2-1-2018

Seismic performance of steel-reinforced concrete composite columns of older and modern construction

Mayer Gerges Farag

Recommended Citation

APA Citation

Farag, M. (2018).*Seismic performance of steel-reinforced concrete composite columns of older and modern construction* [Master's Thesis, the American University in Cairo]. AUC Knowledge Fountain. https://fount.aucegypt.edu/etds/710

MLA Citation

Farag, Mayer Gerges. *Seismic performance of steel-reinforced concrete composite columns of older and modern construction*. 2018. American University in Cairo, Master's Thesis. *AUC Knowledge Fountain*. https://fount.aucegypt.edu/etds/710

The American University in Cairo

The School of Science and Engineering

Seismic Performance of Steel-Reinforced concrete Composite Columns of Older and Modern Construction

A thesis Submitted to

The Department of Construction Engineering

In partial fulfillment of the requirement for the degree of

Masters of Science in Construction Engineering

BY

Mayer Gerges Farag

B.Sc in Construction Engineering

Under the Supervision of

Wael M. Hassan, Ph.D., P.E., S.E.

Visiting Assistant Professor
American University in Cairo

June2017

Acknowledgement

I would never have been able to finish my dissertation without God's support, the guidance of my advisor, help from friends, and support from my family and wife.
First and foremost, praise and thanks goes to God for the many blessings he undeservingly bestowed upon me. I used to say that my abilities may be limited, but I
promise you will be surprised by the amount of effort I exert towards success, thanks to God.

I would like to express my deepest gratitude to my advisor, Dr. Wael Hassan, for his excellent guidance, caring, patience, and providing me with an excellent atmosphere for doing research. He has given me intellectual freedom in my work, supported my attendance at various conferences, and demanded a high quality of work in all my endeavors. Additionally, I would like to thank my committee members Dr. Khaled Nassar, Dr. Sherif Safar, and Dr. Ahmed El-Gendy for their interest in my work.

I would like to thank Dr. Walid Mostafa, Eng. Amr Al Kady, and Mr. Ahmed Madbouly and other workers in the laboratory who patiently helped me throughout specimen tests over the past three years. My research would not have been possible without their support.

Special thanks goes to Eng. SamerSafwat and my staff, who as good friends, tirelessly and with much enthusiasm gave their time and effort to support me, especially running my business while studying. I consider them core partners in this research.

I would also like to thank my parents, and my younger brother, Joney. They were always supporting me and encouraging me with their best wishes. Consultant engineer/ GergesMalak is not only my father but also he is a leader, teacher and it is an honor for me to be his son.

Finally, I would like to thank my wife, Mareez. She was wholeheartedly supporting me and stood by my side through the good and bad times. I owe her.
Special dedication goes to my two daughters Perla and Pretty, who are my source of inspiration, passion, strength and happiness.

Abstract

Existing concrete buildings lacking seismic details are well known to cause most losses during earthquakes so there is no wonder they are nicknamed killer buildings. In every new earthquake we see more evidence of their vulnerability. Ordinary building are taking the most focus of researchers from all over the world because of the majority of building are reinforced concrete. But one of the most widely used structure system contains steel reinforced concrete (SRC) composite columns. This type has been used since early of 1950 and nowadays most high rise or non-prismatic buildings are built using SRC composite columns.

This Experimental study presented addresses the seismic performance of (SRC) composite columns experiencing shear and flexural failures using different concrete grades and confinement details to mimic both existing buildings with old construction details and modern buildings designed and built according to modern codes and construction practices. Test specimens represent exterior columns modeled based on a typical seismic design of a 30-story prototype new core wall-frame tall building and a 20-story prototype gravity existing building. Test parameters considered in this study are target failure mode, axial load ratio, percentage of longitudinal steel, structural steel section, concrete grade, and the transverse reinforcement volumetric ratio. Tests aim to characterize and compare the cyclic response of SRC columns with old and modern construction details. In particular, shear capacity, flexural capacity, residual axial capacity, deformation capacity and engineering demand parameters under different test variables are sought. Backbone curves for numerical simulation of seismic performance of SRC columns are presented. There are fourteen tested specimens divided to three groups; four specimens were tested as pilot, three specimens were tested representing modern building flexure deficient column and seven specimens for old building: five shear deficient specimens and two flexure deficient specimens. This work came out with many conclusions and recommendations for old and modern buildings to overcome the deficiency of SRC composite column.

Retrofitting shear deficient SRC columns under high axial loads (>40%) and flexure deficient columns under high axial loads (higher than the balanced load, i.e. compression controlled failure) experiencing moderate to strong ground shaking seems inevitable.

Contents

List of Figures

Chapter 2

Chapter 3

Chapter 4

Chapter 5

Chapter 6

LIST OF TABLES

Chapter 2

Chapter 3

Chapter 4

Chapter 5

1. Chapter

(1) Introduction

Modern construction industry is witnessing a substantial increase in the number, heights and architectural irregularity of tall buildings. This has naturally led to exceeding the building code height or irregularity limitations, which in return has raised the need for using non-prescriptive design or performance-based engineering. In addition, the real-estate developers increasingly demand smaller column and shear wall sections to maximize building usable and sellable space, particularly in mega-cities' business districts. Moreover, the existing building stock in many active seismic zones includes many seismically deficient buildings that were built before enforcing seismic details in the 1980s. Steel-reinforced concrete (SRC) composite columns and/or high strength concrete columns are being increasingly utilized in tall buildings to achieve these goals. Additionally, many existing buildings utilize SRC columns that are not seismically detailed. Practicing engineers face a major problem which is that is performance-based earthquake nonlinear modeling and design of SRC columns are poorly informed by laboratory tests and nonlinear seismic design guidelines due to test scarcity. Literature reveals a serious lack of knowledge of the seismic behavior of SRC composite columns subjected to simulated seismic loading conditions. There are a small number of tests available to justify deriving seismic backbone curves for macro-modeling purposes. Numerical criteria to distinguish the seismic modes of failure of such columns are not available.

Existing building with composite column in seismic areas since 1960s, no seismic backbones exist for SRC column, no criteria for seismic failure mode, shear strength expressions under higher axial loads are uncertain, no information on axial capacity following shear failure, no information on drift capacity under different axial load levels and even in newly designed SRC column with seismic details on modern codes there are still no seismic backbone recommendations available, all these reasons are the motivation to take the challenge to go through this research. Finally, one of the most important point this hard work research is retrofitting such shear and flexure deficient columns experiencing moderate to strong ground shaking under high axial loads seems inevitable. In addition, the steel section web and shear studs work to over-strength the column in shear. Thus, the shear failure of columns designed according to ACI 318-14 and AISC 341-2008 is not likely

2. Chapter (2)
Background and Literature Review

1. Definition

A steel-concrete composite (SRC) column is a compression member, compressing either a concrete encased hot-rolled steel section or a concrete filled hollow section of hot-rolled steel. It is generally used as a load-bearing member in a composite framed structure.(AIJ 1987)

2. History

Early 1900’s – steel beams encased in concrete for fireproofing

1931 – Empire State Building’s entire steel frame was encased in concrete

1988 – Bank of China “mega truss” of composite columns

Late 1990s – Pacific First Cent (AIJ 1987)

3. Applications of composite column

- Extra capacity in concrete column for no increase in dimension
- Large unbraced lengths in tall open spaces –Lower story in high rise buildings – Airport terminals, convention centers
- Corrosion, fireproof protection in steel buildings •Composite frame –high rise construction

- Transition column between steel, concrete systems
- Toughness, redundancy as for blast, impact (Larry Griffis)

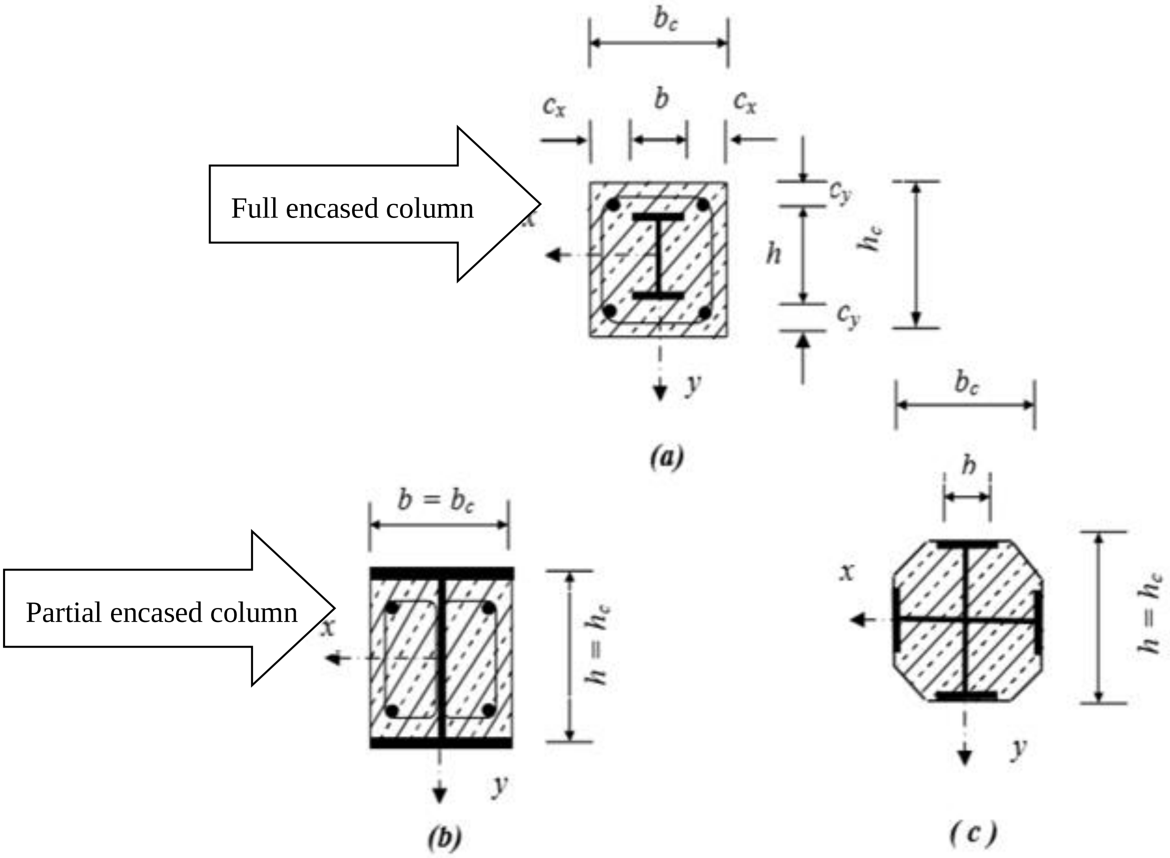

Full encased column

Partial encased column

Figure 2.1: Typical cross-sections of fully and partially concrete encased columns

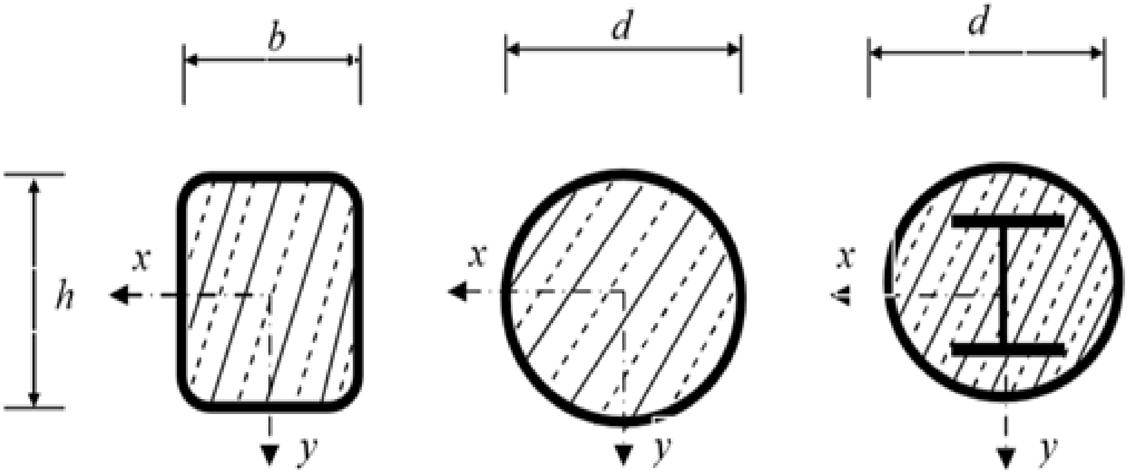

Figure 2.2: Typical cross-sections of concrete filled tubular sections

Typical cross-sections of composite columns with fully concrete encased steel section and two partially concrete encased steel sections are illustrated in **Figure 2.1(a)**, **Figure 2.1(b, c)** and **Figure 2.2**show three typical cross-sections of concrete filled hollow sections. Note that there is no requirement to provide additional steel re-bars for concrete filled hollow composite sections, except for requirements for fire resistance where appropriate.

4. Mechanism of Axial Load Resistance:

In a composite column both the steel and the concrete sections would resist the external loading by bond and friction. Supplementary reinforcement in the concrete encasement prevents excessive spalling of concrete, both under normal load and fire conditions.

5. Construction Advantages:

With the use of composite columns along with composite decking and composite beams, it is possible to erect high rise structures in an extremely efficient manner. There is quite a vertical spread of construction activity carried out simultaneously at any time, with numerous trades working simultaneously. For example

6. Advantages of composite columns:

- Increased strength for a given cross sectional dimensions.
- Good fire resistance
- Corrosion protection in encased columns.
- Significant economic advantages over either structural steel or reinforced concrete alternatives.
- Identical cross sections with different load and moment resistances can be produced by varying steel thickness, the concrete strength or reinforcement. This allows the outer dimensions of a column to be held constant over a number of floors in a building, thus simplifying the construction and architectural detailing.
- Erection of high rise-building in an extremely efficient manner.
- Formwork is not required for concrete filled tubular sections.

7. Cyclic Test on SRC Composite Columns

7.1.Rocles and Paboojian. (1992)

Rocles and Paboojian studied six composite column specimens to test lateral stiffness transverse shear resistance, degree of concrete confinement to achieve good ductility, and effectiveness of shear studs in resisting lateral loading. The next figure and table**Figure 2.3** and **Table 2.1**show the specimens' details.

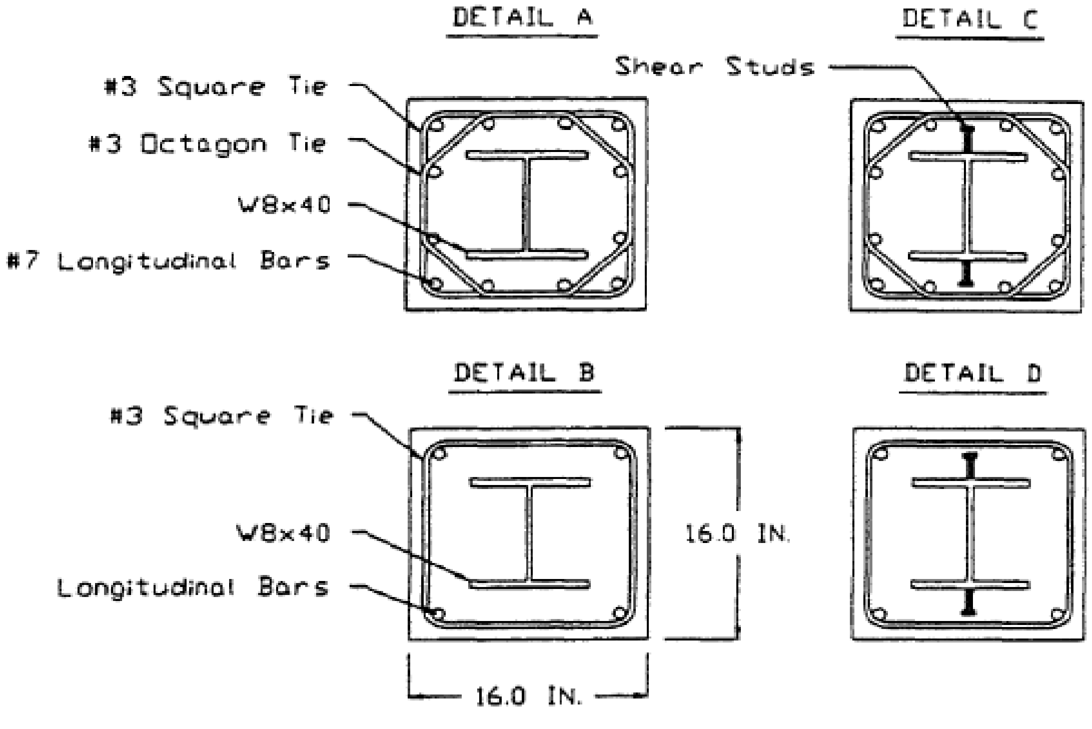

Figure 2.3: Specimens' details (Rocles and Paboojian 1992)

Table 2.1: Specimens' details (Rocles and Paboojian 1992)

Spec No.	d_b (in)	$\frac{A_S}{A_g}$	s (in)	L (in)	Detail Type	s_{max} (in)
1	0.875	0.019	5.0	98	A	4.1
2	1.375	0.023	2.5	98	B	6.5
3	0.875	0.028	3.75	76	A	4.1
4	1.125	0.016	3.75	76	B	5.3
5	0.875	0.028	3.75	76	C	4.1
6	1.125	0.016	3.75	76	D	5.3

1 in. = 2.54 cm.

dp: longitudinal steel par's diameter

As/Ag: longitudinal steel bars' area / gross column cross section area

s: hoop spacing

L: specimen length

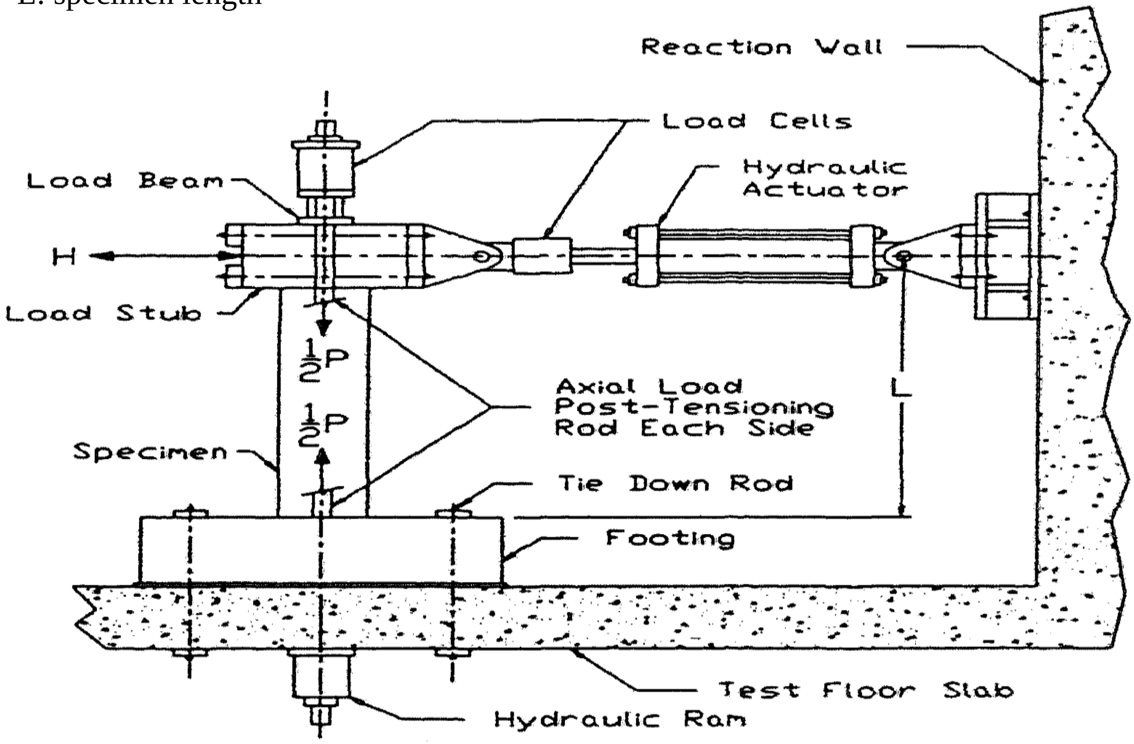

Figure 2.4: Test setup (Rocles and Paboojian 1992)

Figure 2.4 shows the test setup used to test specimens. Based on the test results reported, the following conclusions were mentioned:

- Longitudinal bar buckling must be prevented to preserve the integrity of the member.
- The flexure strengths predicted by the several codes are conservative such as ACI-318-14
- The design of composite columns for shear should be based on the concrete being required to resist all shear at service load levels.
- Shear studs in composite column are neither effective nor required to develop lateral stiffness and flexure capacity.

According to these results, the authors did not mention the seismic behavior of composite columns. There is also a commentary on the point of shear studs which are not effective because shear studs prevent the steel shape from slipping from the concrete section. Next tables show all chen’s specimens; details and results with self-study according to the available data and curves from his work.

7.1.1 Studying Rocles and Paboojian’ specimens

Table 2.2: Rocles and Paboojian specimens’ strength details

ID	Fcu (Mpa)	F'c (Mpa)	Fy (Mpa)	Fyst (Mpa)	Fysec (Mpa)
1A	42.88	34.30	434.40	276.00	372.30
2B	38.38	30.70	434.40	276.00	372.30
3A	44.00	35.20	434.40	276.00	372.30
4B	42.88	34.30	434.40	276.00	372.30
5C (studs)	38.38	30.70	434.40	276.00	372.30
6D (studs)	44.00	35.20	434.40	276.00	372.30

Table 2.3: Rocles and Paboojian specimens' dimensions details

ID	b mm	t mm	H mm	Em. mm	H/Em.
1A	406.40	406.40	812.80	0.00	0.00
2B	406.40	406.40	812.80	0.00	0.00
3A	406.40	406.40	812.80	254.00	3.20
4B	406.40	406.40	812.80	254.00	3.20
5C (studs)	406.40	406.40	812.80	254.00	3.20
6D (studs)	406.40	406.40	812.80	254.00	3.20

Table 2.4: Rocles and Paboojian specimens' concrete and steel bars details

ID	Ac (mm2)	As (mm2)	As/ Ag	Ø mm	#	S mm	Vs/Vc %	Øst mm	#/ m'
1A	165160.96	3138.06	0.02	22	12	127.0	0.61	8.	8.
2B	165160.96	3798.70	0.02	35	4	63.50	0.68	8	16
3A	165160.96	4624.51	0.03	22	12	95.25	0.82	8	11
4B	165160.96	2642.58	0.02	29	4	95.25	0.46	8	11
5C (studs)	165160.96	4624.51	0.03	22	12	95.25	0.82	8.	11
6D (studs)	165160.96	2642.58	0.02	29	4	95.25	0.46	8	11

Table 2.5: Rocles and Paboojian specimens' steel section details

ID	Asec (mm2)	Bf mm	Tf mm	Hw mm	tw mm	Asec/Ag%
1A	7548.37	206.00	14.20	181.20	9.10	4.57
2B	7548.37	206.00	14.20	181.20	9.10	4.57
3A	7548.37	206.00	14.20	181.20	9.10	4.57
4B	7548.37	206.00	14.20	181.20	9.10	4.57
5C (studs)	7548.37	206.00	14.20	181.20	9.10	4.57
6D (studs)	7548.37	206.00	14.20	181.20	9.10	4.57

Table 2.6: Rocles and Paboojian specimens' loading capacity

ID	Axial Load (KN)	ALRt	ALRc	VC axial	Vs (KN)	Vc (kn)	VN KN	Vsteel sec.
1A	1490	0.18	0.26	25.8125	166.57	74.0723	240.64	368.34
2B	1490	0.19	0.29	24.4204	333.14	70.0774	403.22	368.34
3A	1490	0.17	0.26	26.1490	222.09	75.0378	297.13	368.34
4B	1490	0.18	0.26	25.8125	222.09	74.0723	296.17	368.34
5C (studs)	1490	0.19	0.29	24.4204	222.09	70.0774	292.17	368.34
6D (studs)	1490	0.17	0.26	26.1490	222.09	75.0378	297.13	368.34

Table 2.7: Rocles and Paboojian specimens' shear and moment capacity

ID	Mp KNM	Mp H KNM	Vp KN	Vp H KN
1A	395	454.25	485.97	558.871
2B	413	474.95	508.12	584.338
3A	402	462.30	494.59	568.775
4B	388	446.20	477.36	548.967
5C (studs)	388	446.20	477.36	548.967
6D (studs)	387	445.05	476.13	547.552

Table 2.8: Rocles and Paboojian specimens' available test output data

ID	Failure mood	Mpeak Test KNM	Vpeak Test	Vy KN	V80% KN	VR KN
1A	flexural failure	625.7	56.00	45.00	44.80	35.00
2B	flexural failure	592.79	N/A	N/A	N/A	N/A
3A	flexural failure	784.4	86.00	75.00	80.00	80.00
4B	flexural failure	670.54	N/A	N/A	N/A	N/A
5C (studs)	flexural failure	776	N/A	N/A	N/A	N/A
6D (studs)	flexural failure	667.7	N/A	N/A	N/A	N/A

Table 2.9: Rocles and Paboojian specimens' available test output drift data

ID	Δp%	Δy%	Δ80%	ΔR%
1A	8.44	4.16	2.29	2.55
2B	------	------	------	------
3A	7.8	4.16	1.77	1.77
4B	------	------	------	------
5C (studs)	------	------	------	------
6D (studs)	------	------	------	------

Table 2.10: Rocles and Paboojian specimens' ductility and comparison

ID	Vy/Vpeak%	VR/VP%	µΔ	µf
1A	80.36	63	5.5	3.02
2B				
3A	87.21	93	4.25	2.27
4B	------	------	------	------
5C (studs)	------	------	------	------
6D (studs)	------	------	------	------

7.2.Chen et al (2007)

Chen conducted an experimental study of twenty six specimens to study the seismic behavior of SRC composite members and their influence parameters. They used only three shapes with changing other parameters such as axial load ratio, longitudinal steel ratio, steel shape ratio, embedded steel shape length, and transverse steel ratio. **Table 2.11** and **Figure 2.5**&**Figure 2.6**

Table 2.11: Material properties of the test specimens (Chen et al 2007)

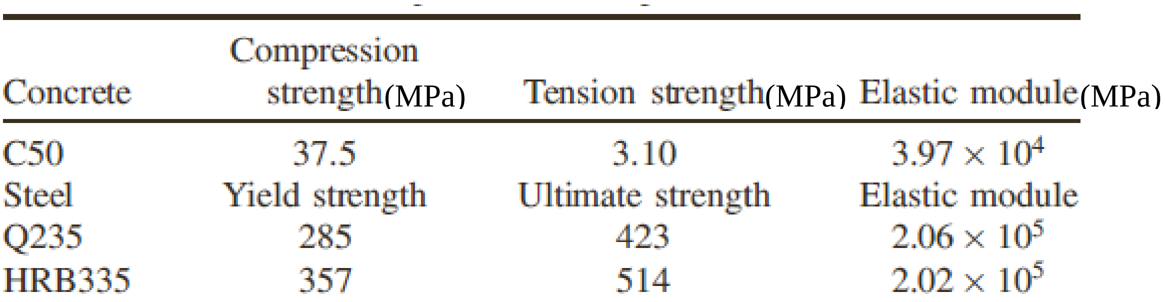

Concrete	Compression strength(MPa)	Tension strength(MPa)	Elastic module(MPa)
C50	37.5	3.10	3.97×10^4
Steel	Yield strength	Ultimate strength	Elastic module
Q235	285	423	2.06×10^5
HRB335	357	514	2.02×10^5

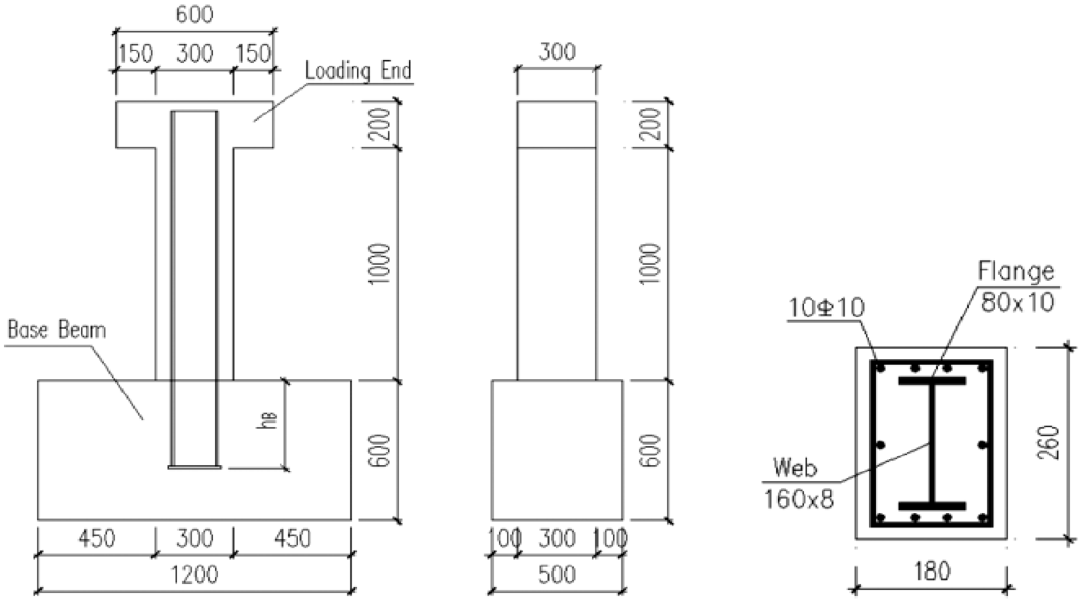

Figure 2.5: Chen's first section details (Chen et al 2007)

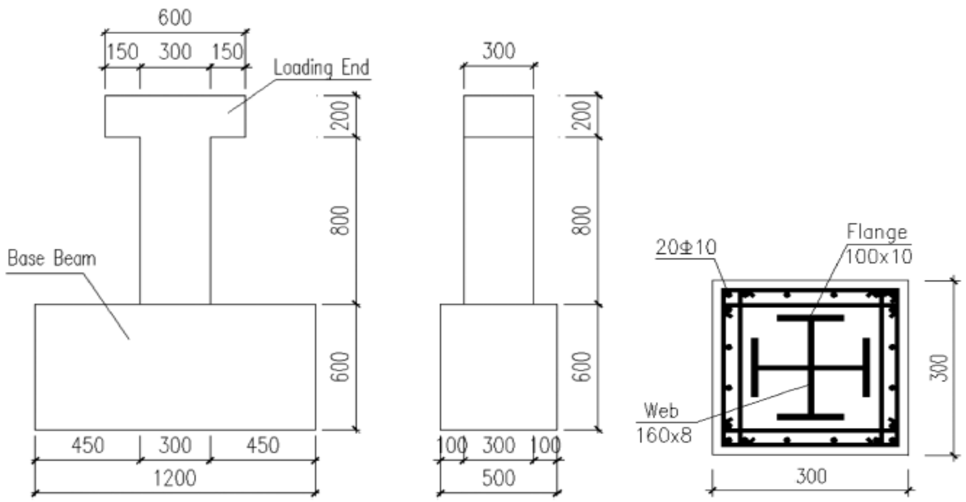

Figure2.6: Chen's second Section details (Chen et al 2007)

After their experiments on 26 specimens under cyclic loading, the author concluded that:

- The steel concrete composite columns display bending failure mode under seismic load.
- The axial compression ratio is an important factor that affects the seismic behavior of steel concrete columns.
- Stirrup ratio is also an important factor to affect the seismic behavior of steel concrete composite column.
- Steel shape also affects the seismic behavior of steel concrete composite column.
- The minimum value of the stirrups ratio of steel concrete composite column can be reduced by 15% over the current limit value.
- The minimum value of the embedded depth of steel concrete composite column can be 2.5inChen et al’s (2007); results; it was not mentioned anything about the backbone curve of composite columns under seismic loading in a nonlinear building.

Next tables show all chen's specimens; details and results with self-study according to the available data and curves from his work.

7.2.1. Studying Chen et al' specimens

Table 2.12: Chen et al specimens' strength details

ID	Fcu (Mpa)	F'c (Mpa)	Fy (Mpa)	Fyst (Mpa)	Fysec (Mpa)
SRC1-1-1	37.50	30.00	357.00	276.00	423.00
SRC1-1-2	37.50	30.00	357.00	276.00	423.00
SRC1-2-1	37.50	30.00	357.00	276.00	423.00
SRC1-2-2	37.50	30.00	357.00	276.00	423.00
SRC1-3-1	37.50	30.00	357.00	276.00	423.00
SRC1-3-2	37.50	30.00	357.00	276.00	423.00
SRC2-1-1	37.50	30.00	357.00	276.00	423.00
SRC2-1-2	37.50	30.00	357.00	276.00	423.00
SRC2-2-1	37.50	30.00	357.00	276.00	423.00
SRC2-2-2	37.50	30.00	357.00	276.00	423.00
SRC2-3-1	37.50	30.00	357.00	276.00	423.00
SRC2-3-2	37.50	30.00	357.00	276.00	423.00
SRC3-1-1	37.50	30.00	357.00	276.00	423.00
SRC3-1-2	37.50	30.00	357.00	276.00	423.00
SRC3-2-1	37.50	30.00	357.00	276.00	423.00
SRC3-2-2	37.50	30.00	357.00	276.00	423.00
SRC3-3-1	37.50	30.00	357.00	276.00	423.00
SRC3-3-2	37.50	30.00	357.00	276.00	423.00

Table 2.13: Chen et al specimens' dimensions details

ID	b mm	t mm	H mm	Em. mm	H/Em.
SRC1-1-1	180.00	260.00	1100.00	366.67	3.00
SRC1-1-2	180.00	260.00	1100.00	440.00	2.50
SRC1-2-1	180.00	260.00	1100.00	366.67	3.00
SRC1-2-2	180.00	260.00	1100.00	550.00	2.00
SRC1-3-1	180.00	260.00	1100.00	366.67	3.00
SRC1-3-2	180.00	260.00	1100.00	366.67	3.00
SRC2-1-1	180.00	260.00	1100.00	366.67	3.00
SRC2-1-2	180.00	260.00	1100.00	366.67	3.00
SRC2-2-1	180.00	260.00	1100.00	366.67	3.00
SRC2-2-2	180.00	260.00	1100.00	366.67	3.00
SRC2-3-1	180.00	260.00	1100.00	366.67	3.00
SRC2-3-2	180.00	260.00	1100.00	366.67	3.00
SRC3-1-1	180.00	260.00	1100.00	366.67	3.00
SRC3-1-2	180.00	260.00	1100.00	366.67	3.00
SRC3-2-1	180.00	260.00	1100.00	366.67	3.00
SRC3-2-2	180.00	260.00	1100.00	440.00	2.50
SRC3-3-1	180.00	260.00	1100.00	366.67	3.00
SRC3-3-2	180.00	260.00	1100.00	550.00	2.00

Table 2.14: Chen et al specimens' concrete and steel bars details

ID	Ac mm2	As mm2	As/Ag	Ø mm	#	S mm	Vs/Vc %	Øst mm	#/m'
SRC1-1-1	46800	785.4	0.02	10	10	53	0.90	6.5	19
SRC1-1-2	46800	785.4	0.02	10	10	53	0.90	6.5	19
SRC1-2-1	46800	785.4	0.02	10	10	65	0.74	6.5	15
SRC1-2-2	46800	785.4	0.02	10	10	65	0.74	6.5	15
SRC1-3-1	46800	785.4	0.02	10	10	80	0.60	6.5	13
SRC1-3-2	46800	785.4	0.02	10	10	80	0.60	6.5	13
SRC2-1-1	46800	785.4	0.02	10	10	43	1.15	6.5	23
SRC2-1-2	46800	785.4	0.02	10	10	43	1.15	6.5	23
SRC2-2-1	46800	785.4	0.02	10	10	53	0.90	6.5	19
SRC2-2-2	46800	785.4	0.02	10	10	53	0.90	6.5	19
SRC2-3-1	46800	785.4	0.02	10	10	65	0.74	6.5	15
SRC2-3-2	46800	785.4	0.02	10	10	65	0.74	6.5	15
SRC3-1-1	46800	785.4	0.02	10	10	37	1.30	6.5	27
SRC3-1-2	46800	785.4	0.02	10	10	37	1.30	6.5	27
SRC3-2-1	46800	785.4	0.02	10	10	43	1.15	6.5	23
SRC3-2-2	46800	785.4	0.02	10	10	43	1.15	6.5	23
SRC3-3-1	46800	785.4	0.02	10	10	53	0.90	6.5	19
SRC3-3-2	46800	785.4	0.02	10	10	53	0.90	6.5	19

Table 2.15: Chen et al specimens' steel section details

ID	**Asec (mm2)**	**Bf mm**	**Tf mm**	**Hw mm**	**tw mm**	**Asec/Ag%**
SRC1-1-1	2880	100	10	160	8	6.15
SRC1-1-2	2880	100	10	160	8	6.15
SRC1-2-1	2880	100	10	160	8	6.15
SRC1-2-2	2880	100	10	160	8	6.15
SRC1-3-1	2880	100	10	160	8	6.15
SRC1-3-2	2880	100	10	160	8	6.15
SRC2-1-1	2880	100	10	160	8	6.15
SRC2-1-2	2880	100	10	160	8	6.15
SRC2-2-1	2880	100	10	160	8	6.15
SRC2-2-2	2880	100	10	160	8	6.15
SRC2-3-1	2880	100	10	160	8	6.15
SRC2-3-2	2880	100	10	160	8	6.15
SRC3-1-1	2880	100	10	160	8	6.15
SRC3-1-2	2880	100	10	160	8	6.15
SRC3-2-1	2880	100	10	160	8	6.15
SRC3-2-2	2880	100	10	160	8	6.15
SRC3-3-1	2880	100	10	160	8	6.15
SRC3-3-2	2880	100	10	160	8	6.15

Table 2.16: Chen et al specimens' loading capacity

ID	Axial Load (KN)	AL R t	AL R c	VC axia l KN	Vs (KN)	Vc (kn)	VN KN	Vsteel sec. KN
SRC1-1-1	702.	0.27	0.50	5.94	162.35	17.04	179.39	324.86
SRC1-1-2	702	0.27	0.50	5.94	162.35	17.04	179.39	324.86
SRC1-2-1	702	0.27	0.50	5.94	132.38	17.04	149.42	324.86
SRC1-2-2	702	0.27	0.50	5.94	132.38	17.04	149.42	324.86
SRC1-3-1	702	0.27	0.50	5.94	107.56	17.04	124.60	324.86
SRC1-3-2	702	0.27	0.50	5.94	107.56	17.04	124.60	324.86
SRC2-1-1	912.6	0.35	0.65	5.94	200.11	17.04	217.15	324.86
SRC2-1-2	912.6	0.35	0.65	5.94	200.11	17.04	217.15	324.86
SRC2-2-1	912.6	0.35	0.65	5.94	162.35	17.04	179.39	324.86
SRC2-2-2	912.6	0.35	0.65	5.94	162.35	17.04	179.39	324.86
SRC2-3-1	912.6	0.35	0.65	5.94	132.38	17.04	149.42	324.86
SRC2-3-2	912.6	0.35	0.65	5.94	132.38	17.04	149.42	324.86
SRC3-1-1	1053	0.40	0.75	5.94	232.56	17.04	249.60	324.86
SRC3-1-2	1053	0.40	0.75	5.94	232.56	17.04	249.60	324.86
SRC3-2-1	1053	0.40	0.75	5.94	200.11	17.04	217.15	324.86
SRC3-2-2	1053	0.40	0.75	5.94	200.11	17.04	217.15	324.86
SRC3-3-1	1053	0.40	0.75	5.94	162.35	17.04	179.39	324.86
SRC3-3-2	1053	0.40	0.75	5.94	162.35	17.04	179.39	324.86

Table 2.17: Chen et al specimens' shear and moment capacity

ID	Mp KNM	Mp H KNM	Vp KN	Vp H KN
SRC1-1-1	62.00	71.30	56.36	64.818
SRC1-1-2	62.00	71.30	56.36	64.818
SRC1-2-1	62.00	71.30	56.36	64.818
SRC1-2-2	62.00	71.30	56.36	64.818
SRC1-3-1	62.00	71.30	56.36	64.818
SRC1-3-2	62.00	71.30	56.36	64.818
SRC2-1-1	55.00	63.25	50.00	57.500
SRC2-1-2	55.00	63.25	50.00	57.500
SRC2-2-1	55.00	63.25	50.00	57.500
SRC2-2-2	55.00	63.25	50.00	57.500
SRC2-3-1	55.00	63.25	50.00	57.500
SRC2-3-2	55.00	63.25	50.00	57.500
SRC3-1-1	46.00	52.90	41.82	48.091
SRC3-1-2	46.00	52.90	41.82	48.091
SRC3-2-1	46.00	52.90	41.82	48.091
SRC3-2-2	46.00	52.90	41.82	48.091
SRC3-3-1	46.00	52.90	41.82	48.091
SRC3-3-2	46.00	52.90	41.82	48.091

Table 2.18: Chen et al specimens' available test output data

ID	Failure mood	Mpeak KNM	Vpeak KNM	Vy KN	V80% KN	VR KN
SRC1-1-1	Shear failure	-----	-----	-----	-----	-----
SRC1-1-2	Shear failure	162.25	147.50	133.75	118.00	100.00
SRC1-2-1	Shear failure	-----	-----	-----	-----	-----
SRC1-2-2	Shear failure	144.10	131.00	112.00	104.80	83.34
SRC1-3-1	Shear failure	-----	-----	-----	-----	-----
SRC1-3-2	Shear failure	176.00	160.00	138.20	128.00	100.00
SRC2-1-1	Shear failure	166.38	151.25	141.34	125.87	100.00
SRC2-1-2	Shear failure	-----	-----	-----	-----	-----
SRC2-2-1	Shear failure	154.00	140.00	117.50	112.00	97.50
SRC2-2-2	Shear failure	-----	-----	-----	-----	-----
SRC2-3-1	Shear failure	158.07	143.70	114.55	115.00	20.00
SRC2-3-2	Shear failure	-----	-----	-----	-----	-----
SRC3-1-1	Shear failure	167.09	151.90	135.00	121.52	90.00
SRC3-1-2	Shear failure	-----	-----	-----	-----	-----
SRC3-2-1	Shear failure	162.25	147.50	132.50	118.00	92.50
SRC3-2-2	Shear failure	-----	-----	-----	-----	-----
SRC3-3-1	Shear failure	176.00	160.00	136.36	128.00	65.46
SRC3-3-2	Shear failure	-----	-----	-----	-----	-----

Table 2.19: Chen et al specimens' available test output drift data

ID	Δp	Δy	Δ80%	ΔR
SRC1-1-1	-----	-----	-----	-----
SRC1-1-2	1.73	0.82	2.95	3.64
SRC1-2-1	-----	-----	-----	-----
SRC1-2-2	1.36	0.95	2.95	3.27
SRC1-3-1	-----	-----	-----	-----
SRC1-3-2	1.36	0.82	2.55	3.09
SRC2-1-1	1.37	1.18	2.45	3.00
SRC2-1-2	-----	-----	-----	-----
SRC2-2-1	1.37	0.59	1.91	2.27
SRC2-2-2	-----	-----	-----	-----
SRC2-3-1	1.18	0.68	1.91	2.27
SRC2-3-2	-----	-----	-----	-----
SRC3-1-1	1.36	0.68	2.73	3.14
SRC3-1-2	-----	-----	-----	-----
SRC3-2-1	1.36	0.68	2.36	2.73
SRC3-2-2	-----	-----	-----	-----
SRC3-3-1	1.36	0.91	1.95	2.36
SRC3-3-2	-----	-----	-----	-----

Table 2.20: Chen et al specimens' ductility and comparison

ID	Vy/Vpeak %	VR/VP %	μΔ	μf
SRC1-1-1	-----	-----	-----	-----
SRC1-1-2	90.68	67.80	3.633	2.67
SRC1-2-1	-----	-----	-----	-----
SRC1-2-2	85.50	63.62	3.1	2.43
SRC1-3-1	-----	-----	-----	-----
SRC1-3-2	86.38	62.50	3.12	2.26
SRC2-1-1	93.45	66.12	2.077	2.19
SRC2-1-2	-----	-----	-----	-----
SRC2-2-1	83.93	69.64	3.22	1.68
SRC2-2-2	-----	-----	-----	-----
SRC2-3-1	79.71	13.92	2.8	1.92
SRC2-3-2	-----	-----	-----	-----
SRC3-1-1	88.87	59.25	3.96	2.30
SRC3-1-2	-----	-----	-----	-----
SRC3-2-1	89.83	62.71	3.42	2
SRC3-2-2	-----	-----	-----	-----
SRC3-3-1	85.23	40.91	21.15	1.73
SRC3-3-2	-----	-----	-----	-----

According to Rocles and Paboojian and Chen’ specimens’ study, the initial yield drift of shear failure mood specimens are a reference source of our study shear specimens and the impeded length ratio of steel section will be taken as resulted to be in all specimens will be illustrated in this experimental study.

7.2.2. Sezen(17 years ago)

Sezen tested four full-scale column specimens to show the response of existing columns in old building under seismic loading. Although Sezen tested conventional concrete columns under seismic loading, not composite columns, the target of his tests was similar to the target of this study: that is to get the actual behavior of the column under the seismic loading. This study depends on Sezen’s setup to reach to the same level as how he simulated the column as it is in the actual building. What is similar between this study and his are the specimens’ setup and the axial load ratio range due to the same shape of specimens. **Figure 2.7** and **Figure 2.8**show the test setup which is our reference for testing setup due to the similarity of specimens and test target of loading axial and horizontally.

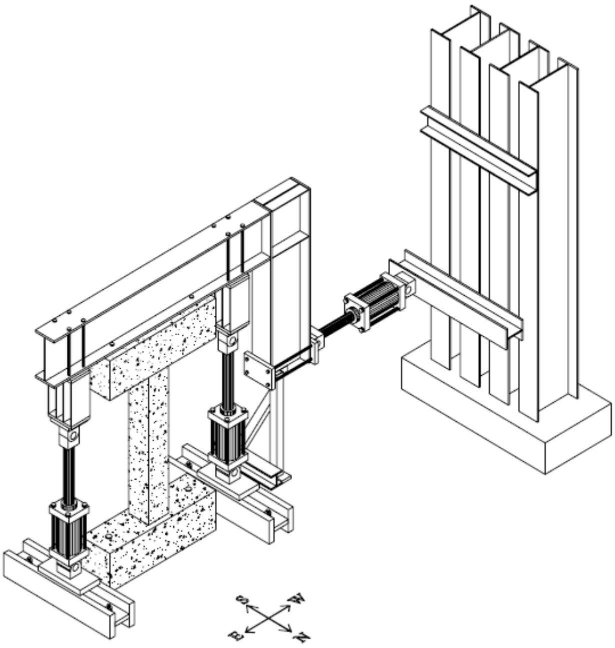

Figure 2.7:Sezen'stest setup

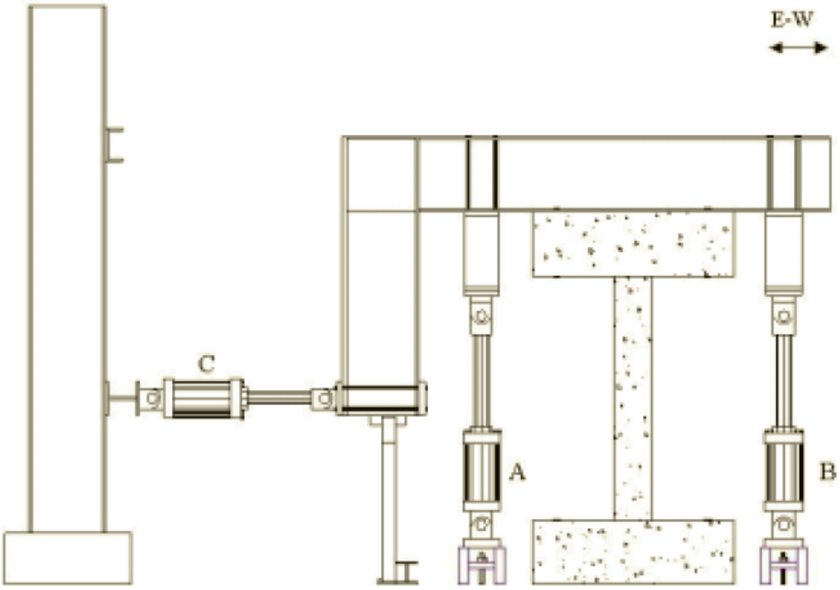

Figure 2.8:Sezen'sloading frame elevation

3. Chapter 3

Design of prototype building

The current series of tests aim to establish more specific cyclic backbone curves of SRC sections. A high-rise building was used as a prototype building to obtain realistic demands on an exterior column of a modern tall building. And 20 story prototype building mimicking old construction was used to obtain the demands on the existing exterior column. The demands on the columns representing existing buildings were estimated based on the axial load ratios prevailing in older construction. Concrete strength used for modern building was $f_c^{'}$=35 MPa and, strength of fc'=27MPa for existing building.

Table 3.1 and **Table 3.2**show the assumed parameters for the high rise prototype building (modern building) and for the existing building.

Table 3.1: The high rise building parameters (Modern construction)

Number of floors	30 floors
Ground floor height	3 m
Total height	90 m
Building area	1765 m^2
Live load	3 KN/m^2
Flooring cover	1.5 KN/m^2
Slab thickness	0.20 m
Load factors	1.4D.L+0.5L.L+EQ
Location	San Francisco
Earthquake combination	100%Y direction + 30%X direction
Shear wall core dimensions	6*0.3 m

Table 3.2: The existing building parameters (Old construction)

Number of floors	20 floors
Ground floor height	3 m
Total height	60 m
Building area	1765 m^2
Live load	3 KN/m^2
Flooring cover	1.5 KN/m^2
Slab thickness	0.20 m
Load factors	1.4D.L+0.5L.L+EQ
Location	San Francisco
Earthquake combination	100%Y direction + 30%X direction
Shear wall core dimensions	6*0.3 m

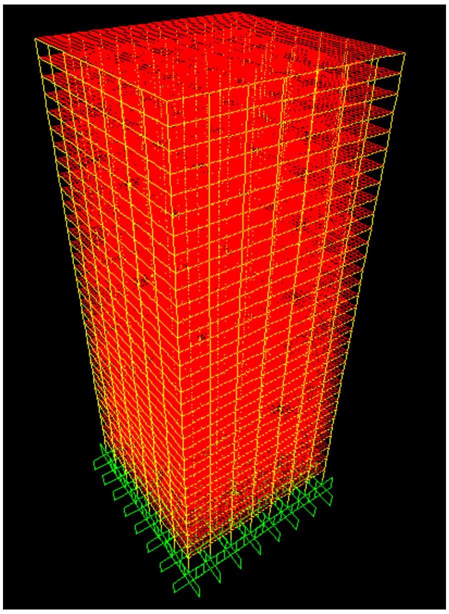

Figure 3.1: The high rise building modeling

According to these parameters and by using SAP2000 for modeling and the response spectra for the San Francisco **Figure 3.2** to model seismic loading, the maximum load of the exterior column for modern building is 25,000 KN. under gravity and earthquake load. The next step was to use the equation for designing the composite column axially section:

P_u = Aa Fya + As Fys + Ac Fc’ (Eq1: ACI 318—14)

P_u = Maximum axial load **Aa** = Cross section area of steel shape = 1-3%**Ac**

Fya = steel shape yield strength

As = Total cross section area of longitudinal steel bars = 2-3%**Ac**

Fys= longitudinal steel bars strength **Ac** = Area cross section of the column

fc’ = Cylinder concrete strength = 80% cubic concrete strength

With this equation the primary design of the column was established which is listed in **Table 3.3.**

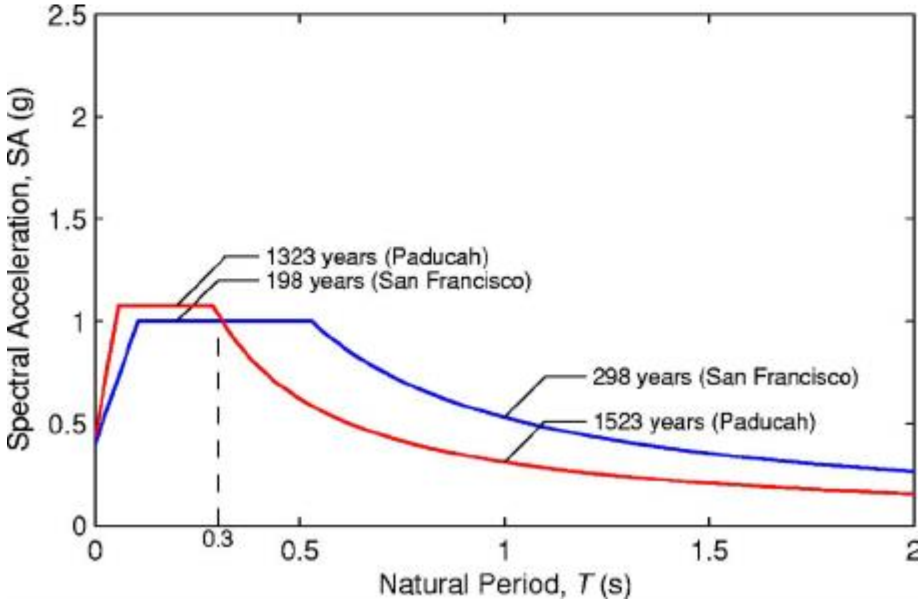

Figure 3.2: Design response spectra for the San Francisco

Table 3.3: Primary modern building column design parameters

Column section	0.75x0.75m
Steel shape	WF 18x86 = 0.0163225 m^2 steel sec. ratio2.9%Ac
Longitudinal steel bars	20 dia. 25mm = 0.01568m^2

As for the existing prototype building based on the modeling, the maximum exterior column axial gravity load was 9500 KN. Using Eq.1,the column design is obtained. However, according to ACI 318—63 which is used to design the existing building columns for gravity load only, there are some differences from the modern ACI 318-14 code.

First, **Aa** = Area cross section of steel shape = 5-9%**Ac** which is much higher than the current practice

As = Total area cross sections of longitudinal steel bars = 2-3%**Ac**

With the same parts of equation only the differences are for steel section and longitudinal bars ratio

Table 3.4: Primary existing column's parameters (old building)

Column section	0.45x0.45 m
Steel shape	WF 10x54 = 0.010125 m^2 Steel sec. ratio 5%Ac
Longitudinal steel bars	12 dia. 25mm =0.00 588 m^2 2.9%Ac

4. Chapter (4)

Experimental Program

The actual column section can be constructed in a real building but still unknown in its behavior under seismic loading. To deal with section and test it, it had to be scaled to fit within the lab capacity. A scaling factor of 0.5 of ground floor height is a very suitable scale to be easy built and tested within the available lab constrains. for column section dimensions it was scaled in first to 0.5 of the original prototype column but after the pilots ‘ test the column dimension reduced from 0.30m x0.30m to be 0.25m x 0.25m. For testing a high-rise building modern column, it was decided to build three specimens with fc’=35 MPa and with height 1.5m as a half scale height of the ground floor of the prototype building. As shown in **Figure 4.2** the column bas dimensions were taken 1.70m in length to be enough for two bolts spacing 1m axis between and extra concrete length 0.35 from two sides. The width was taken 0.6m to be enough for column dimensions which is 0.25 x 0.25 m with 0.175m from two sides to avoid column punching. Finally, the bas depth was taken 0.8 m to be enough for embedment steel section. **Table 4.1** summarizes the specimens’ parameters. According to, Chen et al (2007) and Rocles & Paboojian (1992), the embedment length of the steel shape inside the base is:

H/Em = 2.5

Where **Em**: the embedment length of steel shape

H: the clear height of the column

So, 1.5/Em=2.5 ⟹ Em=0.6m in the base.

1. Shear Studs (Shear Connectors)

According to AISC 360-05, to calculate required shear studs for column, the next equations were used to find length, diameter, and spacing of shear studs as shown in **Figure 4.1**. It was used bolts instead of the studs with same calculated parameters.

- $L \nless 4\, d_s$
- $16mm < d_s < 25mm$
- $d_s \ngtr 2\, t_f$
- $d_h \nless 1.5\, d_s$
- $S = 6\, d_s$

Where:

L: is the length of shear stud: is the shear stud diameter

d_h: is shear stud’s head diameter **S**: is the spacing between shear studs**:** web flange thickness

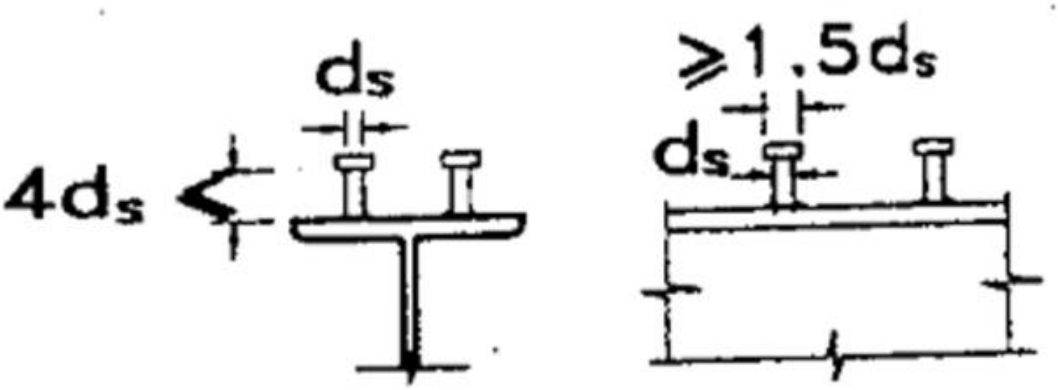

Figure 4.1: Shear studs details

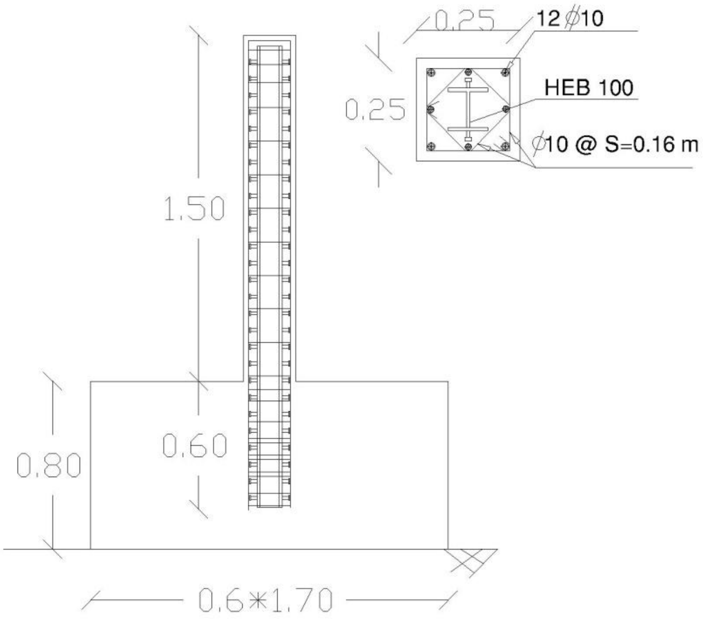

Figure 4.2: Modern building test specimen details

Table 4.1: Modern building test specimens' details

Test target	Number of specimens	f_c' MPa	Column dimensions (m)	Reinforced Steel bars	Steel shape
Conventional concrete	3	35	0.25x0.25x1.5	12 dia. 10 mm Flexure failure	HEB 100

Based on the maximum load, which lab load cell can take (2000 KN), the axial load ratio were calculated. The axial load ratio (ALR) is defined as:

$$ALR = (P_u) / (A_c * f_c')$$

Where P_u is maximum axial load and A_c is the gross section area

Table 4.2: Experimental Modern building specimens' test matrix

Specimens ID	**fc' MPa**	**Failure Mode**	**ALR**	**Stirrups Spacing S**	**Fyst Mpa**	**Steel Shape Ratio**	**Fysec Mpa**	**R. Steel ρ**	**Fybar Mpa**
CSF-10N	35	Flexure Ten.	0.1	0.16m	516	4.16% (H100)	435	2% (12Φ10)	428
CSF-10N	35	Flexure Ten.	0.1	0.075m	516	4.16% (H100)	435	2% (12Φ10)	428
CSF-0N	35	Flexure Ten.	0	0.075m	516	4.16% (H100)	435	2% (12Φ10)	428

1. Specimen instruction

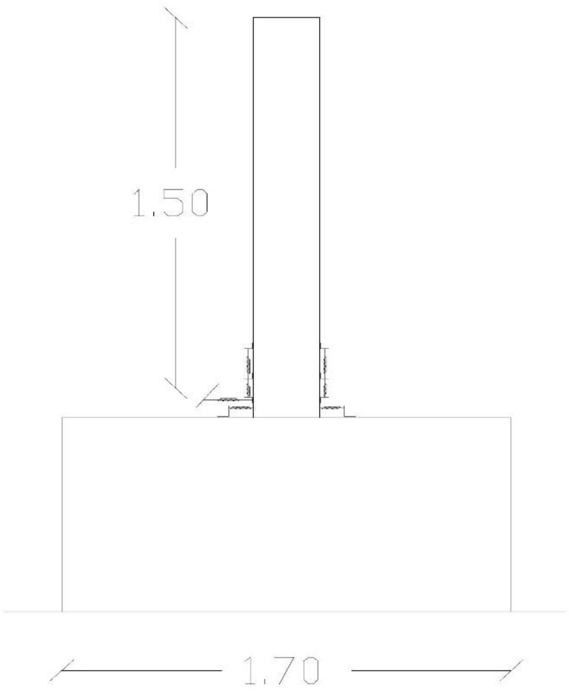

Figure 4.3: Modern building test specimen external instrumentation

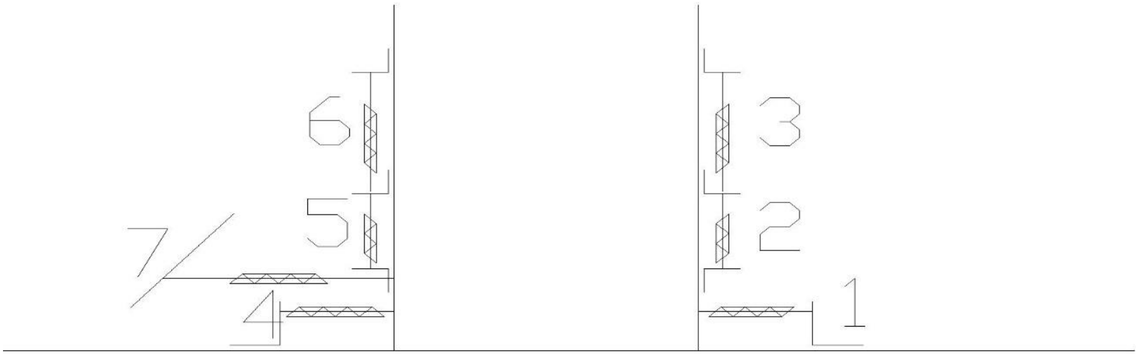

Figure 4.4: Modern building test specimen external instrumentation numbers

There were seven linear variable displacement transducers (LVDTs) to measure each displacement which occur during the test both intension and compression area of the column arranged and numbering as **Table 4.3**:

Table 4.3: Arrangement and numbering of displacement potentiometers of modern building specimens

#	Distance from Base	LVDT Length	Measured length	purpose
1	0.04 m	0.05 m	0.055 m	Slip rotation
2	0.05 m	0.1 m	0.115 m	Tension/ compression displacement
3	0.175 m	0.1 m	0.25 m	Tension/ compression displacement
4	0.04 m	0.05 m	0.055 m	Slip rotation
5	0.05 m	0.1 m	0.12 m	Tension/ compression displacement
6	0.17 m	0.1 m	0.24 m	Tension/ compression displacement
7	0.22 m	0.1 m	0.17 m	Tension/ compression displacement

About 14 strain gages were used to measure strain in stirrups, longitudinal bars, and steel section flanges and web at different distances from base surface to provide sufficient data to give an idea about the behavior of specimen.

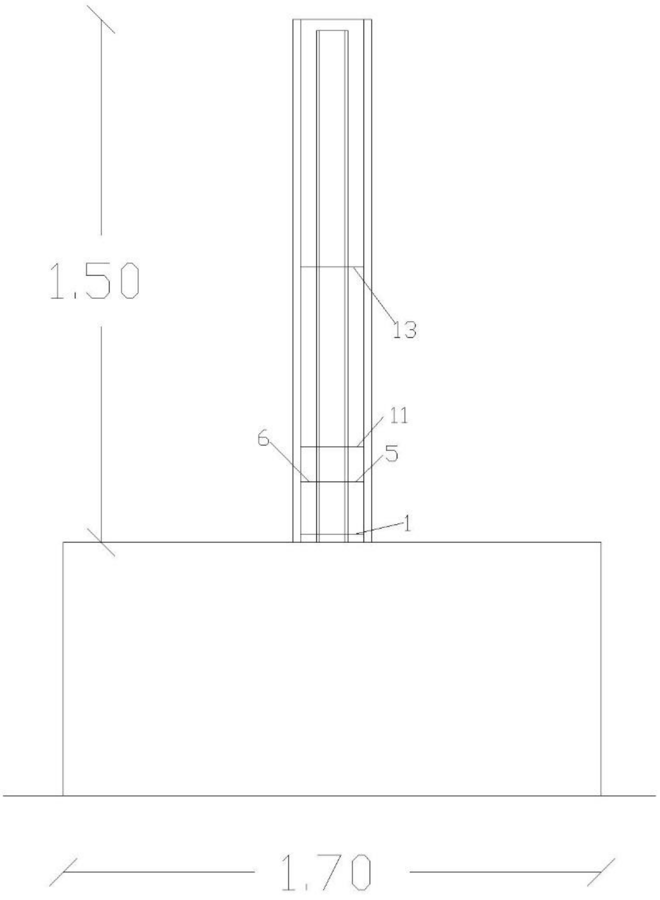

Figure 4.5: Modern building test specimen arrangement hoop strain gages

Table 4.4: Hoop strain gages of modern building specimens

Num.	Distance from base face
1	0.025 m
5	0.19 m
6	0.19 m
11	0.3 m
13	0.87 m

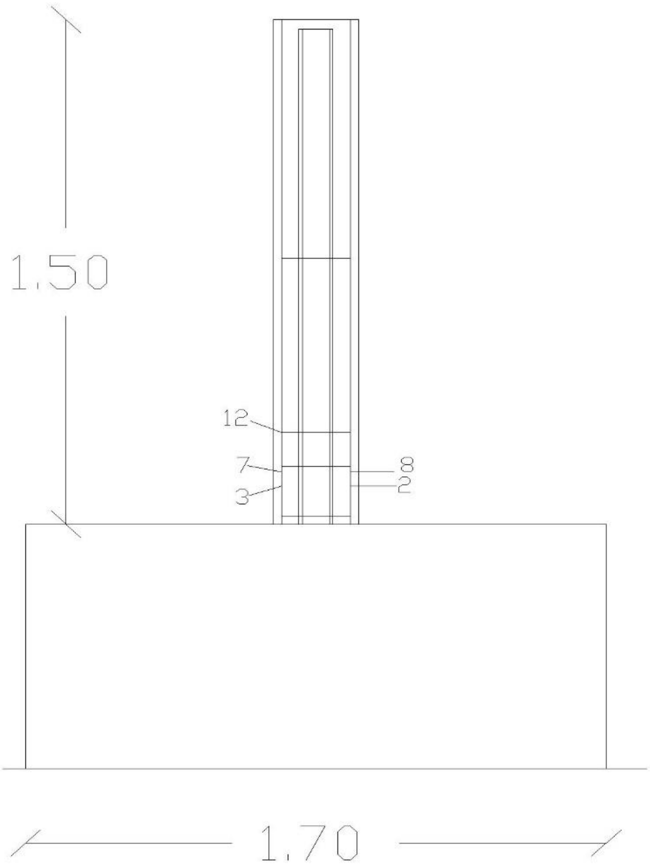

Figure 4.6: Modern building test specimen arrangement of longitudinal bars strain gages

Table 4.5: Longitudinal bars strain gages of modern building specimens

Num.	Distance from base face
2	0.125 m
3	0.125 m
7	0.17 m
8	0.17 m
12	0.30 m

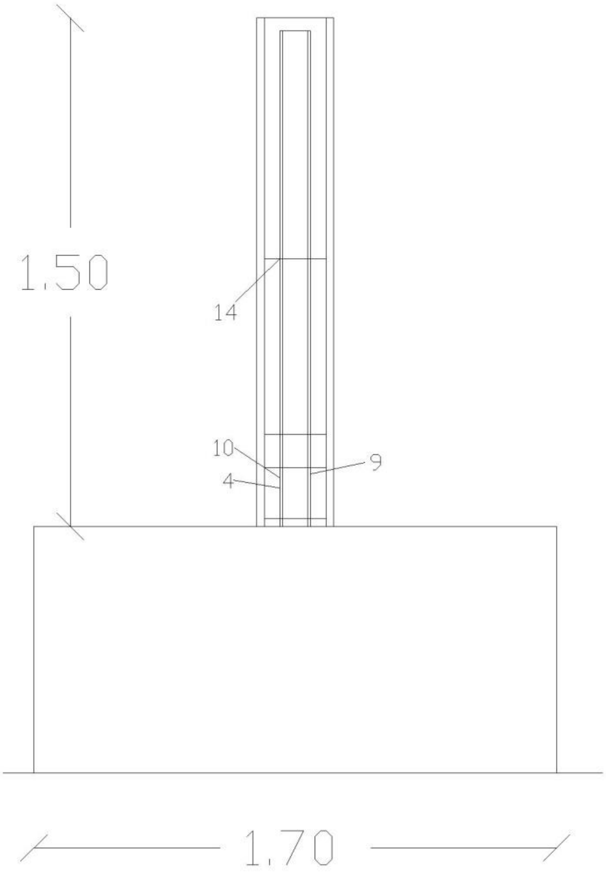

Figure 4.7: Modern building test specimen arrangement of steel section flanges strain gages

Table 4.6: Steel section flanges' strain gages of modern building specimens

Num.	Distance from base face
4	0.125 m
9	0.17 m
10	0.17 m
14	0.87 m

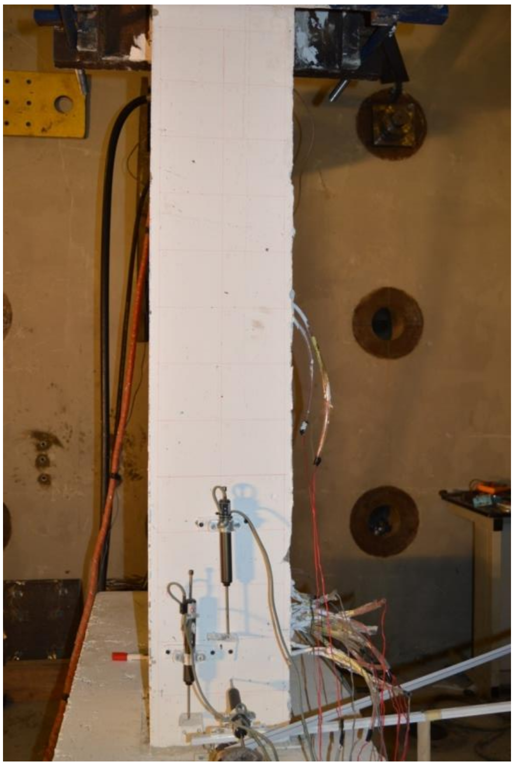

Figure 4.8: Modern building test specimen arrangement of LVDT 4-7

Figure 4.9: Modern building test specimen arrangement of LVDT

For testing column representing existing buildings, seven specimens were built with fc’=27MPa and five of them with height 1m as one third scale of the 3m of the ground floor of the prototype building, using scale 1/3 for shear deficient existing building was necessary to enforce shear failure to reducing the moment values during testing. The other two specimens which are with height 1.5m as same as the modern building's specimens to enlarge the moment values during the test. With the same sequence, to calculate embedment length of steel shape the following equation was used.

$$H/Em = 2.5$$

So, $1/Em=2.5 \Longrightarrow Em= 0.4m$ in the base.

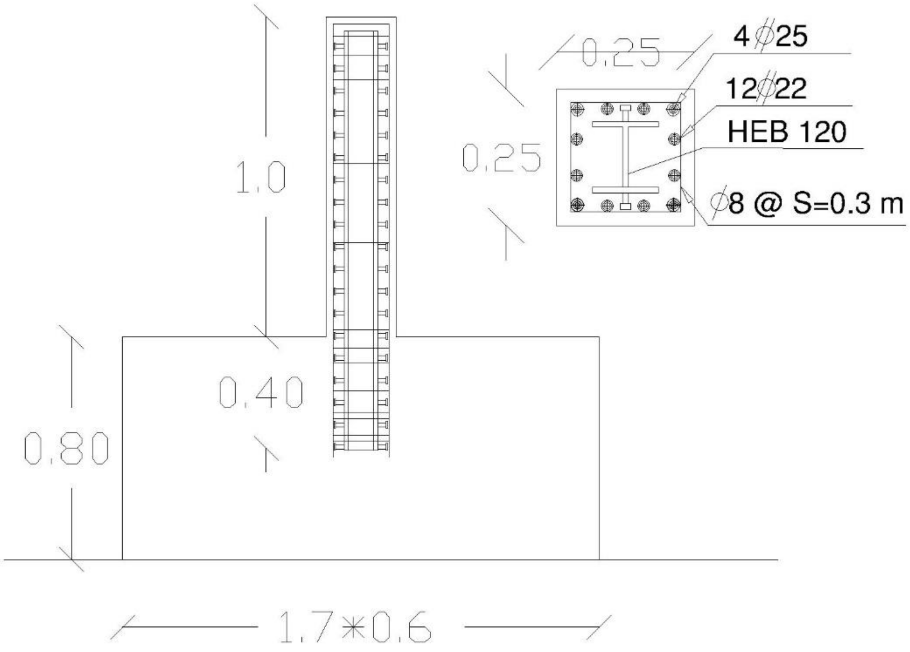

Figure 4.10: Existing building test specimen details

Table 4.7: Existing building test specimens

Number of specimens	f_c' (MPa)	Base dimension	Column dimension	Reinforced Steel bars	Steel shape
5	27	0.8x0.6x1.7 m	0.25x0.25x1 m	(12dia 22 + 4 dia.25) Shear failure	HEB 120
2	27	0.8x0.6x1.7 m	0.25x0.25x1.5 m	(8 dia10) Flexure failure	HEB 120

Table 4.8: Existing specimens test matrix

#	Specimens ID	fc' MPa	Target Failure Mode	ALR	Hoop Spacing	Steel Section Ratio	Reinforcement Steel Ratio
1	CSS15-E	27	Shear	0.15	S=0.30m	5.4% (H120)	7% (12Φ22+ 4Φ25)
2	CSS20-E	27	Shear	0.20	S=0.30m	5.4% (H120)	7% (12Φ22+ 4Φ25)
3	CSS40-E	27	Shear	0.40	S=0.3m	5.4% (H120)	7% (12Φ22+ 4Φ25)
4	CSS60-E	27	Shear	0.60	S=0.3m	5.4% (H120)	7% (12Φ22+ 4Φ25)
5	CSS80-E	27	Shear	0.80	S=0.3m	5.4% (H120)	7% (12Φ22+ 4Φ25)
6	CSF15-E	27	Flexure Ten	0.15	S=0.075m	5.4% (H120)	1% (8Φ10)
7	CSF80-E	27	Flexure Comp	0.8	S=0.075m	5.4% (H120)	1% (8Φ10)

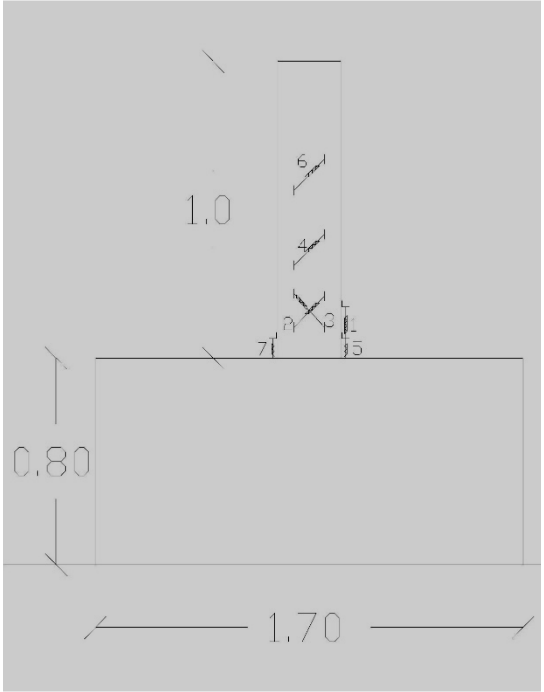

Figure 4.11: Existing building test specimen external instruments

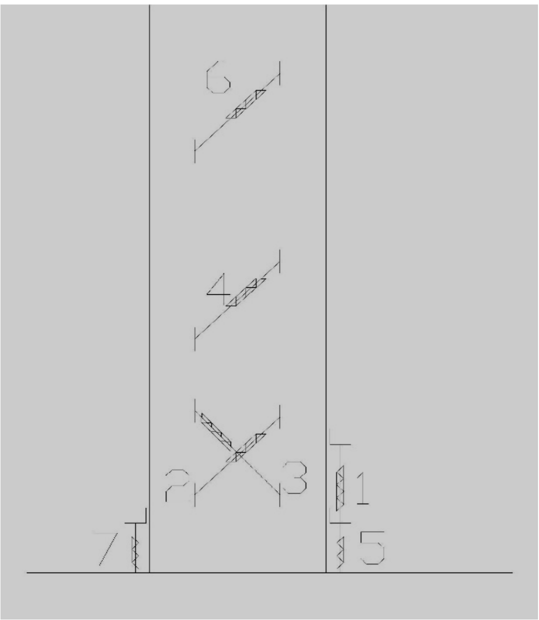

Figure4.12: Existing building test specimen external instrumentation numbers

There were 7 LVDTs to measure each displacement which occur during the test in both tension and compression area of the column arranged and numbering as **Table4.9**.

Table 4.9: Arrangement and numbering of displacement potentiometers of existing building specimens

#	Distance from Base	LVDTs Length	Measured length	purpose
1	0.17 m	0.1 m	0.24 m	tension/compression displacement
2	0.12 m	0.1 m	0.17 m	tension/compression displacement
3	0.11 m	0.1 m	0.15 m	tension/compression displacement
4	0.36 m	0.1 m	0.17 m	tension/compression displacement
5	0.05 m	0.05 m	0.125 m	tension/compression displacement
6	0.65 m	0.1 m	0.115 m	tension/compression displacement
7	0.05 m	0.05 m	0.125 m	tension/compression displacement

1. Test Setup and Loading Protocol

The test setup comprises a horizontal 220k.N. dynamic actuator with a 120 mm tension and compression stroke capacity supported to a strong wall and applying lateral load at the top of the specimen. The lateral loading rate was 0.5 mm per second. A 2000kN vertical load cell connected to a vertical jack that is attached to a loading frame and braced laterally to the reaction wall was used to apply the vertical load. A rolling mechanism was introduced to allow for sliding of the column top under the vertical load. The test setup is shown in **Figure 4.14**, **Figure 4.15**, **Figure 4.16** and **Figure 4.17**.

1.1.Yield displacement Protocol

The specified displacement history used in the experimental investigation of this study was a function of yield displacement. Therefore, it was necessary to predict the yield displacement of the specimens before the tests.

In this study, yield displacement is calculated as the summation of three components: elastic yielding, longitudinal bar slip, and moment curvature displacements. Since the test specimens were tested in single curvature. **Figure 4.13** show displacement protocol example. Two displacement cycles were used prior to reaching theoretical yield displacement followed by three cycles per amplitude after reaching the theoretical yield displacement.

$$\Delta_{y,flex} = \Delta_{ye} + \Delta_{y,slip} + \Delta_{M\text{-}Ø}$$

$$\Delta_{ye} = Ø_y L^2 / 3 \quad + \quad \Delta_{y,slip} = Ø_y d_p f_y / 8U_b + \Delta_{M\text{-}Ø} = fa^3/3EI$$

Where:

L: is the length of column **d_b**: is the bar diameter **U_b** : is a uniform bond stress **$Ø_y$** : yield curvature

f_y: is the steel bar's yield strength **f**: is the conclude horizontal load

I: is the summation of inertia of steel section, steel bars, and concrete

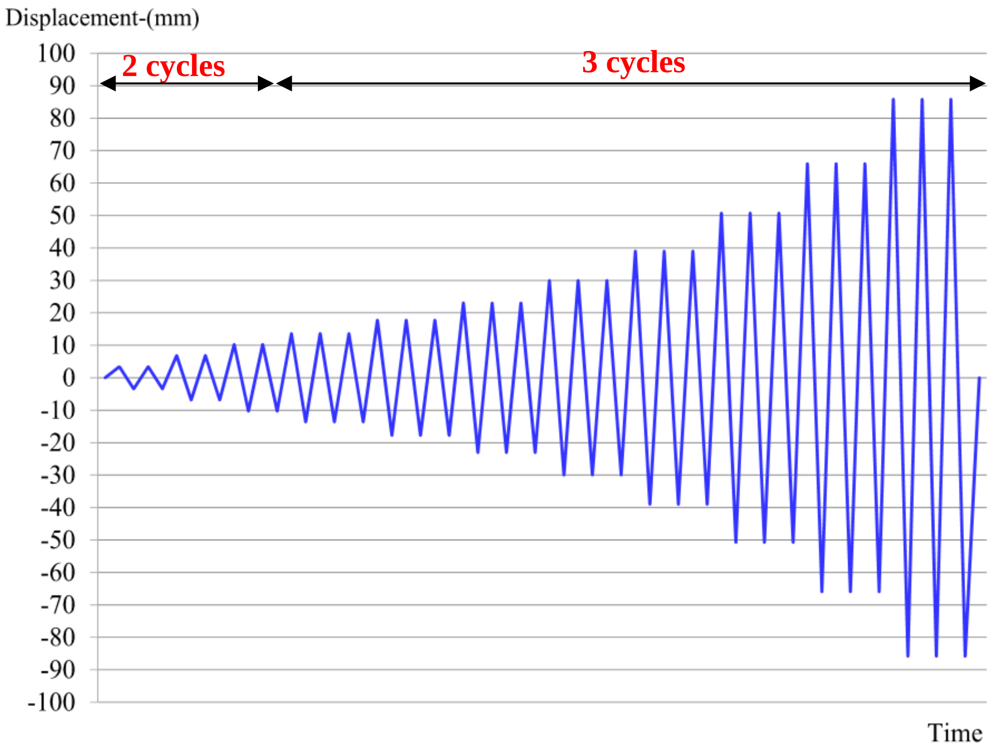

Figure 4.13: Displacement protocol

However, the theoretical yield displacement in shear controlled specimens was much harder to predict, thus it was predicted based on the results of previous literature tests with similar parameters. Seven strain gages and seven LVDTs were used to instrument each test specimen at critical strain locations. A data controller and acquisition systems were used to apply and monitor loading conditions and collect the test data results (Farag, M., and Hassan, W. 2015).**Figure 4.18**: **Figure 4.32** show all steps in preparing specimens starting with steel work, wooden form work, checking dimensions and verticality, fixing strain gages, pouring concrete process and finally curing specimens.

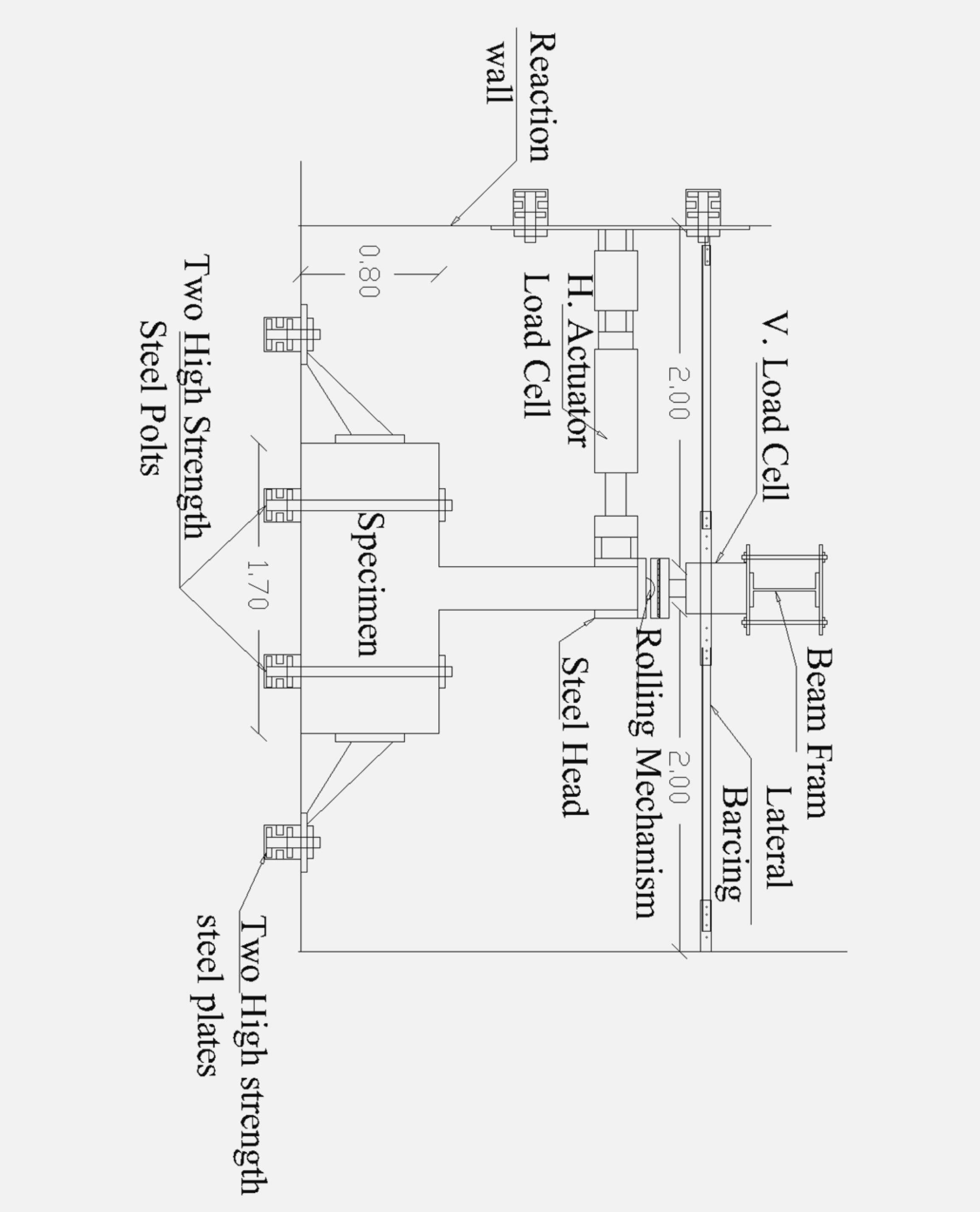

FIGURE 4.14: TEST SETUP

Figure 4.15: Test setup

Figure 4.16: Column head fixation setup

Figure 4.17: Base fixation setup

Figure 4.18: High strength steel rods with lubricate

Figure 4.19: High strength upper steel plate with lubricate

Figure 4.20: Head mechanism of load transfer

4.1. Test specimens' preparation

Figure 4.21: Plywood fair face form work

Figure 4.22: Leveling of specimen column

Figure 4.23: Fixing the specimen frame

Figure 4.24: Making the groves for the tubes of the fixation bolts

Figure 4.25: Checking the stirrups spacing

Figure 4.26: Checking the accuracy of concrete cover

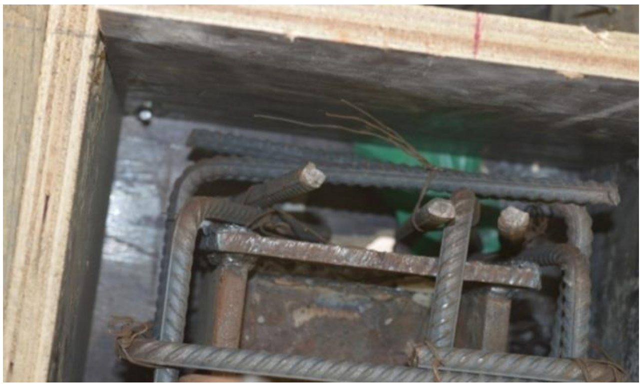

Figure 4.27: The column head

Figure 4.28: Fixing the strain gages as designed

Figure 4.29: Pouring with ready mix concrete

Figure4.30: Checking the leveling during pouring concrete

Figure4.31: Ensuring the strain gages places

Figure 4.32: Finishing the pouring face of concrete

Figure 4.33: Pouring all specimens

Figure 4.34: Final check after pouring

Figure 4.35: Curing stage of specimens and their sample cylinder and cub samples

5. Chapter 5

Test Results and Observation

This chapter provides a summary of the test results including damage description and test data measured during each test. This chapter also includes a brief description of the data reduction procedures, including calibrations and corrections of offsets, modification for second-order effects, and description of engineering quantities such as moment and average curvature.

Based on visual observations and recorded test data, the performance of each test specimen is addressed. For each specimen, the measured lateral load-displacement relations and plots of other important test parameters are presented. The damage description of specimens and their implications are discussed, and the measured response is compared mainly in terms of applied displacement and load configurations described in the previous chapter. The following sections address the response of each specimen and observations made during each test.

1. Pilot specimens

Four pilot specimens were cast and tested before reaching to the final shape and features of the rest of the specimens in the experimental program. Three specimens showed that the lab capacity is limited to enable specimens to fail because of the scale of the specimens and the over-strength provided by the steel section.

1.1.P1: CSF-10-NP

Figure 5.1shows the shear force-drift ratio hysteresis response of specimen CSF10-NP. The flexural nature of the response is clear through the cycles' shape which also shows a strain hardening trend, reaching a significant drift of about 6.5% without any strength degradation. (Farag and Hassan, 2015)

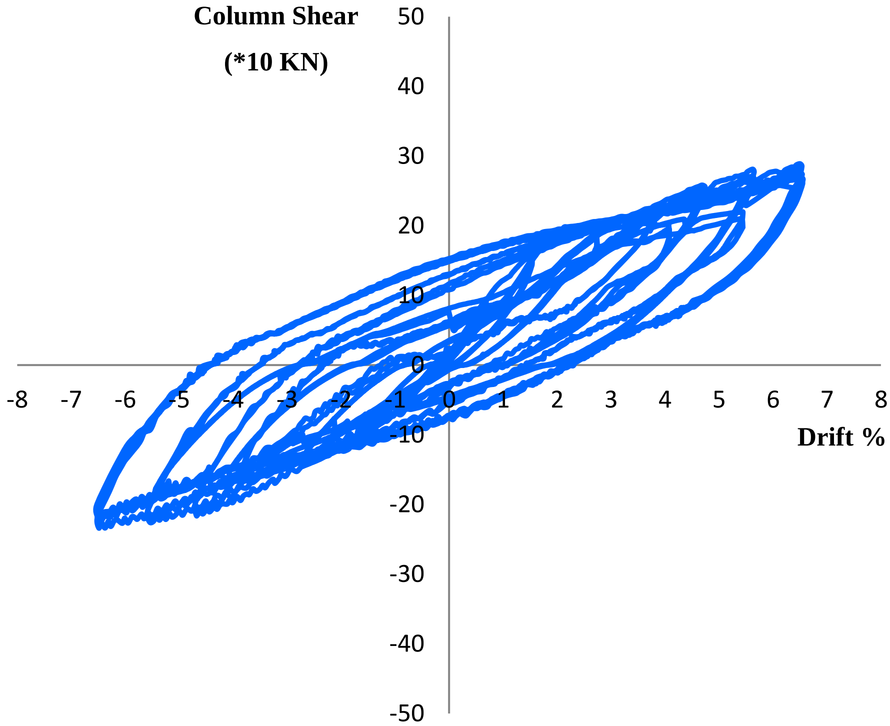

Figure 5.1: Shear force-drift hysteresis response of specimen CSF10-NP

Figure 5.2shows the failure mode of specimen CSF10-NP under the effect of the applied displacement protocol. The specimen was failing in a flexural tension failure mode as predicted in the theoretical analysis. (Farag and Hassan, 2015)

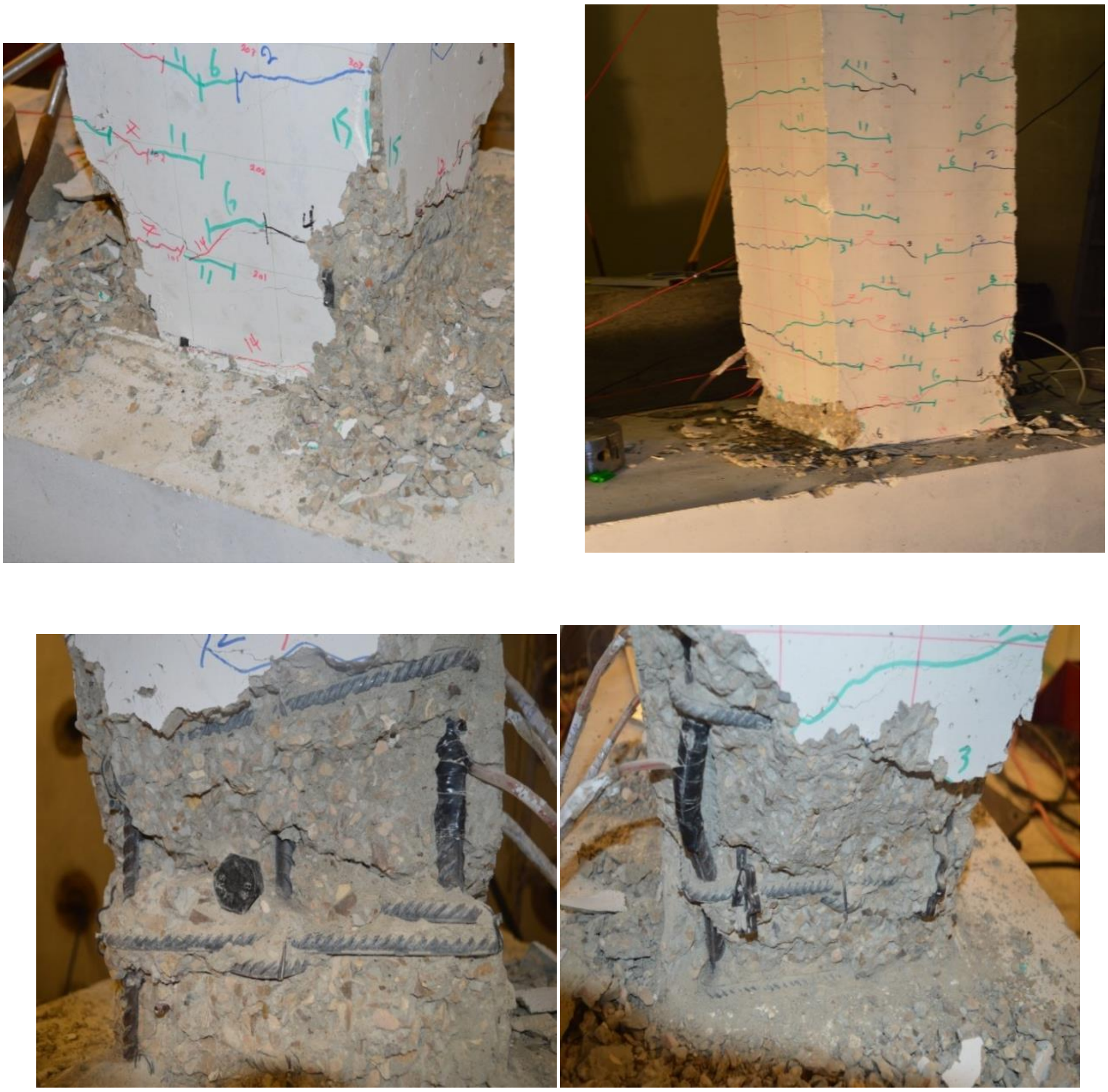

Figure 5.2: Failure mode of specimen CSF10-NP

1.2.P2: CSS-15-NP

Figure 5.3shows the failure mode of specimen CSS15-NP under the effect of the applied displacement protocol. The target failure mode of the specimen was flexural tension failure. According to ACI 318-08, the minimum hoop spacing used was 250 mm. The effect of hoop spacing on the backbone curve will be studied through this study. (Farag and Hassan, 2015)

Figure 5.4shows the shear-drift hysteresis response of specimen CSS15-NP until the test termination drift ratio of about 6.5% due to actuator stroke capacity. A strain hardening trend reached the significant drift of 6.5% without any strength degradation evident. This drift ratio is believed to exceed any practical drift ratio corresponding to collapse prevention limit state. The peak shear value was 490 KN which excessively exceeded the predicted value of 190 KN that was originally expected to correspond to the flexural capacity of the section. (Farag and Hassan, 2015)

Figure 5.3: Failure mode of specimen CSS15-NP

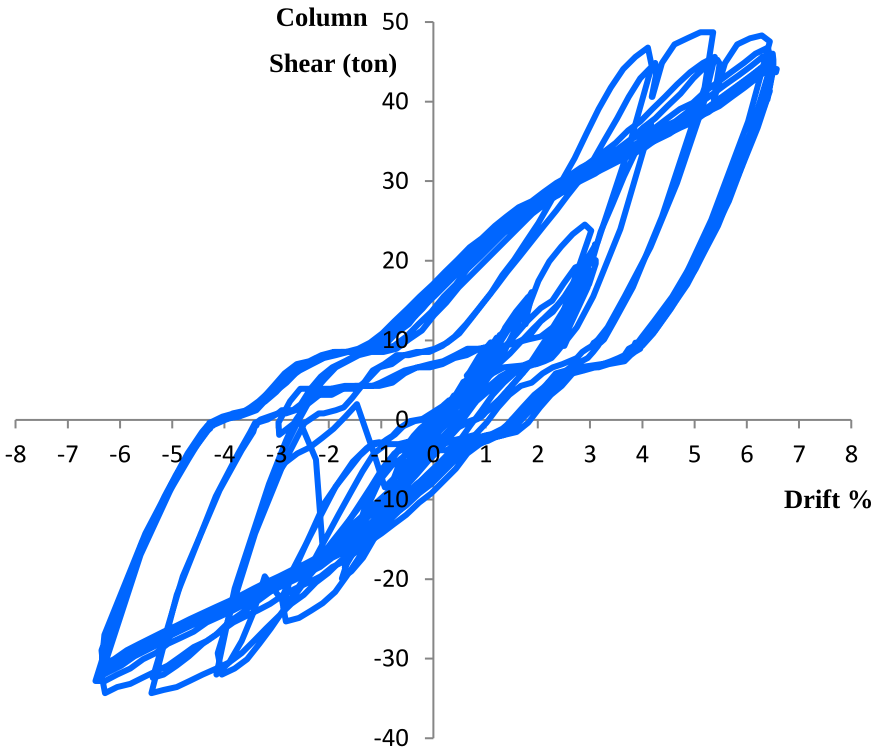

Figure 5.4: Shear force-drift hysteresis response of specimen CSS15-NP

1.3.P3: CSS10-E

Figure 5.5shows the failure mode of specimen CSS10-EP under the effect of the applied displacement protocol. The target failure mode of the specimen was shear failure. The specimen was designed according to ACI 318-63. The hoop spacing was 300 mm. Some shear flexural cracks have appeared during the test. However, the specimen appears to have failed in flexure due to shear over-strength of the embedded steel section. (Farag and Hassan, 2015)

Figure 5.6 shows the shear-drift hysteresis response of specimen CSS10-EP. The specimen initially yielded in flexure; however, large deformation resulting from strain hardening at 90 degree has left hooks of the hoops opened and left the concrete in compression poorly confined. This has resulted in crushing the concrete in compression.(Farag and Hassan, 2015)

Figure 5.5: Failure mode of specimen CSS10-EP

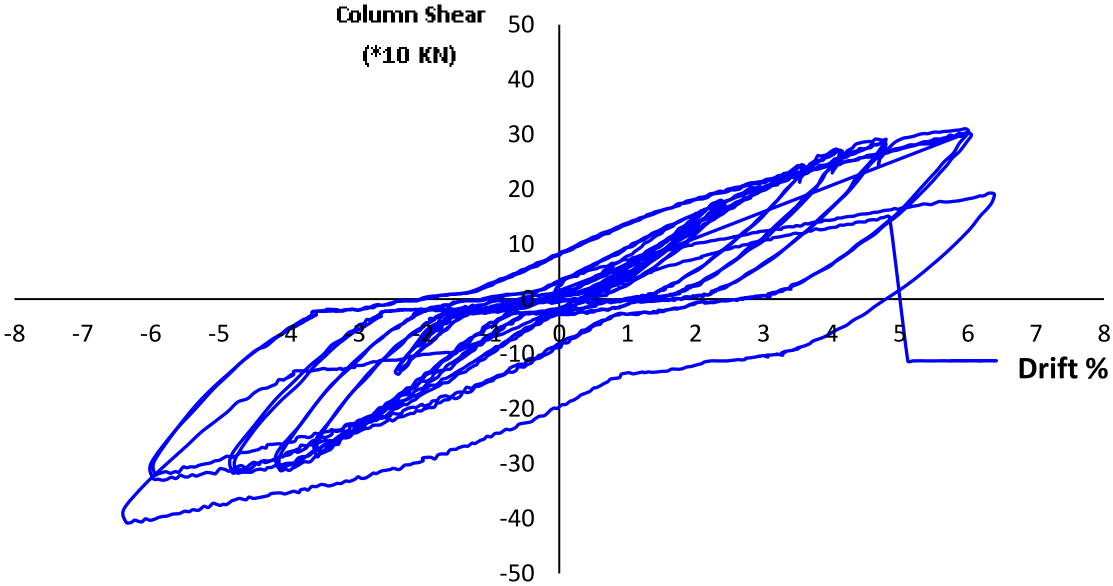

Figure 5.6: Shear force-drift hysteresis response of specimen CSS10-EP

According these three specimens, the section of the column was reduced to be 250 x 250 mm instead of 300x 300 mm with 1.5m height for flexural controlled specimens and 1m height for shear specimens to reduce the failure moment and allow for shear controlled behavior. The fourth specimen was tested to check the new parameters under the lab capacity with 25 cm spacing between hoops for a specimen referring to an existing building according to ACI 318-63.

1.4.P4: CSS-15-E-25

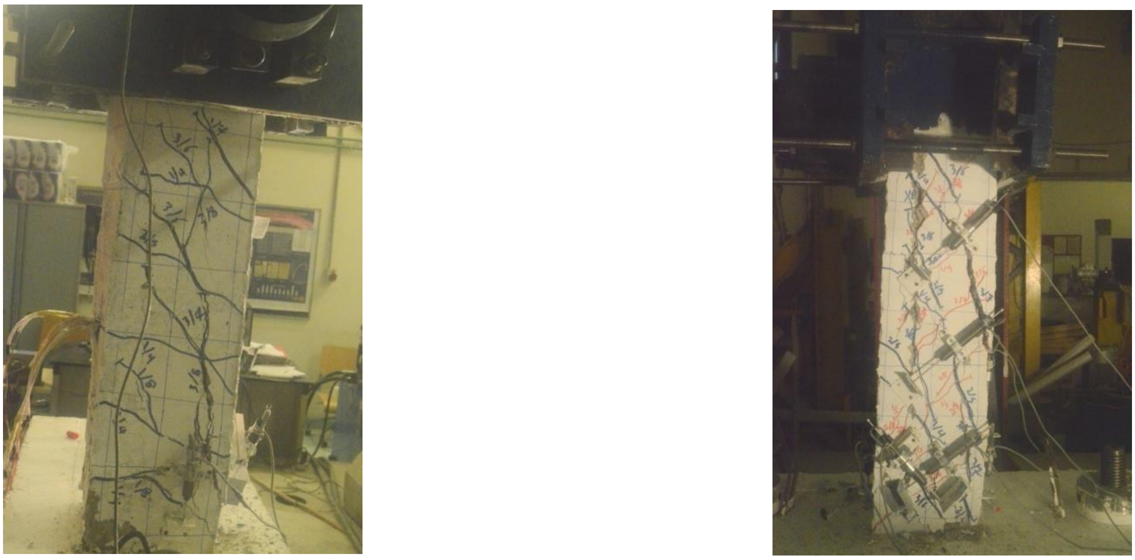

Figure 5.7: Failure mode of specimen CSS15-E-25

Figure 5.7 shows the failure mood of specimen CSS15-E-25.During the testing of specimen CSS15-EP-25, the horizontal load cell reached the maximum load limit of 220 KN. According to **Figure 5.8** shows, it was decided to remove the concrete cover for the column height to check the response of transverse steel (stirrups) and longitudinal bars. No deformation was found. For that, concrete was removed from the entire section to check the steel section; the steel section was not totally affected. Some deformation was found in the longitudinal section due to the side loading for the specimen

As a result, the spacing between stirrups was increased to be 300 mm instead of 250 mm. **Figure 5.10** shows the shear force-drift hysteresis response of specimen.

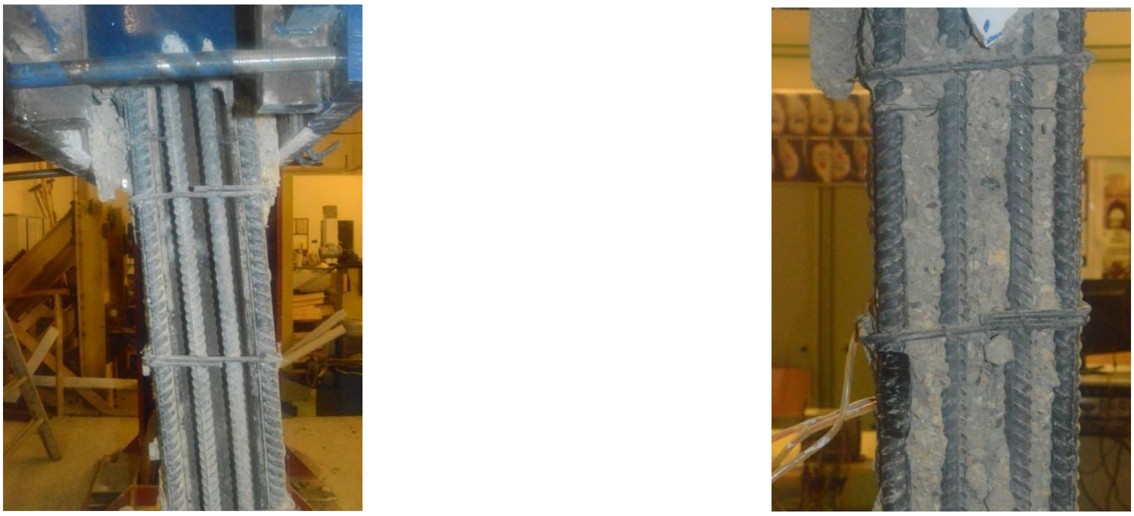

Figure 5.8: Entire section of CSS15-EP-25

Figure 5.9: Damage pattern of specimen CSS15-E-25

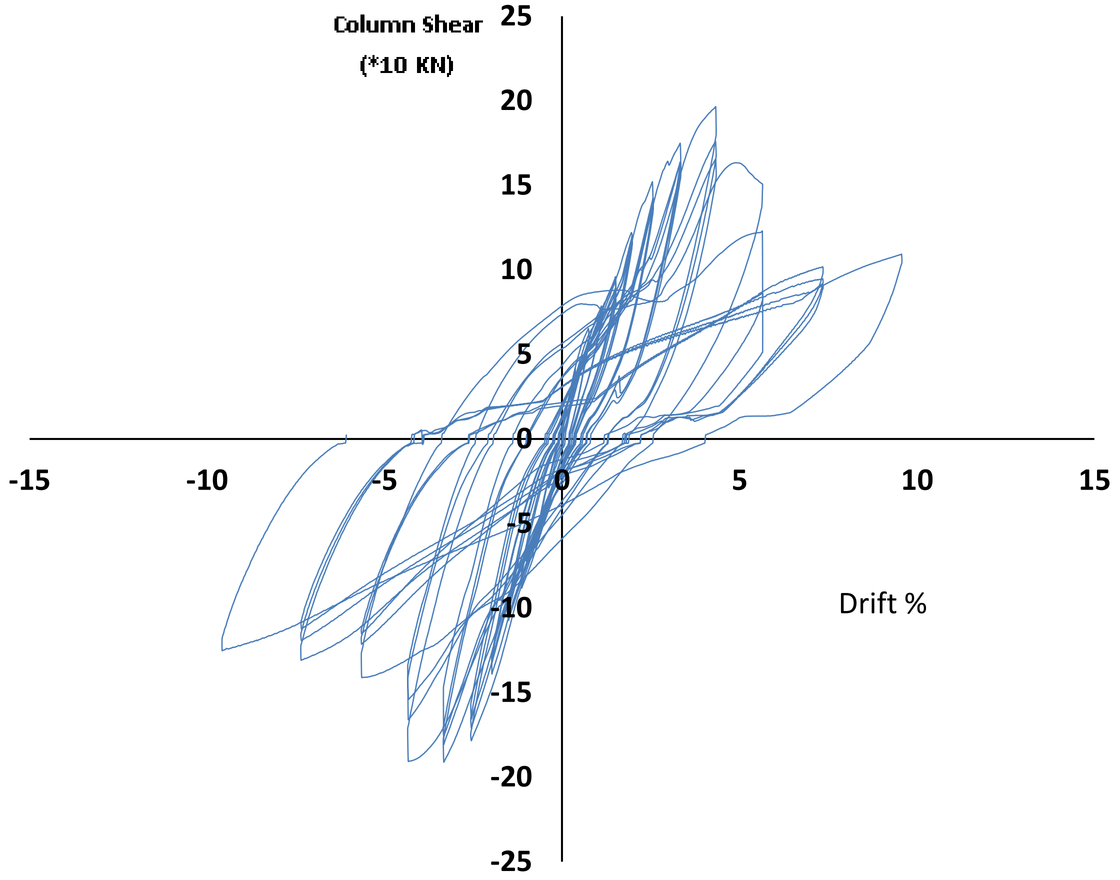

Figure 5.10: Shear force-drift hysteresis response of specimen CSS15-E-25

2. Modern building

2.1.CSF -10-16-N

CSF-10-16-N was subjected to a constant compressive axial load of 262 KN (0.1f'c Ag, where f'c = cylinder compressive concrete strength, and Ag = gross cross sectional area) and cyclic increments of lateral displacements as described in **Figure 4.13**. The theoretical nominal yield displacement was calculated to be equal to 28.1mm. It was noticed that there was inclination of the horizontal actuator load cell with an angel ө=0.0156. This was taken into consideration in the force drift post processing.

During the first two groups of displacement protocol (0.25 Δy and 0.5Δy) there was no cracking. Starting the following displacement cycles of 0.75 of the nominal yield displacement, horizontal hairline cracks (width of less than 1mm.) developed near the bottom of the column.

At these displacement levels, no new cracks were observed around the mid height area of the column. The number of inclined cracks and the crack width on the faces parallel to the lateral loading direction increased as the number and magnitude of the displacement cycles increased. Small horizontal cracks on the faces perpendicular to the lateral loading direction (i.e., on the east and west faces), started to span the width of the column. These relatively straight continuous horizontal cracks opened and closed during each cycle. During displacement cycles at 1.3 of the nominal yield displacement, relatively large crack openings were observed suggesting slip of the longitudinal reinforcing bars from the base.

Figure 5.14 shows 1.5mm wide crack opened between the flexural tension side of the column base and the column at peak lateral displacement.

During displacement cycles at the nominal yield displacement (Δ y = 47.5 mm.), crack opening was wider was wider with no new cracks .the vertical load cell tilted with ɵ=0.058 at the peak of displacement, which was accounted for during post processing The width of the existing horizontal cracks in faces perpendicular to the loading direction increased.

At the beginning of cycle at the displacement level of 136mm (4.87 Δ y), when the specimen was loaded the first time (push or eastward direction, **Figure 5.19**, the cover concrete was luxated at the bottom corner.

In the flexural compression zones, at the bottom of the column, flaking and spalling of concrete were observed.

As the number of cycles increased, the concrete cover crashed and the steel bars appeared. The reinforcing steel bars started to buckle between stirrups spacing near the base at tension and compression sides as shows in **Figures 5.22**.

Figure 5.11: Specimen CSF-10-16-N at initial displacement (Hair cracking)

Figure 5.12: CSF-10-16-NSlipping from base of column at 1.3∆y

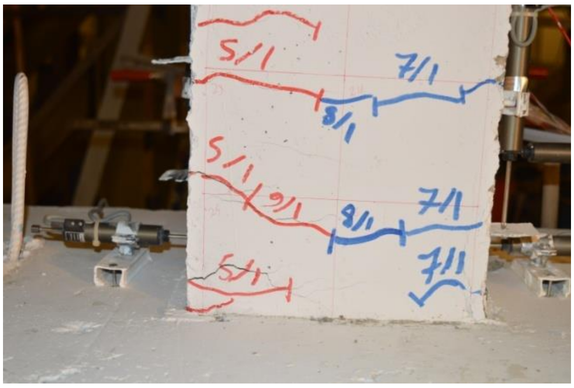

Figure 5.13: Specimen CSF-10-16-N at the compression direction of 2.2∆y

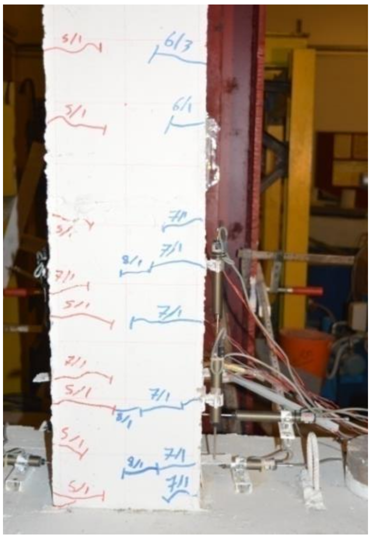

Figure 5.14: Specimen CSF-10-16-N at the tension direction of 2.2Δy

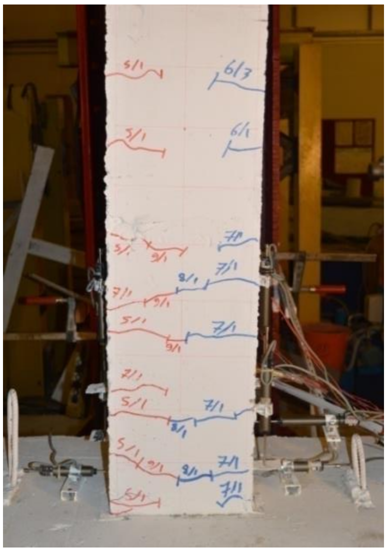

Figure 5.15: Perpendicular side of Specimen CSF-10-16-N at 2.2Δy

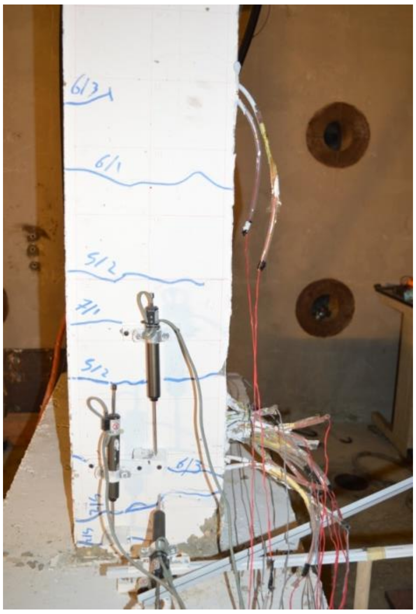

Figure 5.16: CSF-10-16-NCrushing concrete cover at 2.85∆y

Figure 5.17: CSF-10-16-NCrushing concrete cover of 2.85∆y

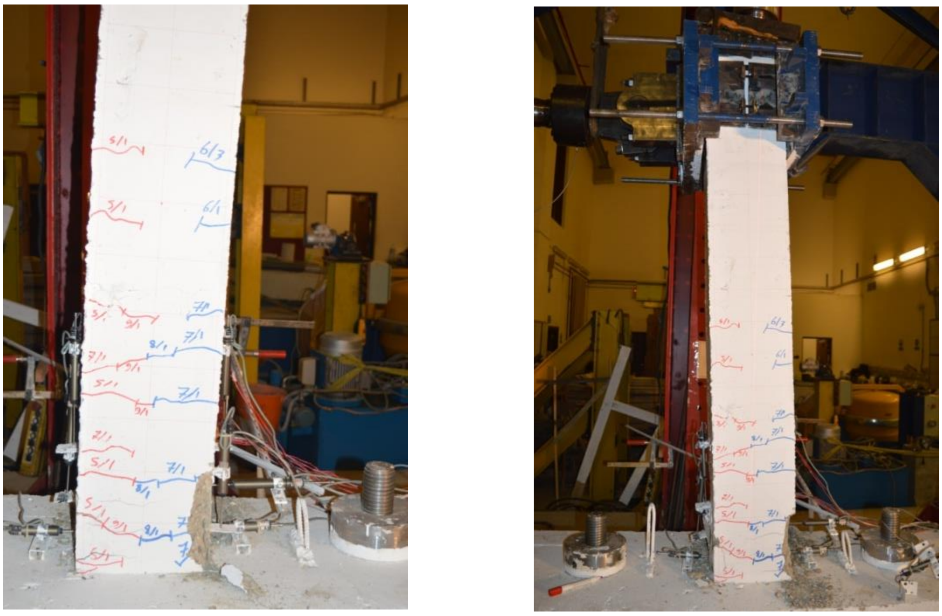

Figure 5.18: CSF-10-16-NCompression and tension of loading of $3.72\Delta y$

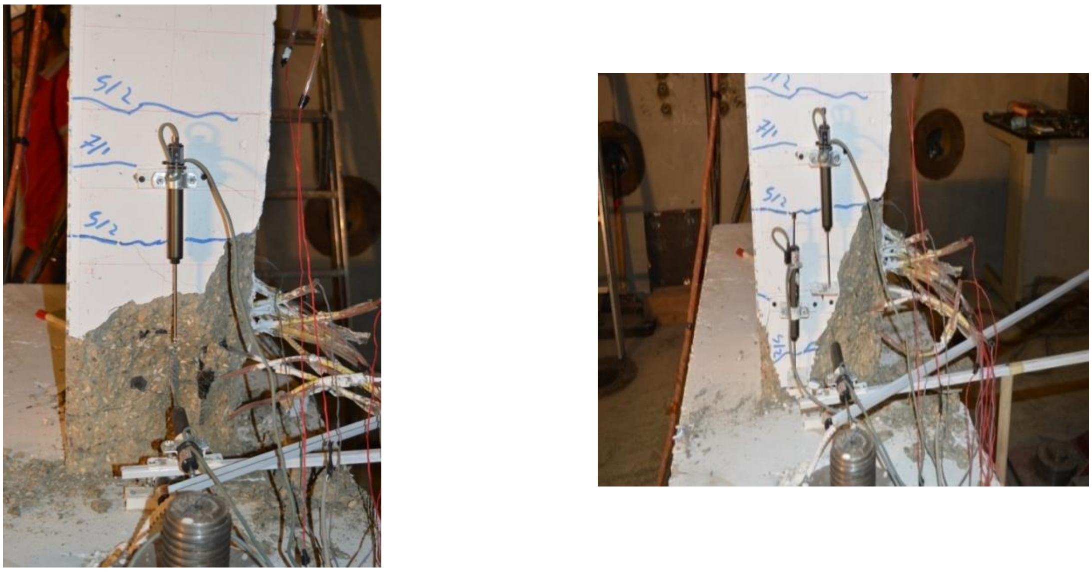

Figure 5.19: CSF-10-16-NCompression side $3.72\Delta y$

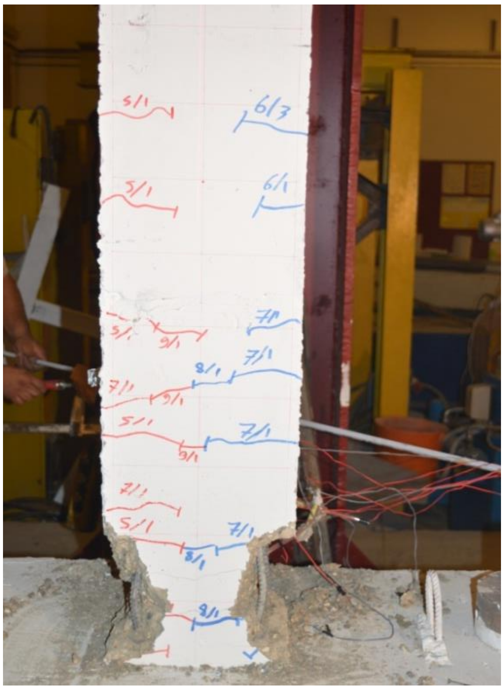

Figure 5.20: Perpendicular side after failure

Figure 5.21: Compression side steel bars buckling

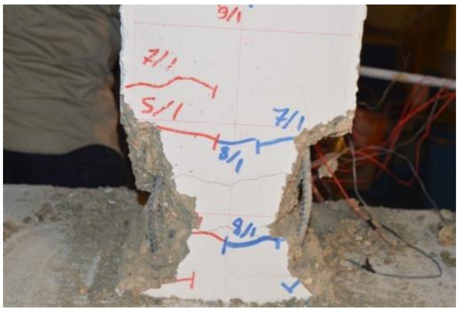

Figure 5.22: Compression and tension sides’ steel bars buckling

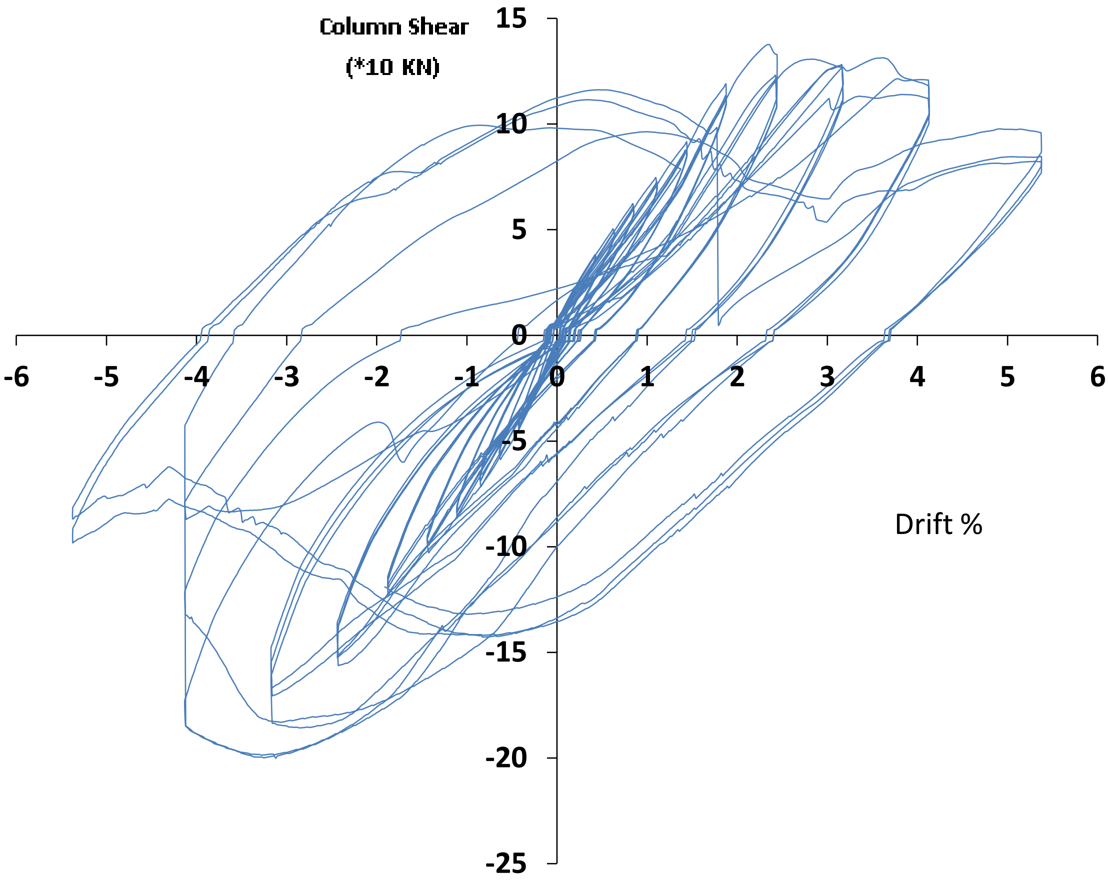

Figure 5.23: Shear force-drift hysteresis response of specimen CSF 10-16-N

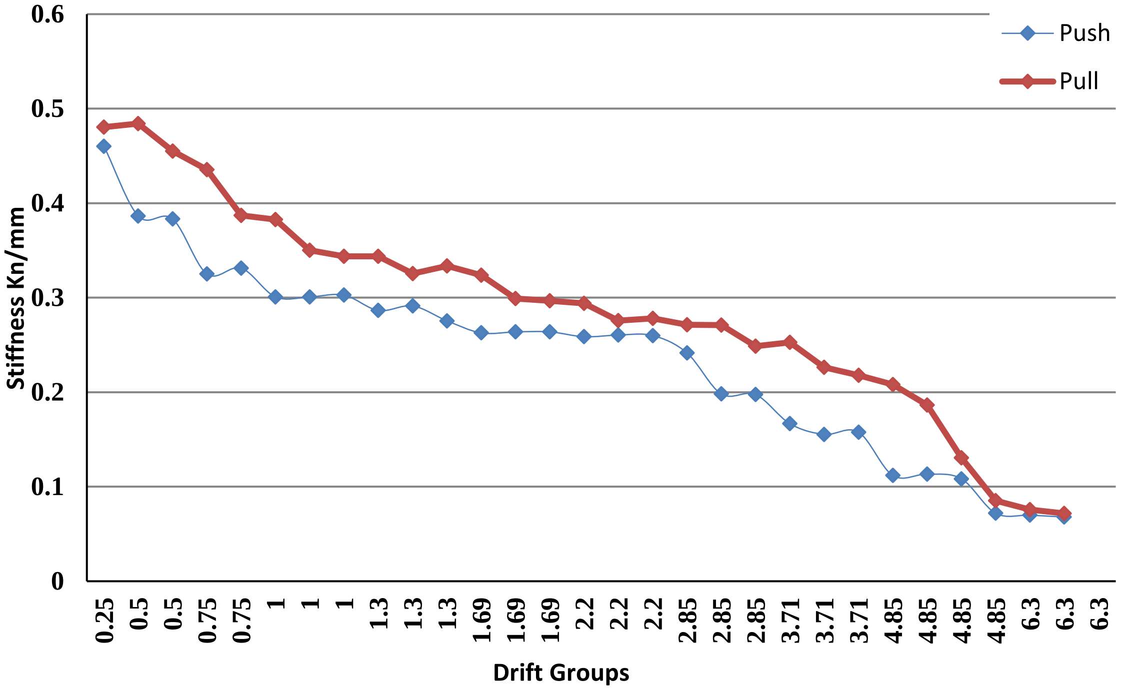

Figure 5.24: Peak to peak stiffness of specimen CSF 10-16-N

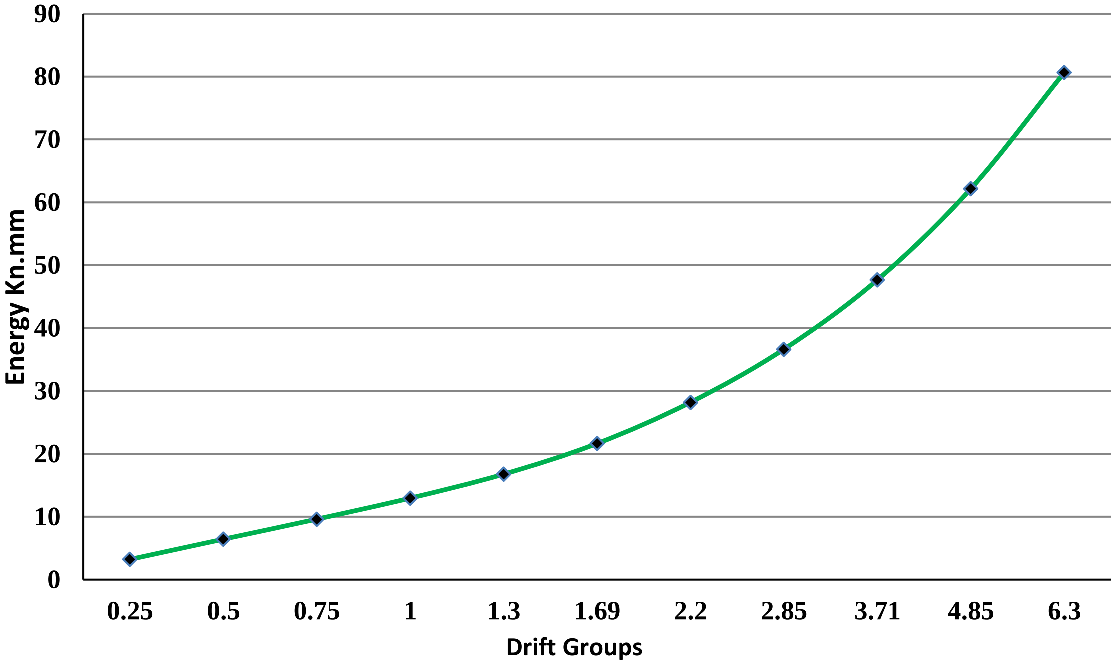

Figure 5.25: Peak to peak Energy of specimen CSF 10-16-N

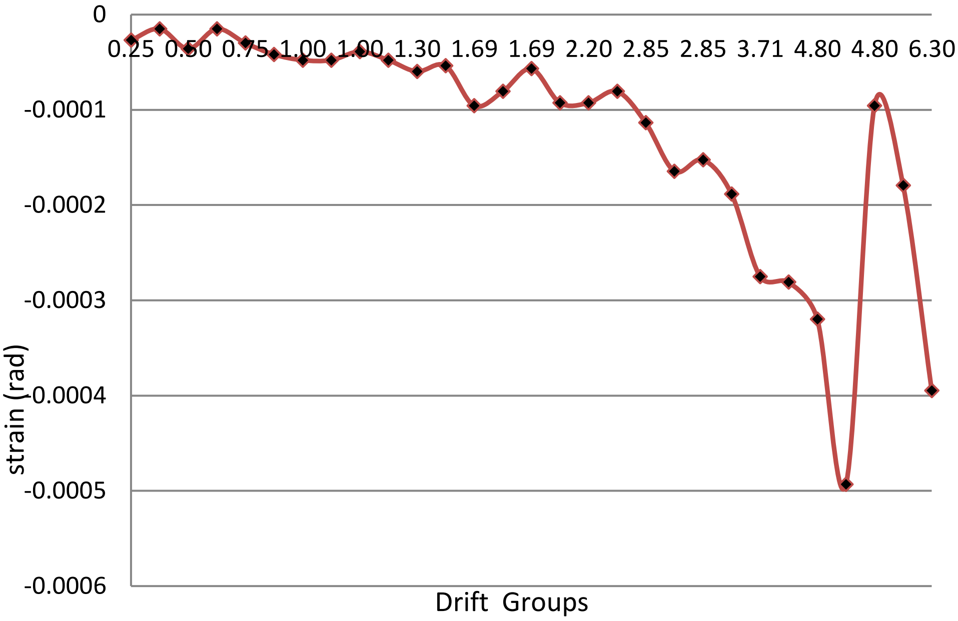

Figure 5.26: Compression shear strain (rad) Vs Drift groups

(Vertical LVDTs 5-12) (Tension side)

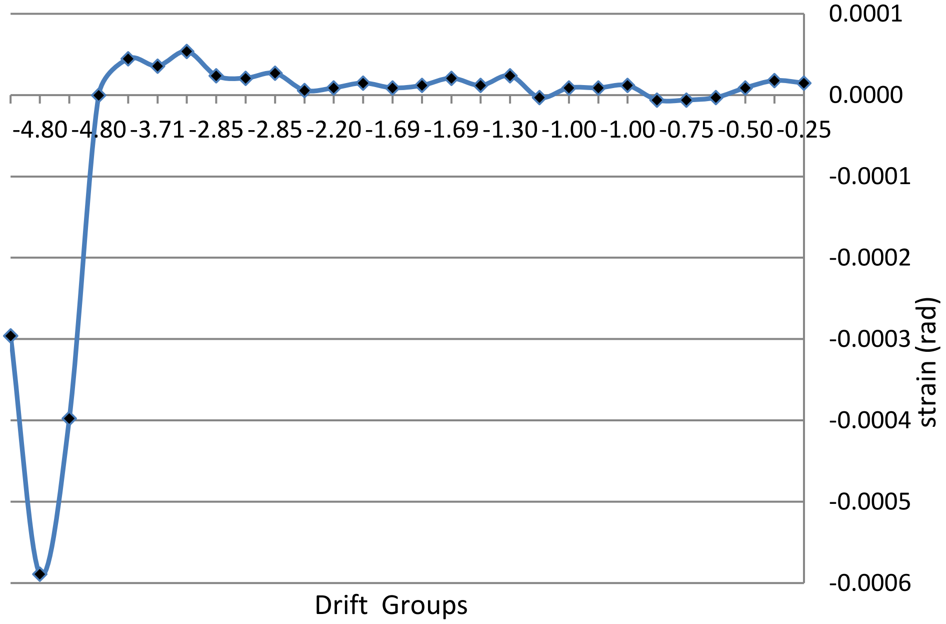

Figure 5.27: Tension shear strain (rad) Vs Drift groups (Vertical LVDTs 5-12) (Tension side)

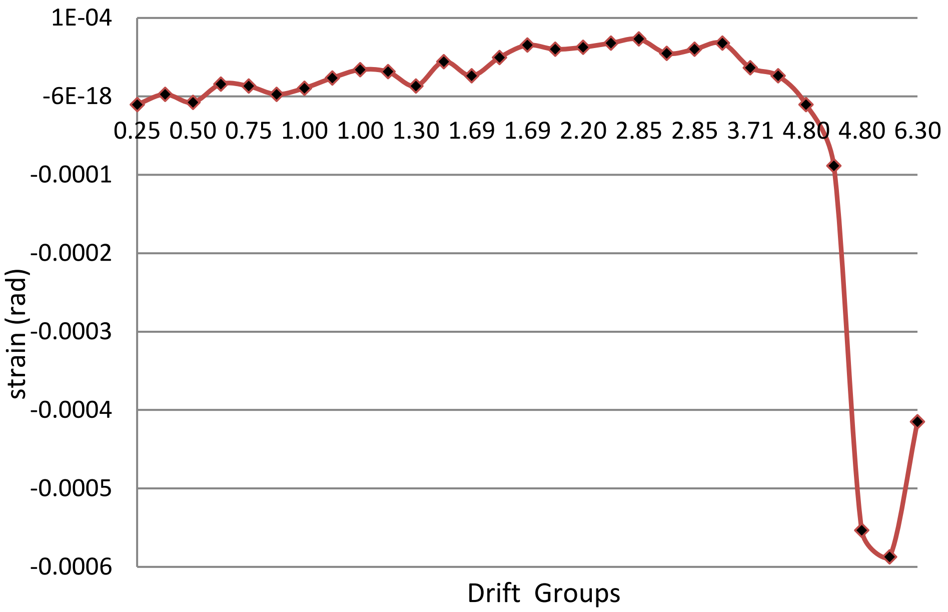

Figure 5.28: Compression shear strain (rad) Vs Drift groups

(Vertical LVDTs 5-12) (Compression side)

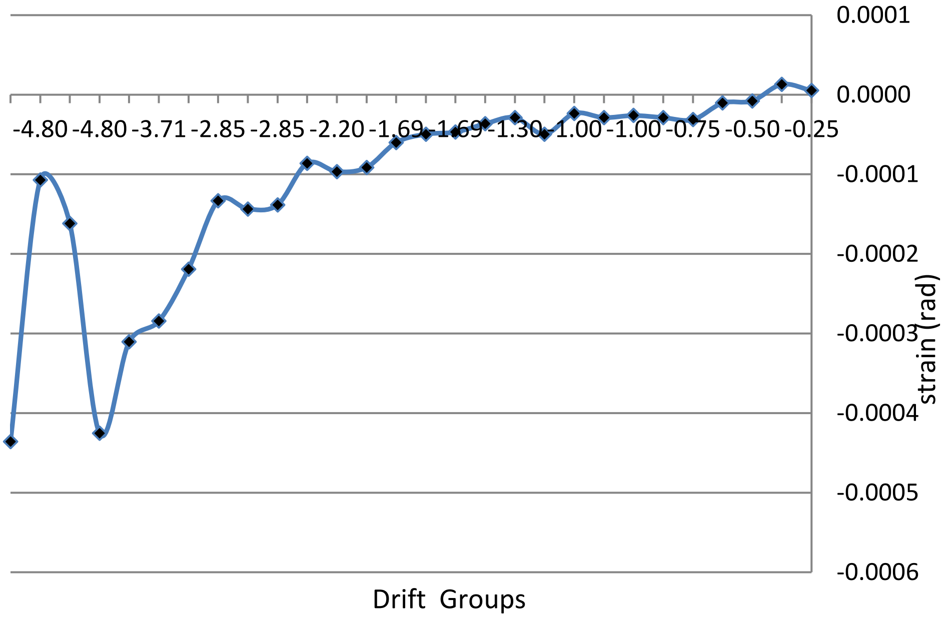

Figure 5.29: Tension shear strain (rad) Vs Drift groups

(Vertical LVDTs 5-12) (Compression side)

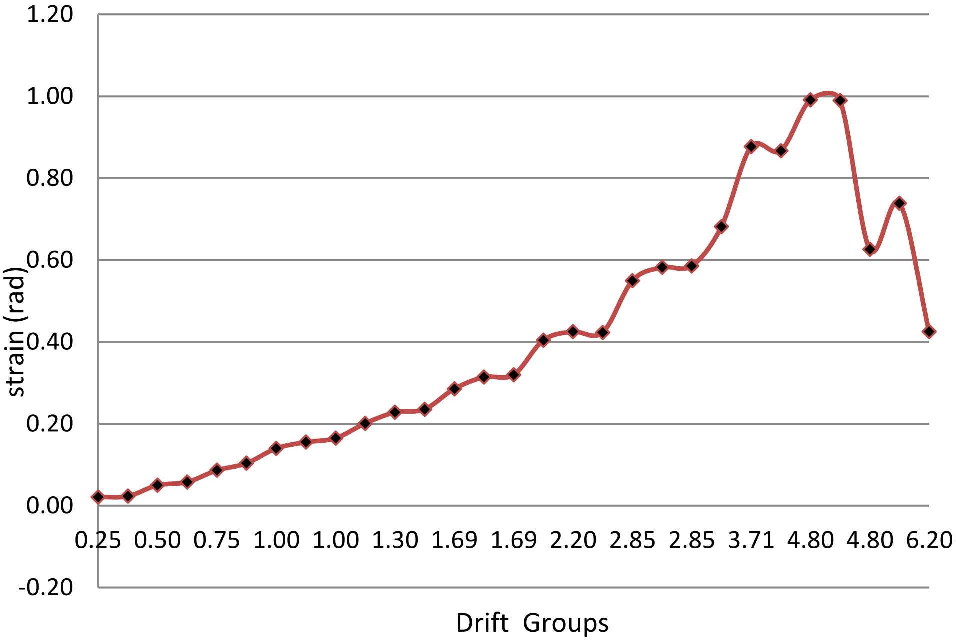

Figure 5.30: Compression flange steel strain Vs Drift groups (125mm)

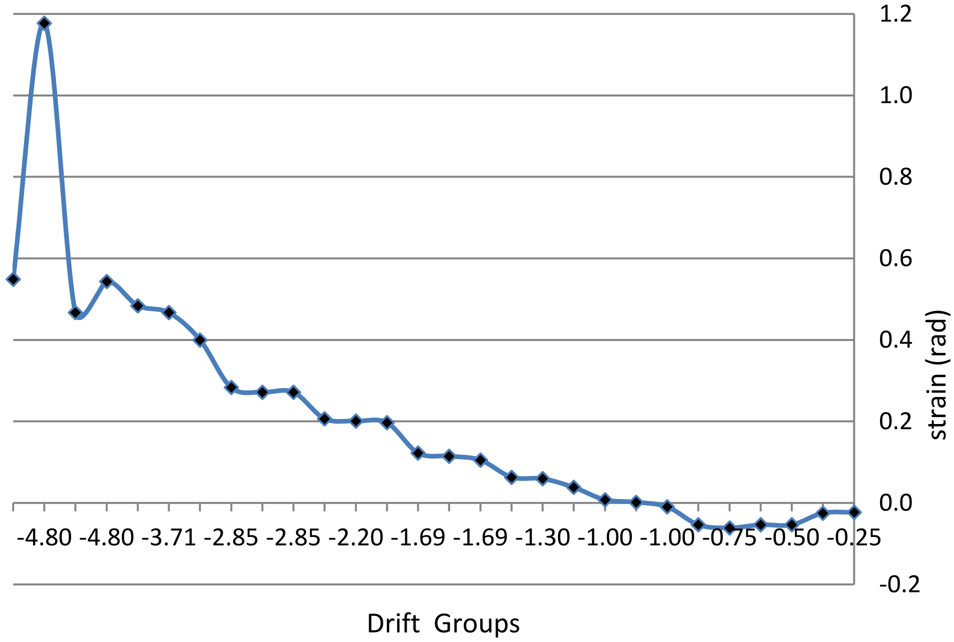

Figure 5.31: Tension flange steel strain Vs Drift groups (12.5mm)

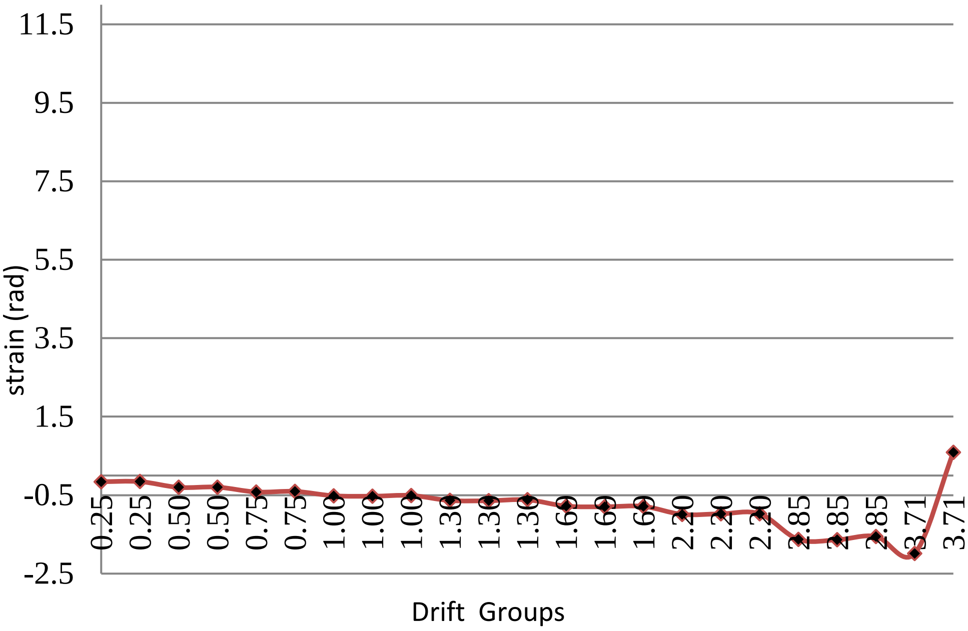

Figure 5.32: Compression steel bar strain Vs Drift groups (125mm) (Compression side)

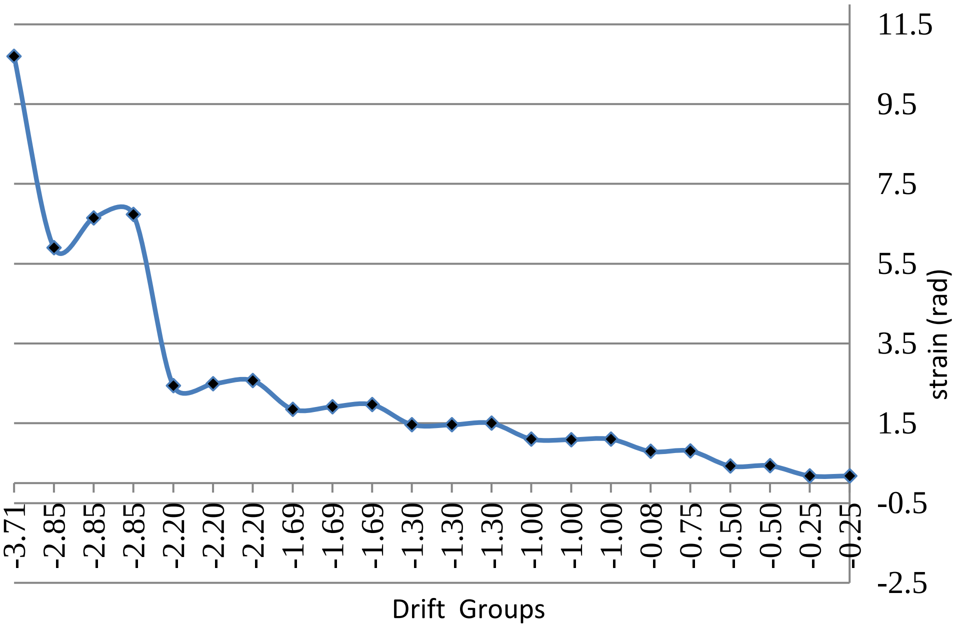

Figure 5.33: Tension steel bar strain Vs Drift groups (125mm) (Compression side)

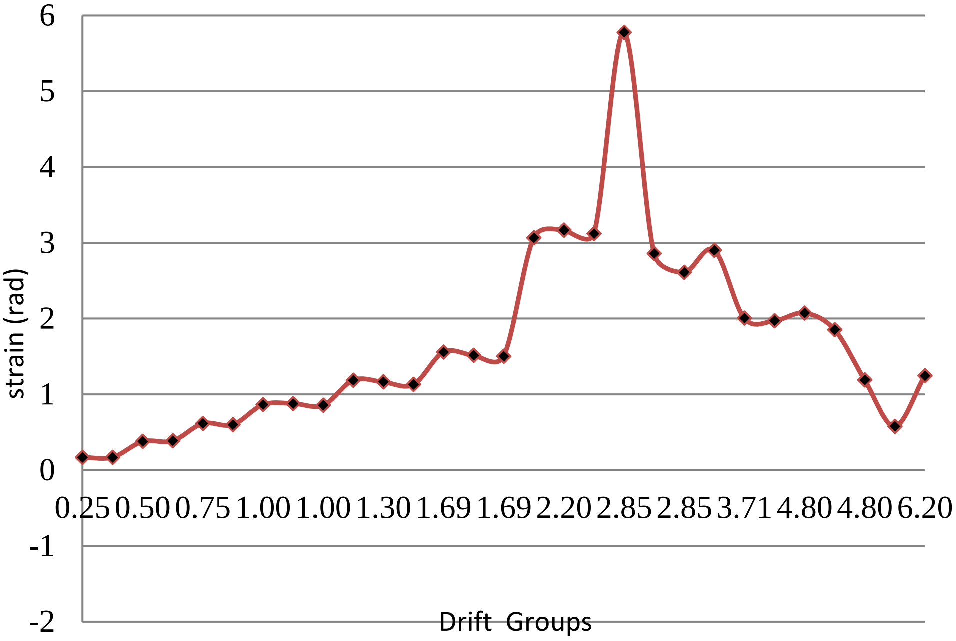

Figure 5.34: **Compression steel bar strain Vs Drift groups (125mm) (Tension side)**

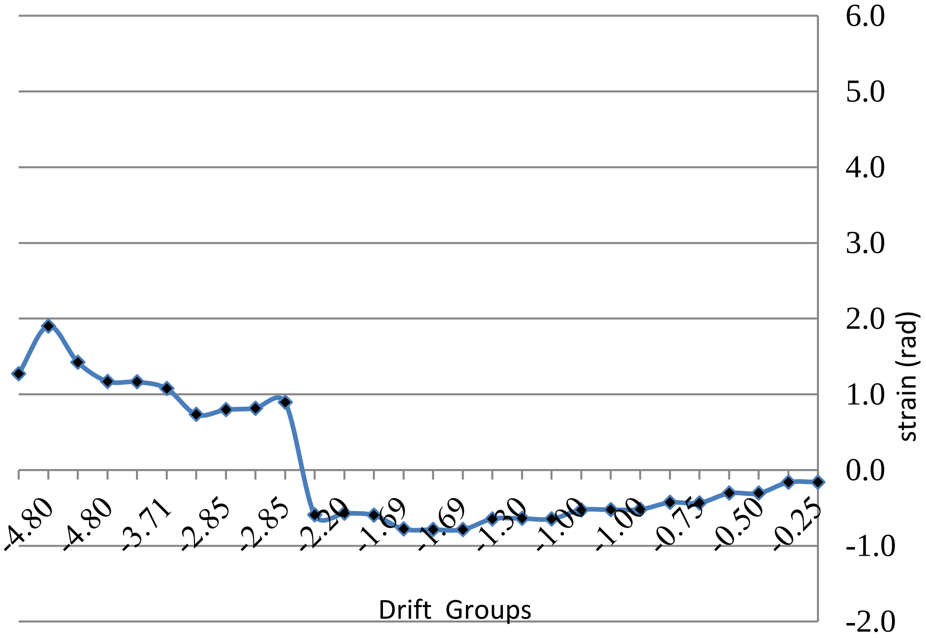

Figure 5.35: **Tension steel bar strain Vs Drift groups (125mm) (Tension side)**

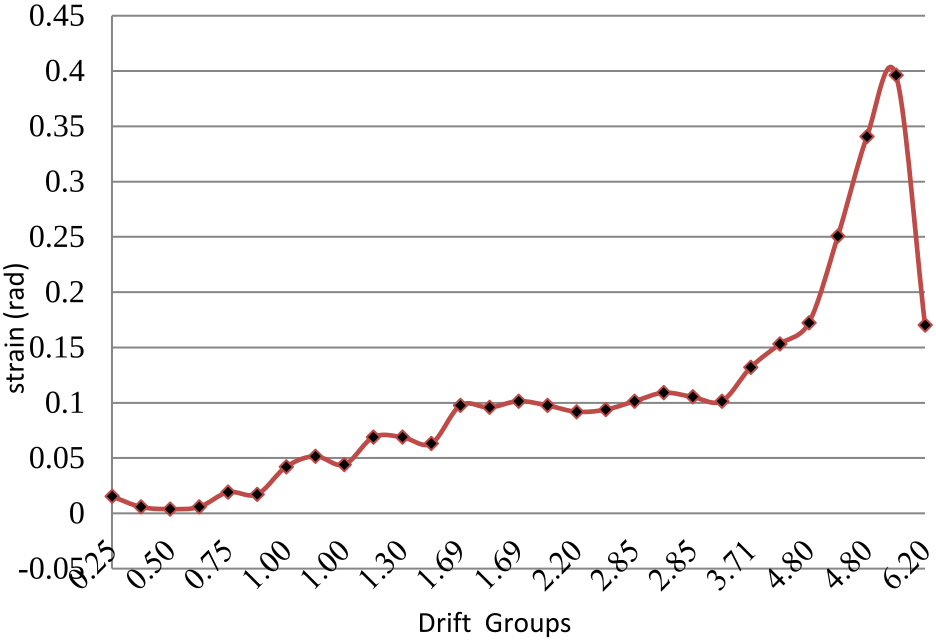

Figure 5.36: Compression steel hoop strain Vs Drift groups (25mm)

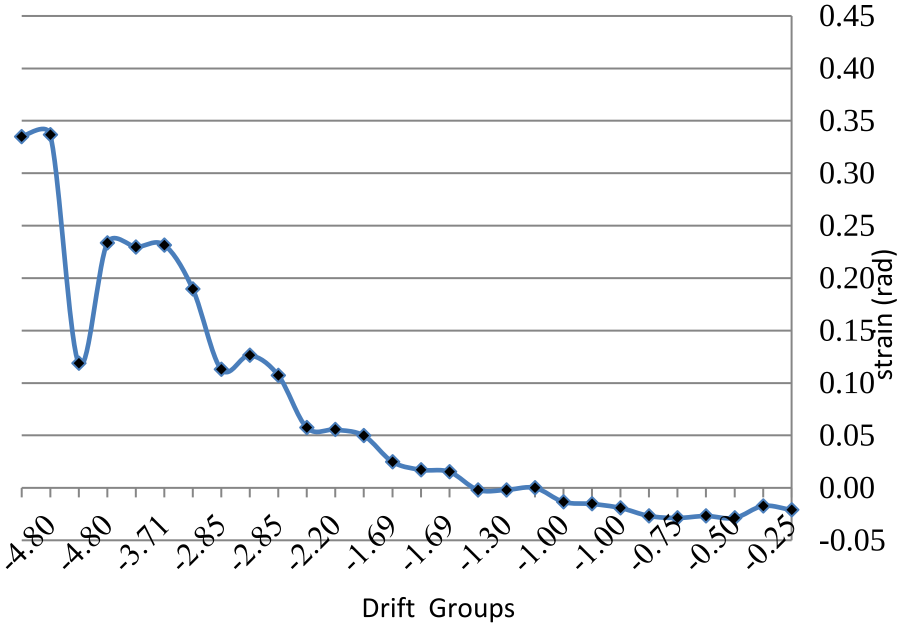

Figure 5.37: Tension steel hoop strain Vs Drift groups (25mm)

2.2.CSF -10-7.5-N

CSF-10-75-N was subjected to a constant compressive axial load of 340 KN (0.1f’c Ag, where f’c = cylinder compressive concrete strength, and Ag = gross cross sectional area) and cyclic increments of lateral displacements as described in **Figure 4.13**. The theoretical nominal yield displacement was calculated to be equal to 28.6 mm Same inclination of the horizontal actuator load cell was noticed with an angel ɵ=0.0156 due to similar specimen height and test setup conditions. This was taken into consideration in the force and drift post processing.

During the first groups of displacement protocol which (0.25 Δy) there was no cracking. Starting the following displacement cycles of 0.5of the nominal yield displacement, horizontal hairline cracks (width of less than 1mm.) developed near the bottom of the column.

At these displacement levels, no new cracks were observed around the mid height area of the column. The number of inclined cracks and the crack width on the faces parallel to the lateral loading direction increased as the number and magnitude of the displacement cycles increased. Small horizontal and inclined cracks on the faces perpendicular to the lateral loading direction (i.e., on the east and west faces), started to span the width of the column. These relatively straight continuous horizontal cracks opened and closed during each cycle. During displacement cycles equal to theoretical Δy displacement cracks opening increased, relatively large crack openings were observed suggesting slip of the longitudinal reinforcing bars from the base at Δ =1.3Δy.

Figure5.41shows 2.5mm wide crack opened between the flexural tension side of the column base and the column at peak lateral displacement. During displacement cycles to the nominal yield displacement (Δ = 5.6 mm.), crack opening was wider was observed without any new cracks.

The width of the existing horizontal cracks in faces perpendicular to the loading direction increased from two sides.

At the beginning of cycling at the displacement level of 62.9mm (2.2 Δ y), when the specimen was loaded the first time (push or eastward direction, **Figure 5.45**, spilling of the cover concrete was observed in the bottom northeast corner and the horizontal load started to decrease after reaching the peak previous. In the flexural compression zones, at the bottom of the column, flaking and spalling of concrete were observed.

As the number of cycles increased, after the concrete cover crashed and the steel bars appeared, there was not any buckling of steel bars but the lower cracks were deep in the column around the cross section as shown in **Figure 5.47**.

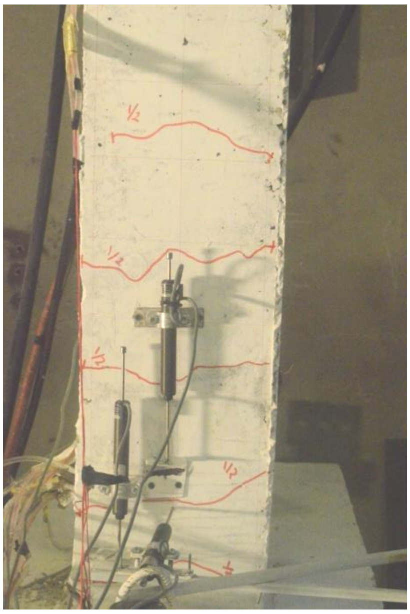

Figure 5.38: Specimen CSF-10-75-N at initial cracking (0.5 Δy)

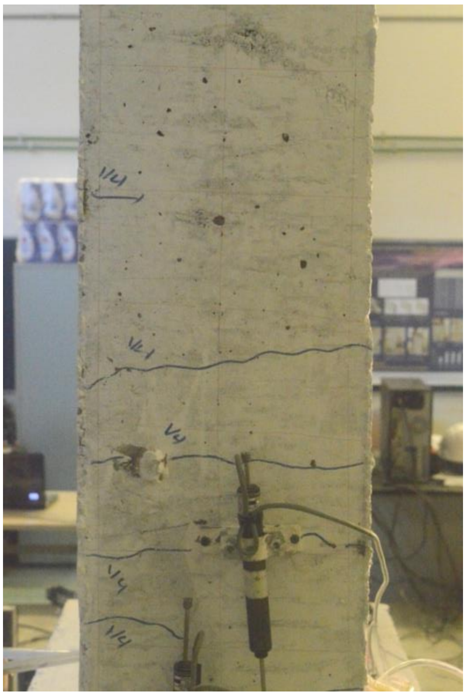

Figure 5.39: CSF-10-75Tension side at Δy

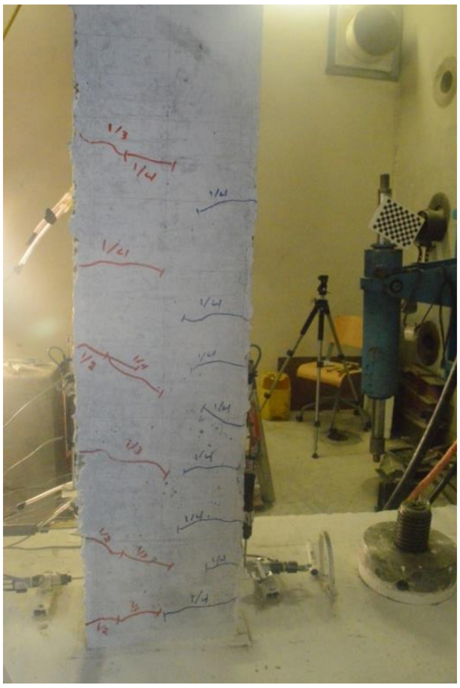

Figure 5.40: CSF-10-75 Perpendicular side at Δy

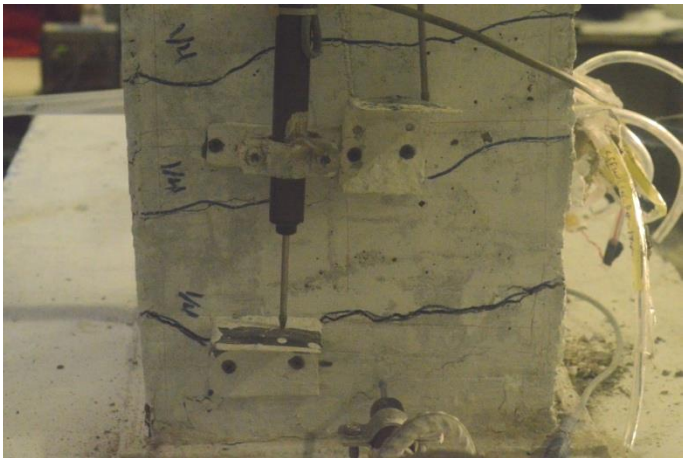

Figure 5.41: CSF-10-75 opening cracks near to base 1.96 ∆y

Figure 5.42: CSF-10-75 Boundary crack before failure

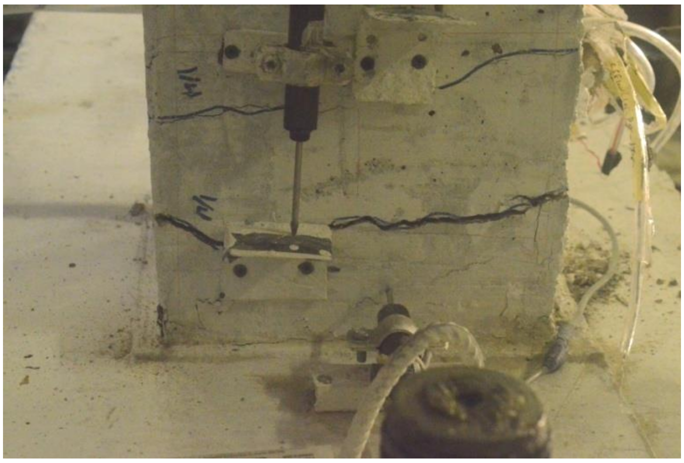

Figure 5.43: CSF-10-75 Crack opining width 2.5mm at first cycle of 2.197 Δy

Figure 5.44: CSF-10-75 Crushing concrete cover mid cycle of (2.197Δy)

Figure 5.45: CSF-10-75 Compression side at (2.85Δy)

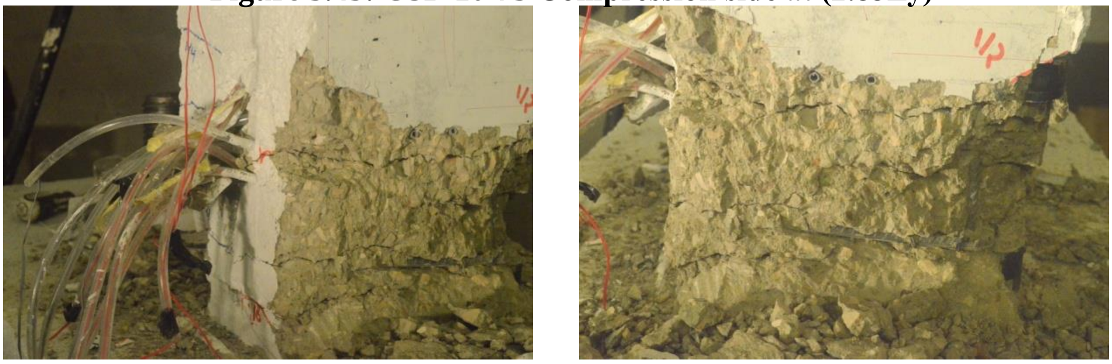

Figure 5.46: CSF-10-75 Deep flexure cracks

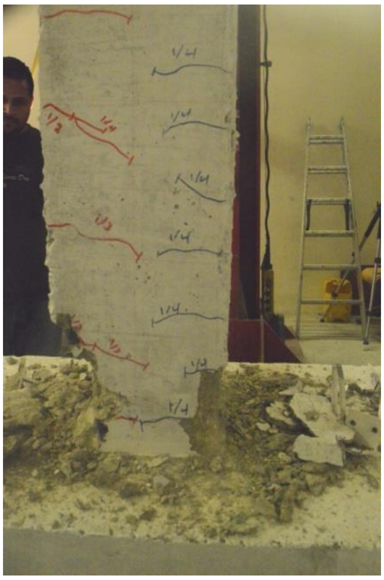

Figure 5.47: CSF-10-75Perpendicular side after failure

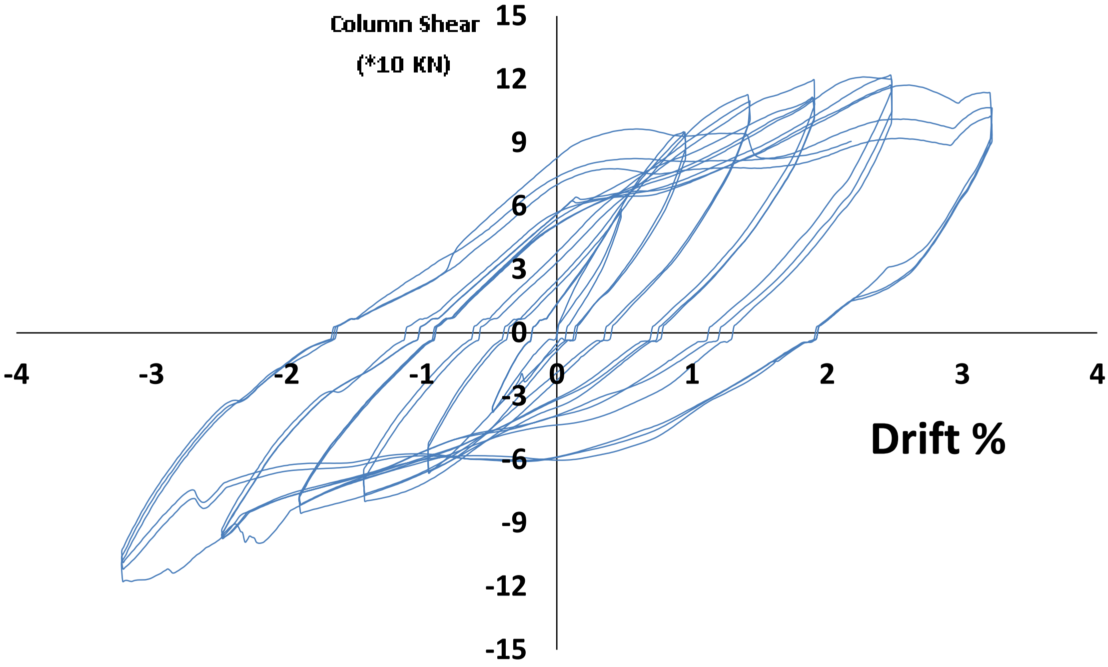

Figure 5.48: Shear force-drift hysteresis response of specimen CSF 10-7.5-N

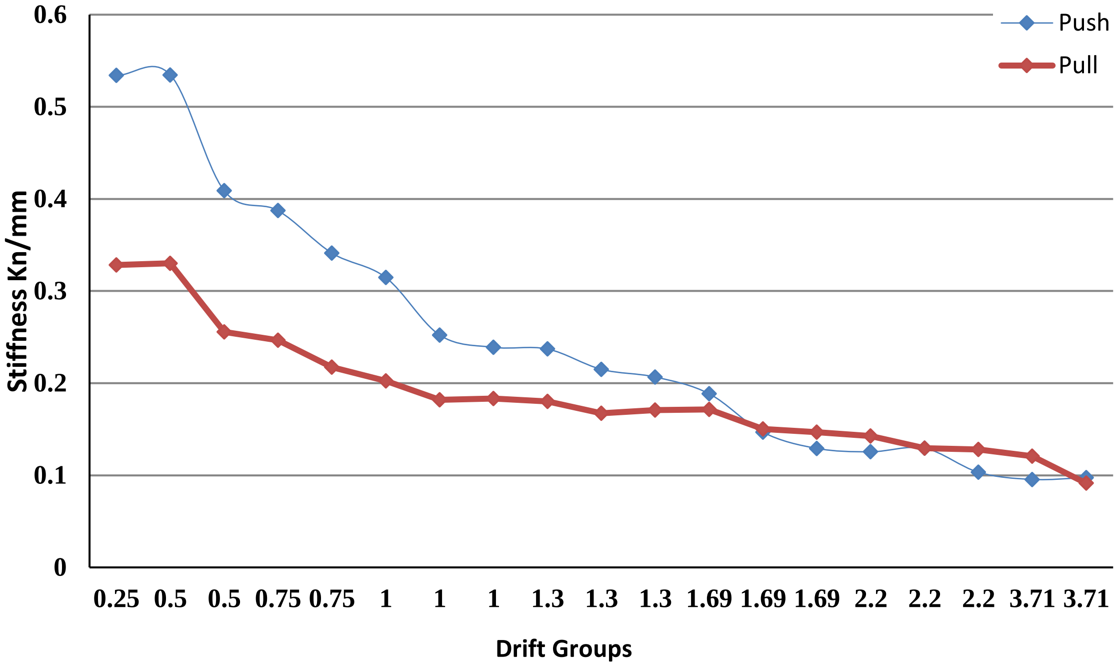

Figure 5.49: Peak to Peak stiffness of specimen CSF 10-7.5-E

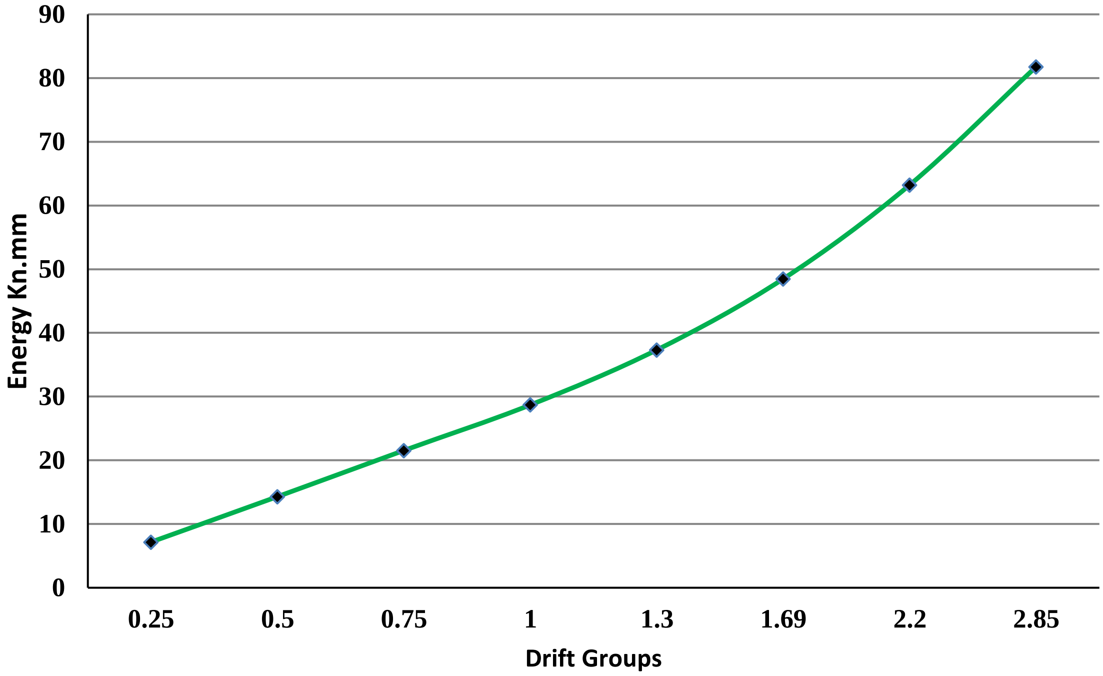

Figure 5.50: Peak to peak Energy of specimen CSF 10-7.5-N

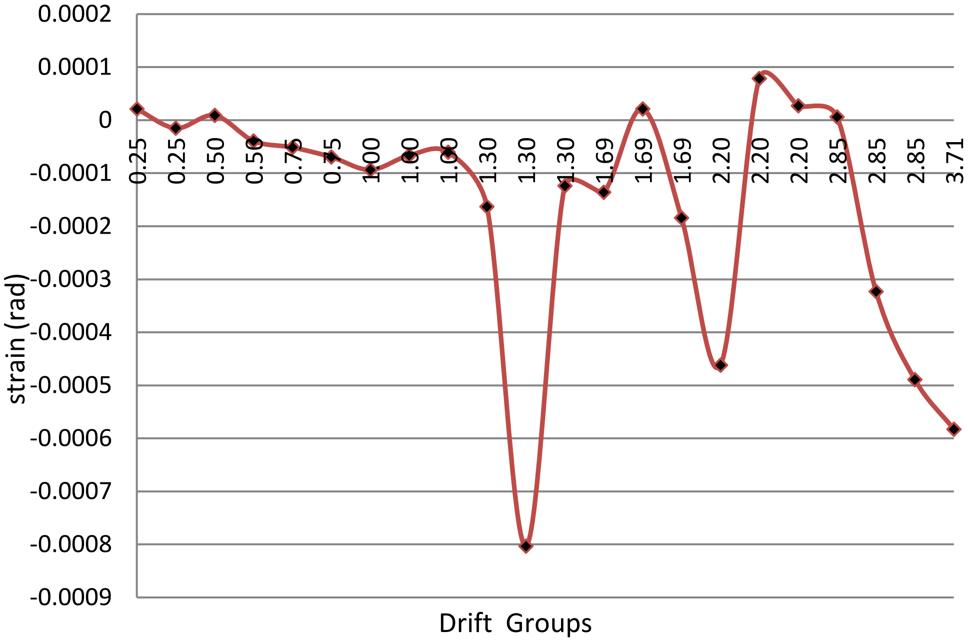

Figure 5.51: CSF-10-75Compression shear strain (rad) Vs Drift groups (Vertical LVDTs 5-12) (Tension side)

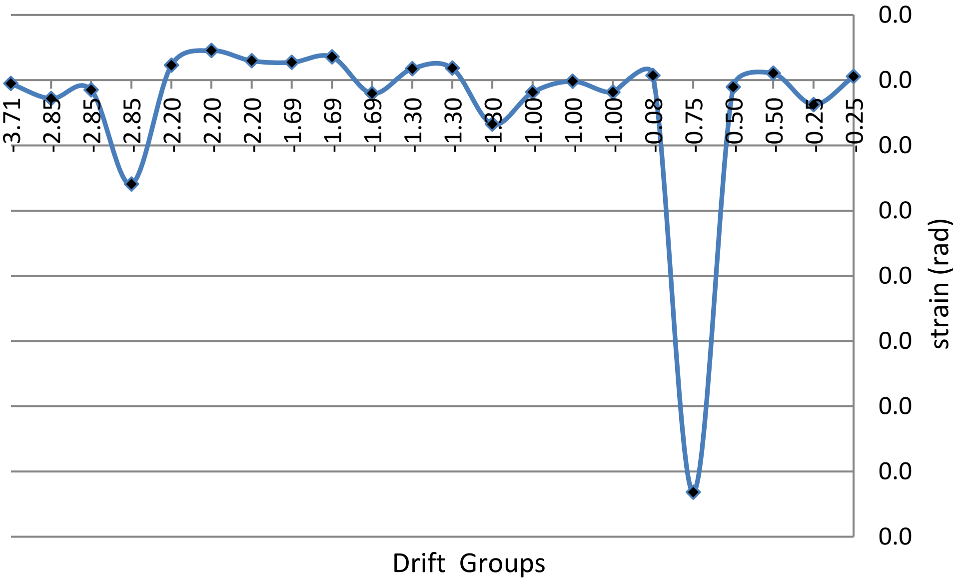

Figure 5.52: CSF-10-75 Tension shear strain (rad) Vs Drift groups (vertical LVDTs 5-12) (tension side)

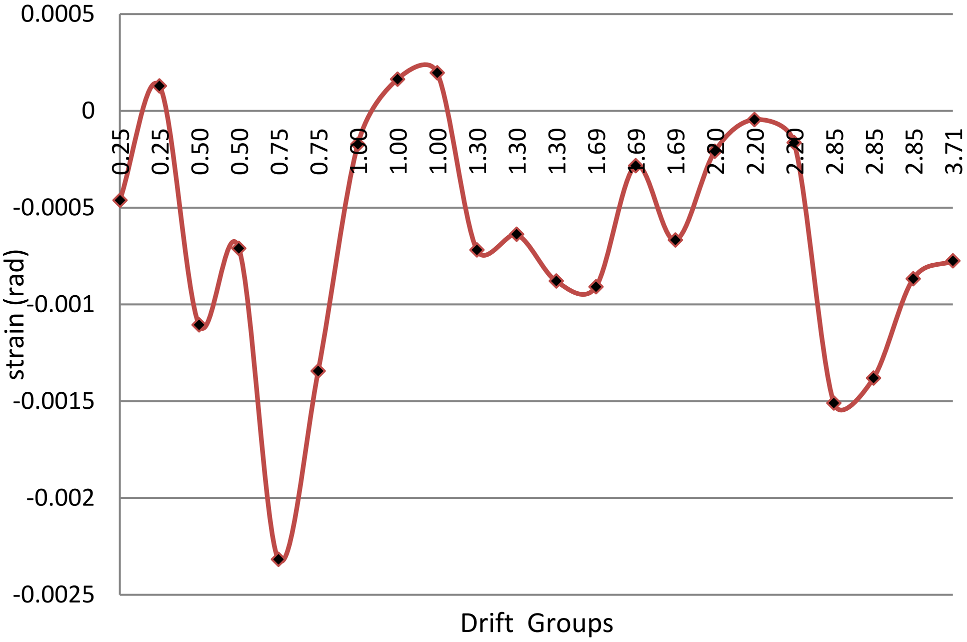

Figure 5.53: CSF-10-75 Compression shear strain (rad) Vs Drift groups (Vertical LVDTs 5-12) (Compression side)

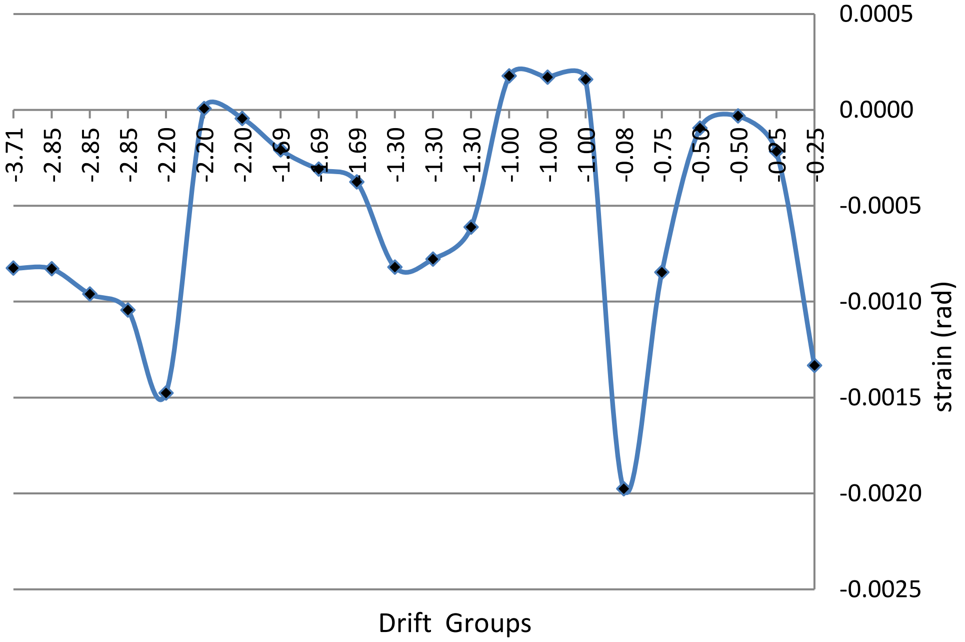

Figure 5.54: CSF-10-75Tension shear strain (rad) Vs Drift groups (vertical LVDTs 5-12) (compression side)

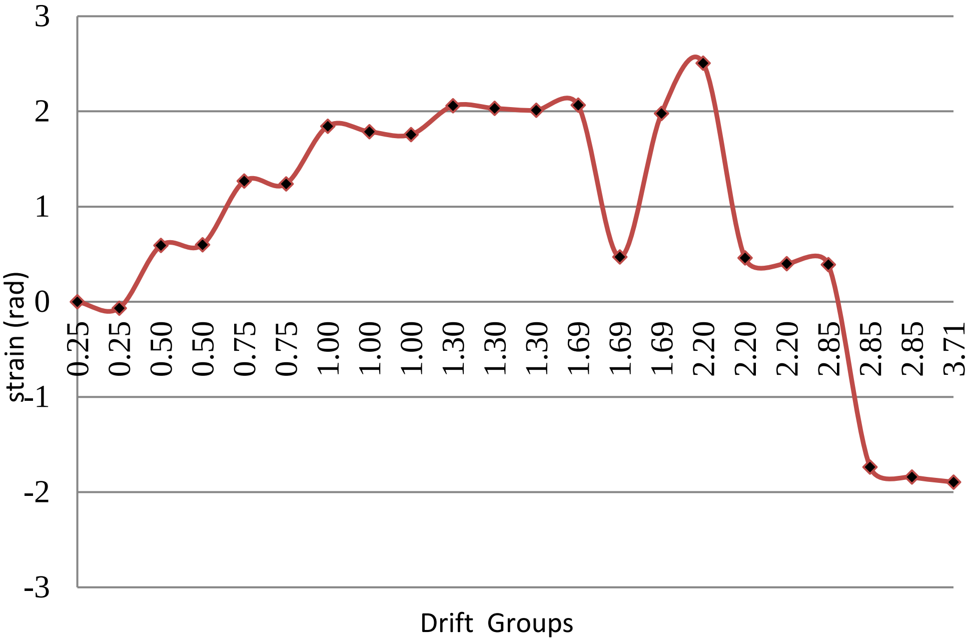

Figure 5.55: CSF-10-75 Compression flange steel strain Vs Drift groups (125mm)

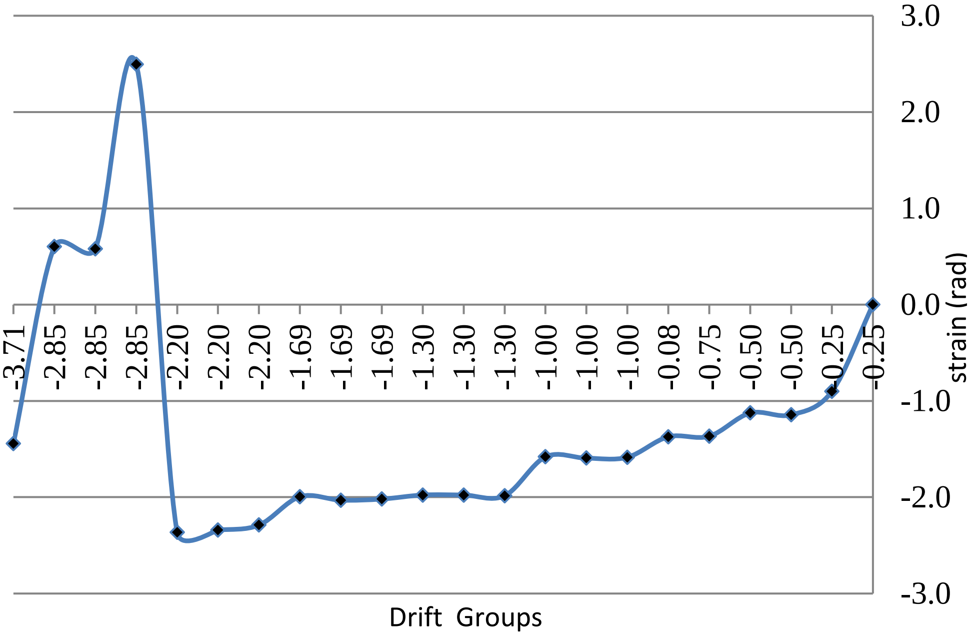

Figure 5.56: CSF-10-75 Tension flange steel strain Vs Drift groups (125mm)

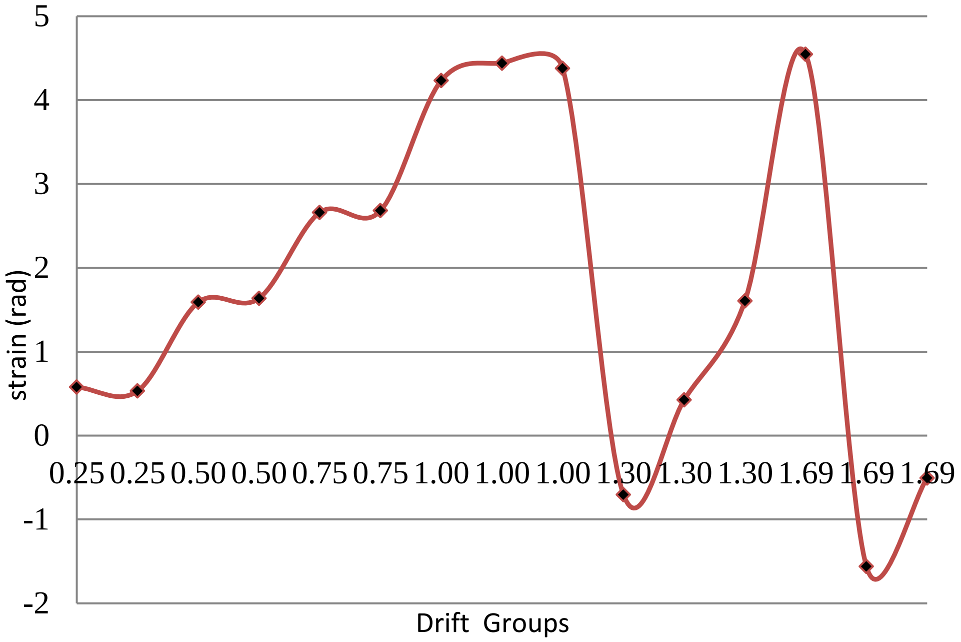

Figure 5.57: CSF-10-75 Compression steel bar strain Vs Drift groups (125mm) (Compression side)

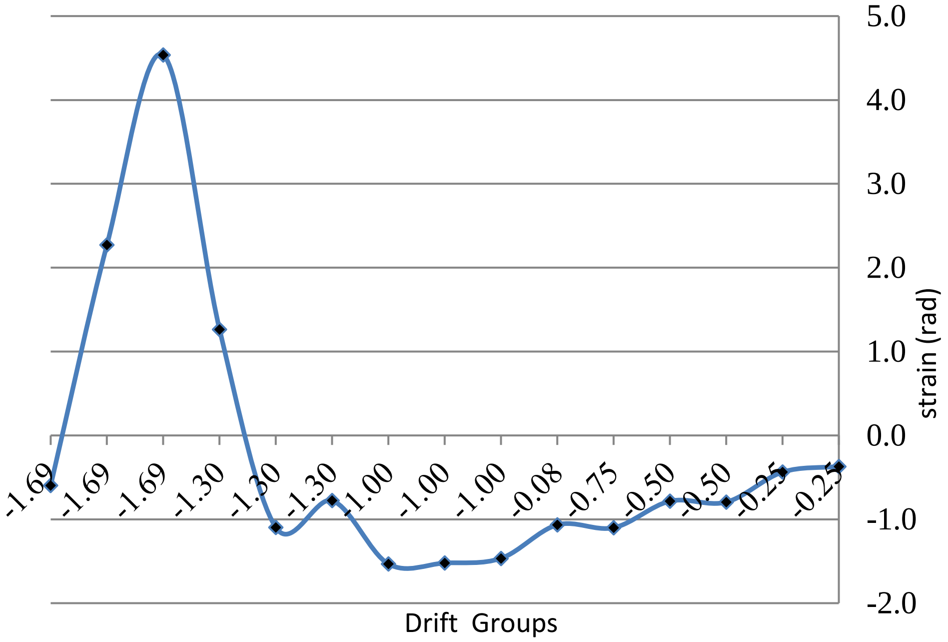

Figure 5.58: CSF-10-75 Tension steel bar strain Vs Drift groups (125mm) (Compression side)

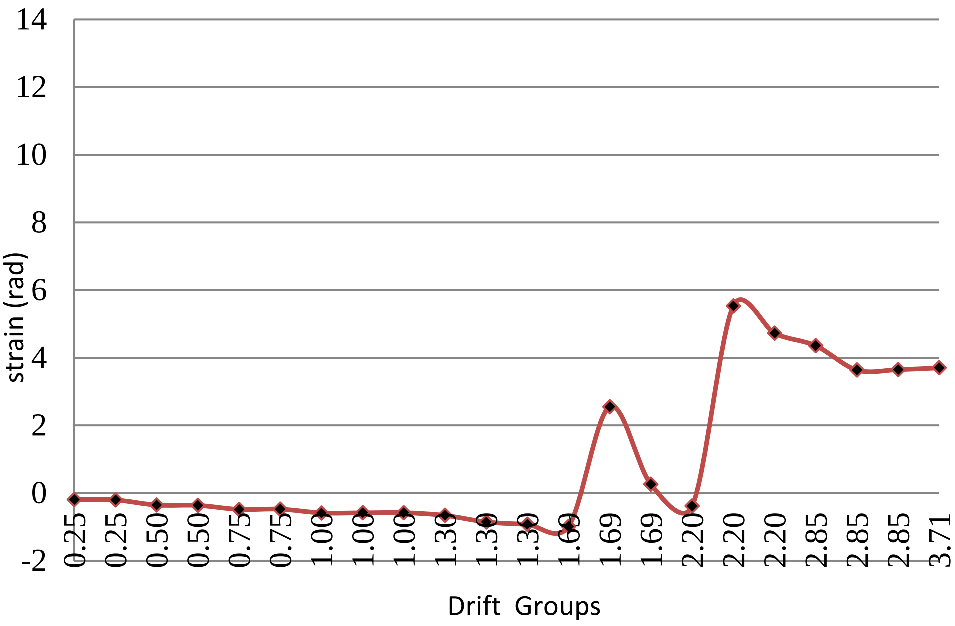

Figure 5.59: CSF-10-75Compression steel bar strain Vs Drift groups (125mm) (Tension side)

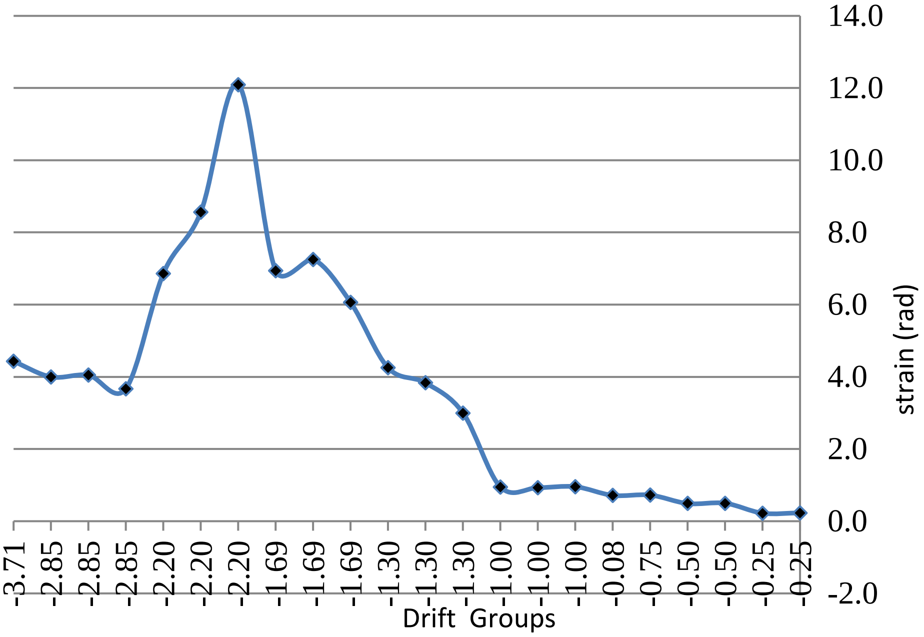

Figure 5.60: CSF-10-75 Tension steel bar strain Vs Drift groups (125mm) (Tension side)

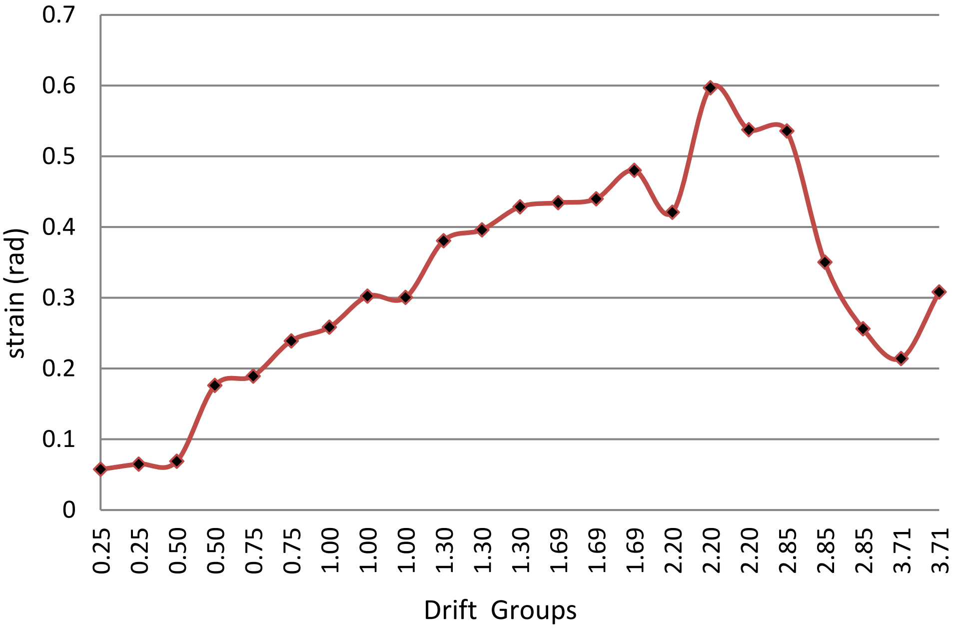

Figure 5.61: CSF-10-75Compression steel hoop strain Vs Drift groups (25 mm)

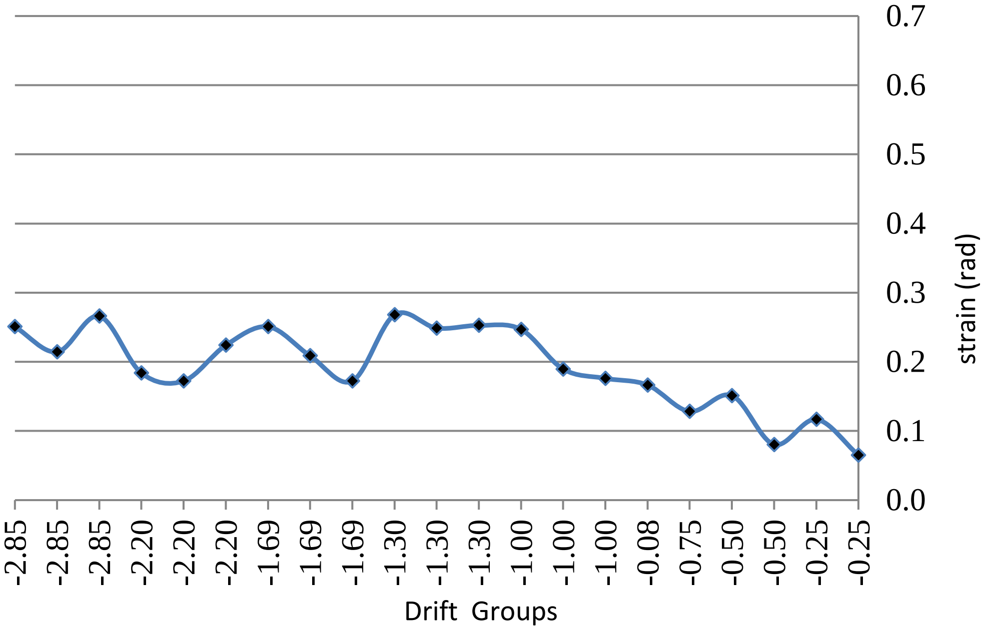

Figure 5.62: CSF-10-75Tension steel hoop strain Vs Drift groups (25mm)

2.3.CSF -0-7.5-N

CSF-0-7.5-N was subjected to no axial load and cyclic increments of lateral displacements as described in **Figure 4.13**. The theoretical nominal yield displacement was calculated to be equal to 29.1 mm. Some inclination of the horizontal actuator load cell was noticed with an angel ɵ=0.0156. This was taken into consideration in the force and drift post processing.

During the first groups of displacement protocol (0.25 and 0.5 Δy) there was no cracking. Starting the following displacement cycles of 0.75of the nominal yield displacement, horizontal hairline cracks (width of less than 1mm.) developed near the bottom of the column.

At these displacement levels, no new cracks were observed around the mid height area of the column. The number of inclined cracks and the crack width on the faces parallel to the lateral loading direction increased as the number and magnitude of the displacement cycles increased. Small horizontal and inclined cracks on the faces perpendicular to the lateral loading direction (i.e., on the east and west faces), started to span the width of the column. These relatively straight continuous horizontal cracks opened and closed during each cycle. During displacement cycles equal to theoretical Δy displacement cracks opening increased, relatively large crack openings were observed suggesting slip of the longitudinal reinforcing bars from the base at the end of
Δ =Δy.

Figure 5.67shows 3.5 mm wide crack opened between the flexural tension side of the column base and the column at peak lateral displacement. During displacement cycles to the nominal yield displacement (Δ = 5.6 mm.), crack opening was wider was observed without any new cracks. The width of the existing horizontal cracks in faces perpendicular to the loading direction increased from two sides.

At the beginning of cycling at the displacement level of 62.9mm (2.2 Δ y), when the specimen was loaded the first time (push or eastward direction, **Figure5.68**, spilling of the cover concrete was observed in the bottom northeast corner and the horizontal load started to decrease after reaching the peak previous. In the flexural compression zones, at the bottom of the column, flaking and spalling of concrete were observed.

As the number of cycles increased, after the concrete cover crashed and the steel bars appeared, there was not any buckling of steel bars but the lower cracks were deep in the column around the cross section as shown in **Figure 5.70.**

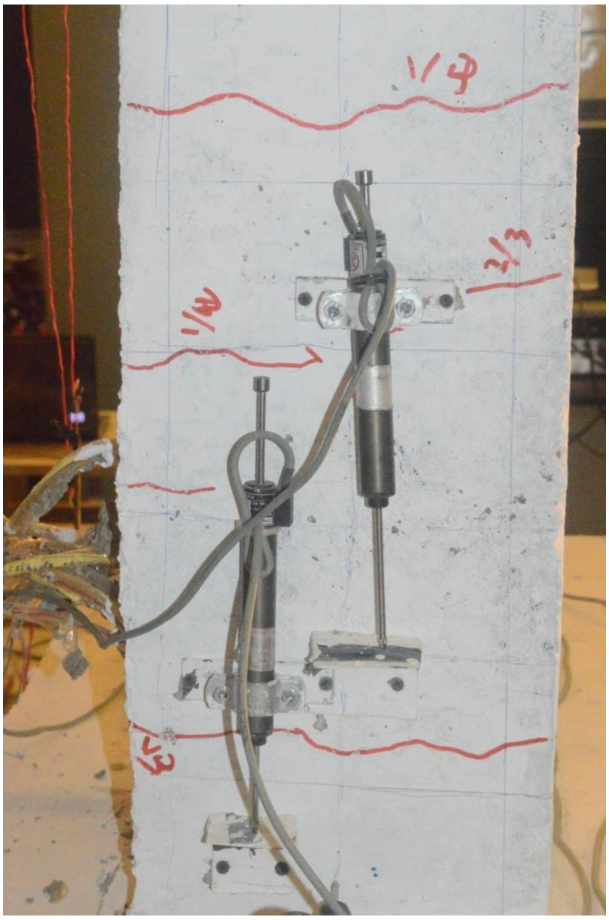

Figure 5.63: SpecimenCSF-0-7.5-N at initial cracking (0.75 ∆y)

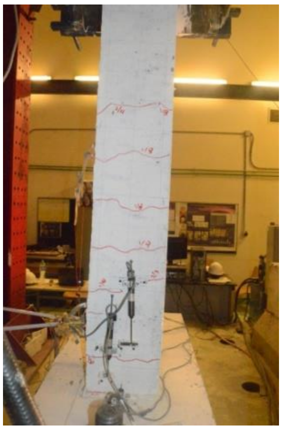

Figure 5.64: CSF-0-7.5-NTension side at Δy

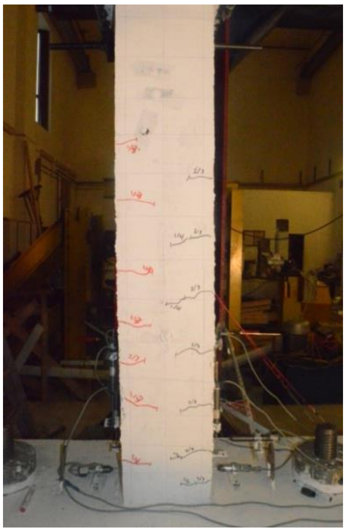

Figure 5.65: CSF-0-7.5-NPerpendicular side at Δy

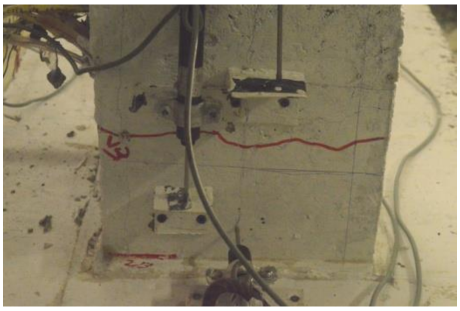

Figure 5.66: CSF-0-7.5-NOpening cracks near to base 1.96 Δy

Figure 5.67: CSF-0-7.5-NCrack opining width 3mm at 2.197 ∆y

Figure 5.68: CSF-0-7.5-NCrushing concrete cover at (2.197∆y)

Figure 5.69: CSF-0-7.5-N Compression side at the end of loading (2.85∆y)

Figure 5.70: End of the test

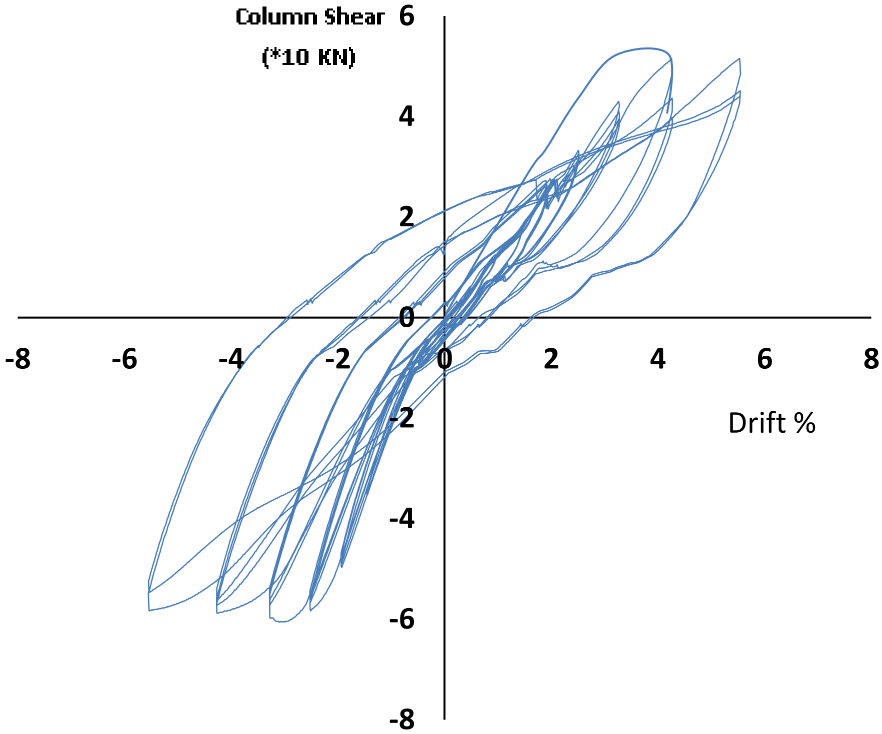

Figure 5.71: Shear force-drift hysteresis response of specimen CSF-0-7.5-N

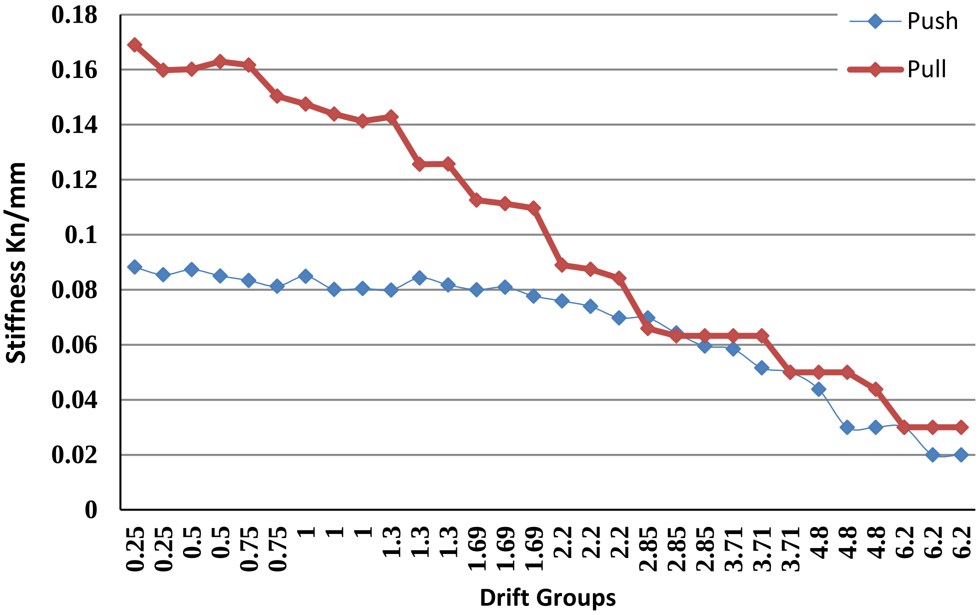

Figure 5.72: Peak to peak stiffness of specimen CSF-0-7.5-N

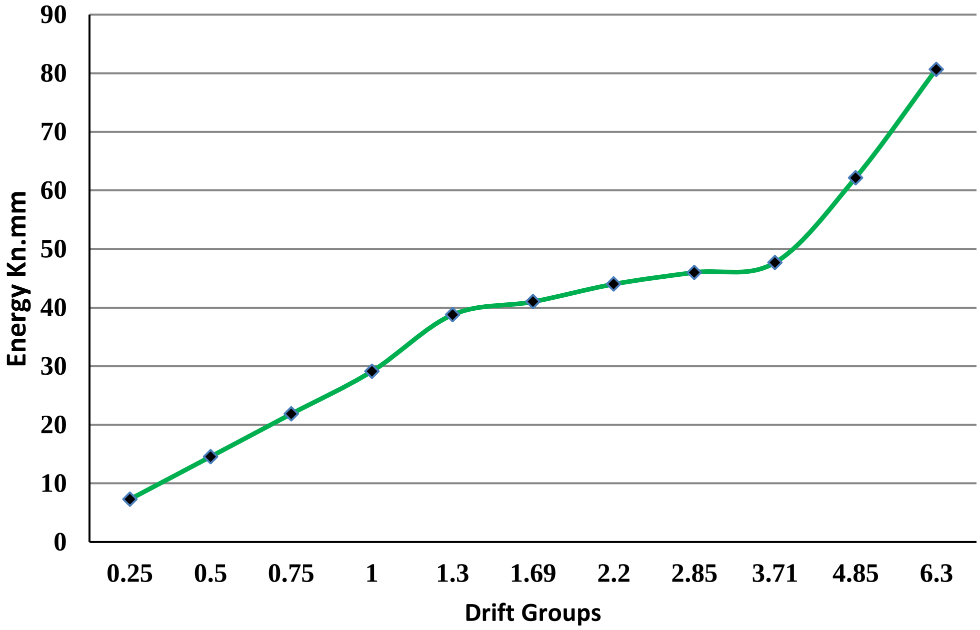

Figure 5.73: Peak to peak Energy of specimen CSF-0-7.5-N

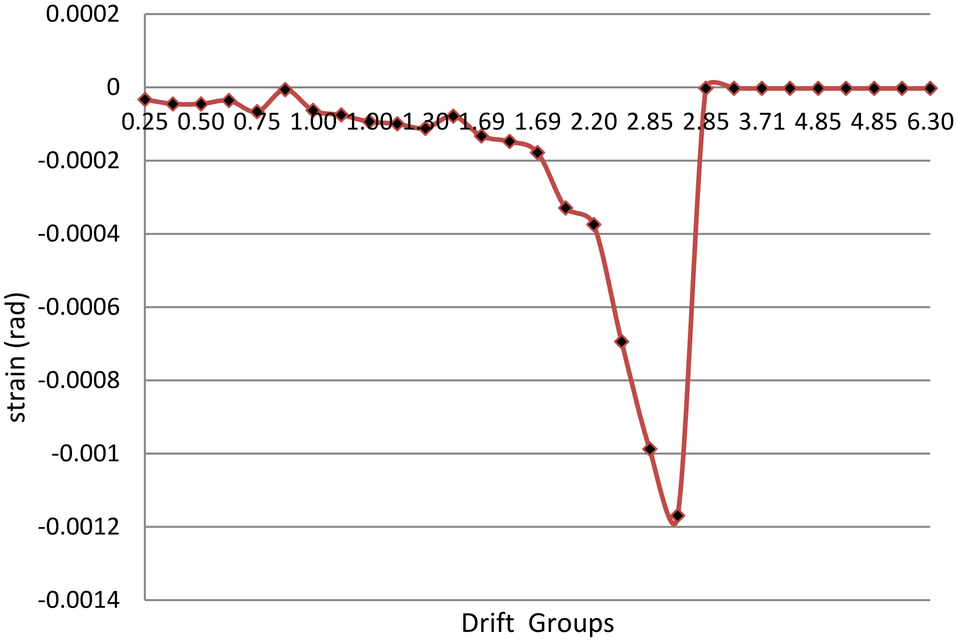

Figure 5.74: CSF-0-7.5-NCompression shear strain (rad) Vs Drift groups

(Vertical LVDTs 5-12) (Tension side)

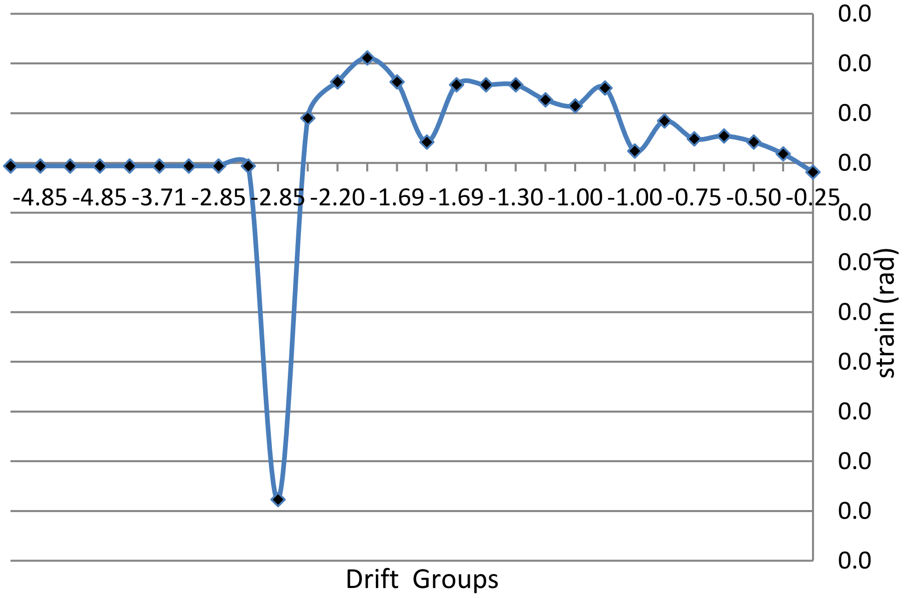

Figure 5.75: CSF-0-7.5-N Tension shear strain (rad) Vs Drift groups

(Vertical LVDTs 5-12) (Tension side)

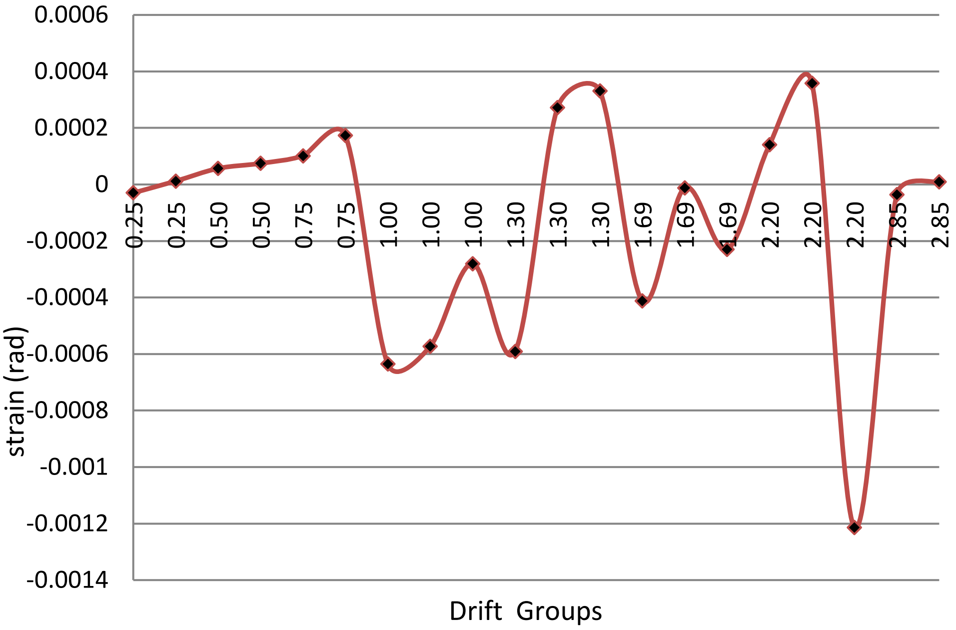

Figure 5.76: CSF-0-7.5-N Compression shear strain (rad) Vs Drift groups (Vertical LVDTs 5-12) (Compression side)

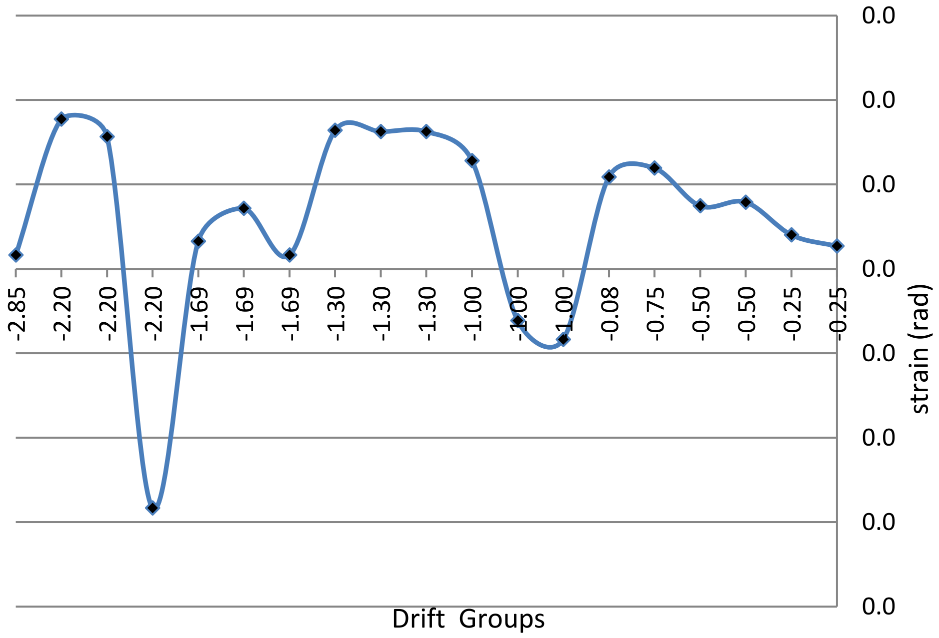

Figure 5.77: CSF-0-7.5-NTension shear strain (rad) Vs Drift groups (vertical LVDTs 5-12) (compression side)

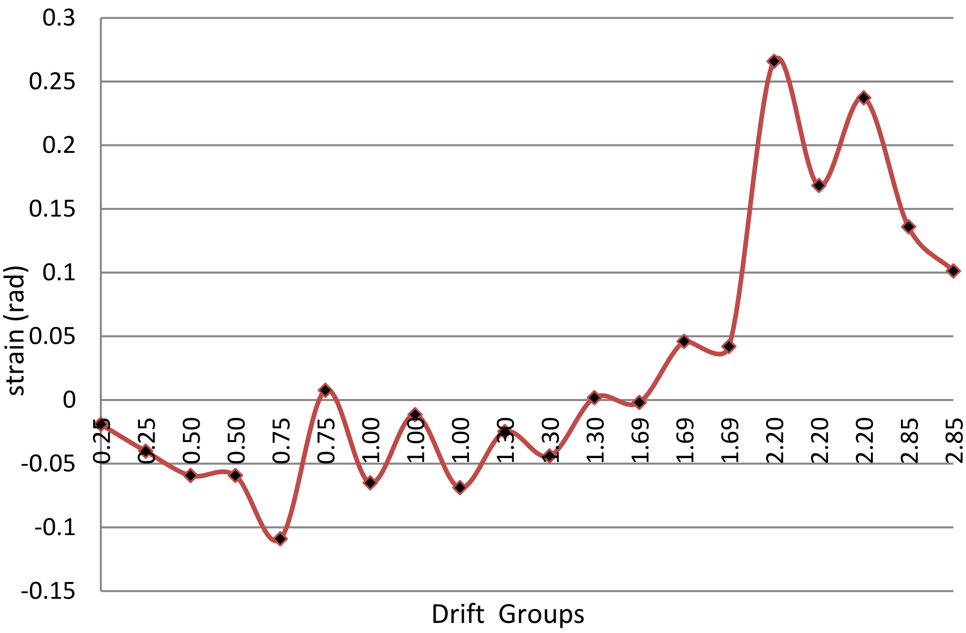

Figure 5.78: CSF-0-7.5-NCompression steel hoop strain Vs Drift groups (25mm)

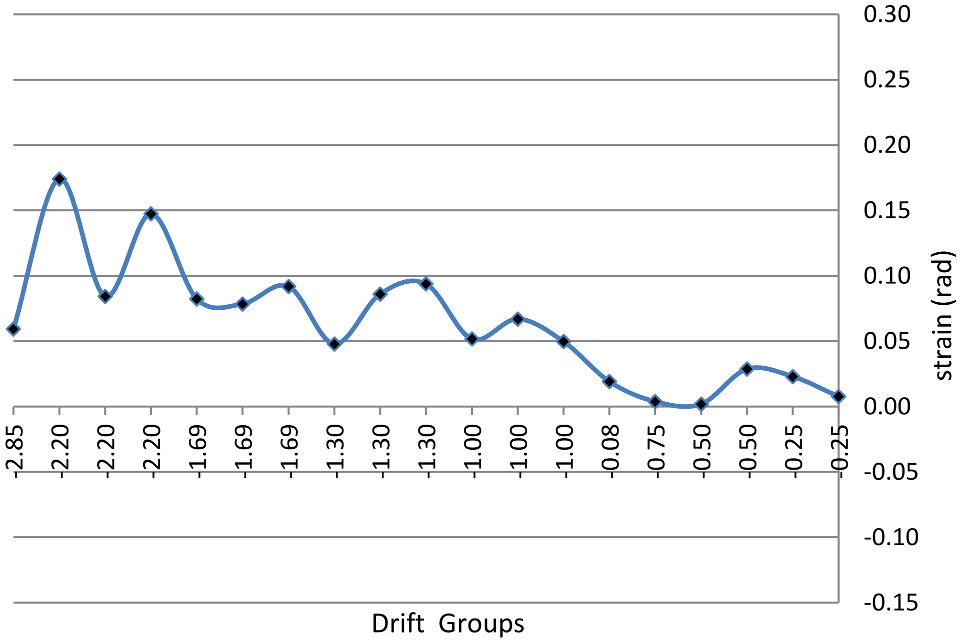

Figure 5.79: CSF-0-7.5-NTension steel hoop strain Vs Drift groups (25mm)

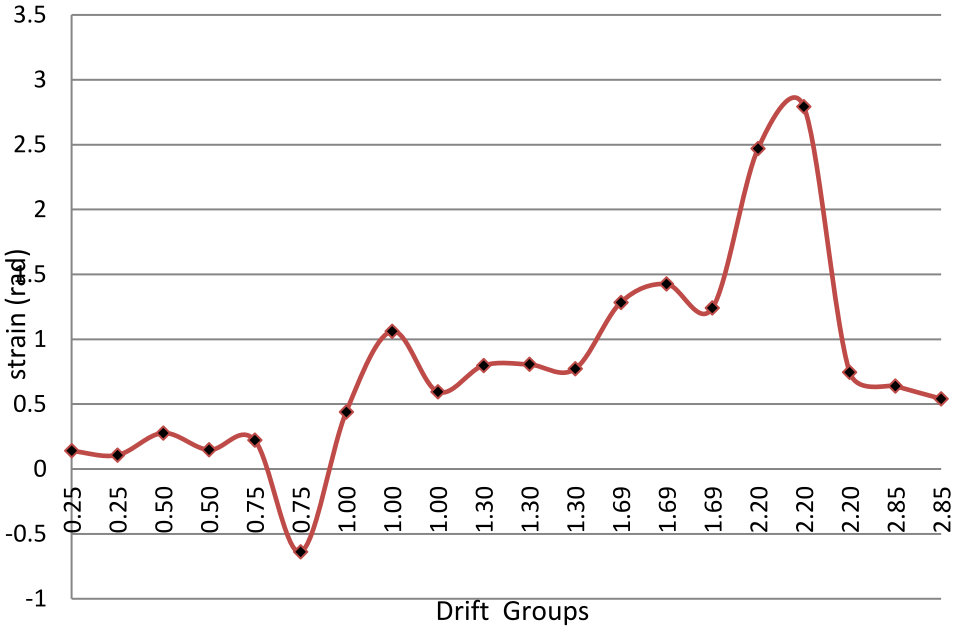

Figure 5.80: CSF-0-7.5-NCompression flange steel strain Vs Drift groups (125mm)

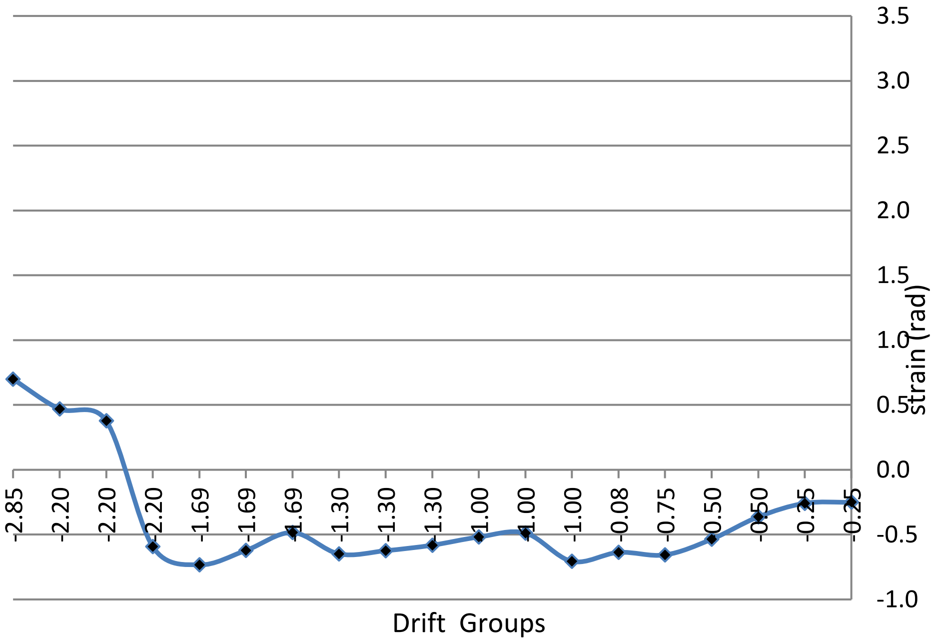

Figure 5.81: CSF-0-7.5-NTension flange steel strain Vs Drift groups (125mm)

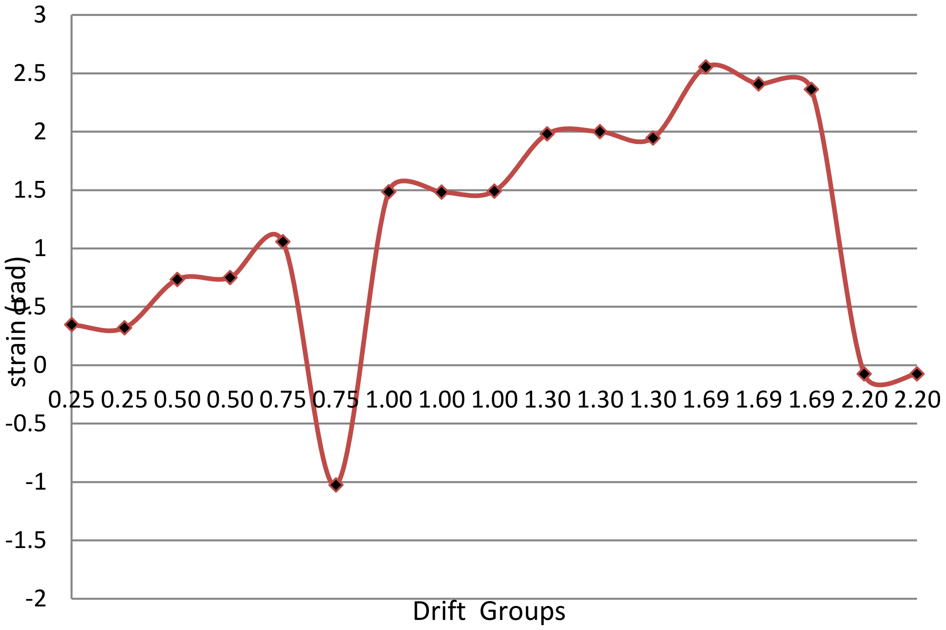

Figure 5.82: CSF-0-7.5-N Compression steel bar strain Vs Drift groups (125mm) (Compression side)

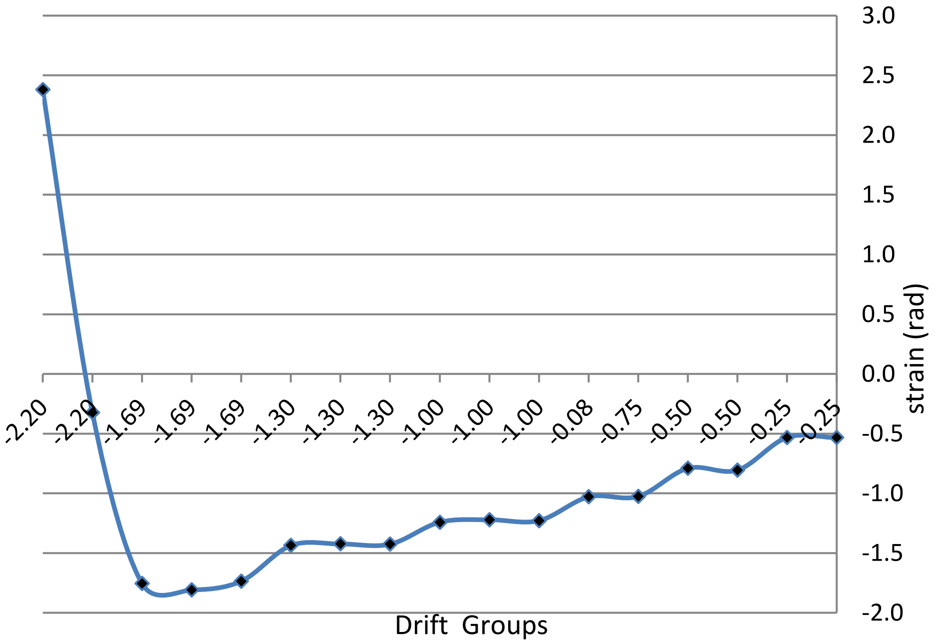

Figure 5.83:CSF-0-7.5-N Tension steel bar strain Vs Drift groups (125mm) (Compression side)

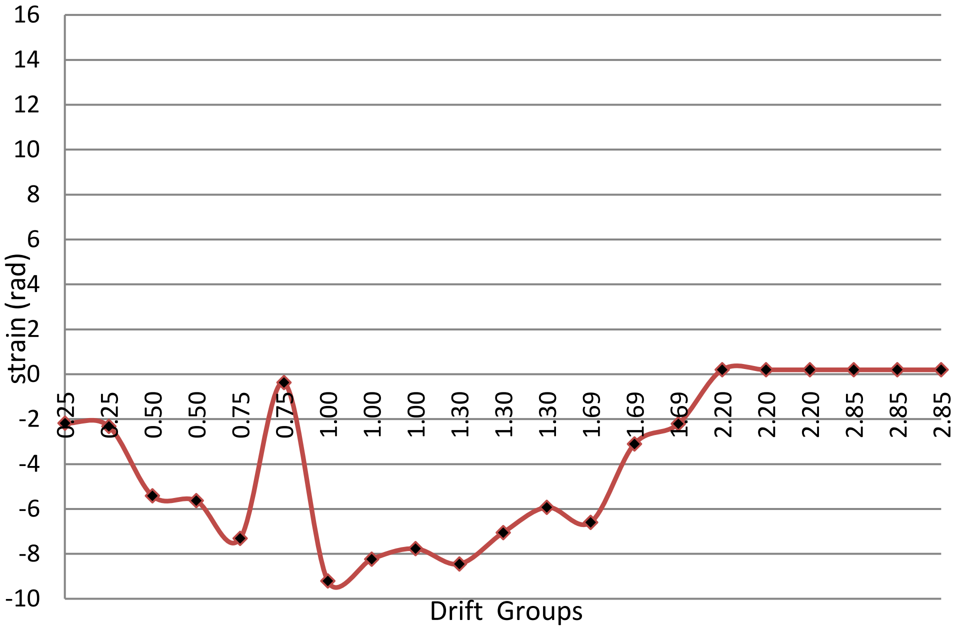

Figure 5.84: CSF-0-7.5-N Compression steel bar strain Vs Drift groups (125mm) (Tension side)

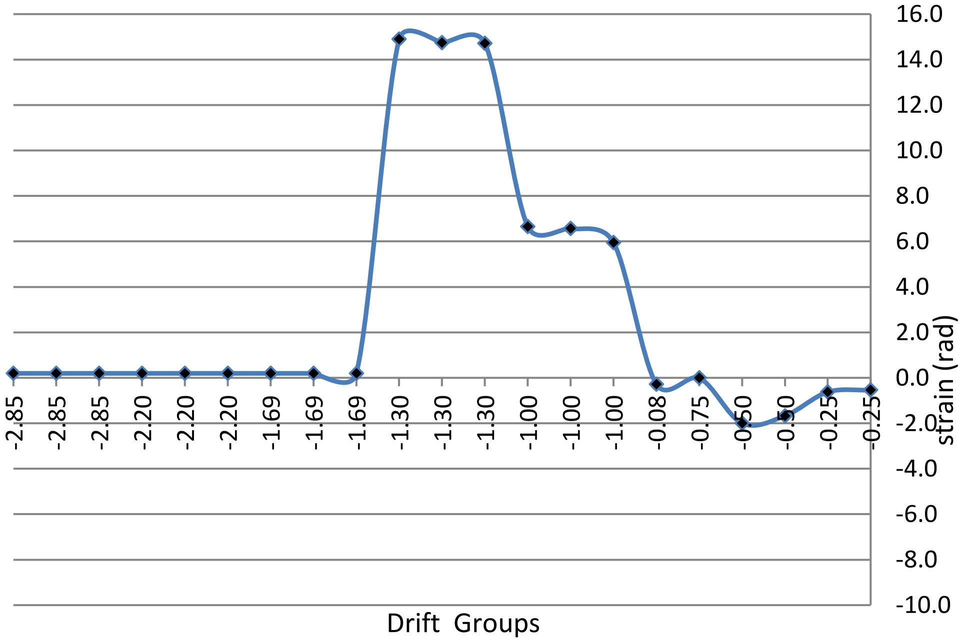

Figure 5.85: CSF-0-7.5-NTension steel bar strain Vs Drift groups (125mm) (Tension side)

Table 5.1 shows the damage sequence for each specimen for each group cycles in displacement protocol. **Figures 5.86, 5.87 and 5.88** show the envelope curve for shear force-drift hysteresis response for specimens to extract values from the curve. **Table 5.2** shows the horizontal load and drift for specimens for the yield, peak, and rapture which are extracted from backbone curves. **Figures 5.89, 5.90 and 5.91** show the comparison of column load capacity from extract program with the actual load from test. To show the damage deference between specimens, **Figure 5.92:97** show the crack pattern for specimens in many levels of loading during the test.

Table 5.1: Qualitative damage description

Cycle	Specimen 1 CSF 10-16cm-N	Specimen 2 CSF 10-7.5cm –N	Specimen3 CSF -0-7.5cm –N
0.25 Δy	No cracks	No cracks	No cracks
0.5 Δy	No cracks	Hair cracks near bottom	No cracks
0.75 Δy	Haircracks	Cracking	Hair cracks
Δy	Cracking	New cracks and widening	Cracking & Slipy
1.3 Δy	Slippy crack and the base and widening	Opening previous cracks and no new cracks	New cracks and widening
1.96 Δy	Opening previous cracks and no new cracks	widening cracks	Yielding
2.2 Δy	Yielding of specimen and opening previous cracks	Horizontal load starting to decrease, Failing	widening cracks
2.85 Δy	Crushing concrete cover near the base	Crushing concrete cover near the base	Crushing concrete cover near the base
3.72Δy	Crushing concrete cover and opening cracks	Losing vertical load and failure end of test	Losing vertical load and failure end of test
4.87Δy	Crushing concrete cover and buckling steel bars	-------------------	-------------------
5.79Δy	Losing vertical load and failure end of test	-------------------	-------------------

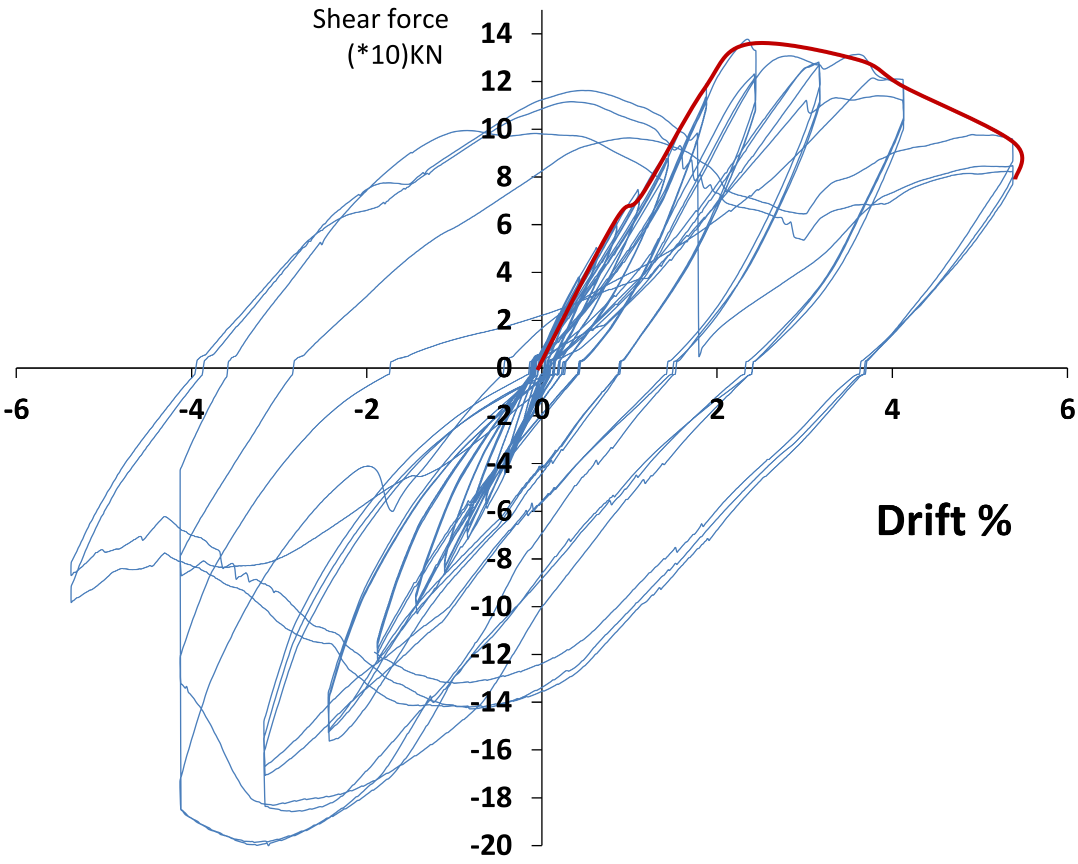

Figure 5.86: Specimen CSF 10-160mm - N backbone curve

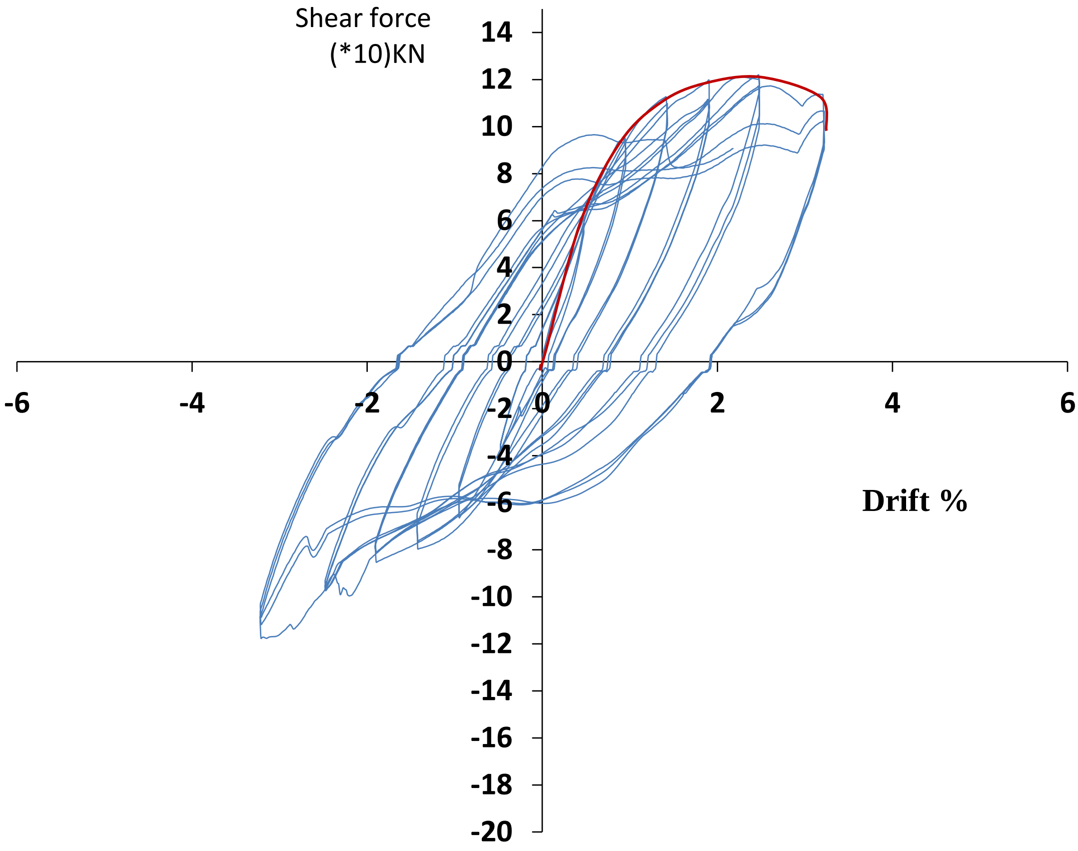

Figure 5.87: Specimen CSF 10-75 mm - N backbone curve

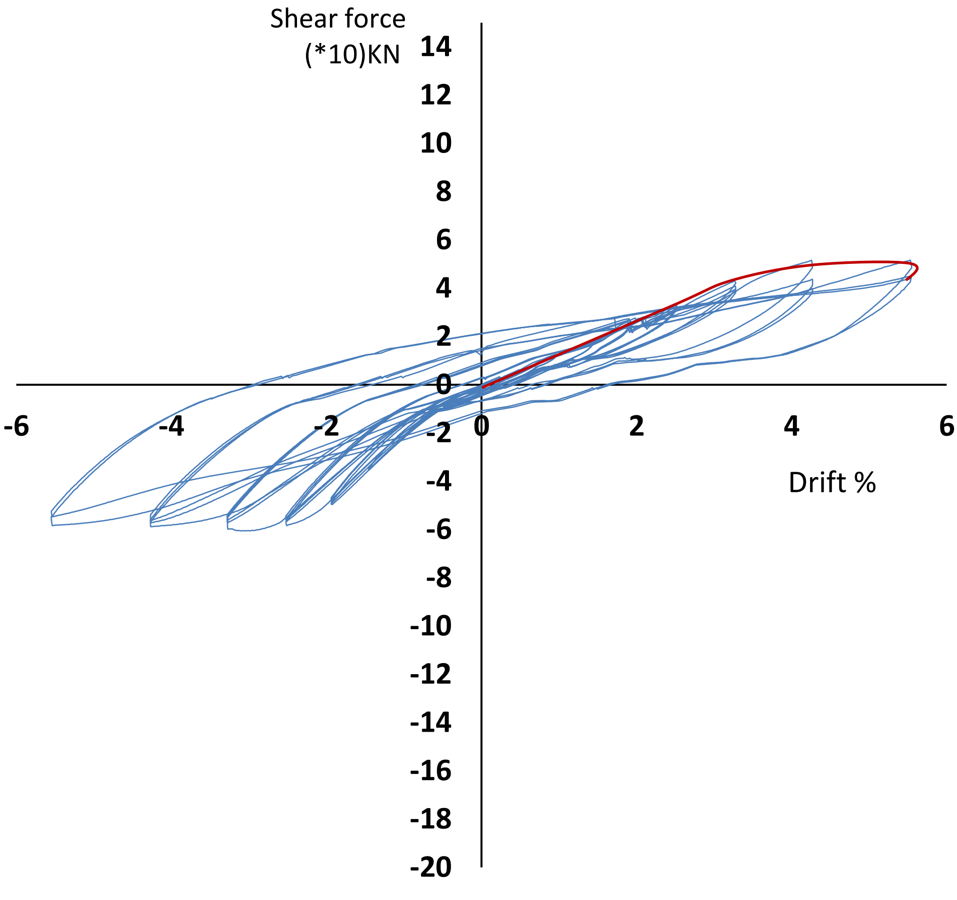

Figure 5.88: Specimen CSF -0-75 mm - N backbone curve

Table 5.2: comparison of Modern building data curve outputs

#	Out put	CSF 10-160mm-N	CSF 10- 75mm -N	CSF 0- 75mm -N
1	VpeakTest	137 KN	122 KN	50KN
2	Mpeak Test	205.5 KN M	183 KN M	75KN M
3	∆Vp%	2.5%	2.3 %	5%
4	VyTest	85 KN	104 KN	45 KN
5	Vy/Vpeak %	62.04 %	85.26 %	90 %
6	∆Vy%	1.3 %	1.15 %	3.8 %
7	V80%	109.6 KN	97.6 KN	40 KN
8	∆V80%	4.8 %	4.3 %	6%
9	VR	92 KN	96 KN	40KN
10	VR/VP %	67.15 %	78.68 %	80%
11	∆ VR	5.35 %	4.4 %	6%
12	µ∆=	3.69 %	3.739 %	1.31%
13	µf=	2.14 %	1.91 %	1.2%

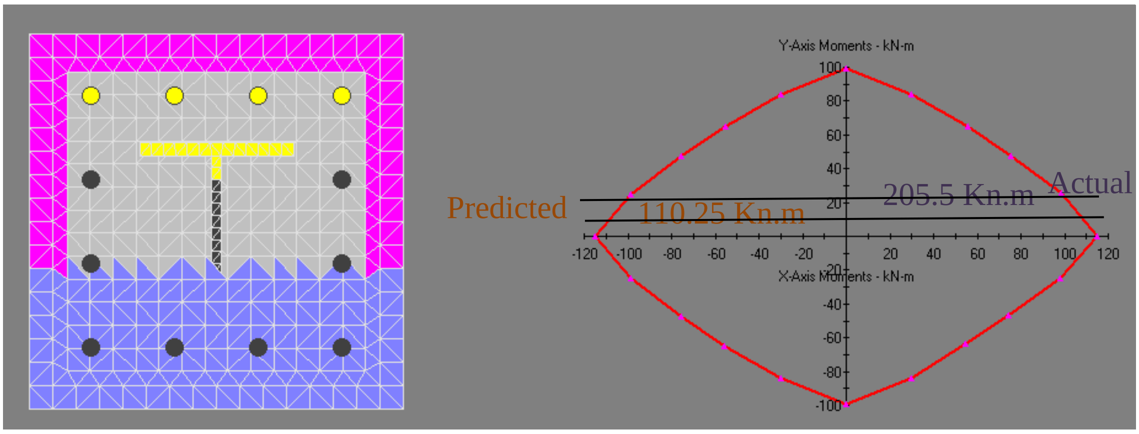

Figure 5.89: Predicted capacity Vs actual capacity of CSF 10-160mm – N

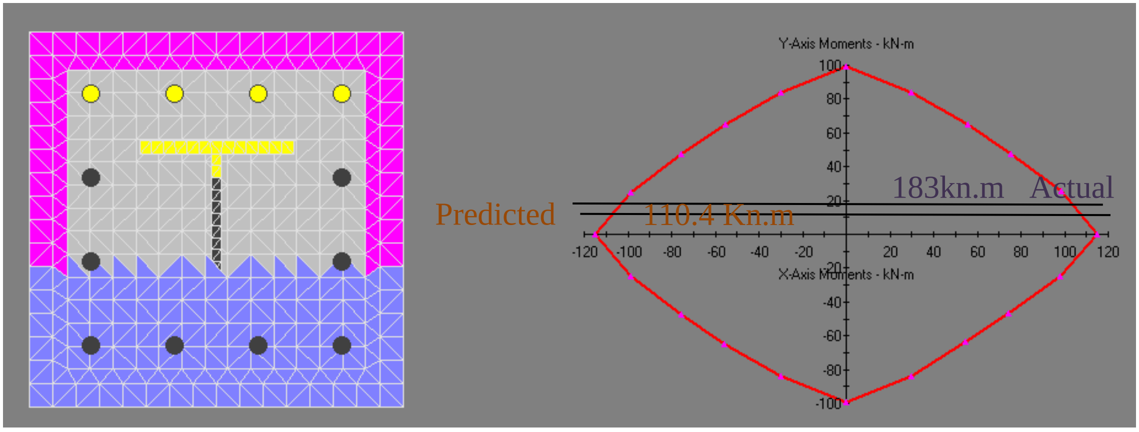

Figure 5.90: Predicted capacity Vs actual capacity of CSF 10- 75mm –N

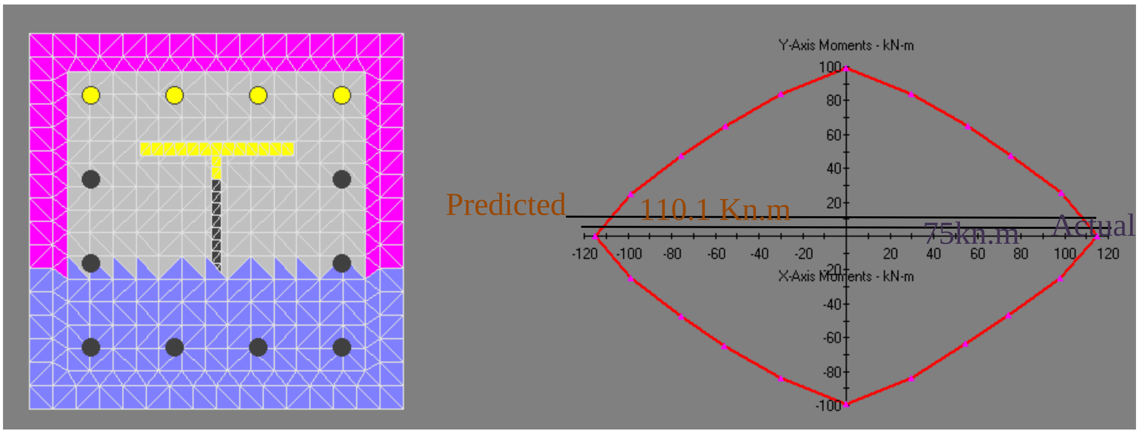

Figure 5.91: Predicted capacity Vs actual capacity of CSF 0- 75mm –N

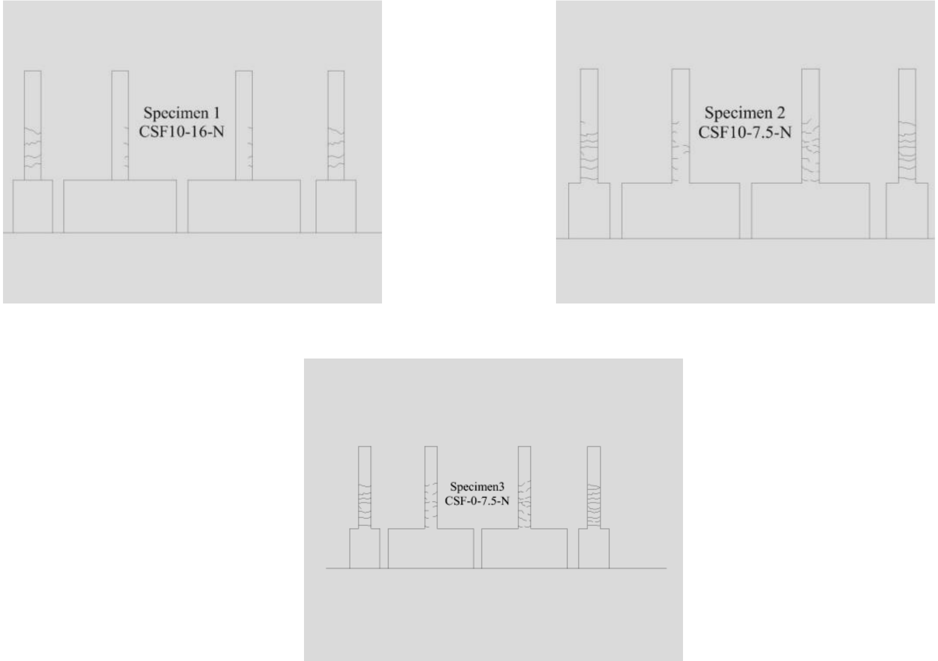

Figure 5.92: Crack pattern at (∆ y) lateral displacement

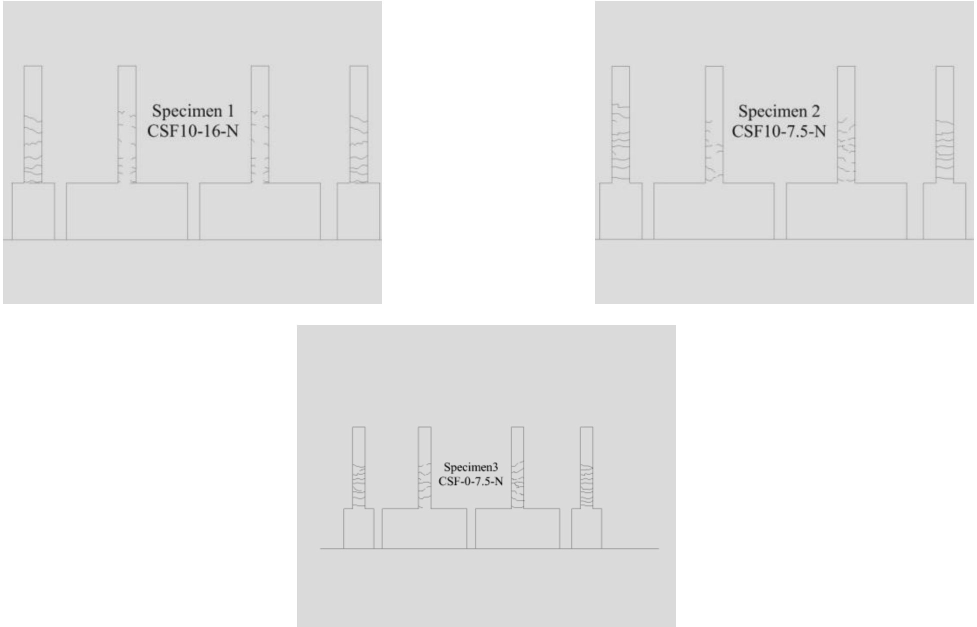

Figure 5.93: Crack pattern at (1.3 ∆ y) lateral displacement

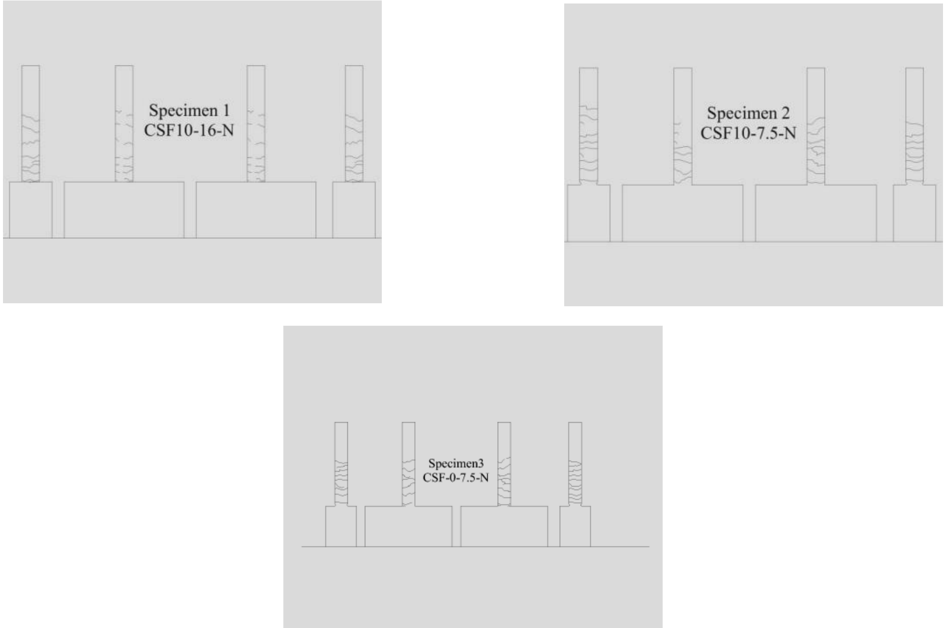

Figure 5.94: Crack pattern at (2.2 ∆ y) lateral displacement

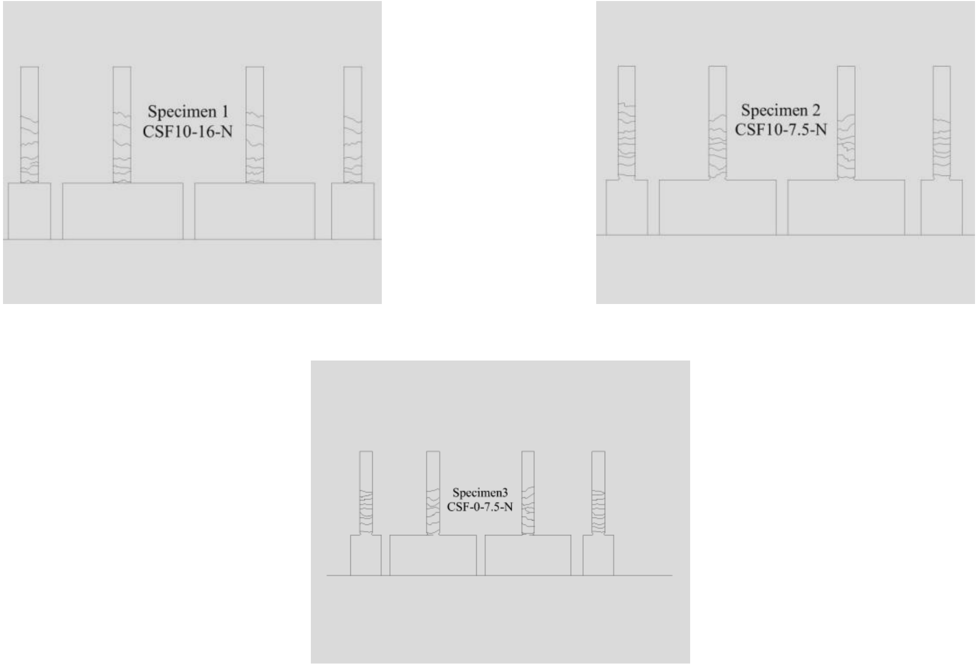

Figure 5.95: Crack pattern at (3.73 ∆ y) lateral displacement

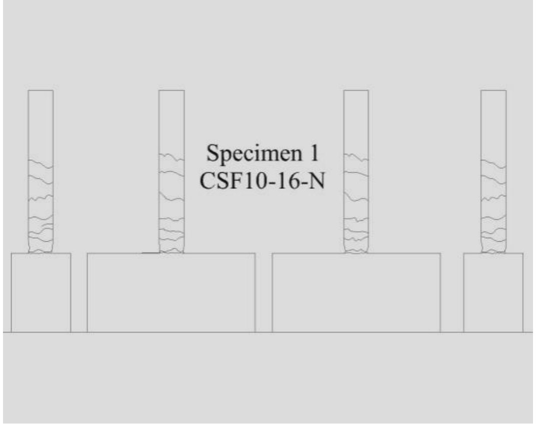

Figure 5.96: Crack pattern at (4.87 Δ y) lateral displacement

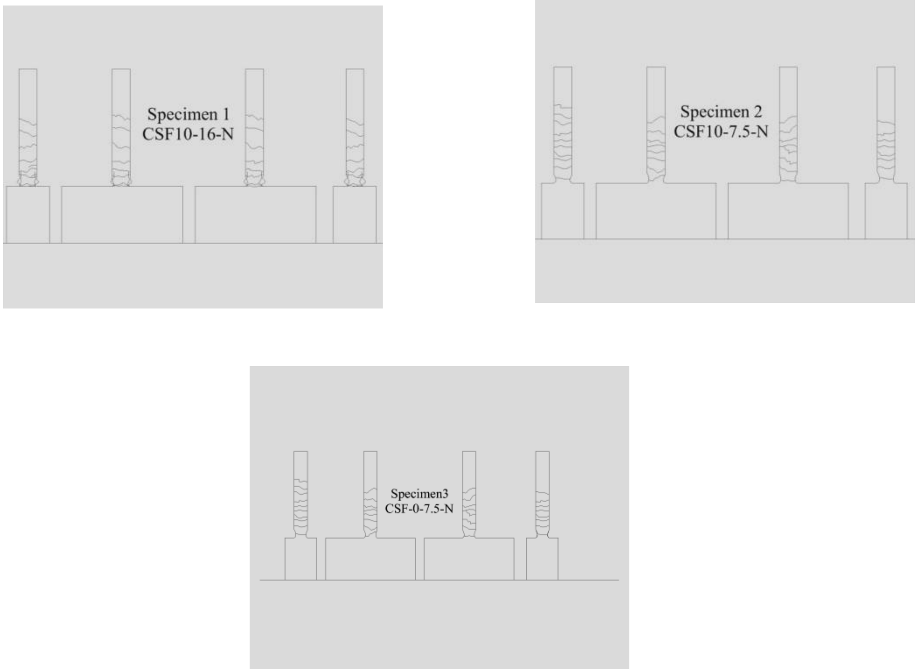

Figure 5.97: Crack pattern at (End of the test) lateral displacement

5.3. Existing building:

3.1.Shear deficient Specimens

1. **Specimen CSS-15-E**

CSS -15-Ewas subjected to a constant compressive axial load of 255 KN (0.15f'c Ag, where f'c = cylinder compressive concrete strength, and Ag = gross cross sectional area) and cyclic increments of lateral displacements as described in **Figure 4.13.** The theoretical nominal yield displacement was taken from the previous similar condition test to equal 15.2 mm. Some inclination of the horizontal actuator load cell was noticed with an angel ɵ=0'59'16'. This was taken into consideration in the force and drift post processing.

During the first two groups of displacement protocol (0.25 ∆y and 0.5∆y), there was no cracking. Starting the following displacement cycles of 0.75 of the nominal yield displacement, horizontal hairline cracks (width of less than 1mm.) developed near the bottom of the column. At these displacement levels, no new cracks were observed around the mid height region of the column. The number of inclined cracks and the crack width on the faces parallel to the lateral loading direction increased as the number and magnitude of the displacement cycles increased. Small diagonal shear cracks on the faces perpendicular to the lateral loading direction (i.e., on the east and west faces) were noticed. These relatively straight continuous diagonal cracks opened and closed during each cycle. During displacement cycles of 1.3 of the nominal yield displacement, relatively large crack openings were observed, suggesting a slip of the longitudinal reinforcing bars from the base. **Figure 5.99** shows 1.5mmwide crack opened between tension side of the column base and the column at peak lateral displacement.

During displacement cycles to the nominal yield displacement (Δ y = 33.44 mm.), wider crack opening was observed with no new cracks. The width of the existing horizontal cracks in the faces perpendicular to the loading direction increased especially in the side of pouring concrete. This was normal because the concrete in this side is less compacted than the other side and may have lost some of the gravel aggregate during concrete vibration.

At the beginning of cycle of the displacement level of 43.32mm (2.85 Δ y), the horizontal actuator load cell reached maximum loading capacity (220 KN). The luxation of the concrete cover was observed from middle to top corner of the column. Then the test was stopped and restarted from 2.85 Δy without axial loading force to reduce the horizontal resistance components coming from the axial loading.

In the compression zones, at the bottom of the column, flaking and spalling of concrete were observed at the end of group 3.72 Δy (56.55mm) **Figure 5.102**. As the number of cycles increased, the concrete cover crashed and the steel bars appeared from different areas, as shows in **Figures 5.103**

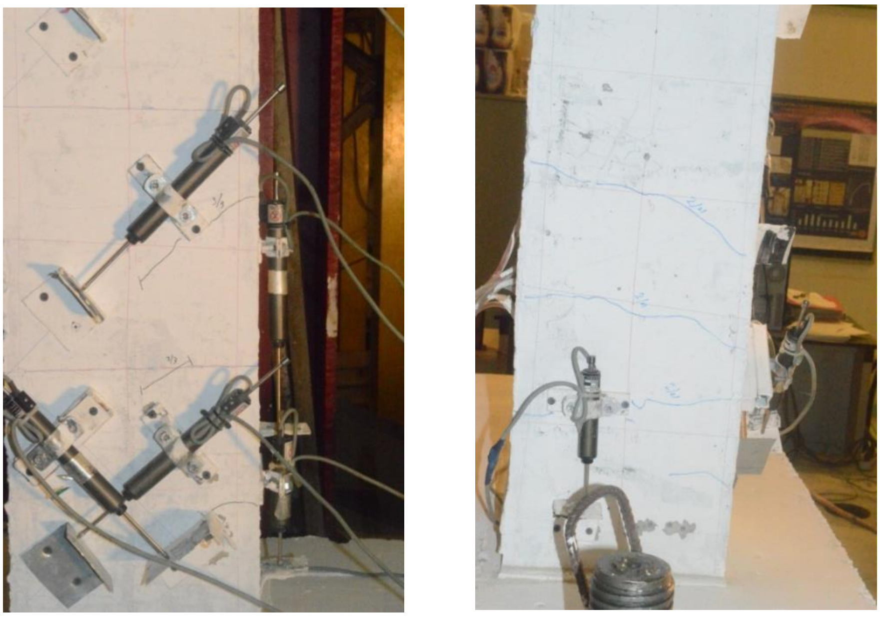

Figure 5.98: Specimen CSS-15-E at initial displacement (hair cracking)

Figure 5.99: starting slipping from base of column at 1.3∆y

Figure 5.100: Specimen CSS-15-E at the tension direction of 2.2∆y

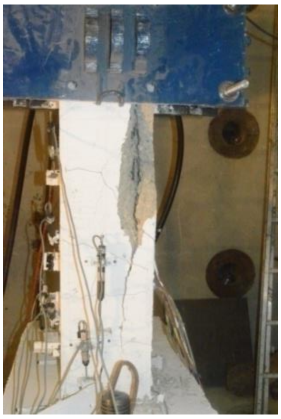

Figure 5.101: CSS-15-ECrushing concrete cover at the compression side at displacement of 2.85∆y

Figure 5.102: CSS-15-E Crushing concrete cover of 3.72∆y

Figure 5.103: CSS-15-ECompression and tension of loading of 3.72∆y

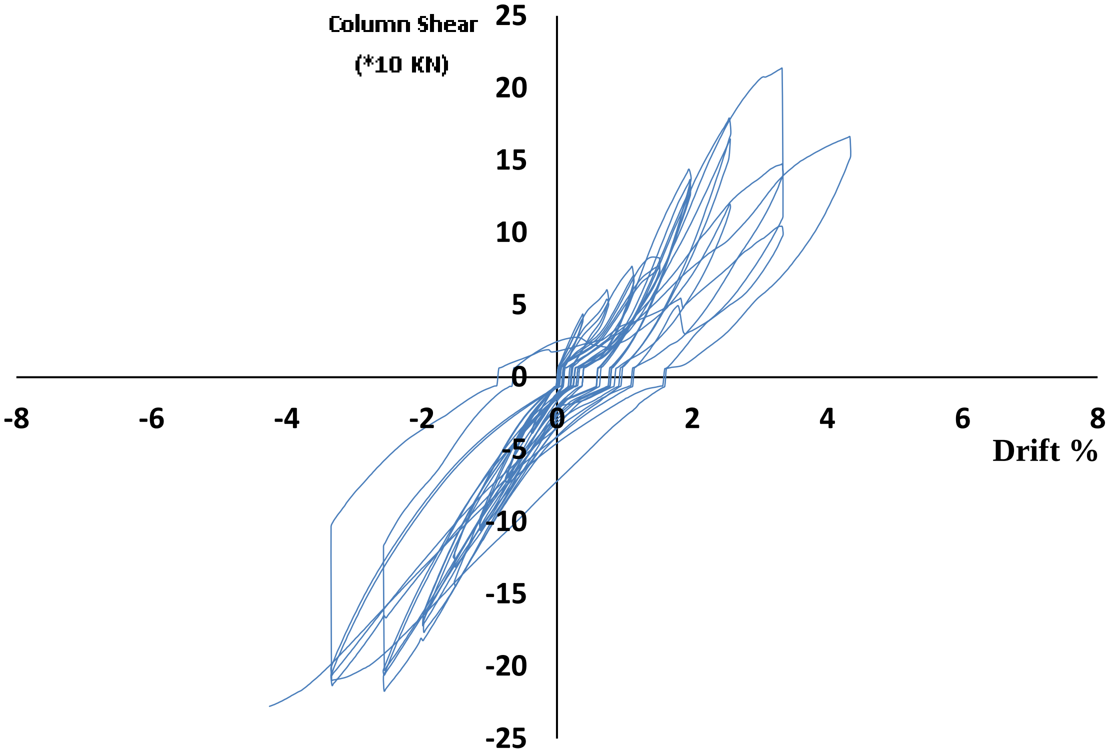

Figure 5.104: Shear force-drift hysteresis response of specimen CSS 15-E

Figure 5.104 shows the shear force-drift ratio hysteresis response of CSS15-E. The peak shear capacity of the specimen was 230 KN. This significantly exceeded the theoretical shear prediction value of AISC 341 which was 124 KN (based on concrete and hoop shear resistance). It is noteworthy that code shear capacity is believed to be based on first shear cracking capacity. The peak shear capacity was reached at 3.1% drift ratio. Thus, the specimen loss in lateral force capacity was reached at 5.8% drift ratio. This drift ratio is considered relatively so high for the typical reinforced concrete existing buildings (with no SRC columns) which generally can tolerate less than 2% drift before collapse. However, this peak drift ratio is considered low if compared to the modern building collapse prevention drift limit state of 4.5% for a single ground motion and 3% for the mean of several ground motions, as per recommended by Tall Building Initiative (2011). The specimen exhibited brittle shear failure with immediate strength degradation following the peak shear strength.

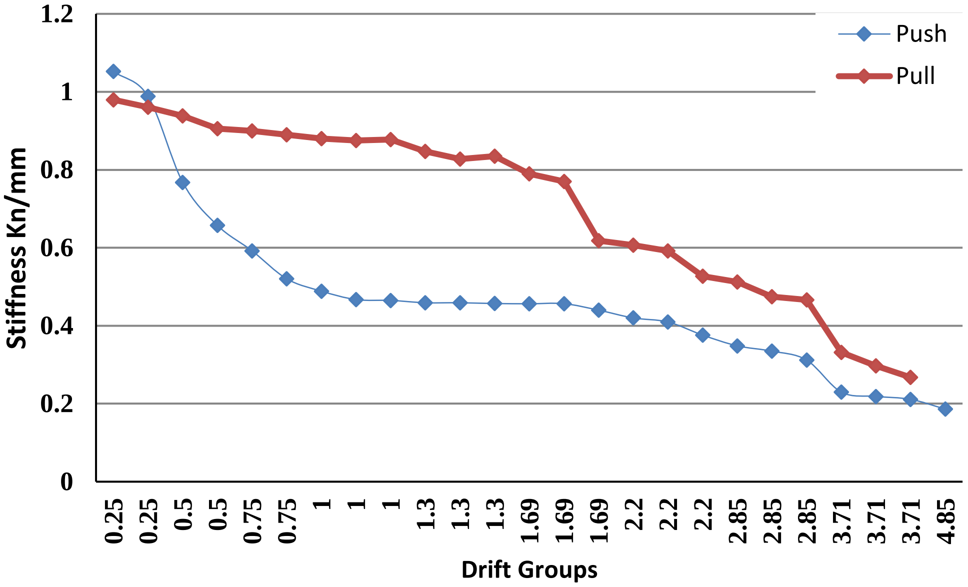

Figure 5.105: Peak to Peak stiffness of specimen CSS-15-E

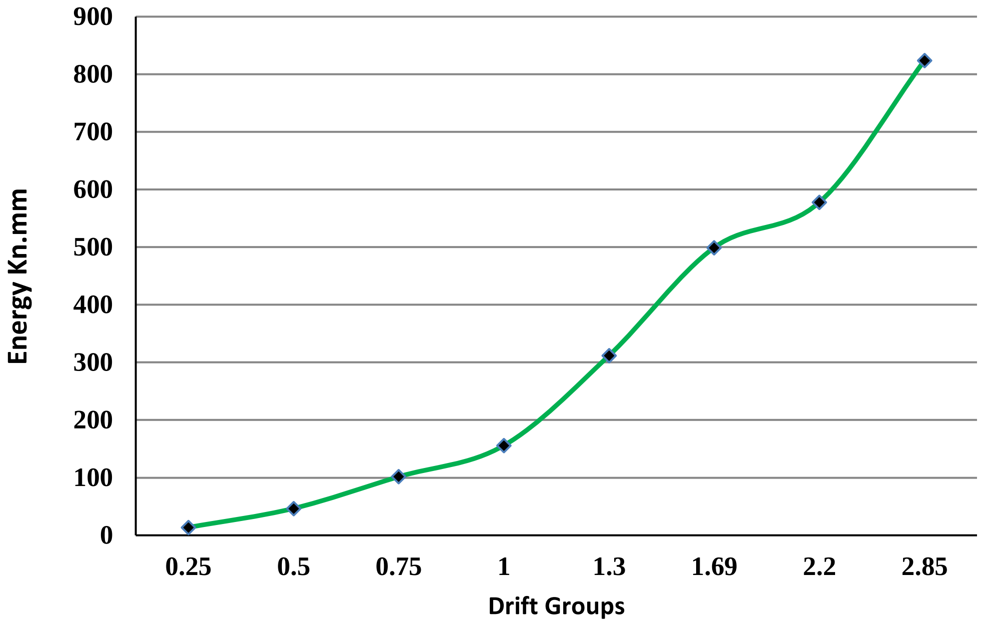

Figure 5.106: Peak to peak Energy of specimen CSS-15-E

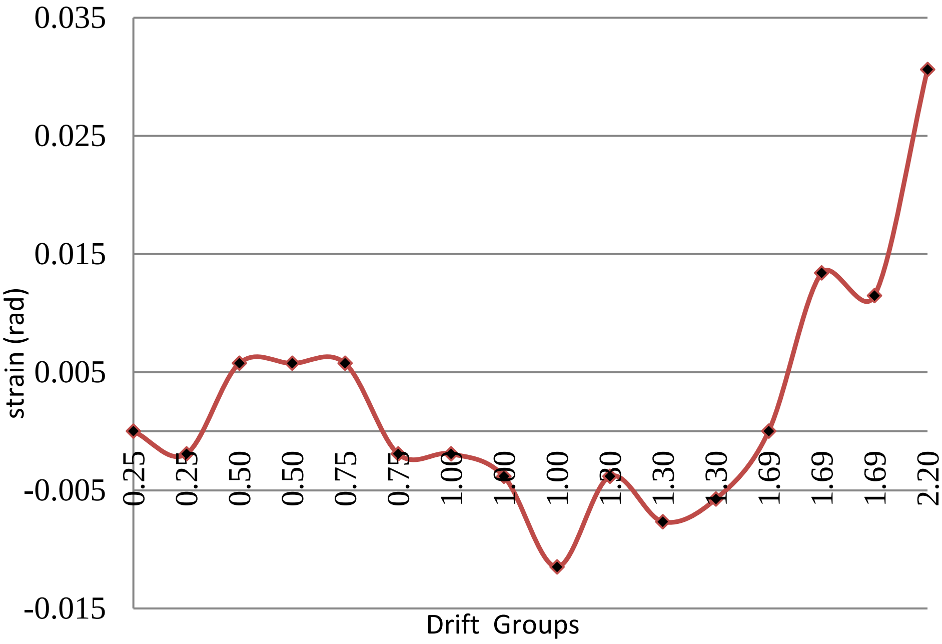

Figure 5.107: CSS-15-ECompression Web steel strain Vs Drift groups (320mm)

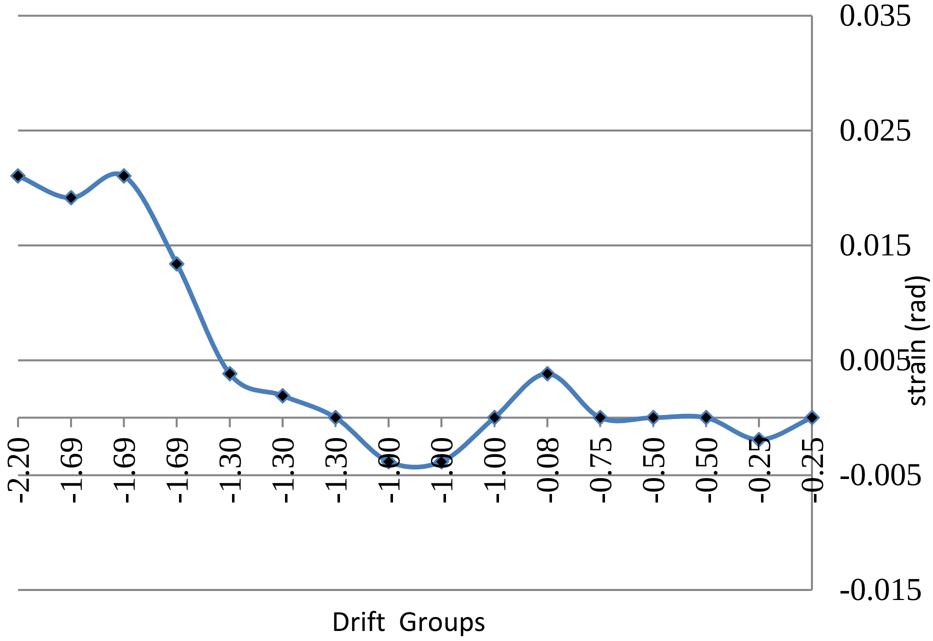

Figure 5.108: CSS-15-ETension Web steel strain Vs Drift groups (320mm)

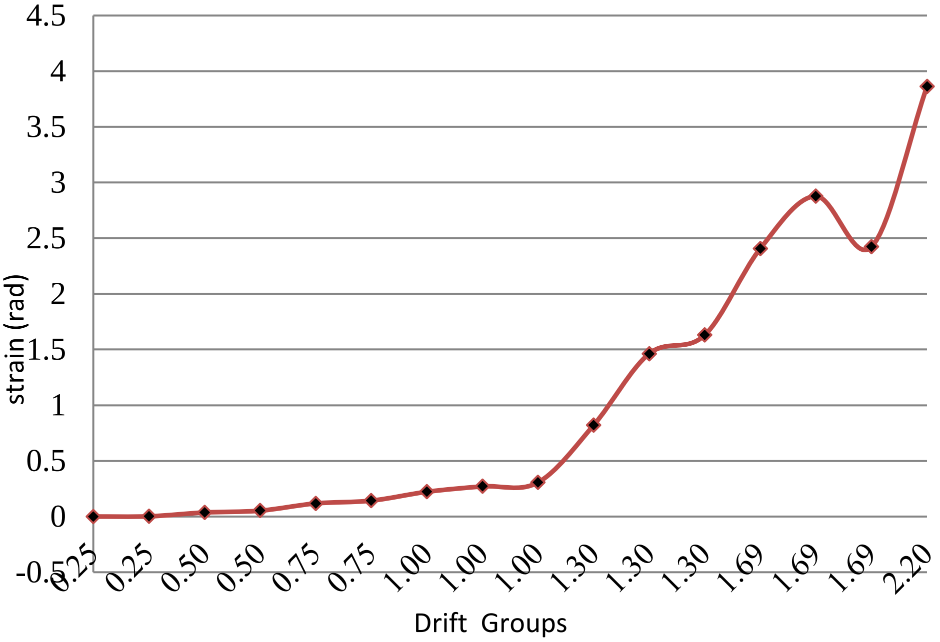

Figure 5.109: CSS-15-ECompression steel hoop strain Vs Drift groups (325mm)

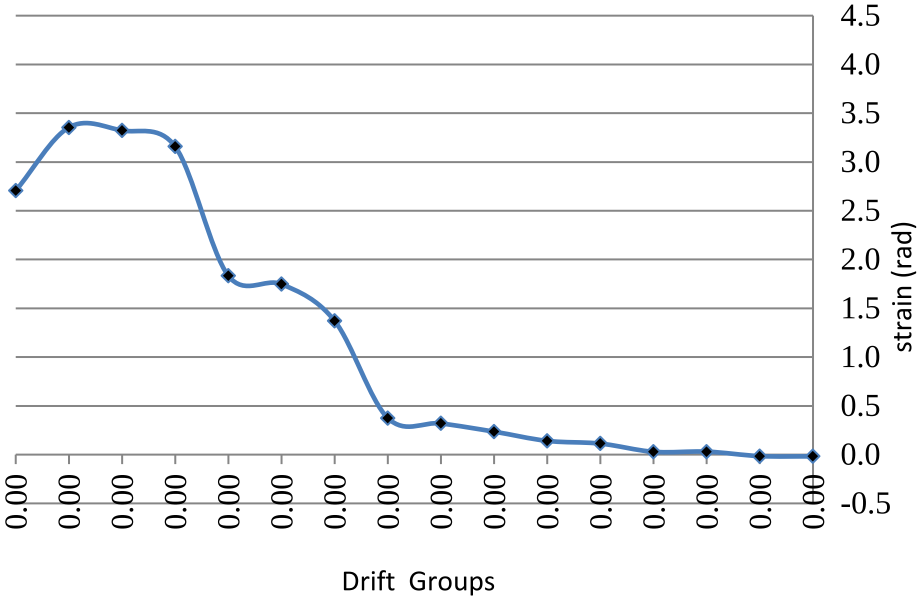

Figure 5.110: CSS-15-ECompression steel hoop strain Vs Drift groups (325mm)

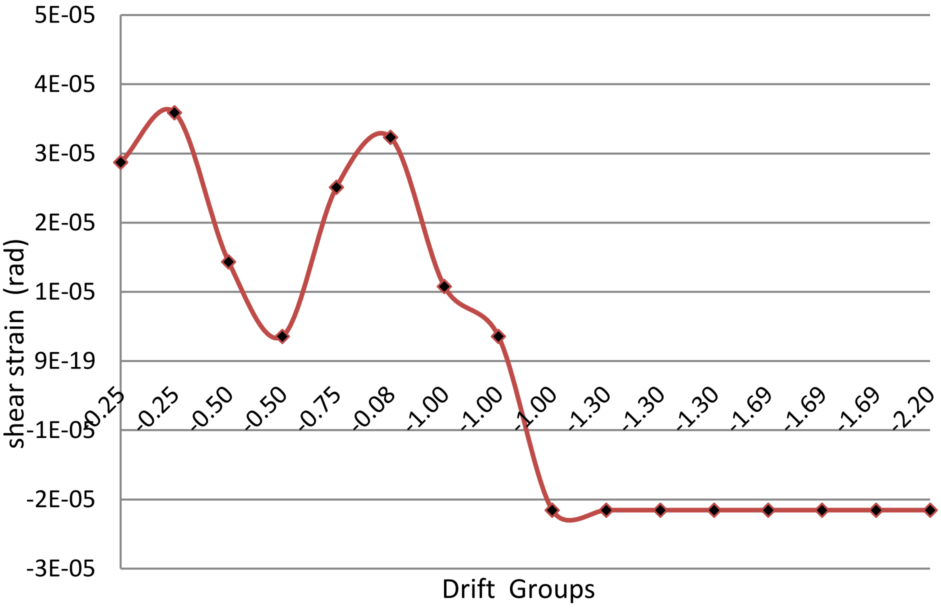

Figure 5.111: CSS-15-E Compression shear strain (rad) Vs Drift groups (Diagonal LVDTs4-27)

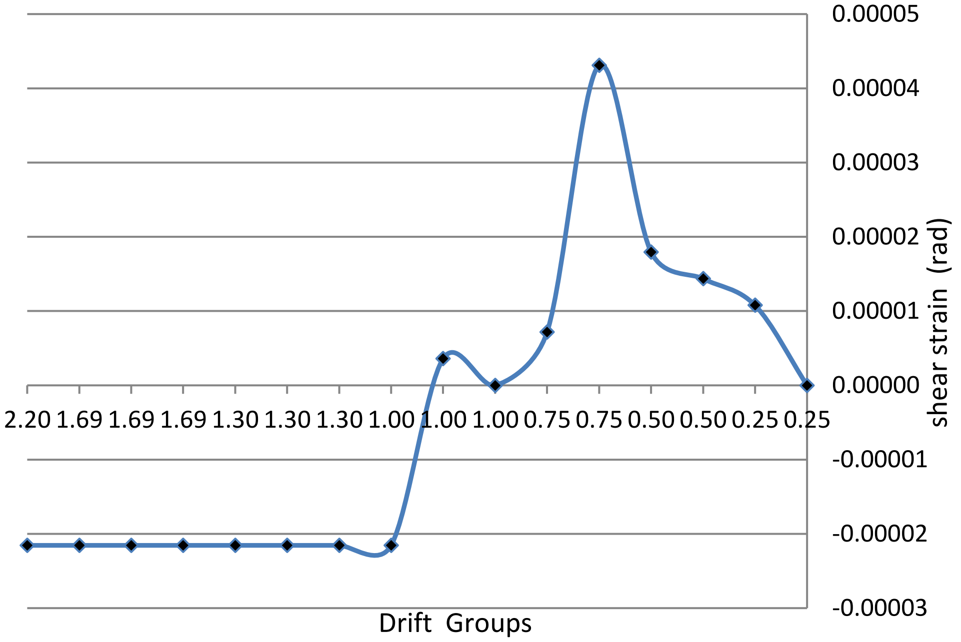

Figure 5.112: CSS-15-ECompression shear strain (rad) Vs Drift groups (Diagonal LVDTs 4-27)

2. Specimen CSS -20-E:

CSS -20-E was subjected to a constant compressive axial load of 465 KN (0.2f’c Ag, where f’c = cylinder compressive concrete strength, and Ag = gross cross sectional area) and cyclic increments of lateral displacements as described in **Figure 4.13**. The theoretical nominal yield displacement was calculated to equal 14.85 mm. Some inclination of the horizontal actuator load cell was noticed with an angel ɵ= 1’17’52.This was taken into consideration in the force and drift post processing. .

During the first groups of displacement protocol (0.25, 0.5, 0.75 Δy) there was no cracking. Starting the following displacement cycles of Δy of the nominal yield displacement, flexure hairline cracks (width of less than 1mm.) and developed near the bottom of the column. The number of inclined cracks and the crack width on the faces parallel to the lateral loading direction increased as the number and magnitude of the displacement cycles increased. Small horizontal and inclined cracks on the faces perpendicular to the lateral loading direction (i.e., on the east and west faces) started to span the width of the column. These relatively straight continuous horizontal cracks opened and closed during each cycle. During displacement cycles equal to theoretical Δy displacement cracks increased opening. Relatively, large crack openings were observed suggesting slip of the longitudinal reinforcing bars from the base atΔ =2.2Δy.

During displacement cycles following the nominal yield displacement (Δ = 2.85 Δy.), more in wide crack opening without any new cracks. Faces perpendicular to the loading direction, the width of the existing diagonal cracks increased from two sides.

At the beginning of cycling at the displacement level of (2.2 Δ y), when the specimen were loaded the first time (push or eastward direction, **Figure 5.115**), luxation of the cover concrete was observed in the bottom northeast corner and the horizontal load started to decrease after reaching the previous peak.

In the flexural compression zones, at the bottom of the column, flaking and spalling of concrete were observed. As the number of cycles increased, after the concrete cover crushed and the steel bars appeared, there was no buckling of steel bars; however, the lower cracks were deep in the column around the cross section as shown in **Figure 5.119**.At the 4.87 Δ y, it stopped loading horizontally and the specimen loaded only with axial load 1850KN to check the axial capacity after seismic loading. The steel section could carry the axial load without failing what was rested from concrete.

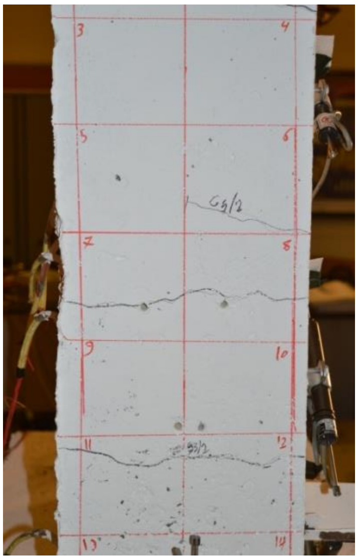

Figure 5.113: Specimen CSS-20-E at initial cracking (1 Δy)

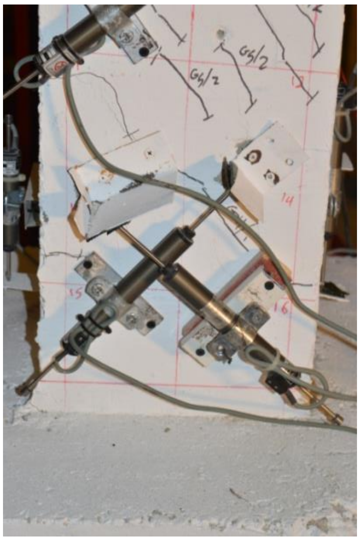

Figure 5.114: CSS-20-E Start slipping at 2.2Δy

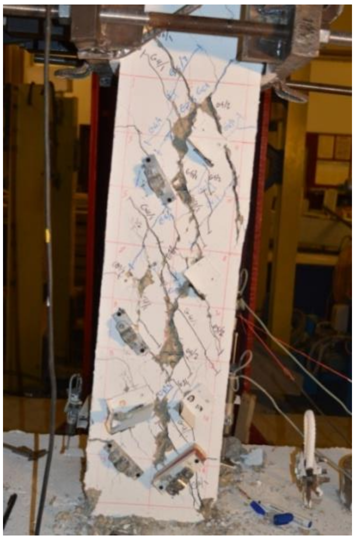

Figure 5.115: CSS-20-EPerpendicular side at 2.2∆y

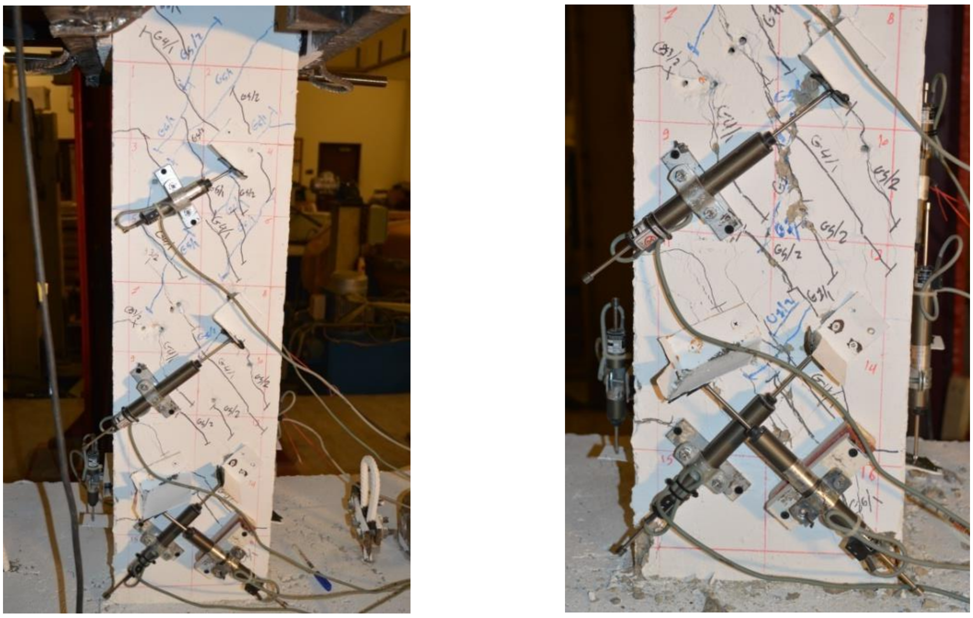

Figure 5.116: CSS-20-EOpening cracks near to base 2.85 ∆y

Figure 5.117: CSS-20-ECrushing concrete cover mid cycle of (2.85 ∆y)

Figure 5.118: CSS-20-ECrushing concrete cover (2.85 ∆y)

Figure 5.119: Final failure of column CSS-20-Econcrete cover (3.71∆y)

Figure 5.120: End of the test

Figure 5.121: Testing was under supervision of Prof. Dr. Wael Hassan

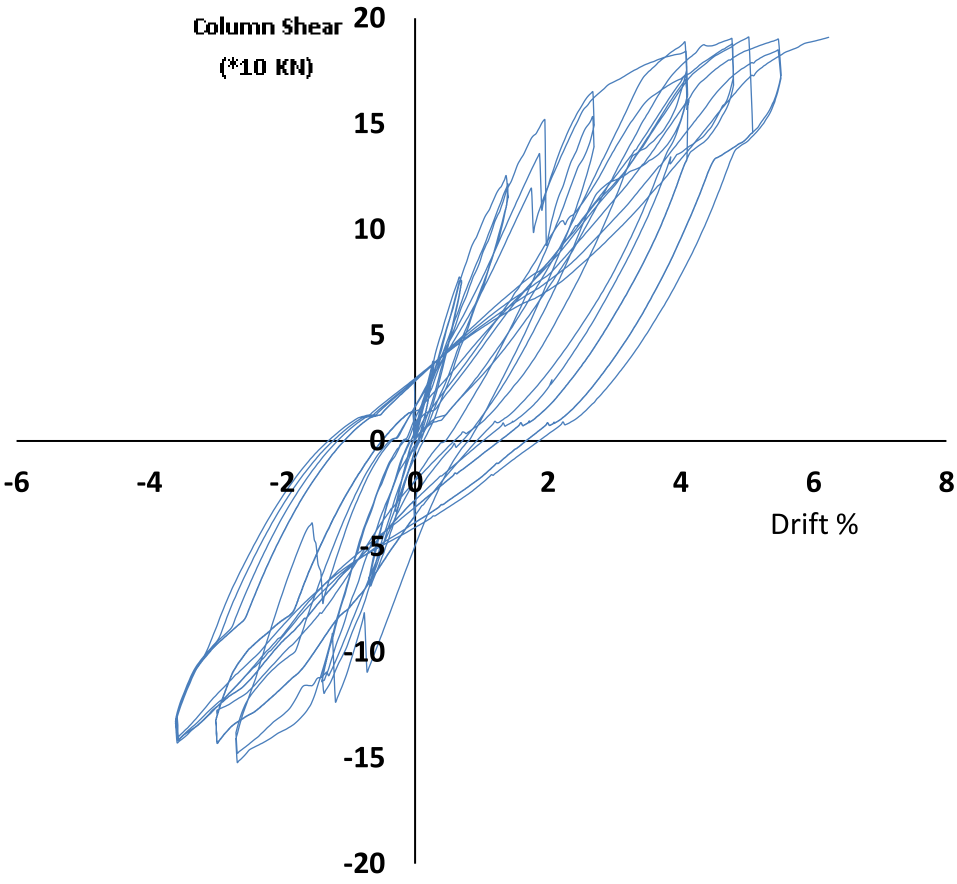

Figure 5.122: Shear force-drift hysteresis response of specimen CSS 20-E

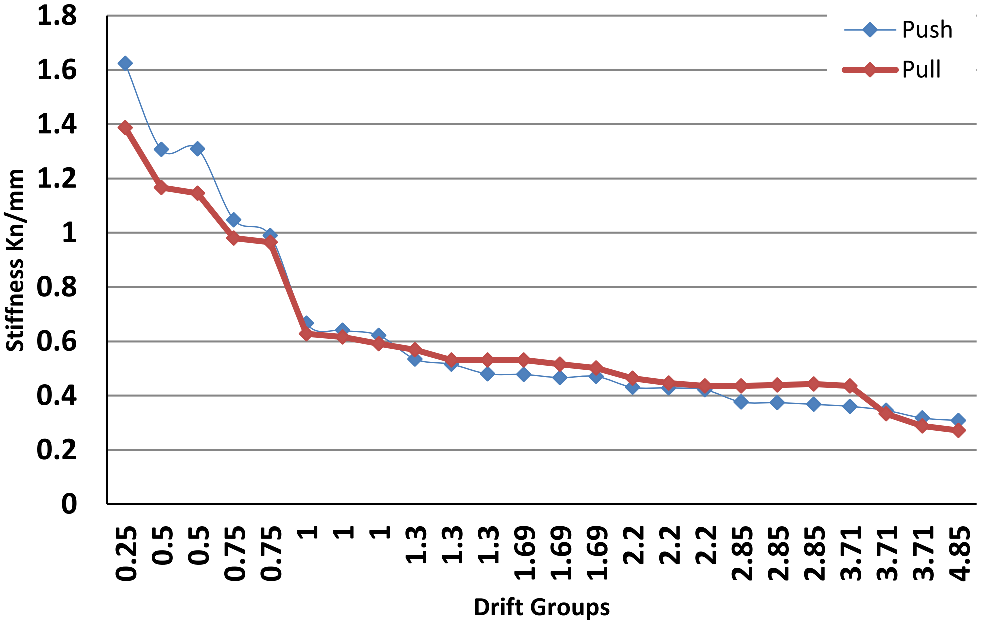

Figure 5.123: Peak to Peak stiffness of specimen CSS 20-E

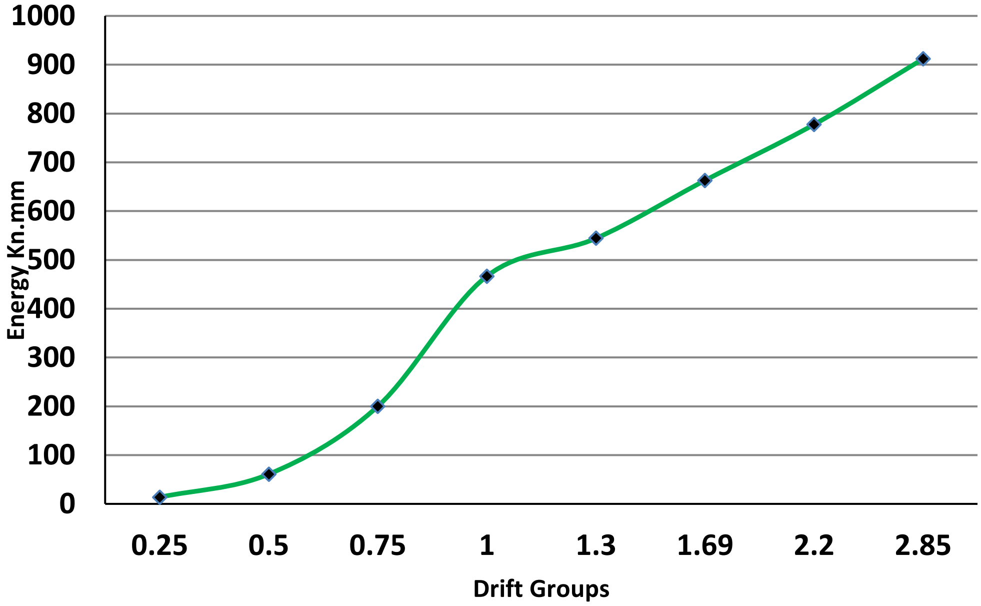

Figure 5.124: Peak to peak Energy of specimen CSS 20-E

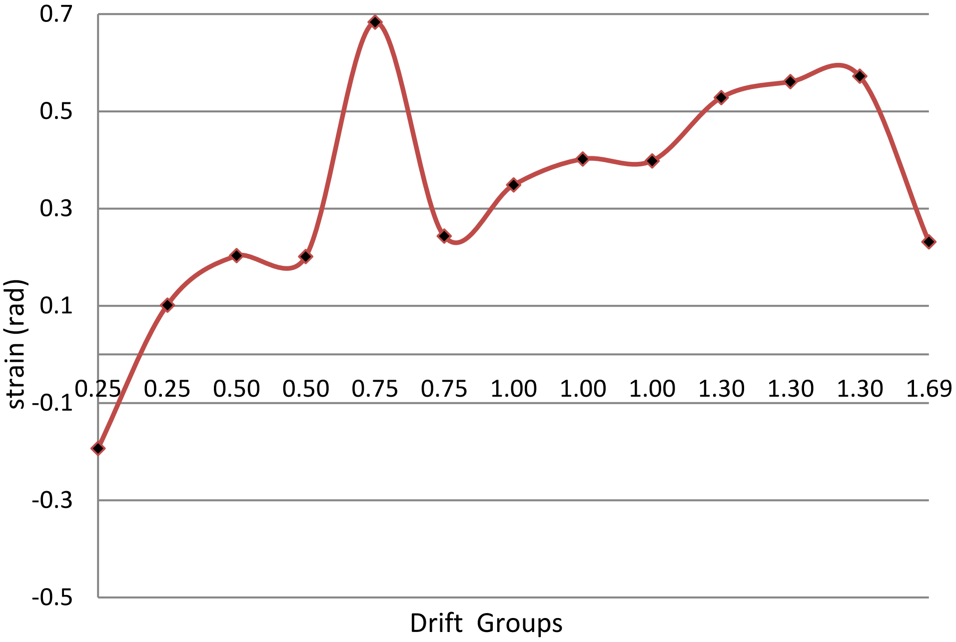

Figure 5.125: CSS-20-E Compression Web steel strain Vs Drift groups (320mm)

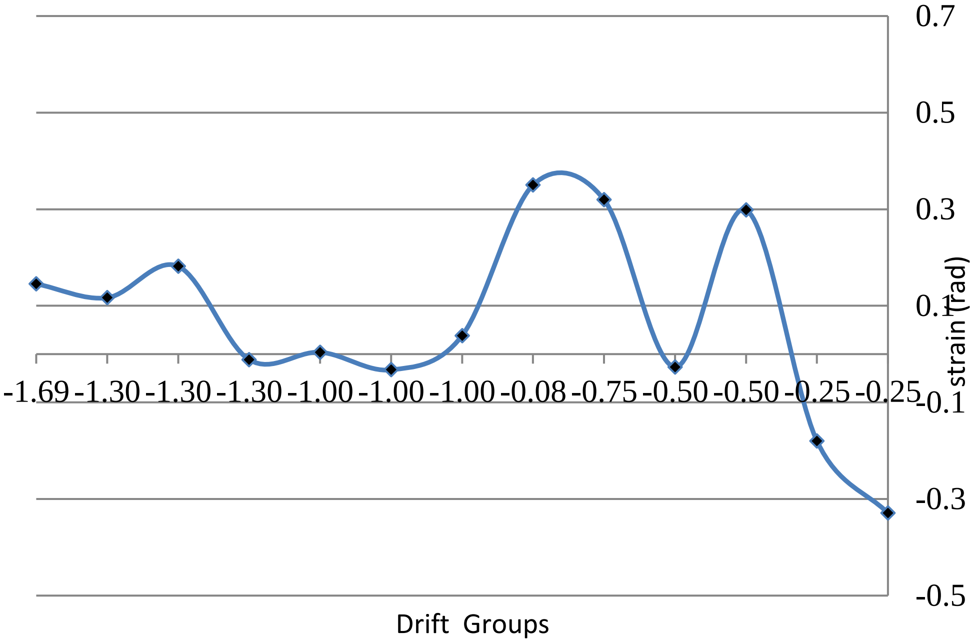

Figure 5.126: CSS-20-E Tension Web steel strain Vs Drift groups (320mm)

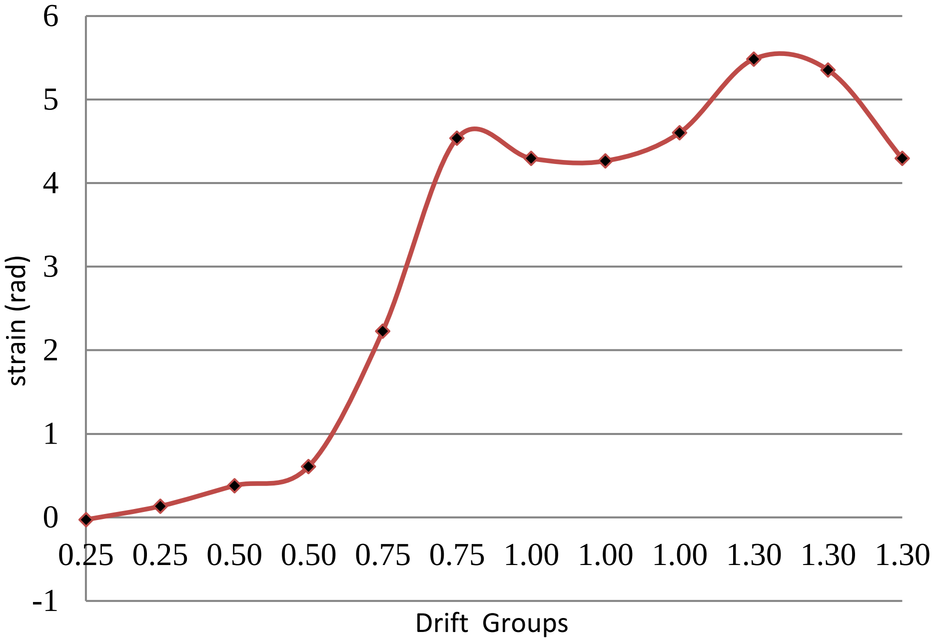

Figure 5.127: CSS-20-ECompression steel hoop strain Vs Drift groups (325mm)

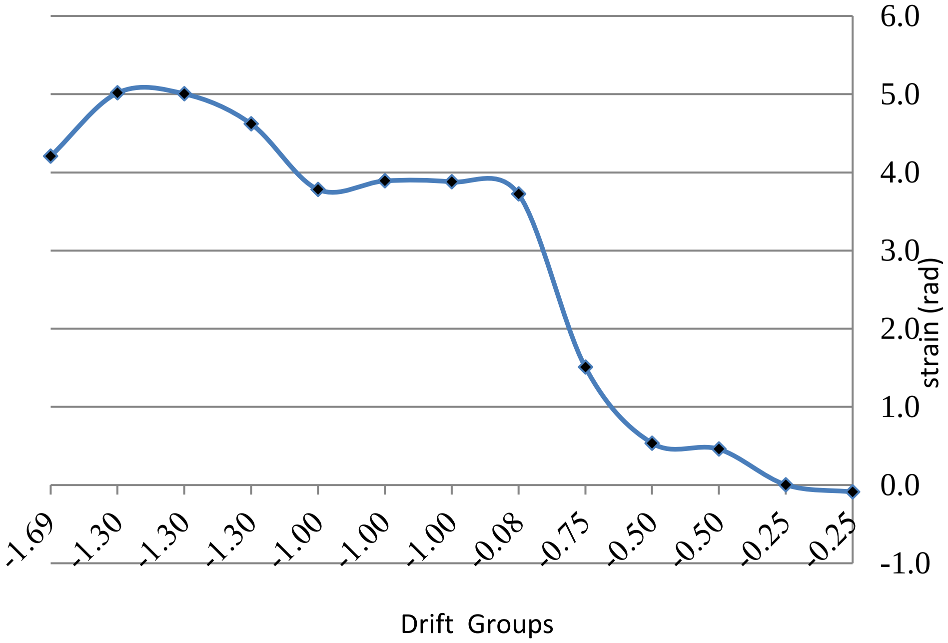

Figure 5.128: CSS-20-E Compression steel hoop strain Vs Drift groups (325mm)

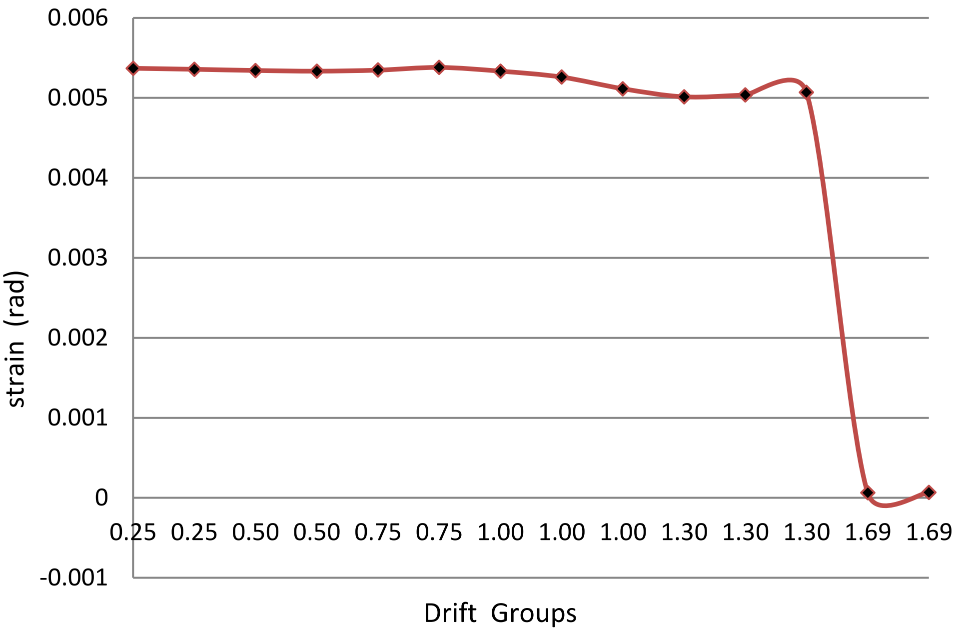

Figure 5.129: CSS-20-ECompression shear strain (rad) Vs Drift groups (Diagonal LVDTs 4-27)

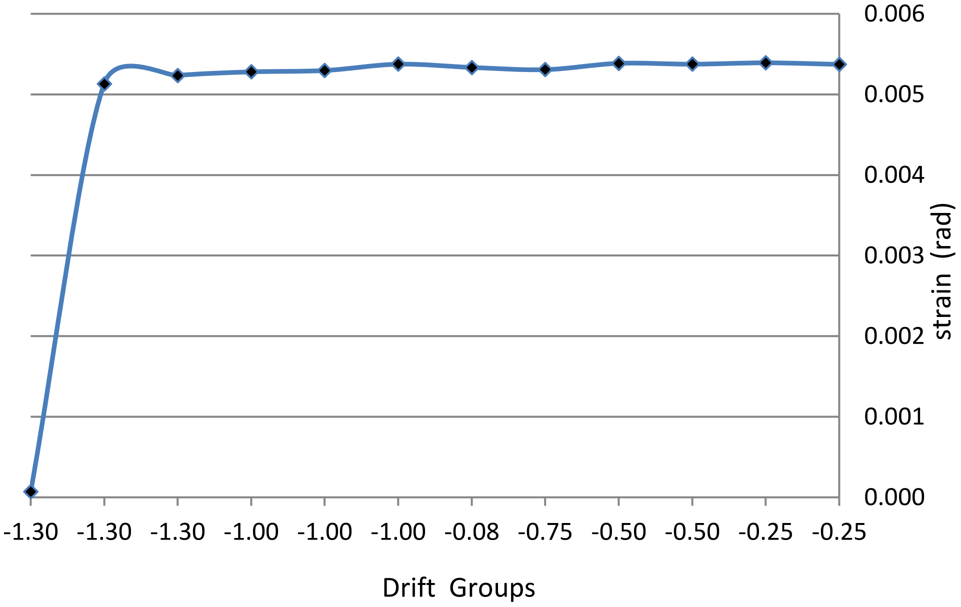

Figure 5.130: CSS-20-ECompression shear strain (rad) Vs Drift groups (Diagonal LVDTs 4-27)

3. Specimen CSS -40-E:

CSS -40-E was subjected to a constant compressive axial load of 670 KN (0.4f'c Ag, where f'c = cylinder compressive concrete strength, and Ag = gross cross sectional area) and cyclic increments of lateral displacements as described in **Figure 4.13**. The theoretical nominal yield displacement was calculated to be equal 13.85 mm. it was noticed the same inclination of the horizontal actuator load cell with an angel
ɵ = 1'17'52. This was taken into consideration in the force and drift post processing.

During the first groups of displacement protocol which (0.25, 0.5 Δy) there were not any cracking. Starting the next displacement cycles of 0.75 Δy of the nominal yield displacement, flexure hairline cracks (width of less than 1mm.) developed near the bottom of the column.

The number of inclined cracks and the crack width on the faces parallel to the lateral loading direction increased as the number and magnitude of the displacement cycles increased. Small horizontal and inclined cracks on the faces perpendicular to the lateral loading direction (i.e., on the east and west faces), started to span the width of the column. These relatively straight continuous horizontal and diagonal cracks opened and closed during each cycle.

During displacement cycles equal to theoretical Δy displacement cracks increased opening, relatively large crack openings were observed suggesting slip of the longitudinal reinforcing bars from the base at Δy.

Figure 5.13 4shows 1.5 mm wide crack opened between the flexural tension side of the column base and the column at peak lateral displacement.

During displacement cycles to the nominal yield displacement (Δ = 1.7 Δy.), more in wide crack opening without any new cracks. Faces perpendicular to the loading direction, the width of the existing diagonal cracks increased from two sides.

At the beginning of cycle at the displacement level of (2.2 Δ y), luxation of the cover concrete was observed in the bottom corner and the horizontal load started to decrease after reaching the peak previous. In the flexural compression zones, at the bottom of the column, flaking and spalling of concrete were observed.

As the number of cycles increased, after the concrete cover crashed and the steel bars appeared, there was not no buckling of steel bars; however the lower cracks were deep in the column around the cross section as shown in **Figure 5.135**. After ending all cycles, the specimen was loaded for 80% of its capacity with 1370 KN without any axial failure.

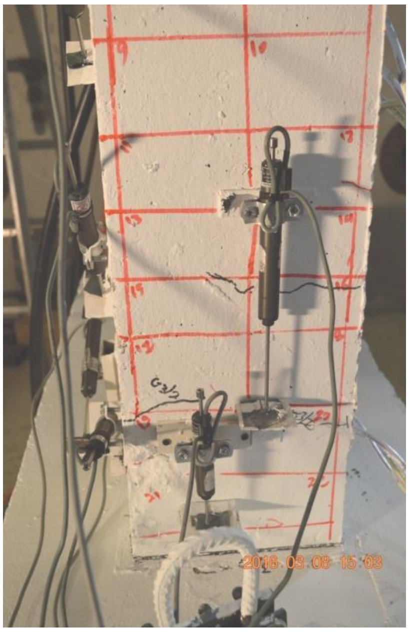

Figure 5.131: Specimen CSS 40-E at initial cracking (1 Δy)

Figure 5.132: CSS 40-E start slipping at ∆y

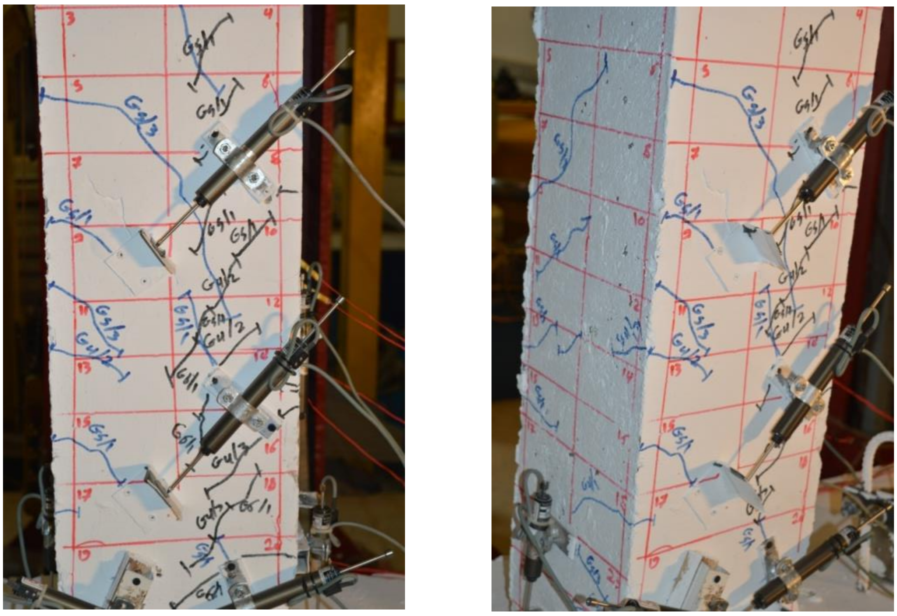

Figure 5.133: CSS 40-Eperpendicular side at 1.3 ∆y

Figure 5.134: CSS 40-ECrushing concrete cover (1.69 ∆y)

Figure 5.135: CSS 40-E Opening cracks2.856 ∆y

Figure 5.136: CSS 40-ECrushing concrete cover (3.71 ∆y)

Figure 5.137: CSS 40-ECrushing column concrete cover (4.8∆y)

Figure 5.138: CSS 40-E failure at the end of the test

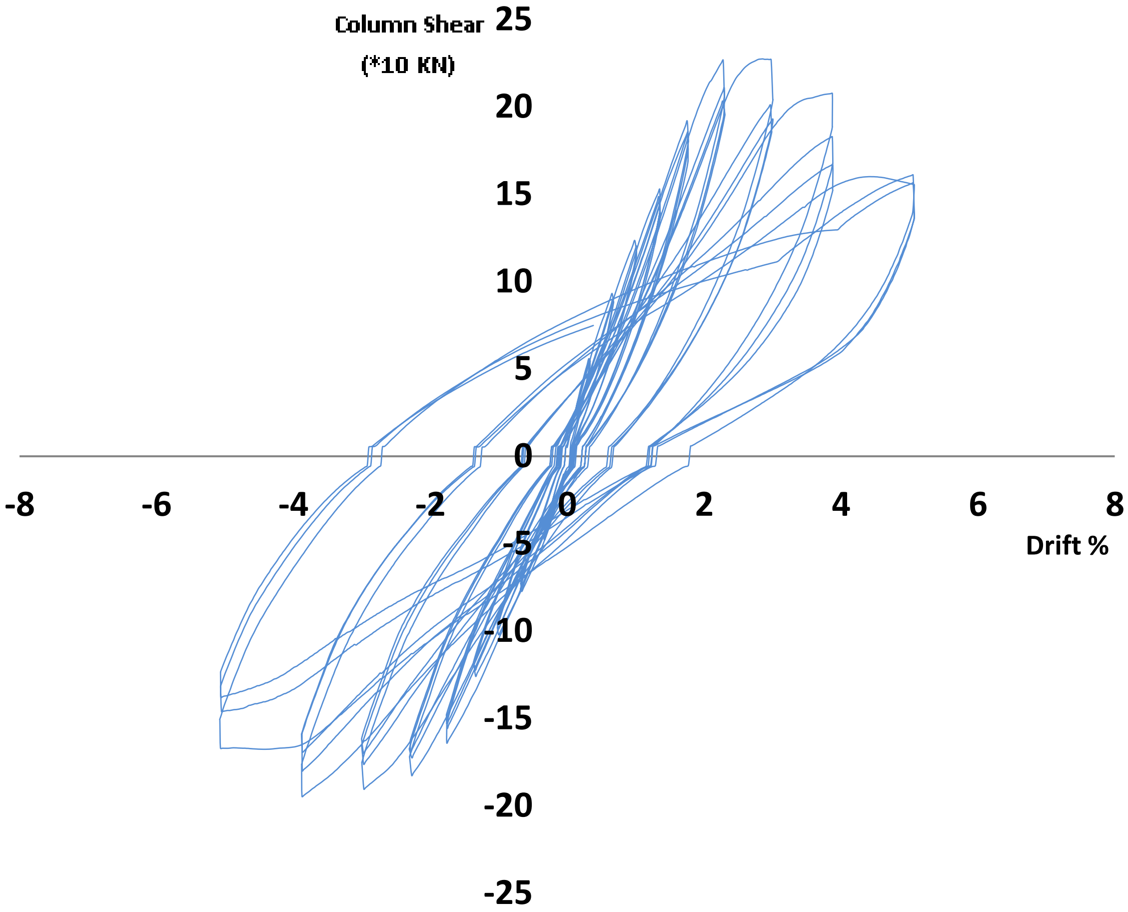

Figure 5.139: Shear force-drift hysteresis response of specimen CSS 40-E

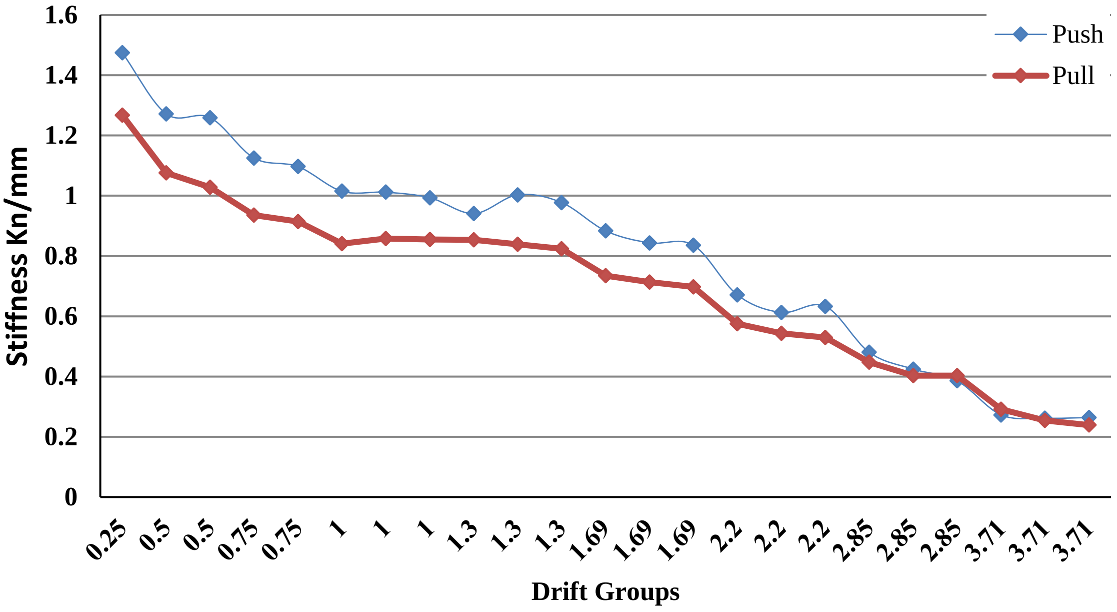

Figure 5.140: Peak to Peak stiffness of specimen CSS 40-E

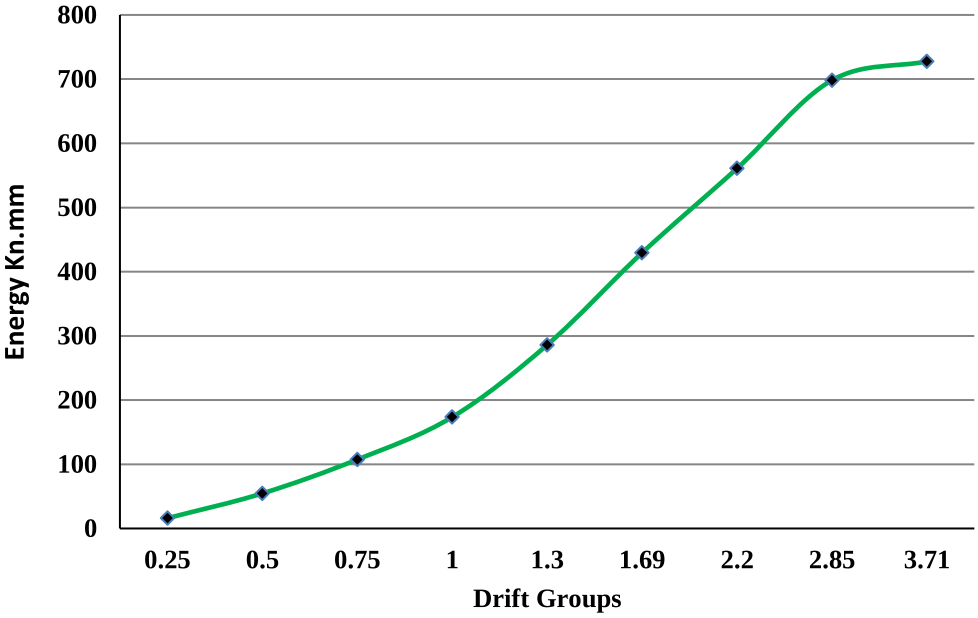

Figure 5.141: Peak to peak Energy of specimen CSS 40-E

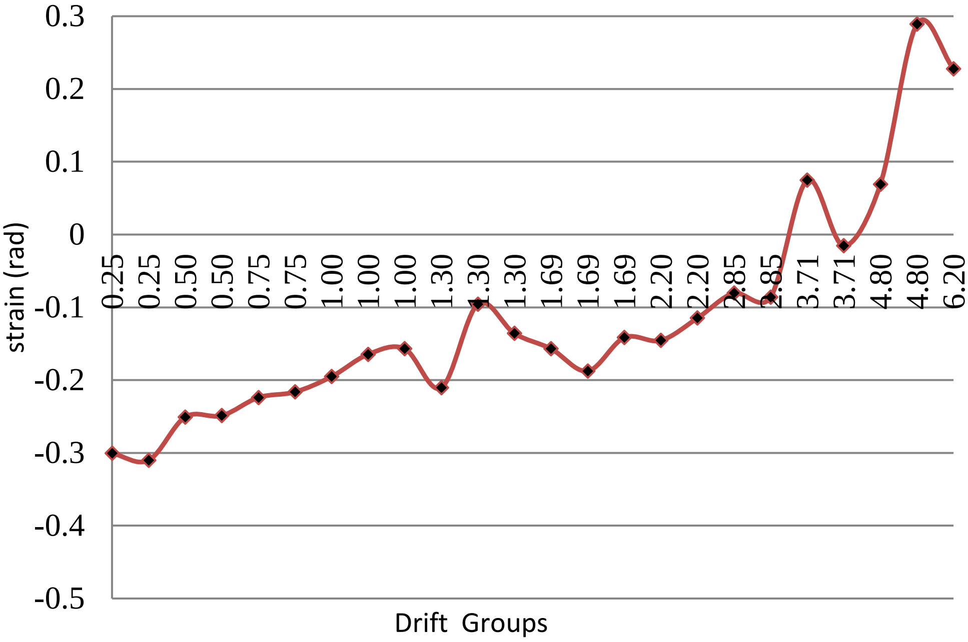

Figure 5.142: **CSS 40-ECompression Web steel strain Vs Drift groups (320mm)**

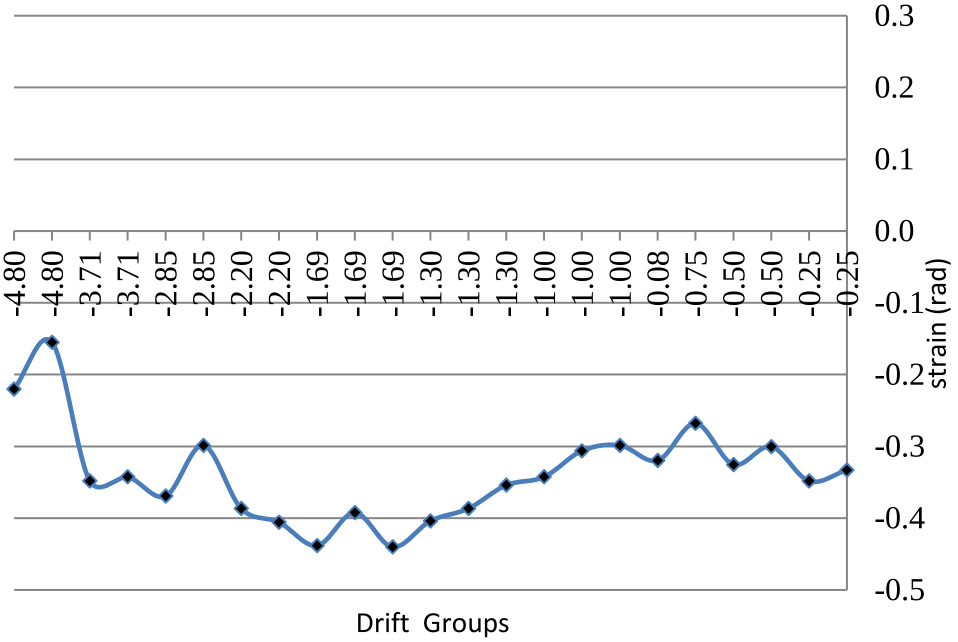

Figure 5.143: **CSS 40-ETension Web steel strain Vs Drift groups (320mm)**

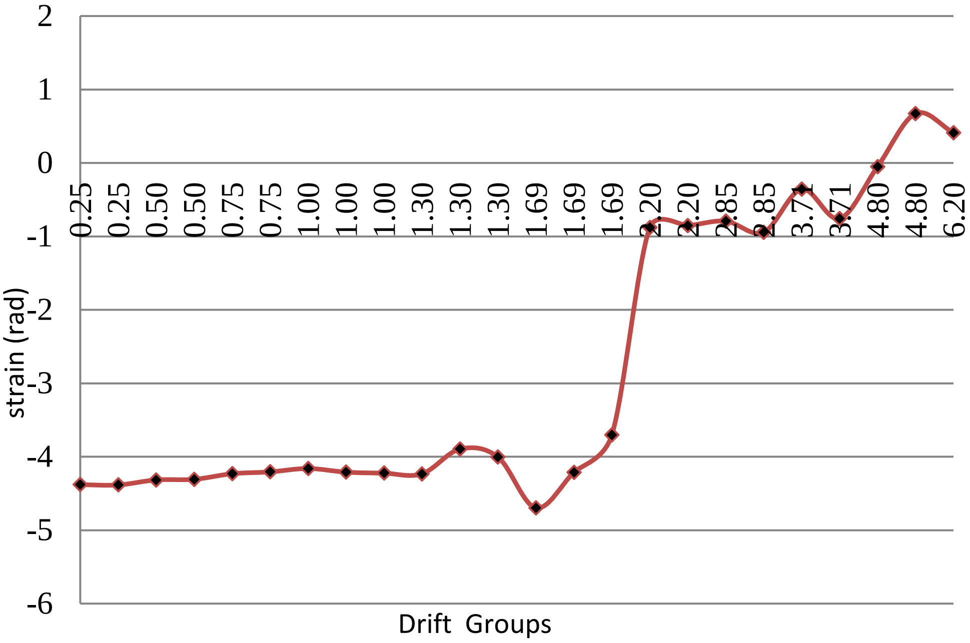

Figure 5.144: CSS 40-ECompression steel hoop strain Vs Drift groups (325mm)

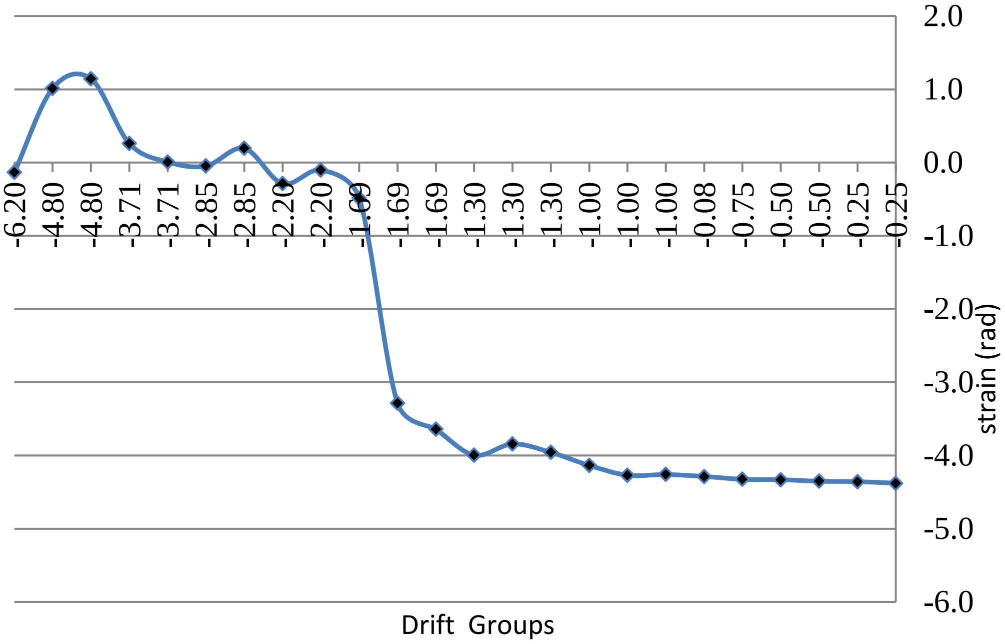

Figure 5.145: CSS 40-E Compression steel hoop strain Vs Drift groups (325mm)

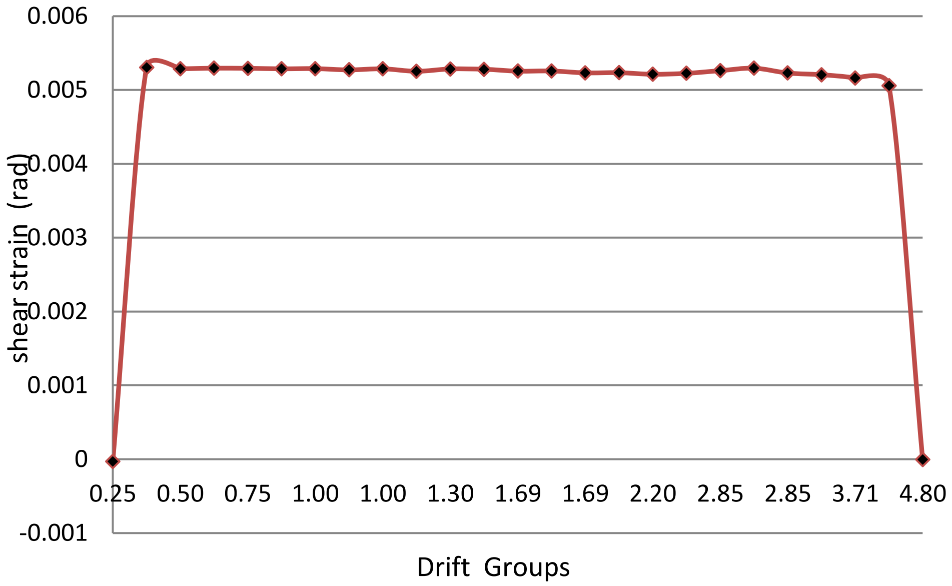

Figure 5.146: CSS 40-ECompression shear strain (rad) Vs Drift groups (Diagonal LVDTs 4-27)

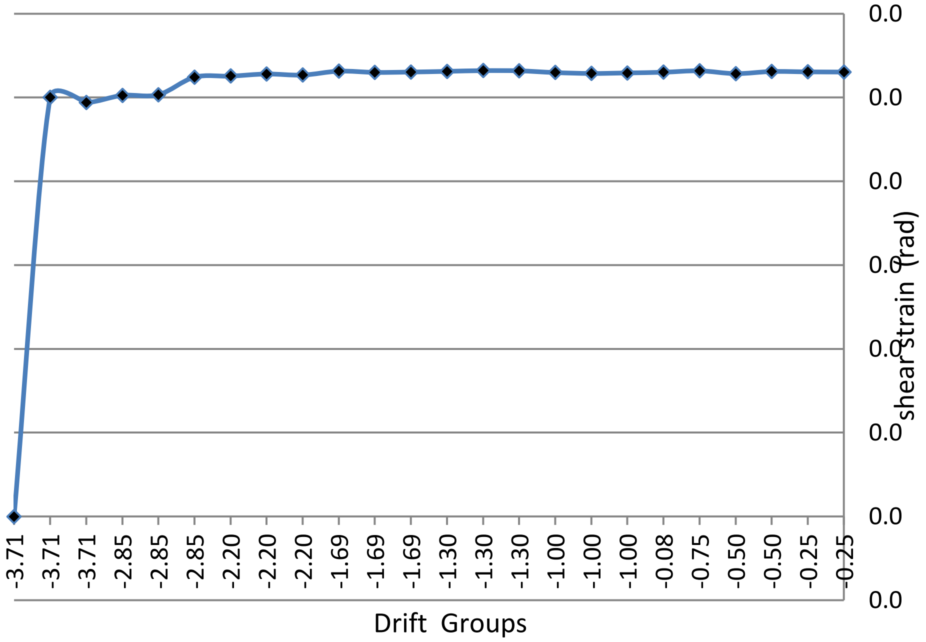

Figure 5.147: CSS 40-E Compression shear strain (rad) Vs Drift groups (Diagonal LVDTs 4-27)

4. Specimen CSS -60-E

CSS -60-E was subjected to a constant compressive axial load of 1400 KN (0.6 f’c Ag, where f’c = cylinder compressive concrete strength, and Ag = gross cross sectional area) and cyclic increments of lateral displacements as described in **Figure4.13**. The theoretical nominal yield displacement was calculated to be equal 13.22 mm. it was noticed the same inclination of the horizontal actuator load cell with an angel ɵ = 1’17’52.This was taken into consideration in the force and drift post processing.

During the first groups of displacement protocol (0.25 Δy) there was no cracking. Starting the following displacement cycles of 0.5 Δy of the nominal yield displacement, flexure hairline cracks (width of less than 1mm.) developed near the bottom of the column.

The number of inclined cracks and the crack width on the faces parallel to the lateral loading direction increased as the number and magnitude of the displacement cycles increased. Small horizontal and inclined cracks on the faces perpendicular to the lateral loading direction (i.e., on the east and west faces), started to span the width of the column. These relatively straight continuous horizontal cracks opened and closed during each cycle. During displacement cycles equal to theoretical 1.3 Δy displacement cracks increased opening, relatively large crack openings were observed suggesting slip of the longitudinal reinforcing bars from the base at Δ = 2.2 Δy. **Figure5.152** shows 2.5 mm wide crack opened between the flexural tension side of the column base and the column at peak lateral displacement.

During displacement cycles to the nominal yield displacement (Δ = Δy.), more in wide crack opening without any new cracks. Faces perpendicular to the loading direction, the width of the existing diagonal cracks increased from two sides.

At the beginning of cycling at the displacement level of (2.2 Δ y), when the specimen was loaded the first time (push or eastward direction), **Figure5.152**, luxation of the cover concrete was observed in the bottom northeast corner and the horizontal load started to decrease after reaching the previous peak.

Specimen CSS-60-E was tested by two conditions. The first loading condition was with axial load ratio 60 % until reaching the peak drift, then second part was loading without axial load to get the degradation curve of the specimen,

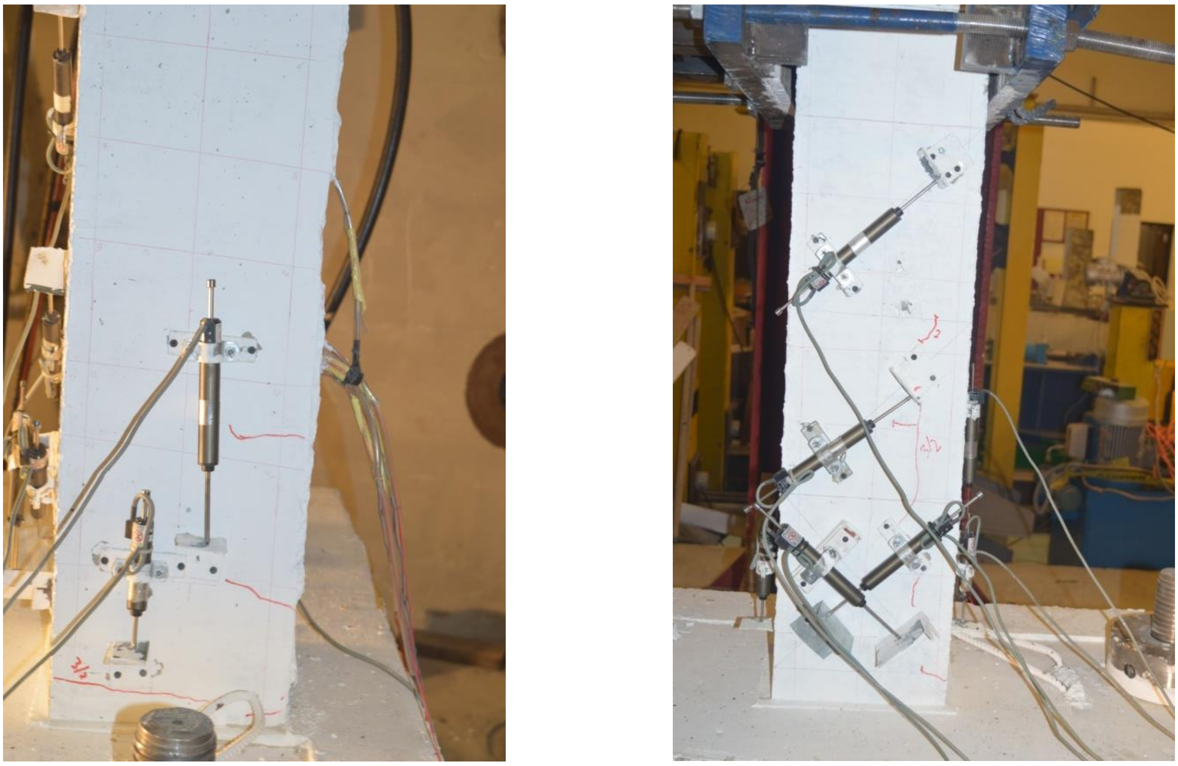

Figure 5.148: Specimen CSS-60-E at initial cracking (0.5 Δy)

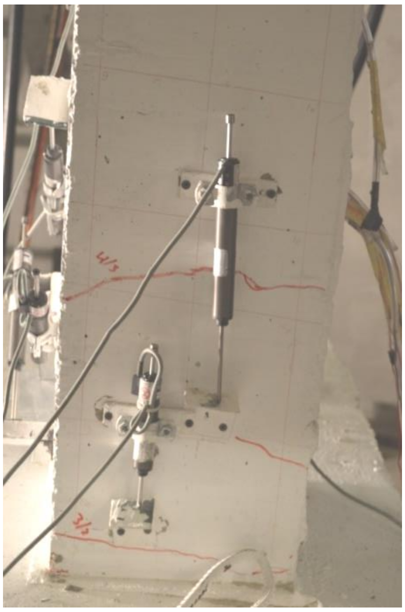

Figure 5.149: CSS 60EStart slipping at2.2∆y

Figure 5.150: CSS-60-EPerpendicular side 1.3∆y

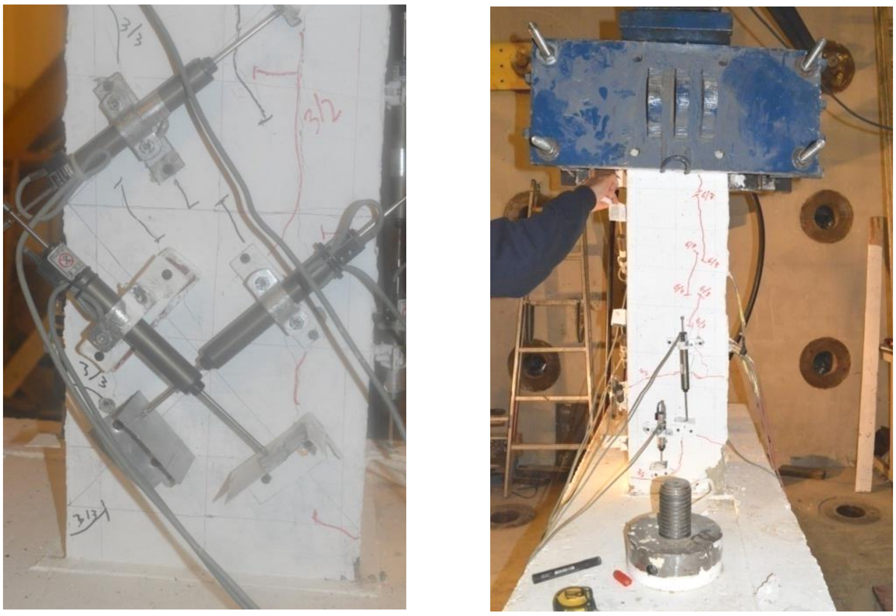

Figure 5.151: CSS-60-ECrushing concrete cover (1.3 ∆y)

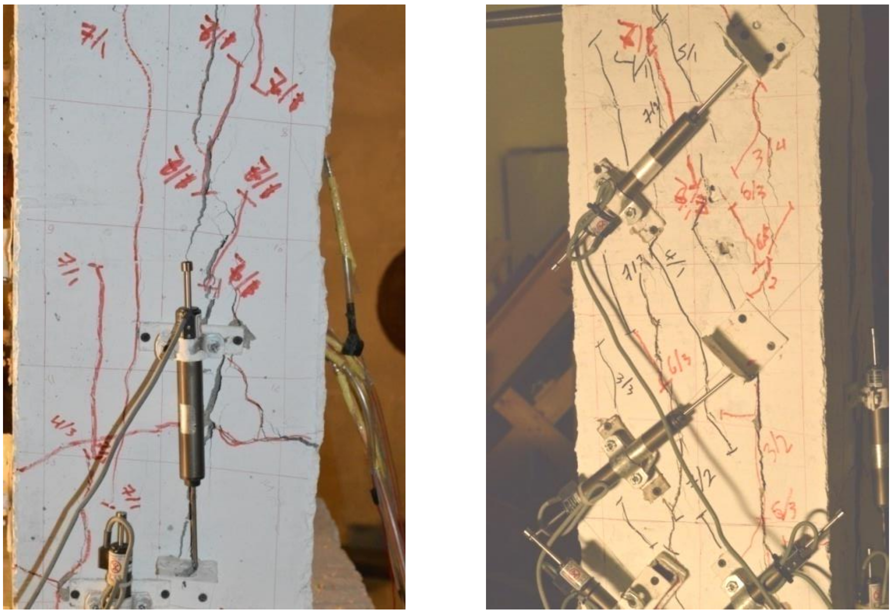

Figure 5.152: CSS-60-E Cracks began to be deeper at (2.2∆y)

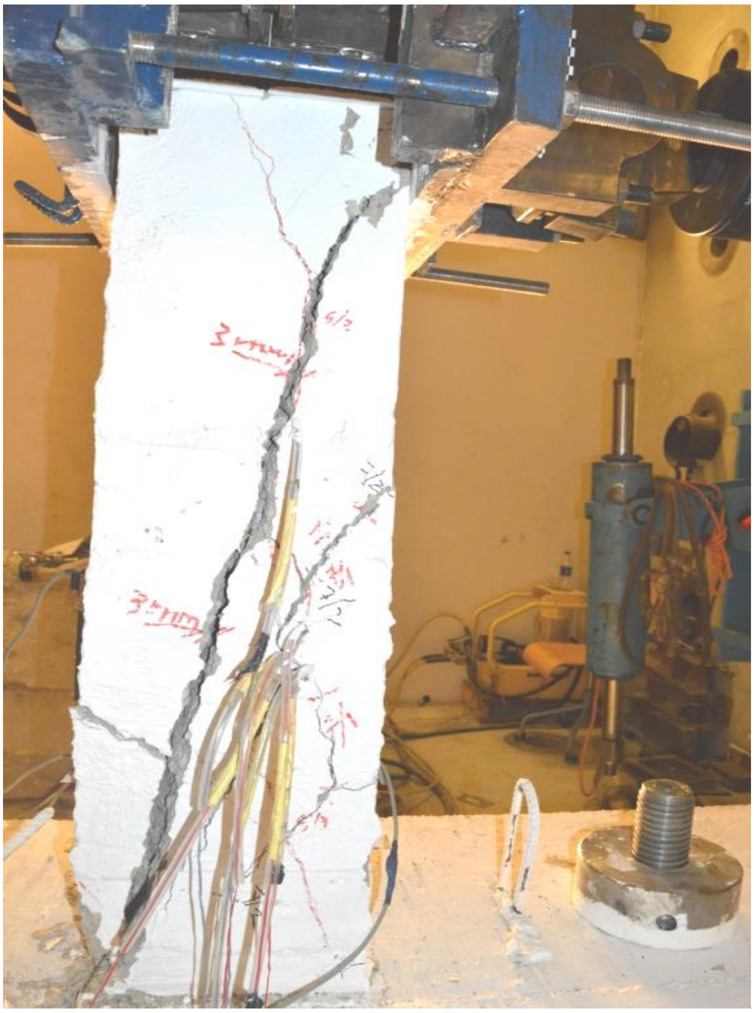

Figure 5.153: CSS-60-E failure at the end of the test

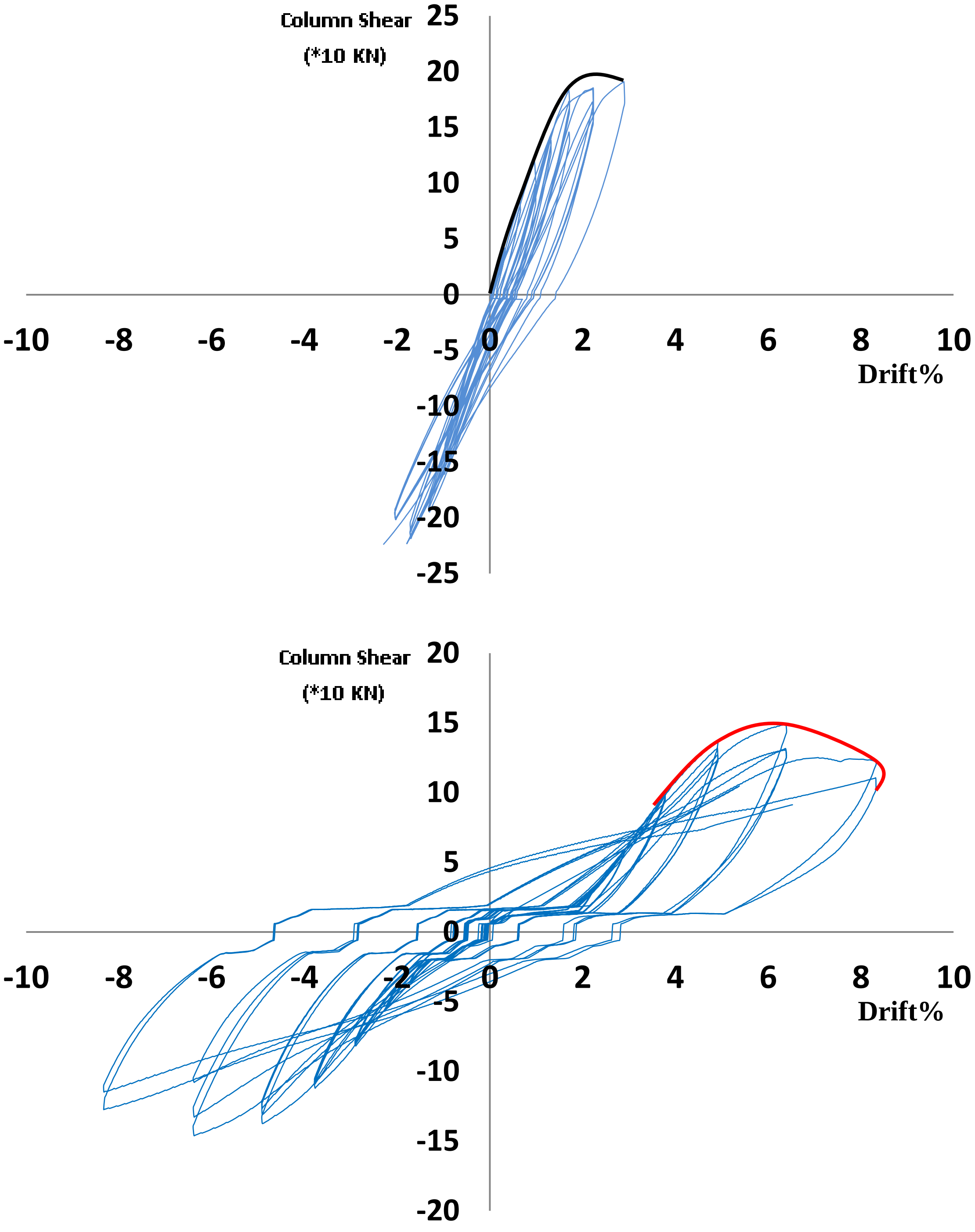

Figure 5.154: Shear force-drift hysteresis response of specimen CSS 60-E

Figure 5.144 shows two shear force drift hysteresis response of specimen CSS60-E. During the test, it was noted a high inclination of axial load cell affected unaccepted eccentricity. It was decided to complete the test with the same loading protocol but without axial load to get the curve slope degradation. The red hysteresis show drift with the response under axial load of 60%, but the blue hysteresis show the drift without axial load, only horizontal load.

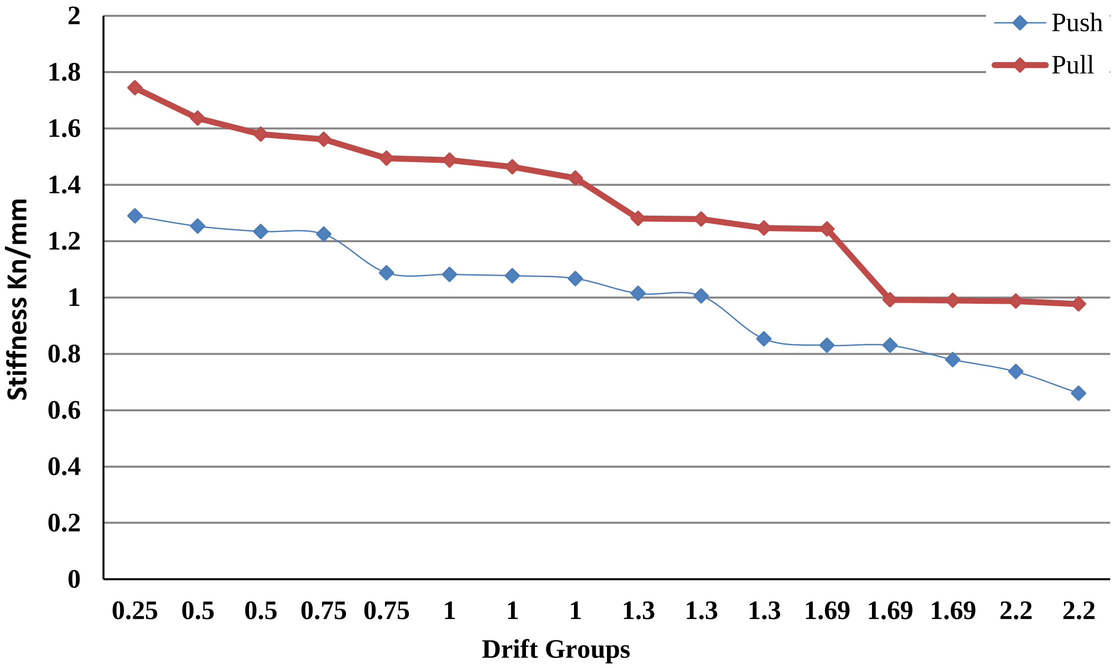

Figure 5.155: Peak to Peak stiffness of specimen CSS-60-E

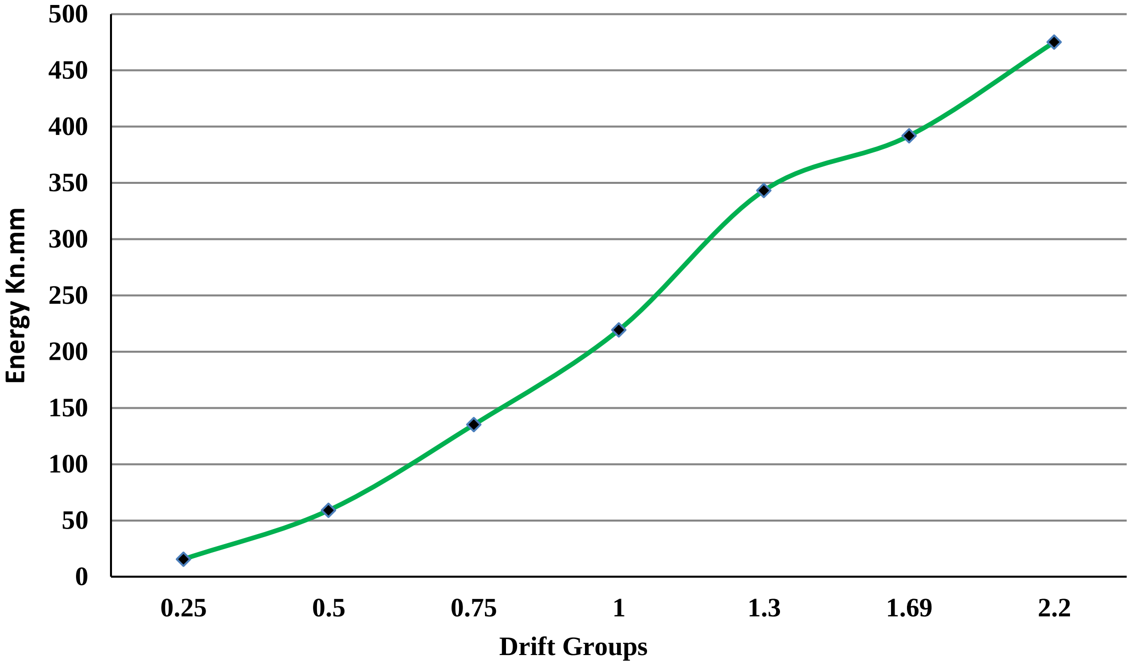

Figure 5.156: Peak to peak Energy of specimen CSS 60-E

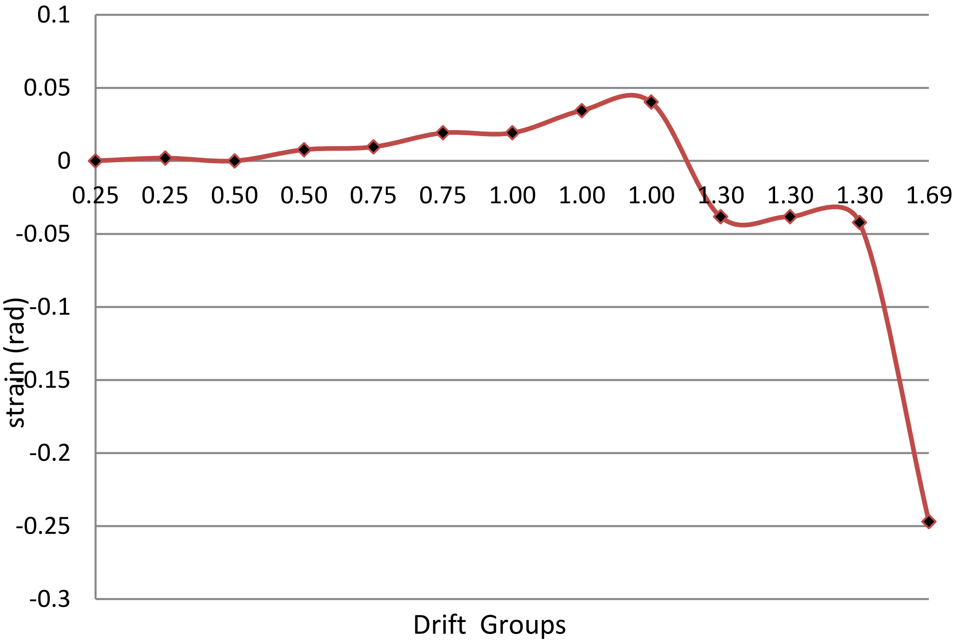

Figure 5.157: CSS-60-ECompression Web steel strain Vs Drift groups (320mm)

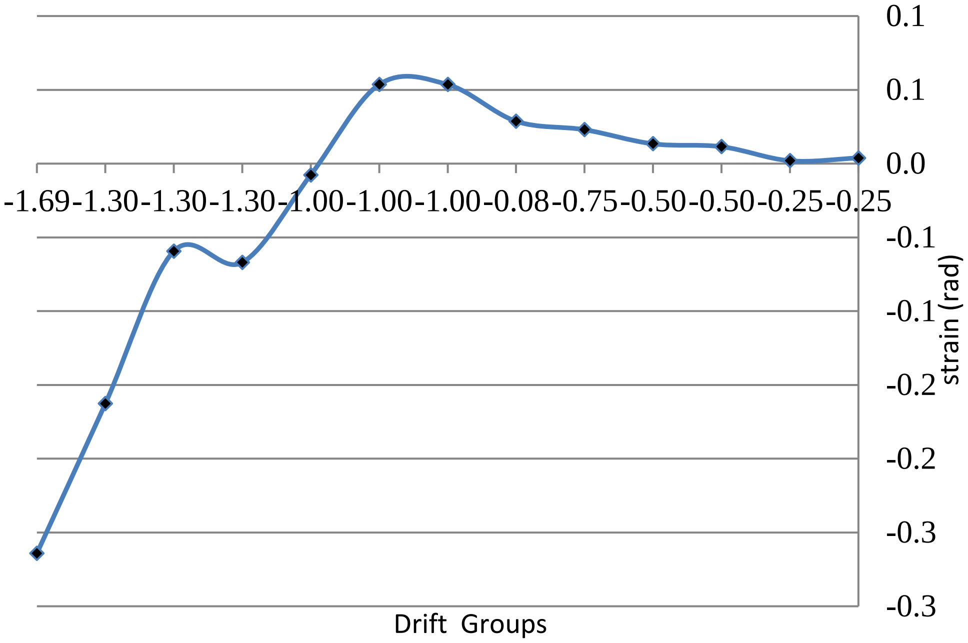

Figure 5.158: CSS-60-ETension Web steel strain Vs Drift groups (320mm)

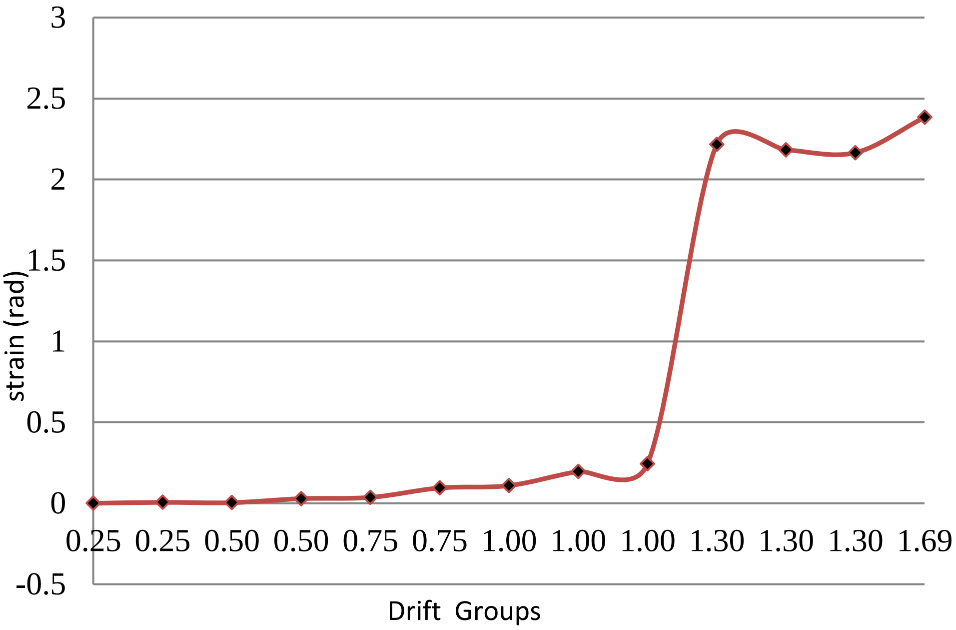

Figure 5.159: CSS-60-ECompression steel hoop strain Vs Drift groups (325mm)

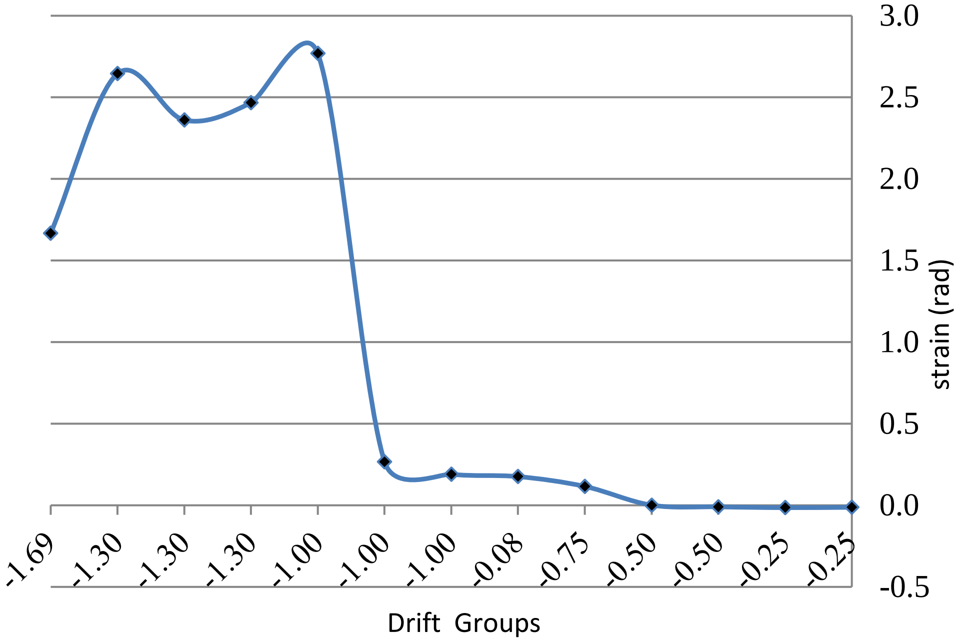

Figure 5.160: CSS-60-ECompression steel hoop strain Vs Drift groups (325mm)

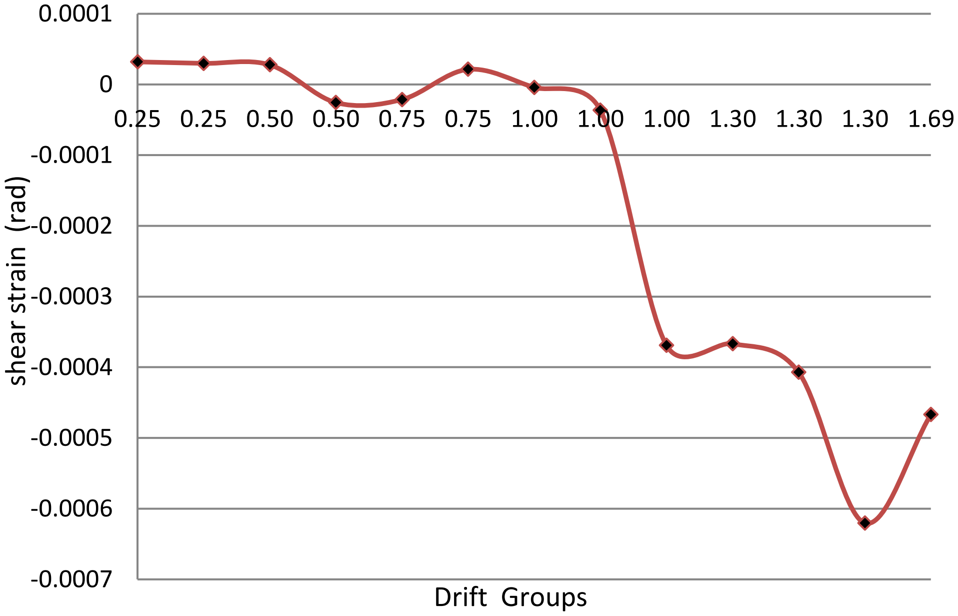

Figure 5.161: CSS-60-ECompression shear strain (rad) Vs Drift groups (Diagonal LVDTs 4-27)

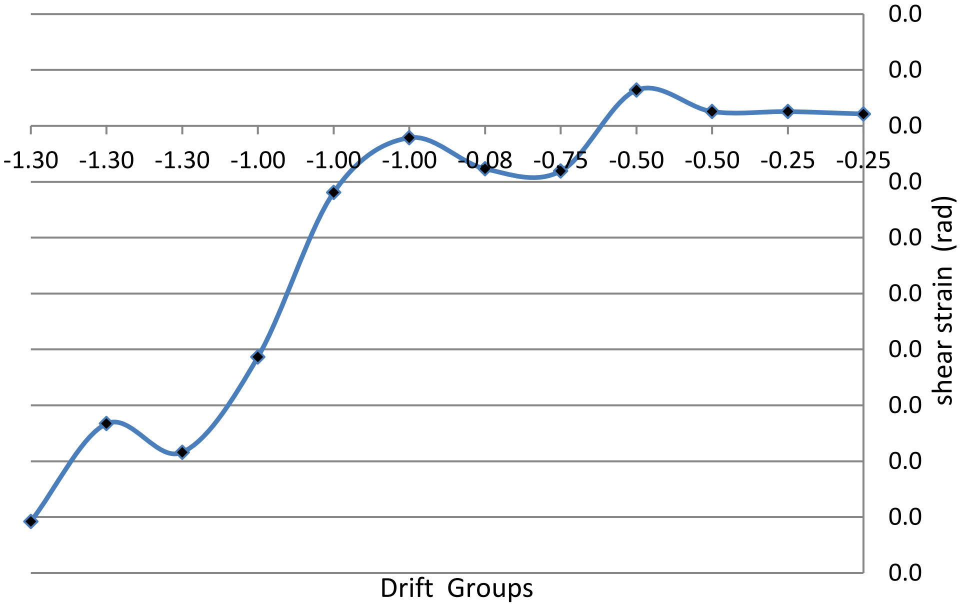

Figure 5.162: CSS-60-ECompression shear strain (rad) Vs Drift groups (Diagonal LVDTs 4-27)

5. Specimen CSS -80-E

CSS -80-Ewas subjected to a constant compressive axial load of 1300 KN (0.8 f'c Ag, where f'c = cylinder compressive concrete strength, and Ag = gross cross sectional area) and cyclic increments of lateral displacements as described in **Figure 4.13**. The theoretical nominal yield displacement was calculated to be equal 13.12 mm. it was noticed the same inclination of the horizontal actuator load cell with an angel ɵ = 1'17'52.This was taken into consideration in the force and drift post processing.

During the first groups of displacement protocol which (0.25Δy) there were not any cracking. Starting end of the next displacement cycles of 0.5 Δy of the nominal yield displacement, flexure hairline cracks (width of less than 1mm.) developed near the bottom of the column.

The number of inclined cracks and the crack width on the faces parallel to the lateral loading direction increased as the number and magnitude of the displacement cycles increased. Small horizontal and inclined cracks on the faces perpendicular to the lateral loading direction (i.e., on the east and west faces), started to span the width of the column. These relatively straight continuous shear cracks opened and closed during each cycle.

During displacement cycles equal to theoretical Δy displacement cracks increased opening, relatively large crack openings were observed suggesting slip of the longitudinal reinforcing bars from the base at Δ = Δy.

Figure5.167 shows 2 mm wide crack opened between the flexural tension side of the column base and the column at peak lateral displacement.

During displacement cycles to the nominal yield displacement (Δ = 1.3 Δy.), more in wide crack opening without any new cracks. Faces perpendicular to the loading direction, the width of the existing diagonal cracks increased from two sides especially the pouring side due to non-compacted concrete cover well.

At the beginning of cycling at the displacement level of (2.2 Δ y), when the specimen was loaded the first time (push or eastward direction, **Figure 5.167**), luxation of the cover concrete was observed in the bottom northeast corner and the horizontal load started to decrease after reaching the peak previous. In the flexural compression zones, at the bottom of the column, flaking and spalling of concrete were observed.

Specimen started to twist around its vertical axis due to losing the concrete capacity to carry load in the beginning of 3.71 Δ y. As the number of cycles increased, the concrete cover crashed and the steel bars appeared.

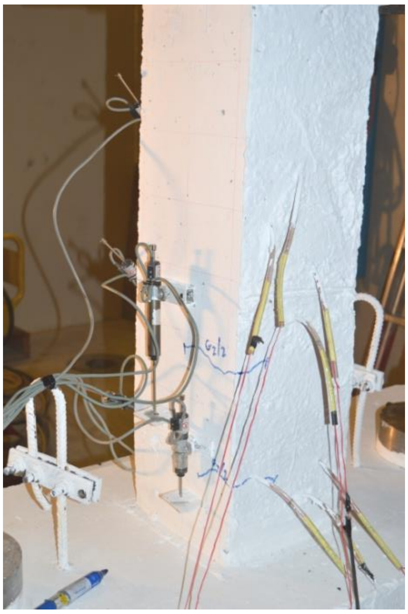

Figure 5.163: Specimen CSS-80-E at initial cracking (0.5 Δy)

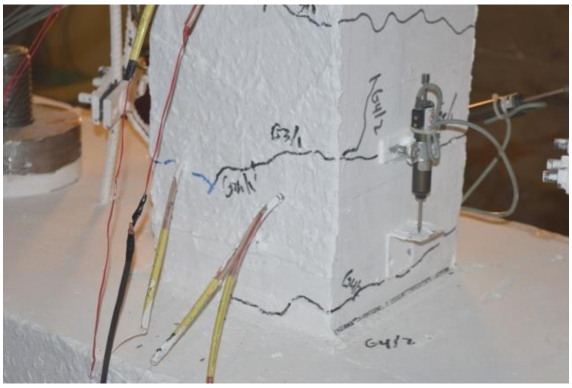

Figure 5.164: CSS-80-EStart slipping at Δy

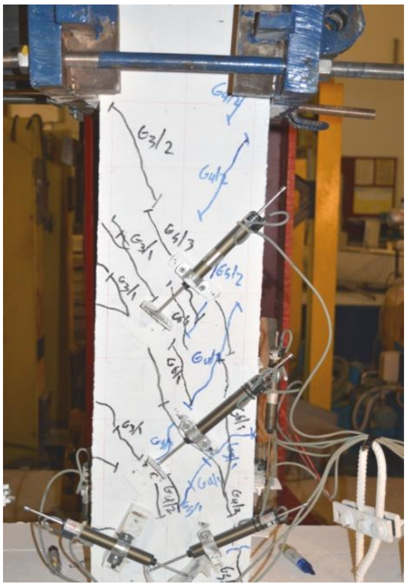

Figure 5.165: CSS-80-EPerpendicular side of 1.7 Δy

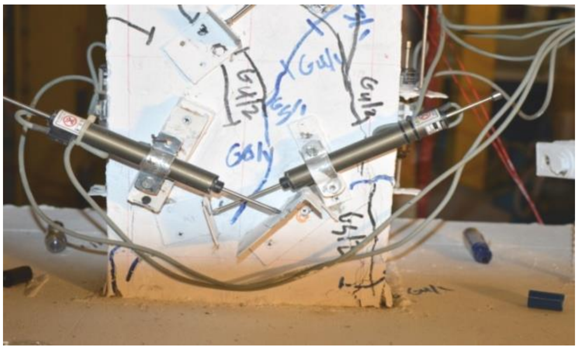

Figure 5.166: CSS-80-EOpening cracks near to base 5 Δy

Figure 5.167: CSS-80-ECrushing concrete cover mid cycle of (2.2 ∆y)

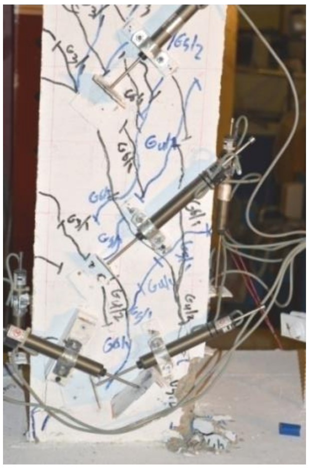

Figure 5.168: CSS-80-ECrushing concrete cover (2.85 ∆y)

Figure 5.169: CSS-80-ECrushing column concrete cover at (2.85∆y)

Figure 5.170: CSS-80-E failure end of the test

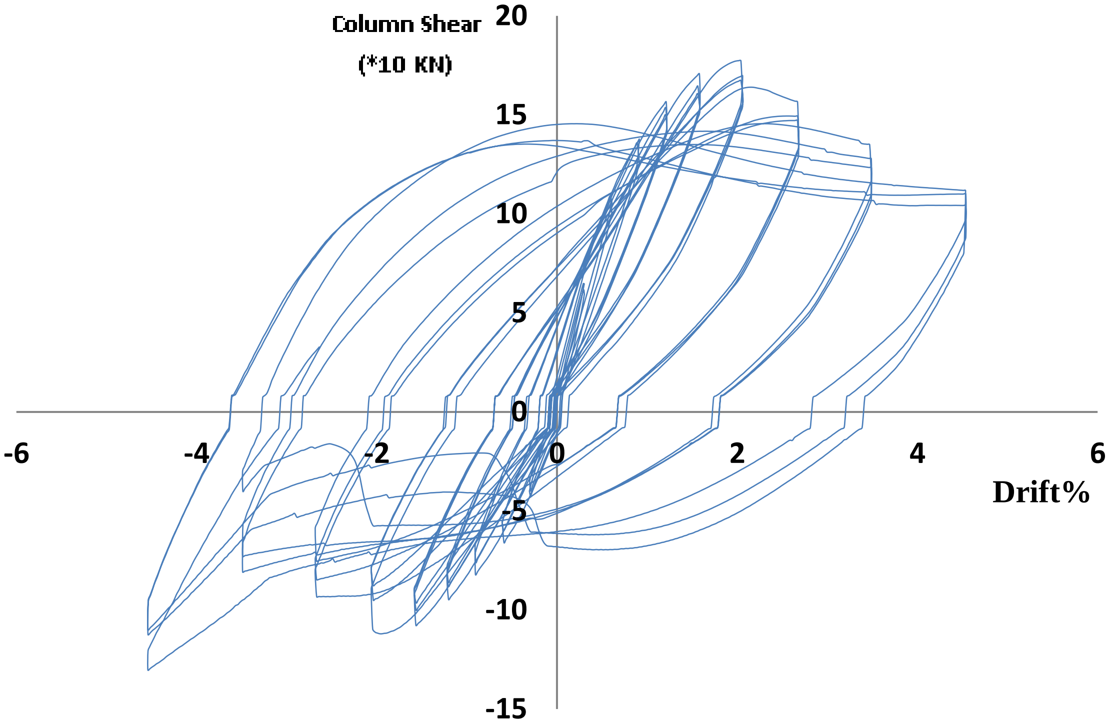

Figure 5.171: Shear force-drift hysteresis response of specimen CSS-80-E

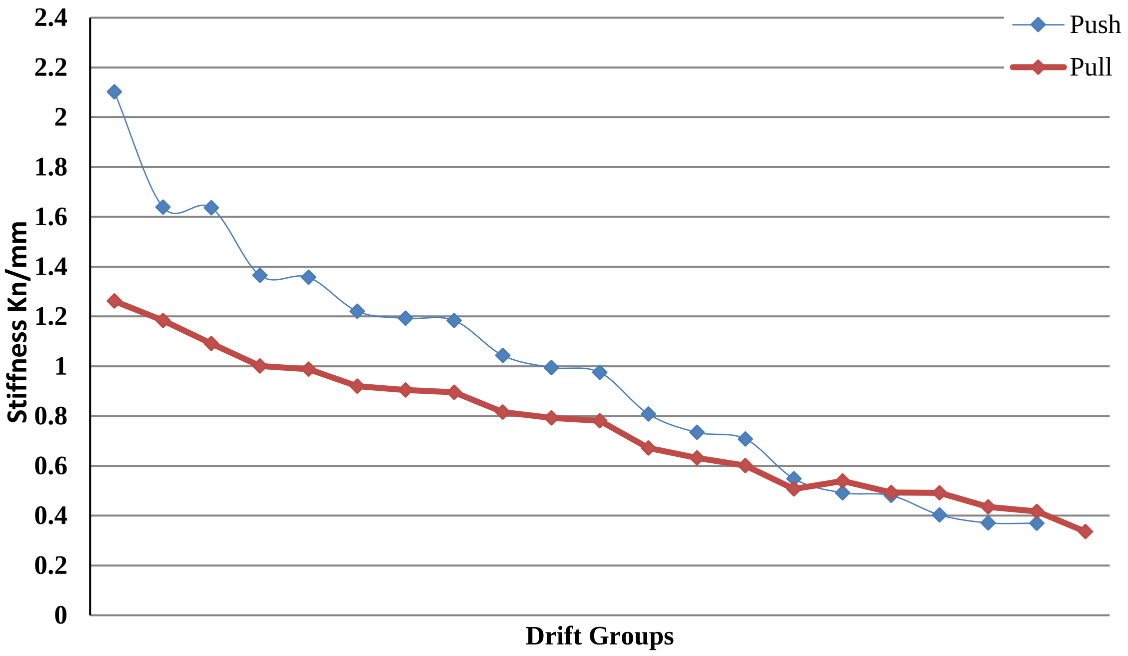

Figure 5.172: Peak to Peak stiffness of specimen CSS 80-E

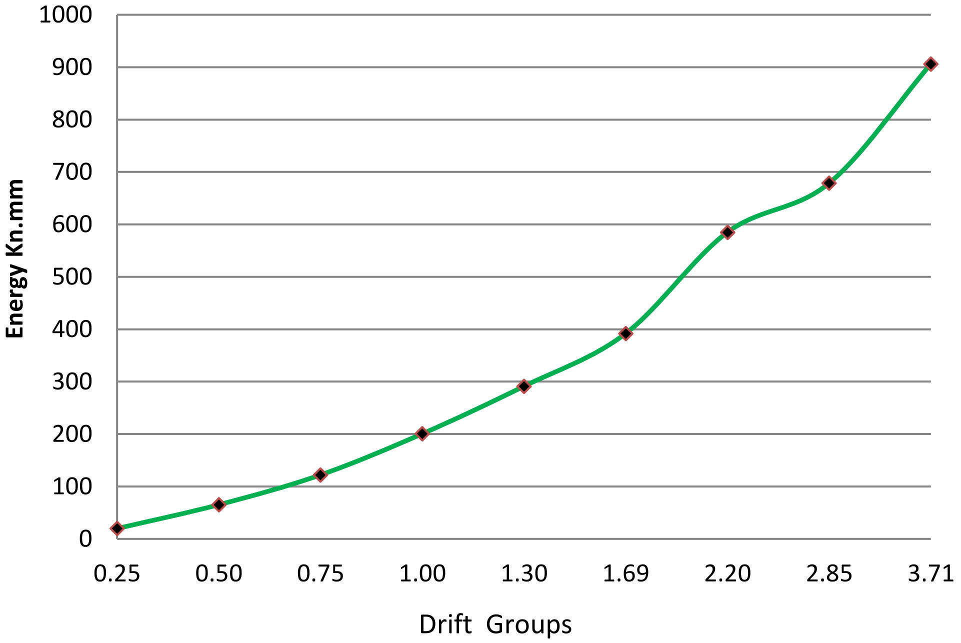

Figure 5.173: Peak to peak Energy of specimen CSS 80-E

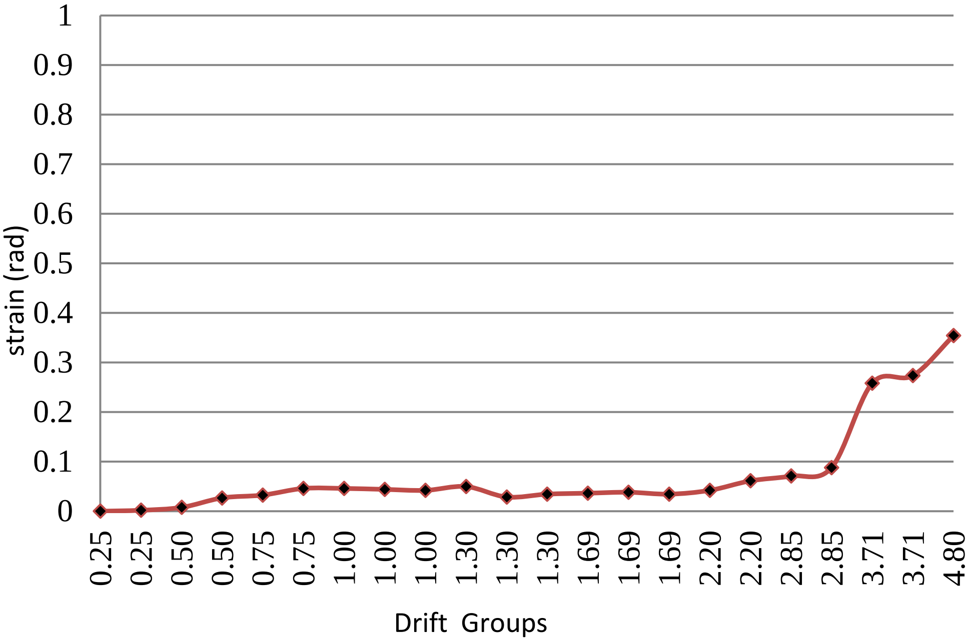

Figure 5.174: CSS-80-ECompression Web steel strain Vs Drift groups (320mm)

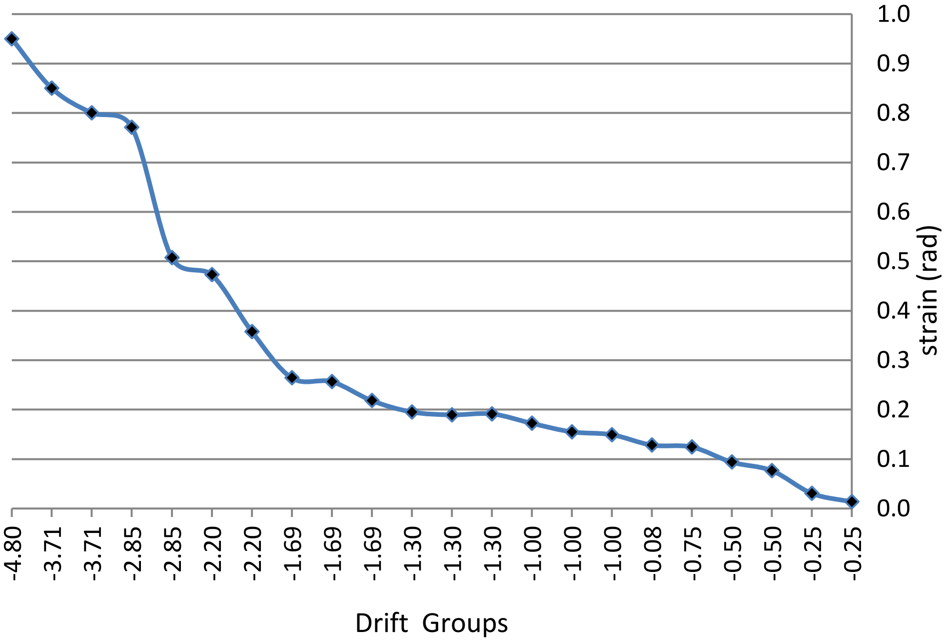

Figure 5.175: CSS-80-ETension Web steel strain Vs Drift groups (320mm)

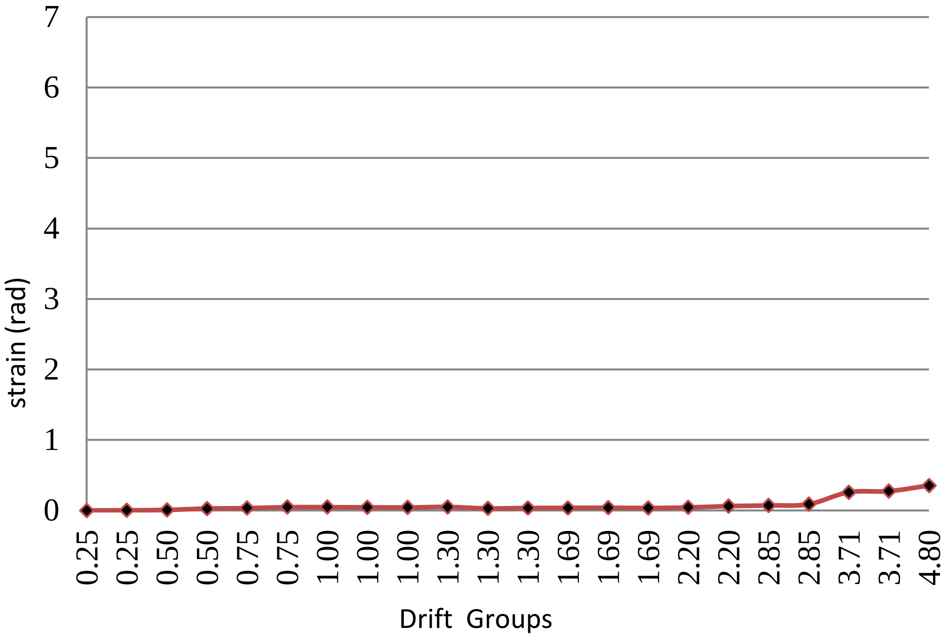

Figure 5.176: CSS-80-ECompression steel hoop strain Vs Drift groups (325mm)

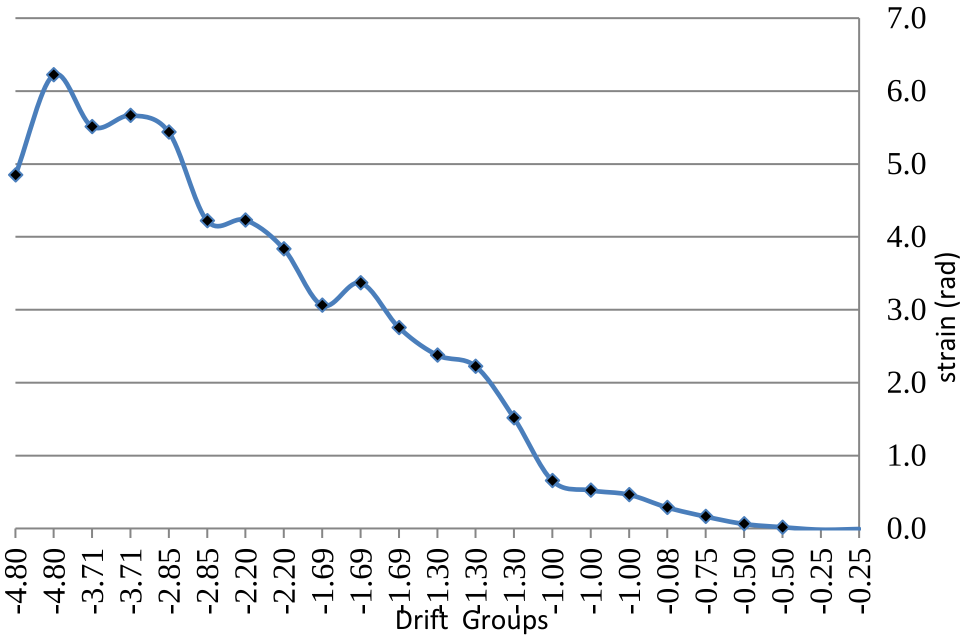

Figure 5.177: CSS-80-ECompression steel hoop strain Vs Drift groups (325mm)

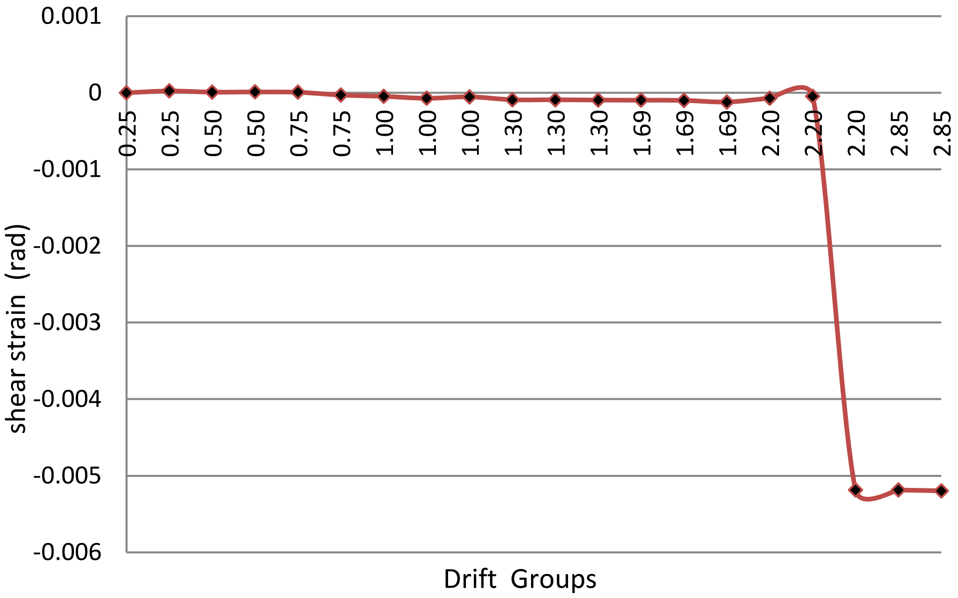

Figure 5.178: CSS-80-ECompression shear strain (rad) Vs Drift groups (Diagonal LVDTs 4-27)

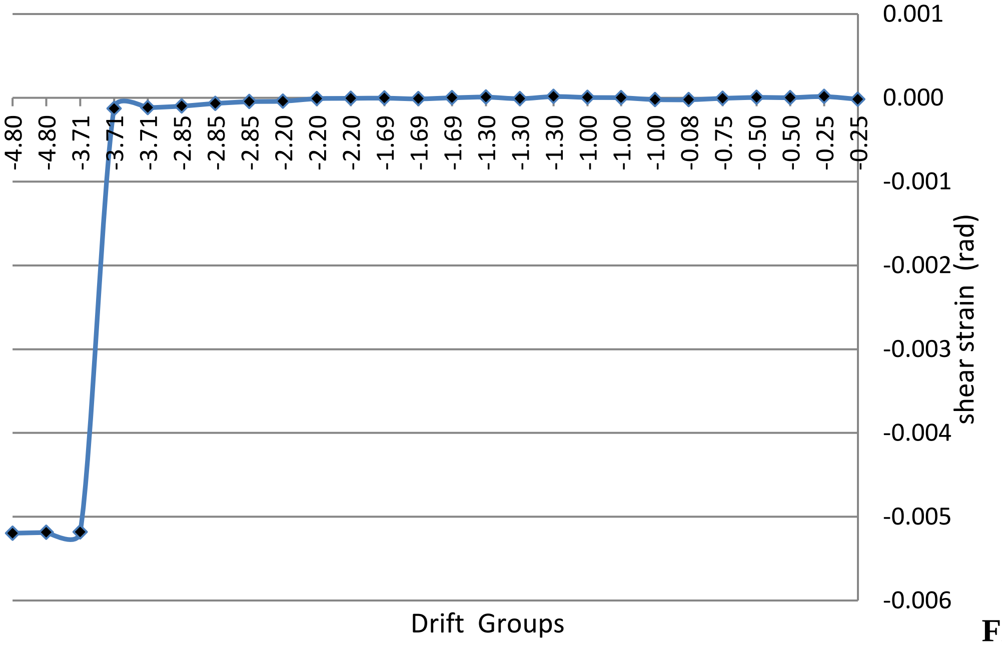

Figure 5.179: CSS-80-ECompression shear strain (rad) Vs Drift groups (Diagonal LVDTs 4-27)

Table 5.3: Qualitative damage description

Cycle	Specimen 1 CSS 15-E	Specimen2 CSS 20-E	Specimen 3 CSS 40-E	Specimen 4 CSS 60-E	Specimen 5 CSS 80-E
0.25 Δy	No cracks	No cracks	No cracks	No cracks	No cracks
0.5 Δy	No cracks	No cracks	No cracks	Hair cracks	Hair cracks
0.75 Δy	Hair cracks	Hair cracks	Hair cracks	Cracking	Cracking
Δy	Yielding and cracking	Yielding and cracking	Slipy and cracking	Slipy and cracking	Slipy and cracking
1.3 Δy	Slipy and cracking	Slipy and cracking	Yielding and cracking	Cracking	Yielding and cracking
1.96 Δy	Opening cracks and no new cracks	Opening cracks & stopping create new cracks	Deeper cracking Shear cracks	Opening cracks and no new cracks	Opening cracks and no new cracks
2.2 Δy	Deeper cracking	Deeper cracking	Deeper cracking	Crushing concrete	Deeper cracking
2.85 Δy	Crushing concrete	Crushing concrete	Crushing concrete	Failing Loading without axial load	Failing
3.72Δy	End of the test	Stopped horizontal loading	End of the test	The specimen twisted	The specimen twisted and the test ended
4.87Δy	---	Axial load 1850KN TEST End	------------	End of the test	------------

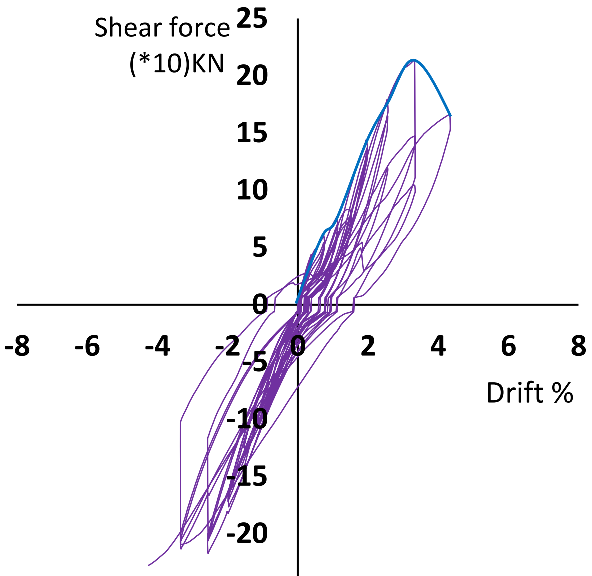

Figure 5.180: Specimen CSS 15 – E backbone curve

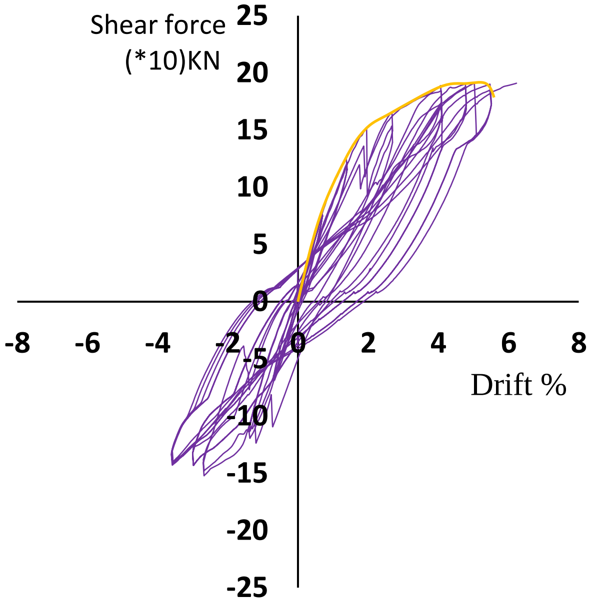

Figure 5.181: Specimen CSS 20-E backbone curve

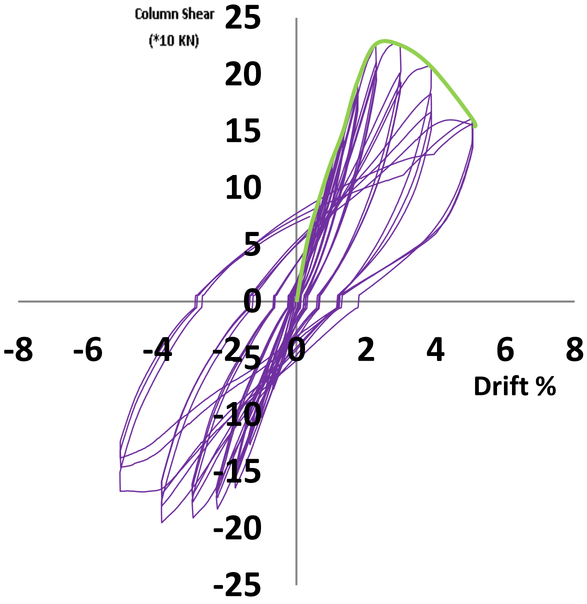

Figure 5.182: Specimen CSS 40-E backbone curve

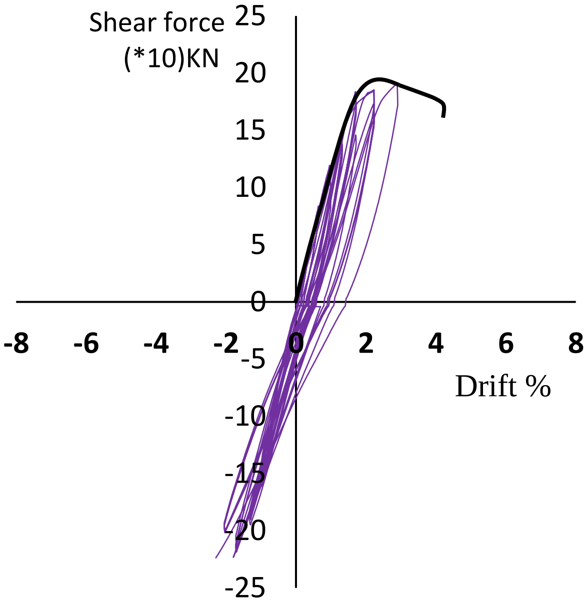

Figure 5.183: Specimen CSS 60-E backbone curve

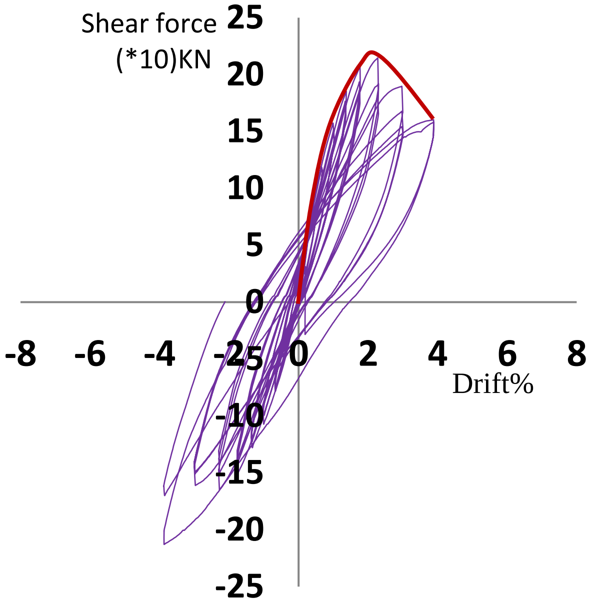

Figure 5.184: Specimen CSS 80-E backbone curve

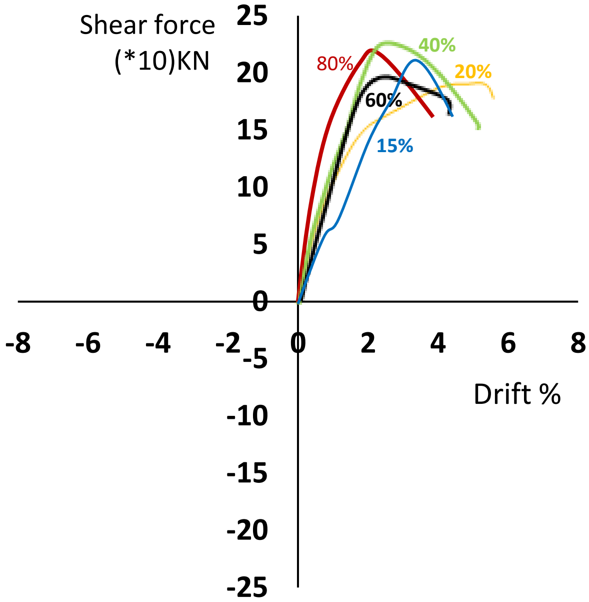

Figure 5.185: Shear deficient old building specimens Backbone curves

Table 5.4: Comparison of modern building data curve outputs

#	Out put	CSS 15-E	CSS 20-E	CSS 40-E	CSS 60-E	CSS 80-E
1	**V peak Test**	230 KN	195 KN	190 KN	192 KN	220 KN
2	**M peak Test**	230 KN M	195 KN M	190 KN M	192 KN M	220 KN M
3	**Δ Vp%**	3.1%	4.2 %	5.1 %	3 %	2 %
4	**Vy Test**	180KN	110 KN	126 KN	180KN	155 KN
5	**Vy/Vpeak %**	78.26 %	56.4 %	66.3 %	93.75 %	70.45 %
6	**ΔVy%**	2.2 %	1.8 %	1.3 %	1.8 %	1.1 %
7	**V80%**	184 KN	156 KN	165 KN	170 KN	176 KN
8	**ΔV80%**	4.6 %	5.6 %	5.5%	4.3 %	3.5 %
9	**VR**	120 KN	153 KN	165 KN	140 KN	162 KN
10	**VR/VP %**	52.17 %	78.46 %	84.6 %	88.54 %	87.56 %
11	**Δ VR**	5.8 %	5.85 %	5.5 %	4.3 %	3.9 %
12	**μΔ= ΔV80/ΔVy**	2 %	3.25 %	4.23 %	2.39 %	3.18 %
13	**μf= ΔVR/ΔVp**	1.87 %	1.39 %	1.39 %	1.43 %	1.95 %

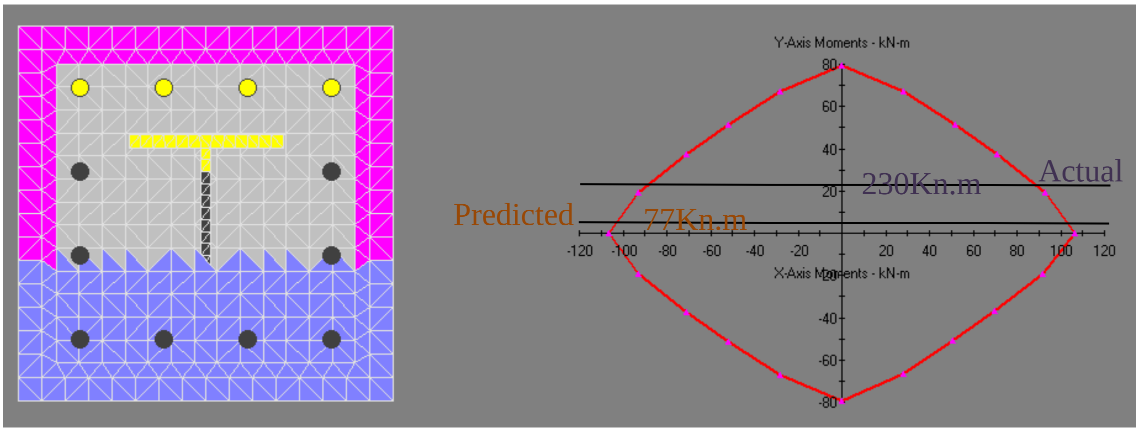

Figure 5.186: Predicted capacity Vs actual capacity of CSS 15-E

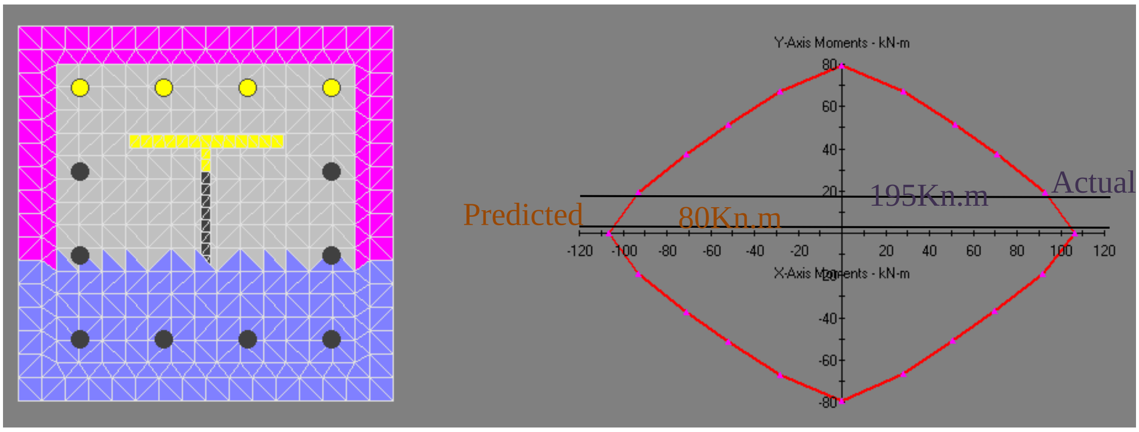

Figure 5.187: Predicted capacity Vs actual capacity of CSS 20-E

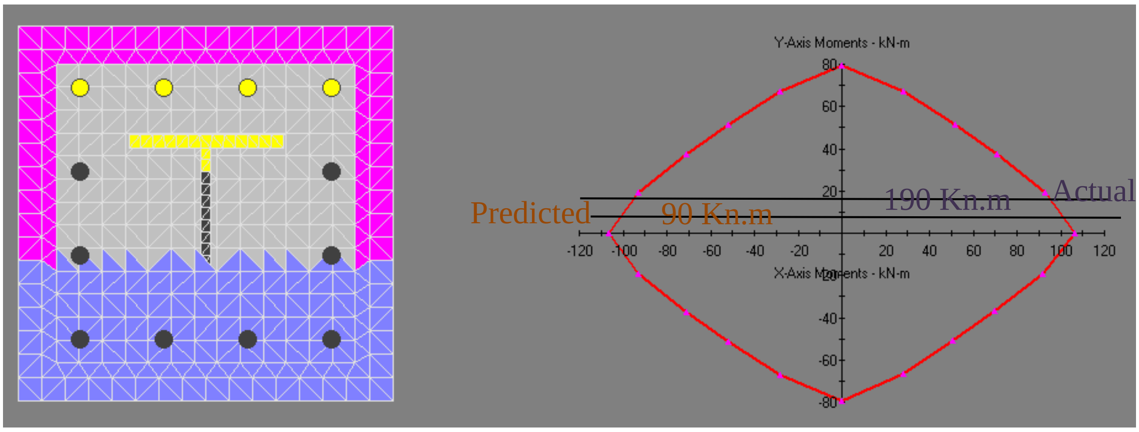

Figure 5.188: Predicted capacity Vs actual capacity of CSS 40-E

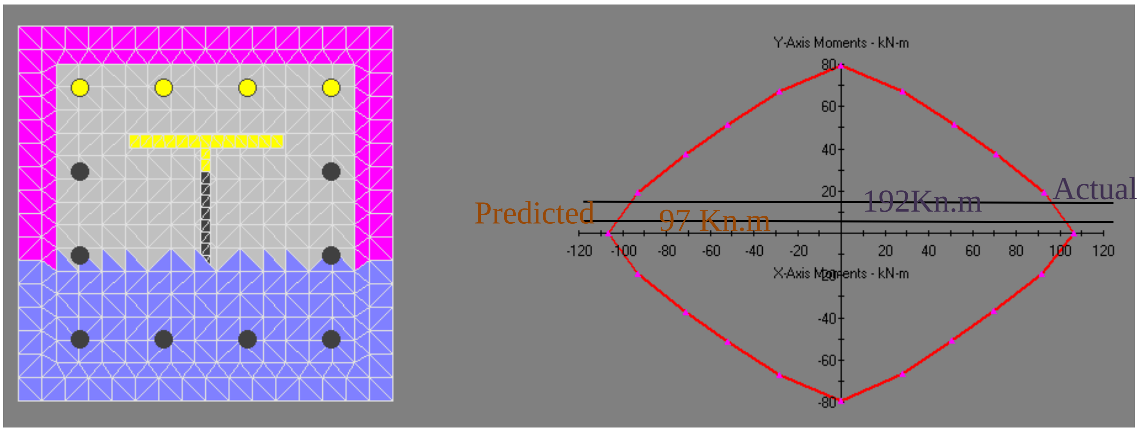

Figure 5.189: Predicted capacity Vs actual capacity of CSS 60-E

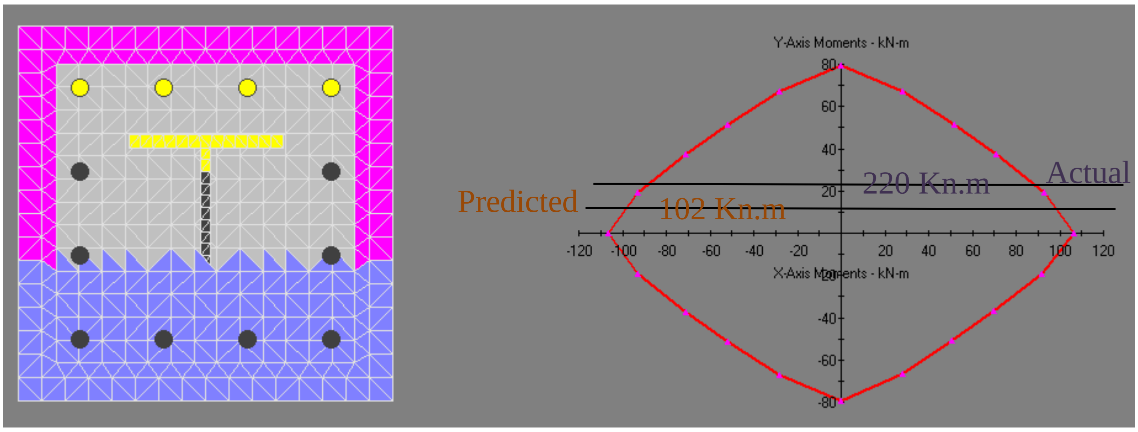

Figure 5.190: Predicted capacity Vs actual capacity of CSS 80-E

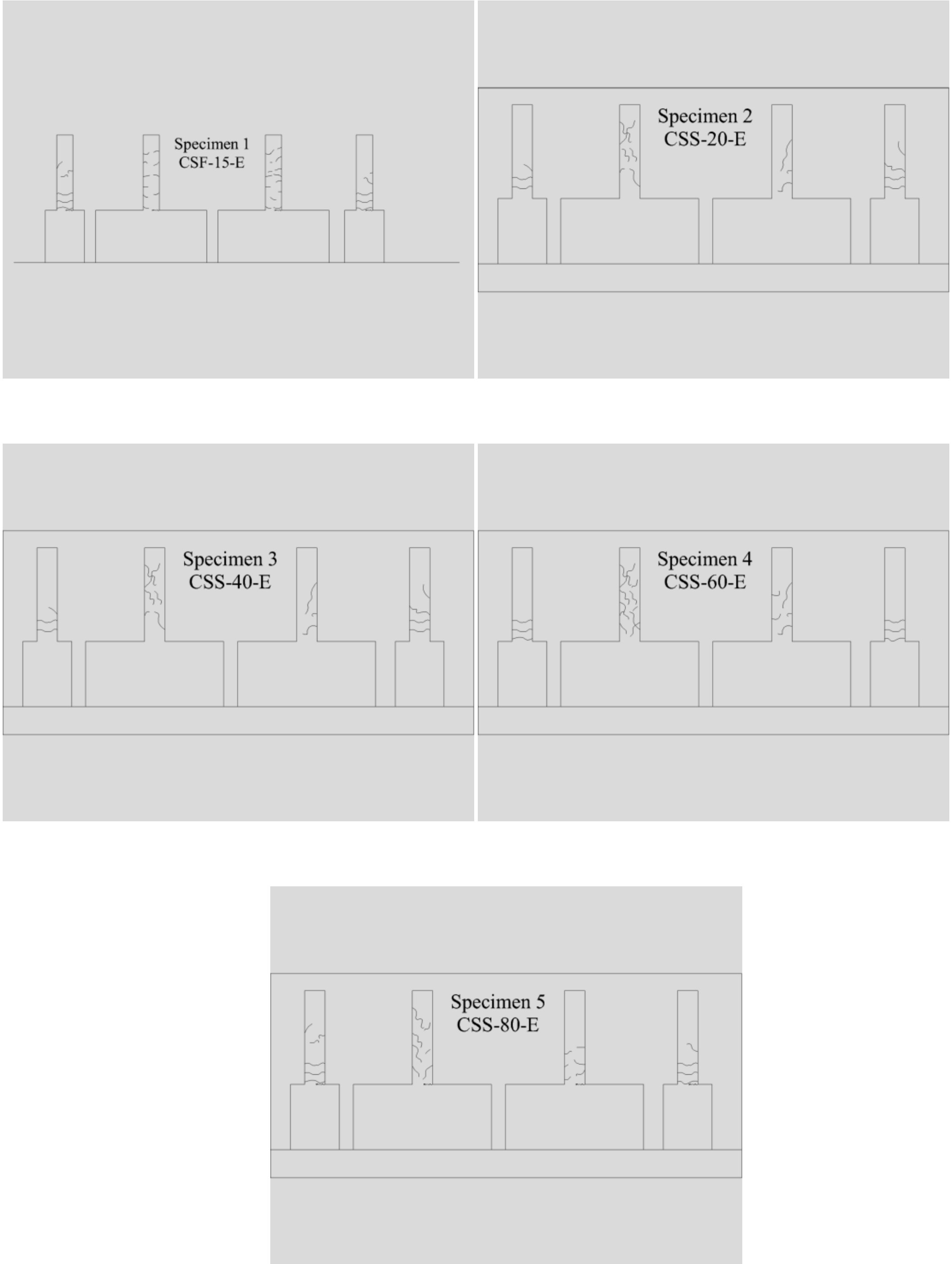

Figure 5.191: Crack pattern at (Δ y) lateral displacement

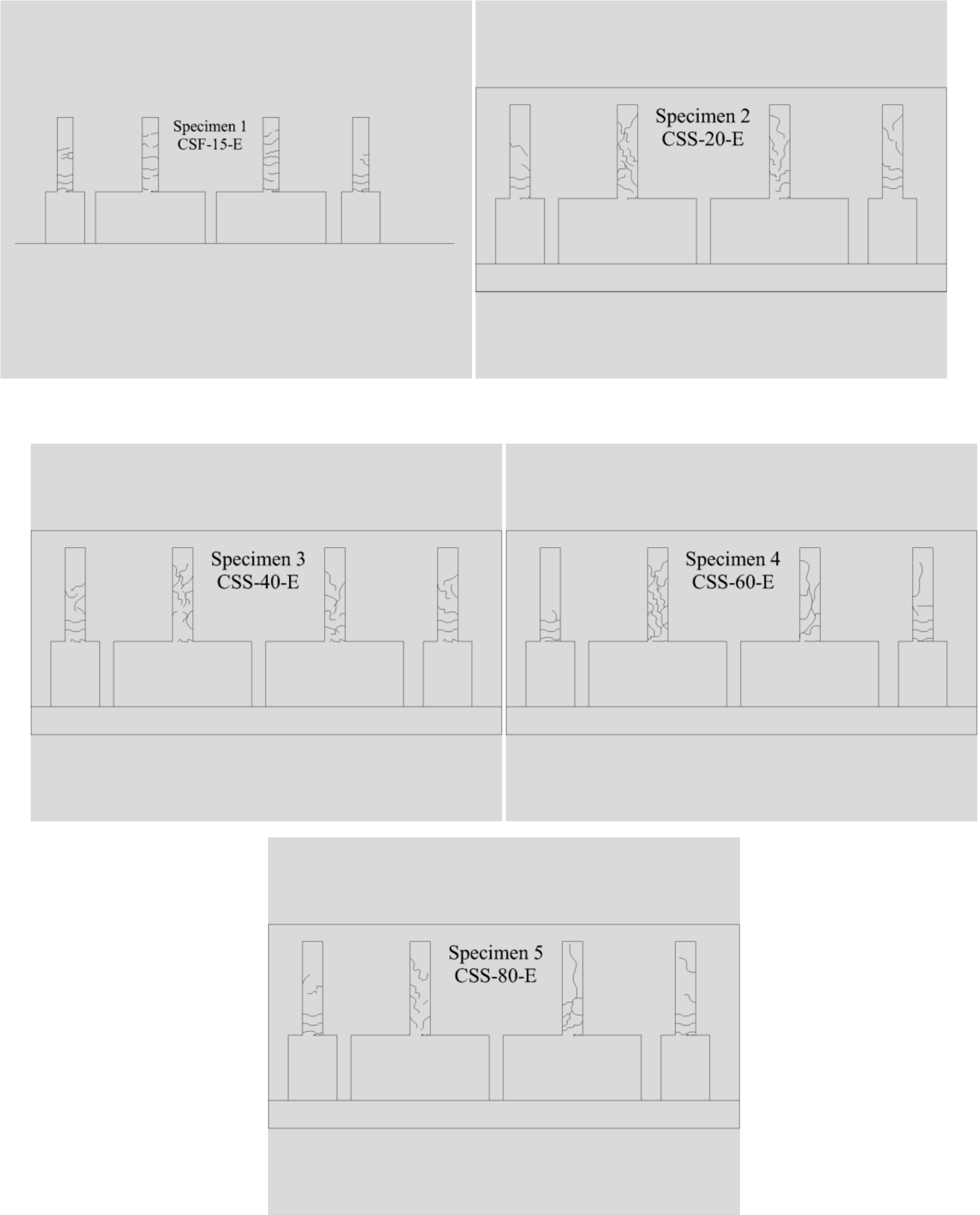

Figure 5.192: Crack pattern at (1.3 ∆ y) lateral displacement

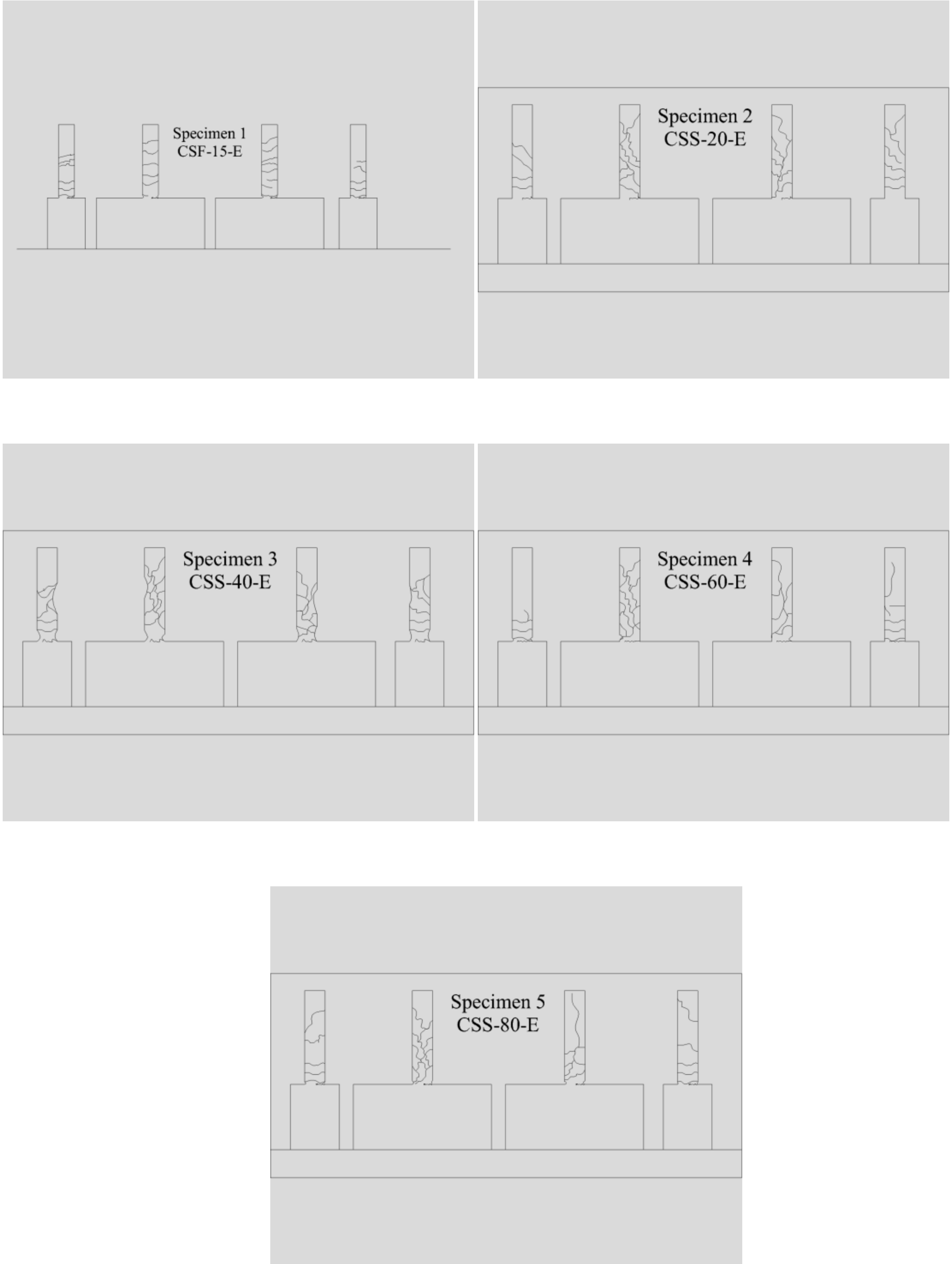

Figure 5.193: Crack pattern at (2.2 Δ y) lateral displacement

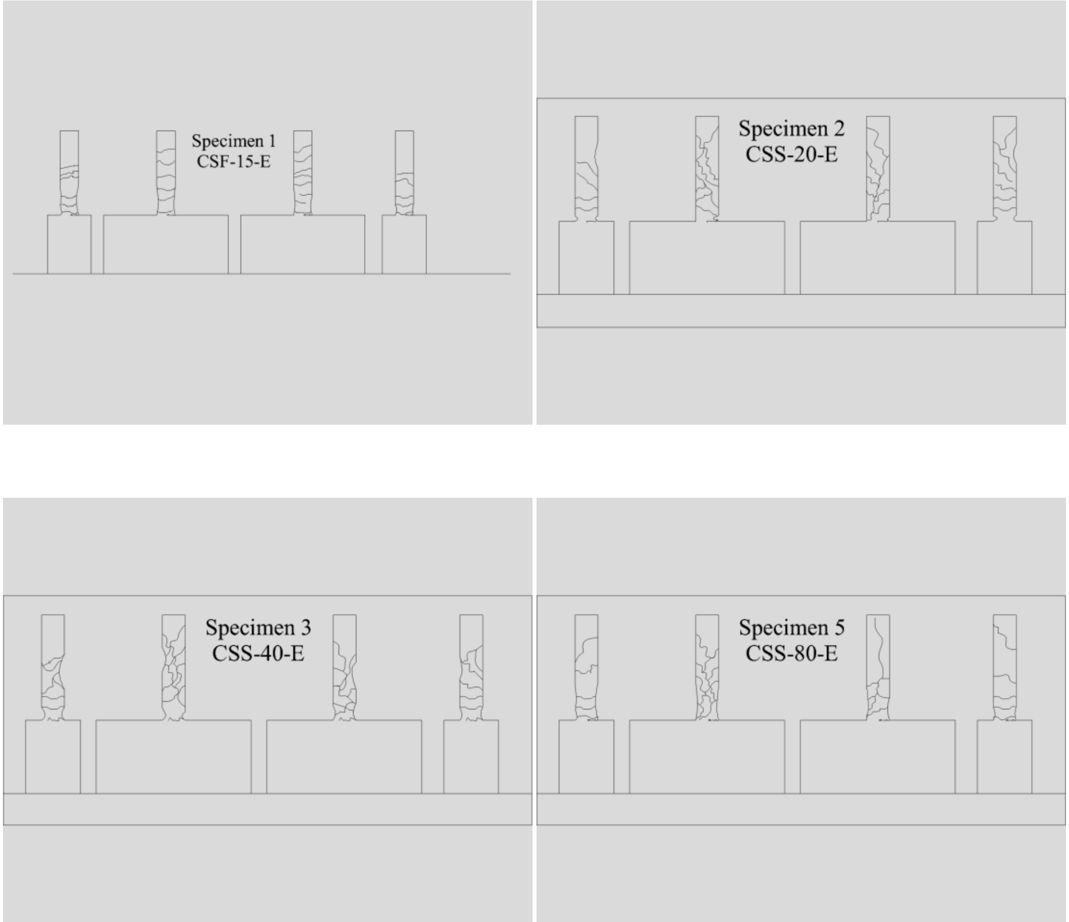

Figure 5.194: Crack pattern at (3.73 Δ y) lateral displacement

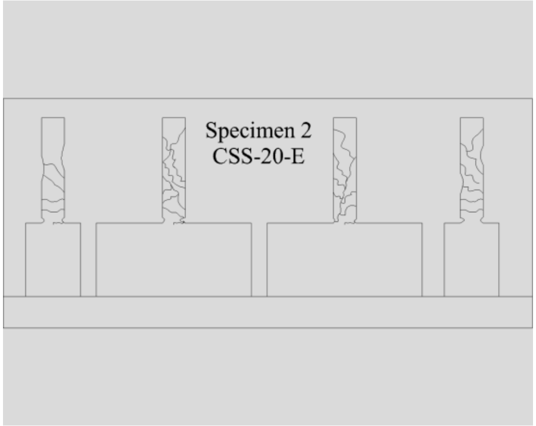

Figure 5.195: Crack pattern at (4.87 ∆ y) lateral displacement

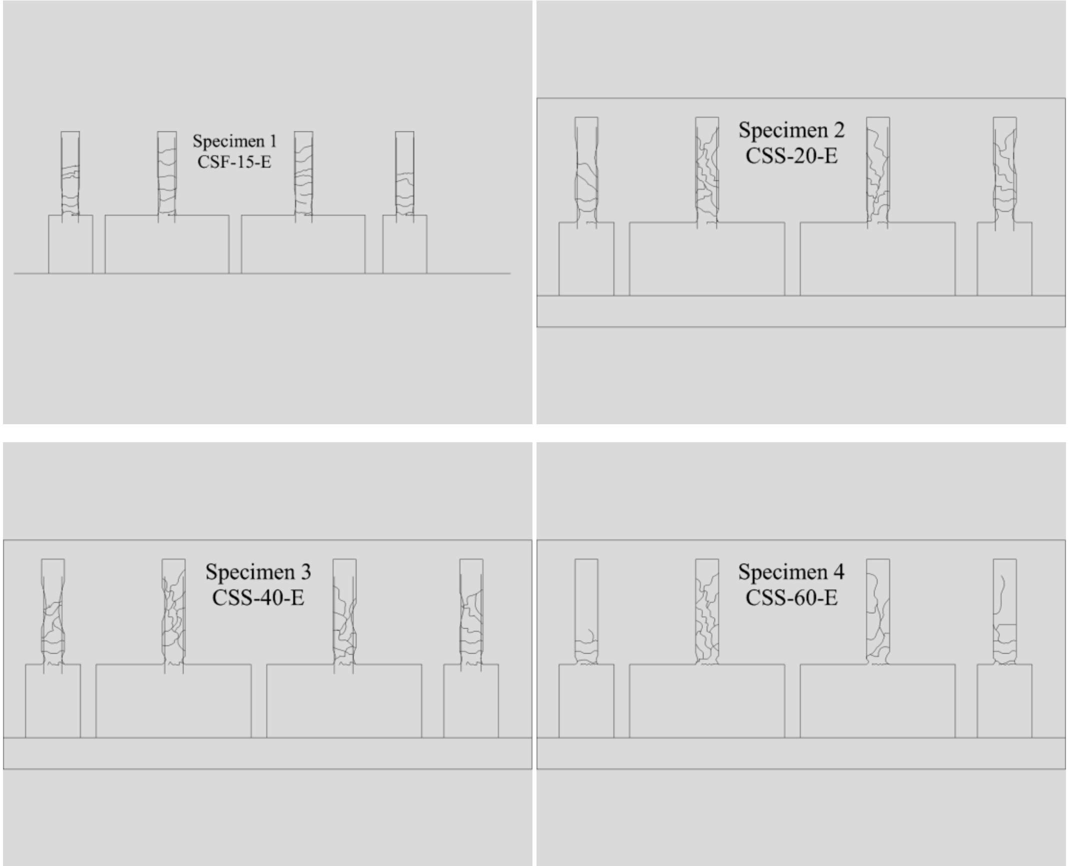

Figure 5.196: Crack pattern at (end of the test) lateral displacement

3.2.Flexure deficient Specimens

1. Specimen CSF -15-E

CSF-15-Ewas subjected to a constant compressive axial load of 270 KN (0.15f’c Ag, where f’c = cylinder compressive concrete strength, and Ag = gross cross sectional area) and cyclic increments of lateral displacements as described in **Figure4.13**. The theoretical nominal yield displacement was calculated to be equal 16.25 mm. It was noticed that there was inclination of the horizontal actuator load cell with an angel ɵ=0’59’16’. This was taken into consideration in the force and drift post processing.

At the end of the first group of displacement protocol (0.25 Δy) there were some flexure cracks. Starting the next displacement cycles, horizontal hairline cracks (width of less than 1mm.) developed near the bottom of the column.

The number of flexure cracks and the crack width on the faces parallel to the lateral loading direction increased as the number and magnitude of the displacement cycles increased. Small diagonal cracks on the faces perpendicular to the lateral loading direction (i.e., on the east and west faces). These relatively straight continuous cracks opened and closed during each cycle.

During displacement cycles to 0.5 of the nominal yield displacement, relatively crack openings were observed suggesting slip of the longitudinal reinforcing bars from the base. **Figure5.199** shows about 2mm wide crack opened between tension side of the column base and the column at peak lateral displacement.

During displacement cycles to the nominal yield displacement (Δ y = 27.378mm.), more in wide crack opening without any new cracks. Faces perpendicular to the loading direction, the width of the existing horizontal cracks increased especially in the side of pouring concrete. It was normal because of concrete in this side is less compacted than the other side and may loss some of the gravel aggregate during vibrating within pouring concrete. Luxation of the concrete cover was observed at the column bottom corner at Δ= 1.69 Δy. In the compression zones, at the bottom of the column, flaking and spalling of concrete were observed at the end of group 2.856 Δy (46.41mm) **Figure 5.201**.

As the number of cycles increased, after the concrete cover crashed and the steel bars appeared from different areas, as shows in **Figures5.201** at middle of 4.8Δy it was found a clear tension flexure failure with cutting in some of buckled longitudinal steel bars without opening in stirrups as shown in **Figure 5.201**.

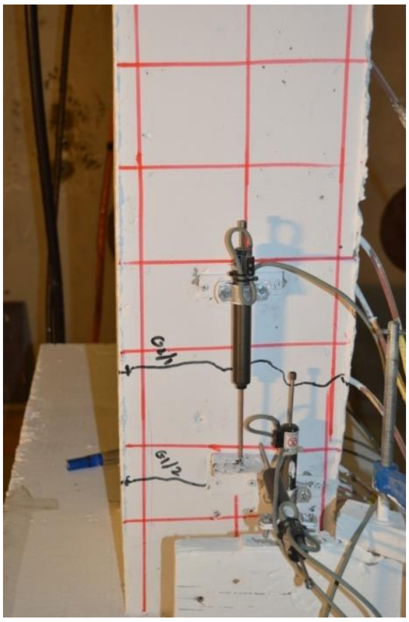

Figure 5.197: Specimen CSF-15-E at initial displacement (Hair cracking)

Figure 5.198: CSF-15-E starting slipping from base of column at 0.5Δy

Figure 5.199: CSF-15-ECrushing concrete cover at 1.69Δy

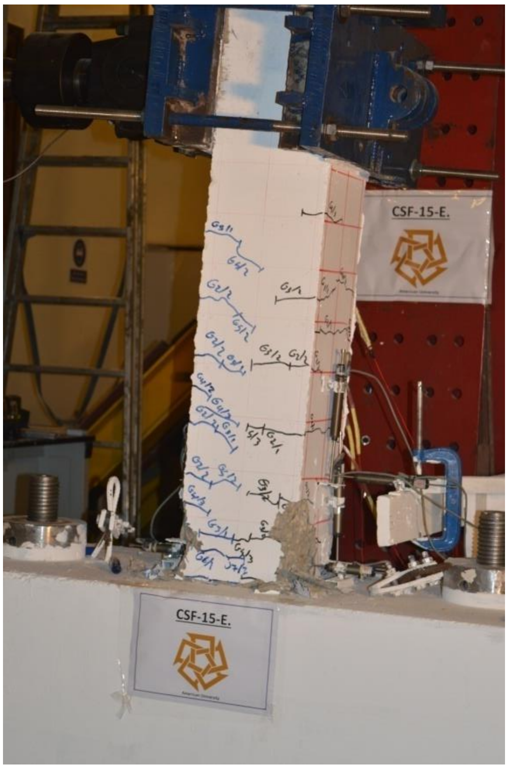

Figure 5.200: Specimen CSF-15-E at the compression direction of 2.856∆y

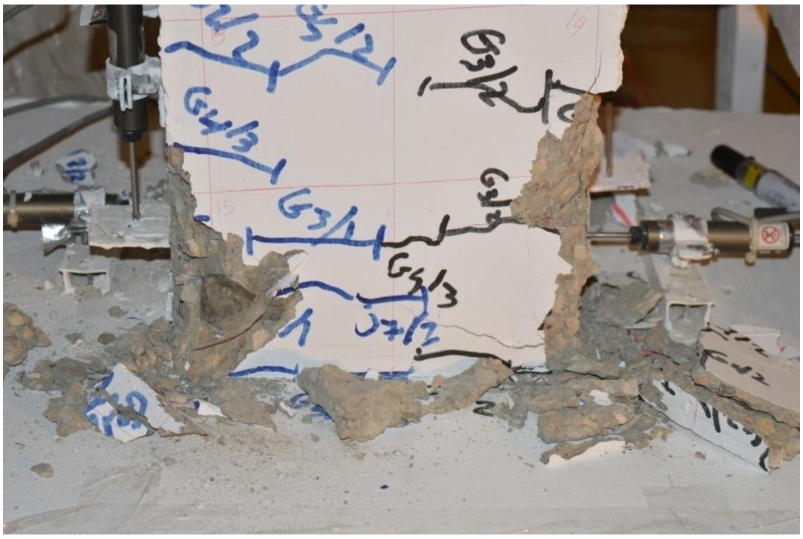

Figure 5.201: CSF-15-ECrushing concrete cover at 2.856∆y

Figure 5.202: Classical tension failure 4.8∆y

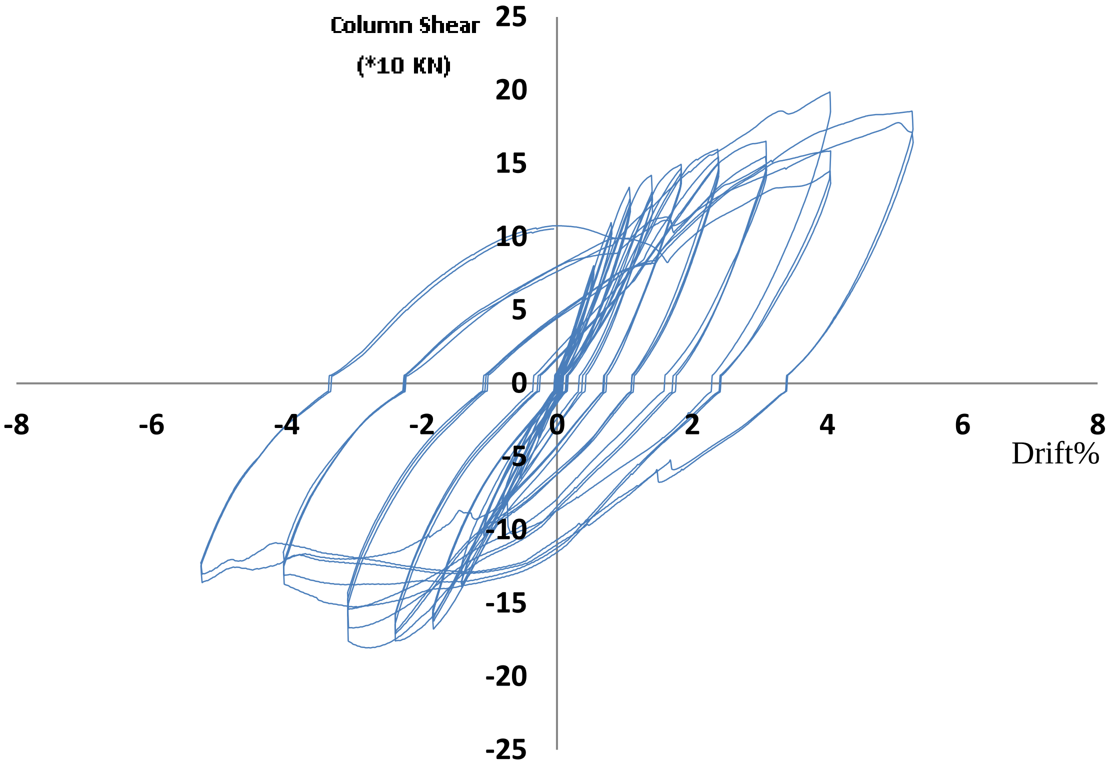

Figure 5.203: Shear force-drift hysteresis response of specimen CSF 15-E

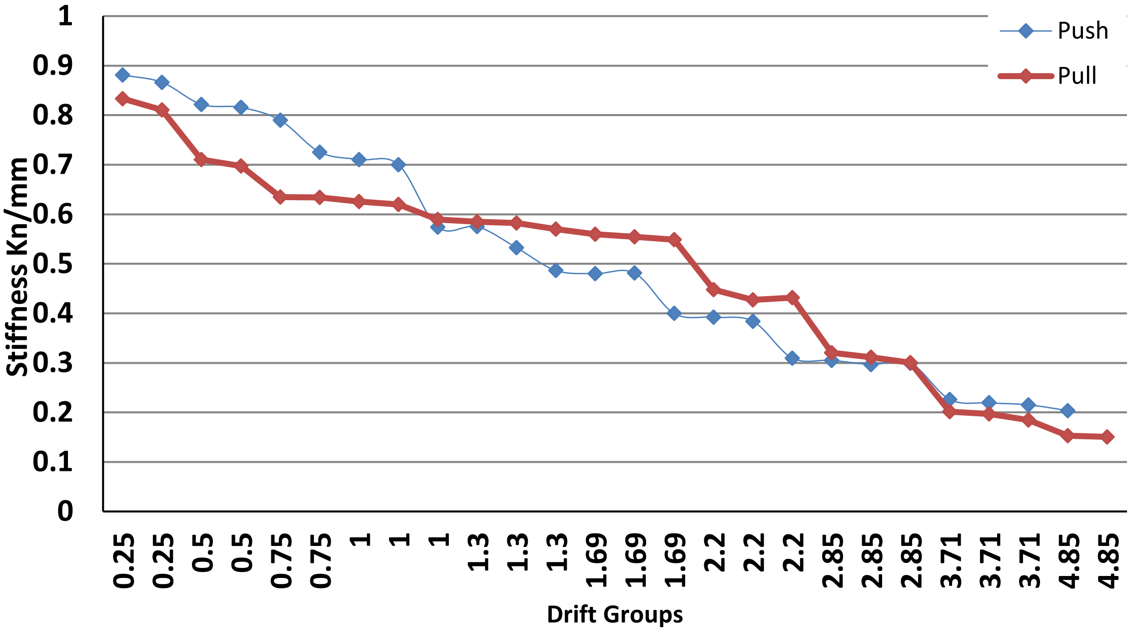

Figure 5.204: Peak to Peak stiffness of specimen CSF 15-E

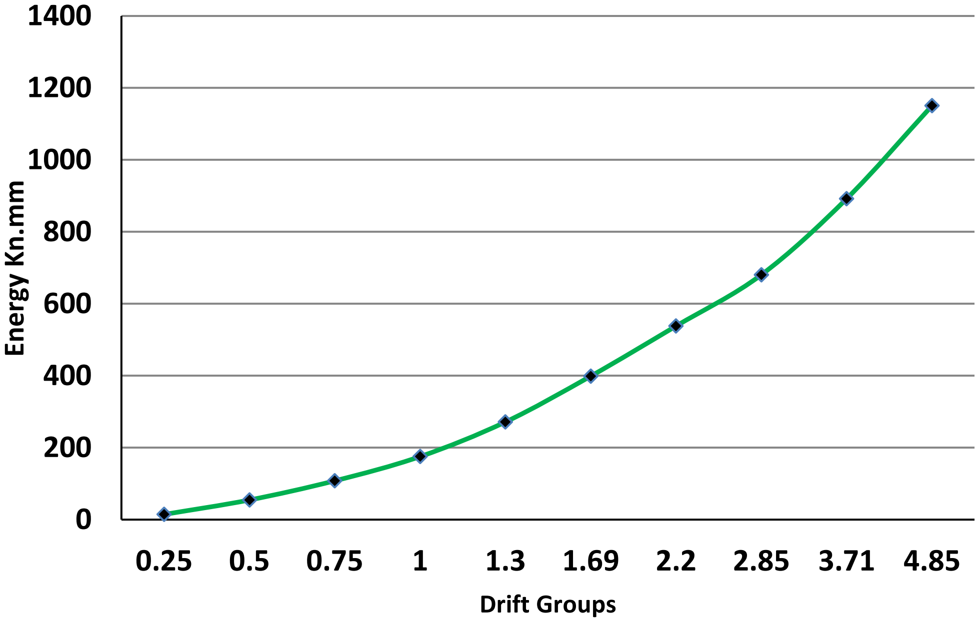

Figure 5.205: Peak to peak Energy of specimen CSF 15-E

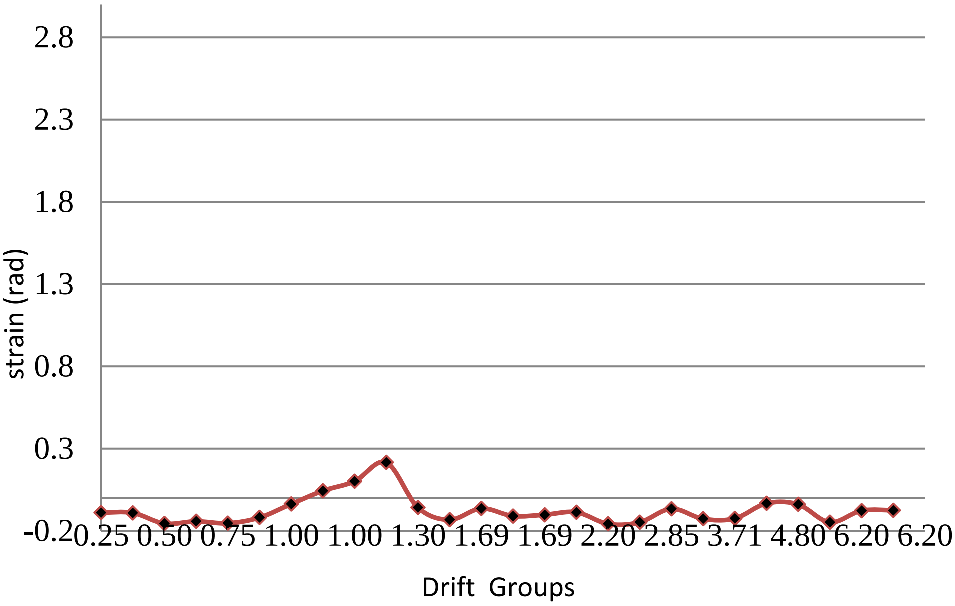

Figure 5.206: CSF-15-ECompression flange steel strain Vs Drift groups (300mm)

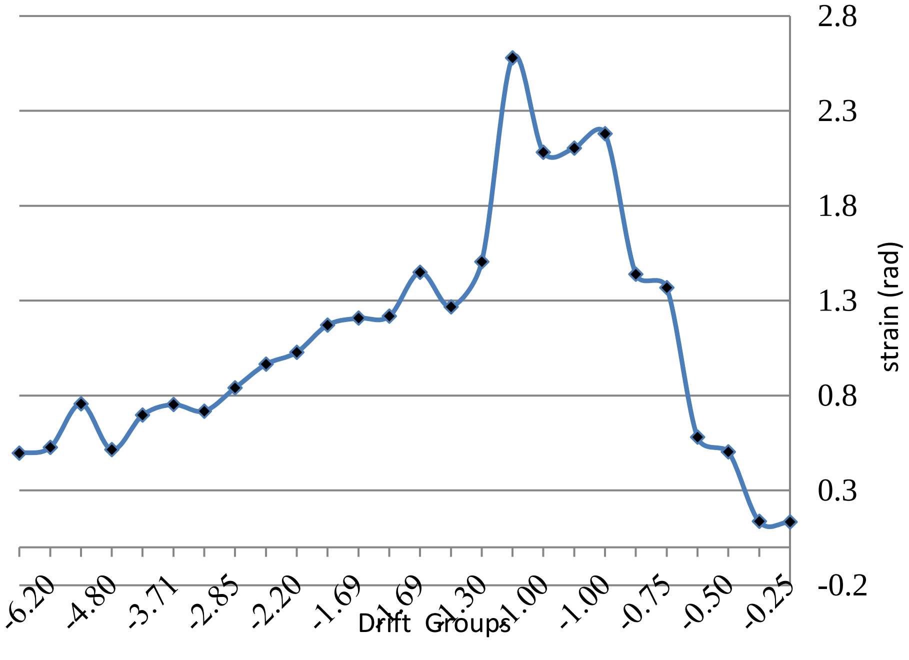

Figure 5.207: CSF-15-E Compression flange steel strain Vs Drift groups (300mm)

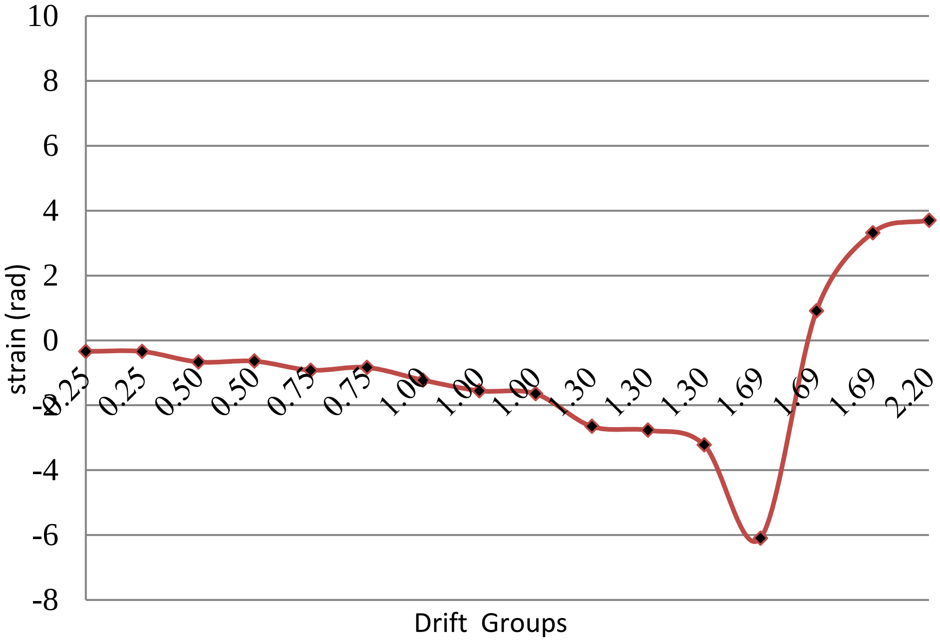

Figure 5.208: CSF-15-E Compression steel bar strain Vs Drift groups (50mm)(Compression side)

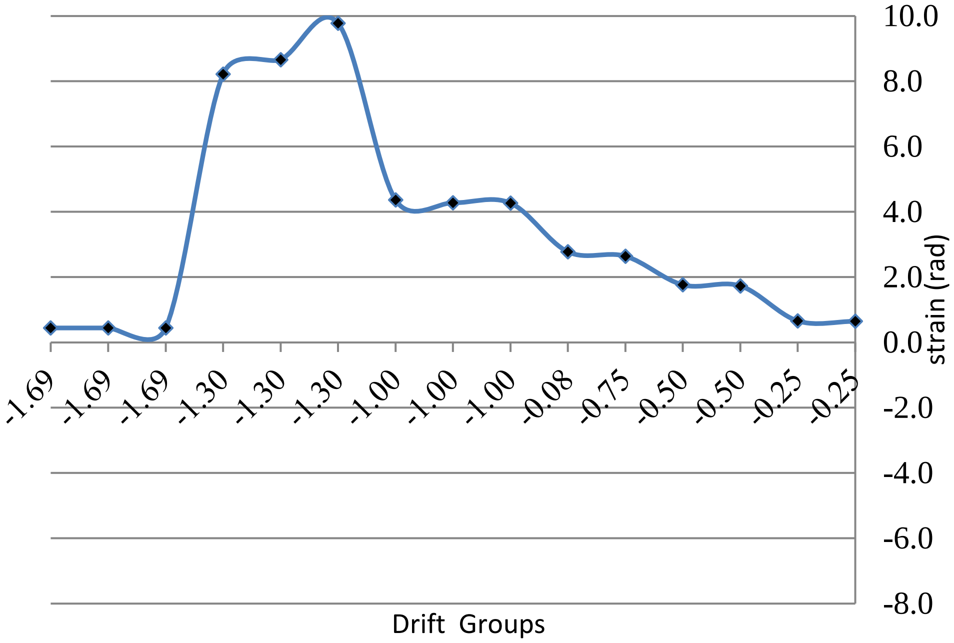

Figure 5.209: CSF-15-E Tension steel bar strain Vs Drift groups (50mm) (Compression side)

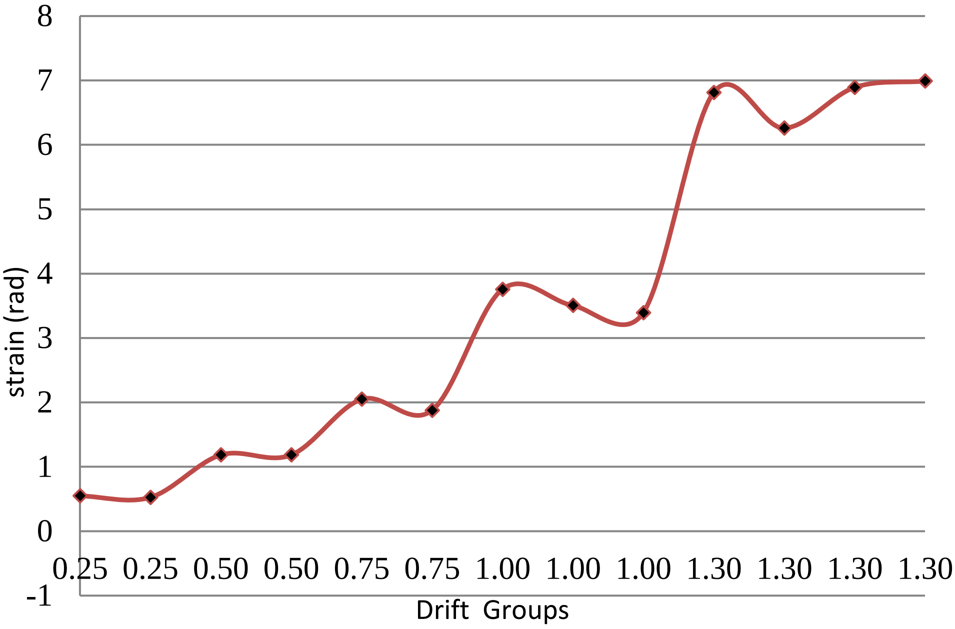

Figure 5.210: CSF-15-ECompression steel bar strain Vs Drift groups (50mm) (Compression side)

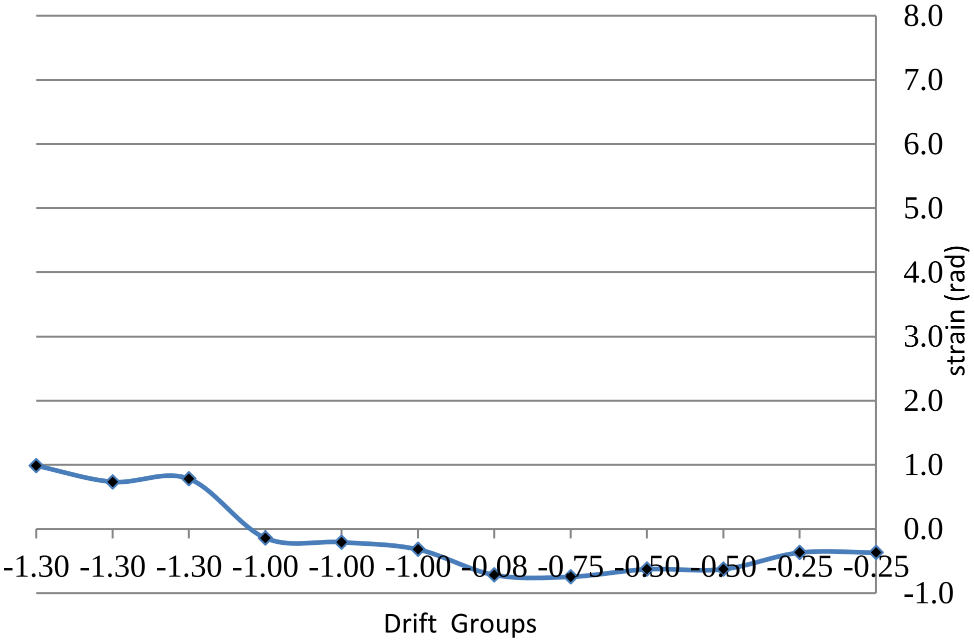

Figure 5.211: CSF-15-ETension steel bar strain Vs Drift groups (50mm) (Compression side)

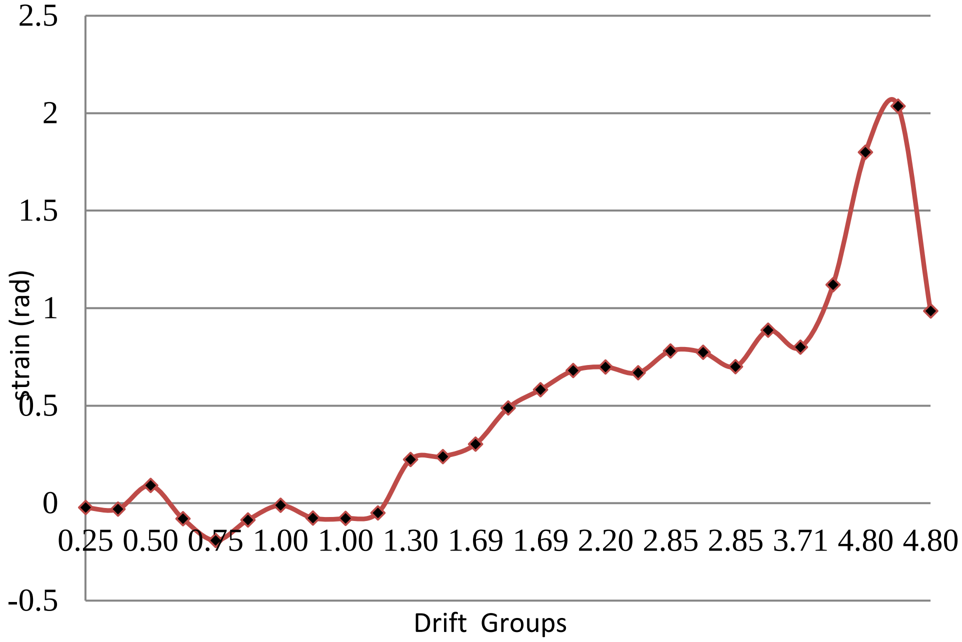

Figure 5.212: CSF-15-ECompression steel hoop strain Vs Drift groups (100mm)

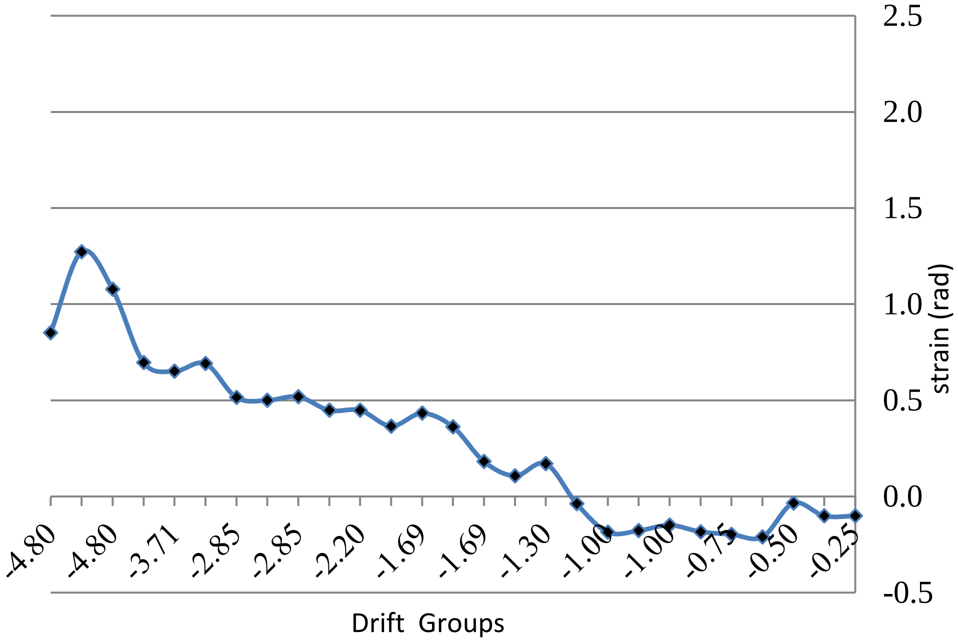

Figure 5.213: CSF-15-ECompression steel hoop strain Vs Drift groups (100mm)

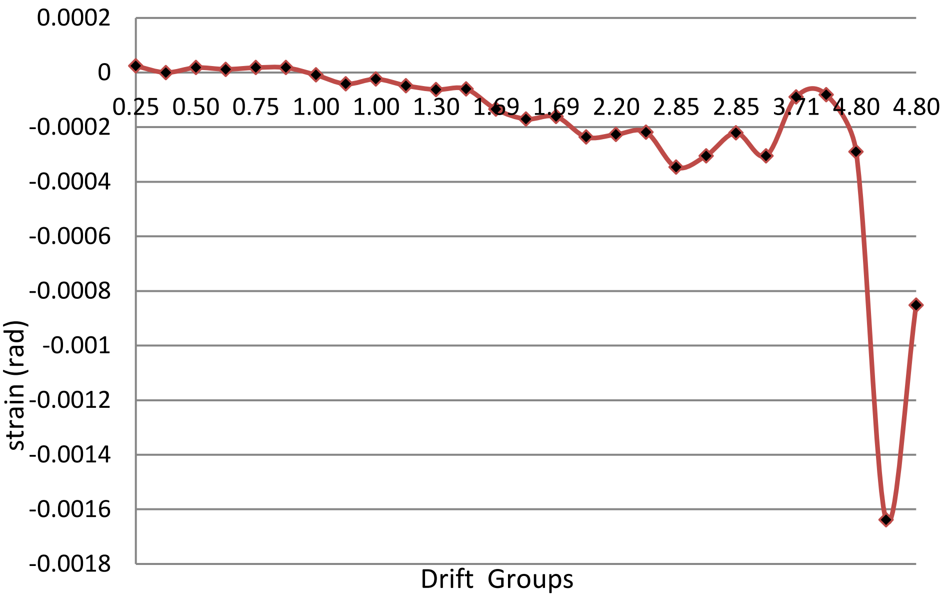

Figure 5.214: CSF-15-ECompression shear strain (rad) Vs Drift group (vertical LVDTs 5-12) (Compression side)

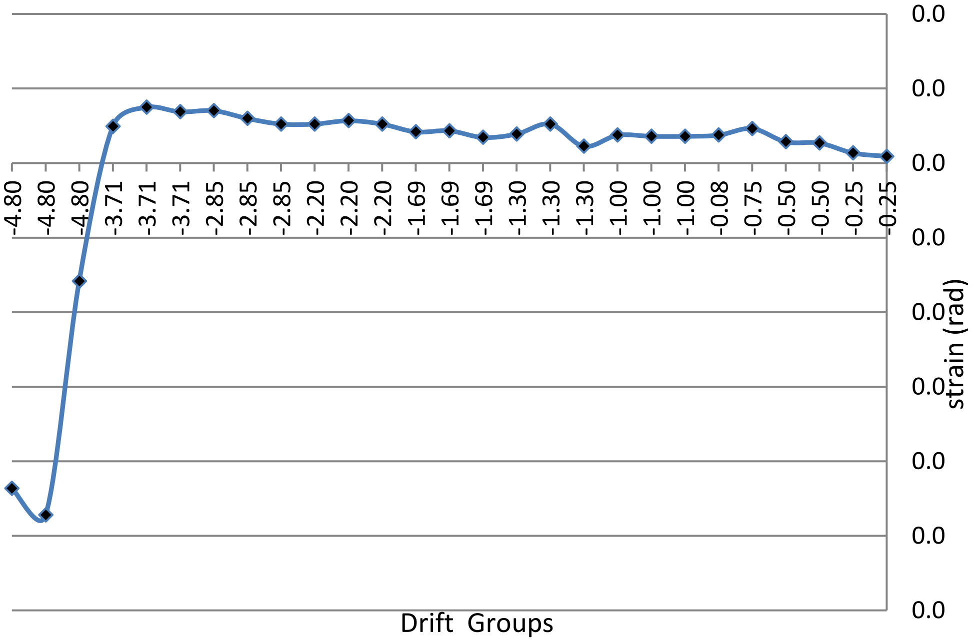

Figure 5.215: CSF-15-ETension shear strain (rad) Vs Drift groups (vertical LVDTs 5-12) (compression side)

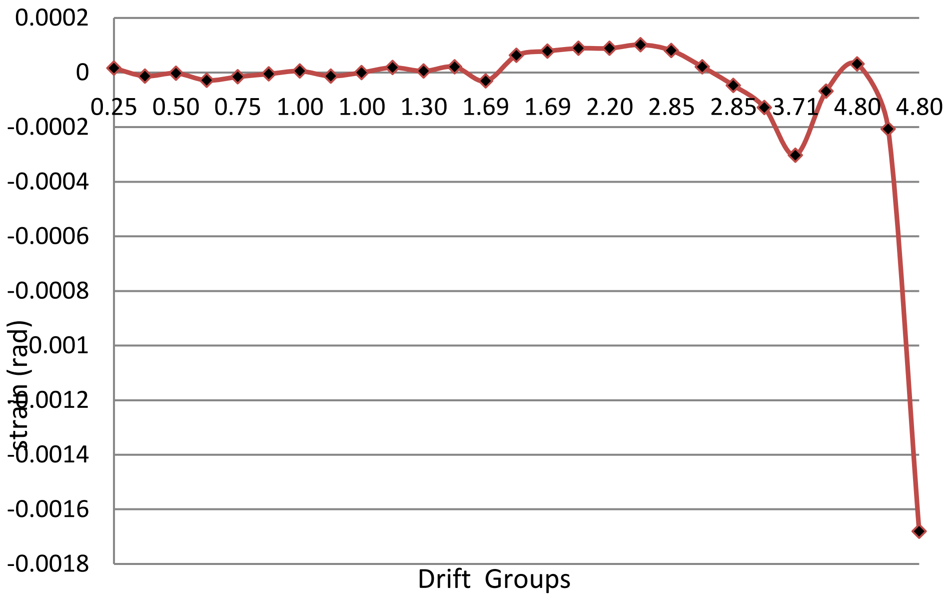

Figure 5.216: CSF-15-ECompression shear strain (rad) Vs Drift groups (Vertical LVDTs 5-12) (Tension side)

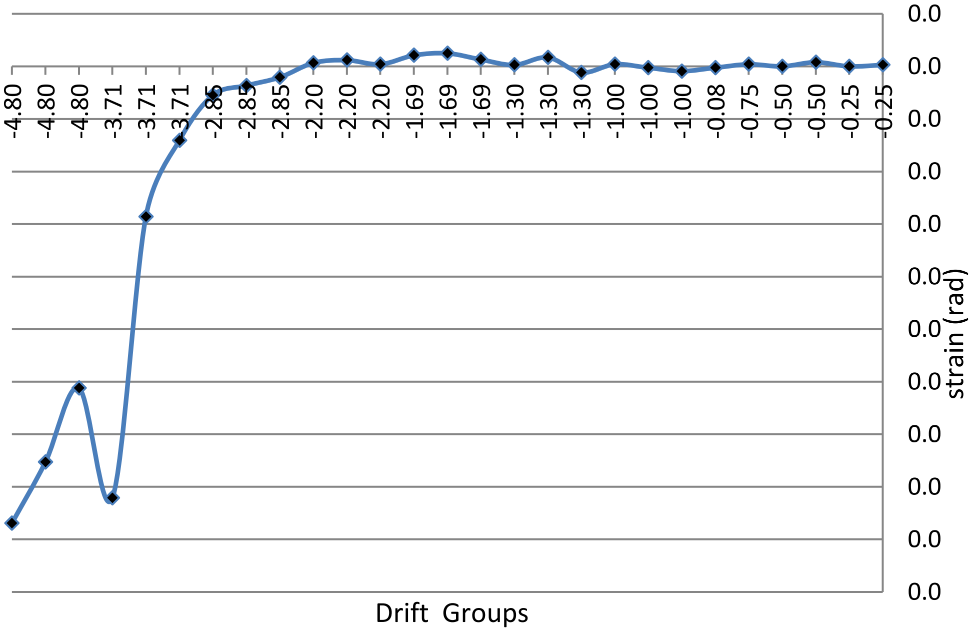

Figure 5.217: CSF-15-ETension shear strain (rad) Vs Drift groups (vertical LVDTs 5-12) (tension side)

2. Specimen CSF-80-E:

CSF -80-Ewas subjected to a constant compressive axial load of 18000 KN (0.8f’c Ag, where f’c = cylinder compressive concrete strength, and Ag = gross cross sectional area) and cyclic increments of lateral displacements as described in **Figure4.13**. The theoretical nominal yield displacement was calculated to be equal 12.2 mm. it was noticed the same inclination of the horizontal actuator load cell with an angel ɵ = 1’17’52. This was taken into consideration in the force and drift post processing.

During the first groups of displacement protocol (0.25Δy) there were not any cracking. Starting the next displacement cycles of 0.5Δy of the nominal yield displacement, flexure hairline cracks (width of less than 1mm.) developed near the bottom of the column.

The number of inclined cracks and the crack width on the faces parallel to the lateral loading direction increased as the number and magnitude of the displacement cycles increased. Small horizontal and inclined cracks on the faces perpendicular to the lateral loading direction (i.e., on the east and west faces), started to span the width of the column. These relatively straight continuous horizontal cracks opened and closed during each cycle. During displacement cycles equal to theoretical Δy displacement cracks increased opening, relatively large crack openings were observed suggesting slip of the longitudinal reinforcing bars from the base at Δ = Δy. **Figure5.221** shows 2 mm wide crack opened between the flexural tension side of the column base and the column at peak lateral displacement.

During displacement cycles to the nominal yield displacement (Δ = 1.3 Δy.), more in wide crack opening without any new cracks. Faces perpendicular to the loading direction, the width of the existing diagonal cracks increased from two sides. At the beginning of cycling at the displacement level of (1.69 Δ y), when the specimen was loaded the first time (push or eastward direction, **Figure 5.222**, luxation of the cover concrete was observed in the bottom northeast corner and the horizontal load started to decrease after reaching the peak previous. In the flexural compression zones, at the bottom of the column, flaking and spalling of concrete were observed.

As the number of cycles increased, after the concrete cover crashed and the steel bars appeared, steel bars was buckled, stirrups hoops opened, local buckling in lower two flanges and the lower cracks were deeply in the column around the cross section as shown in **Figure5.223** at the 4.87 Δ y.

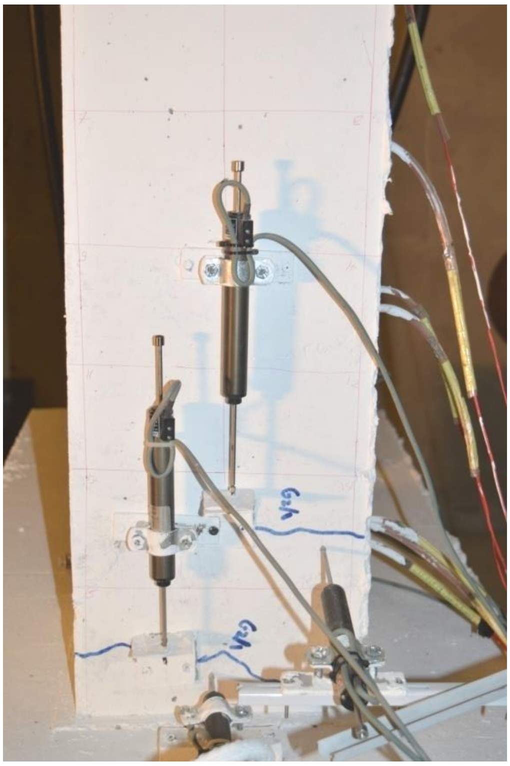

Figure 5.218: Specimen CSF-80-E at initial cracking (0.5 Δy)

Figure 5.219: CSF-80-E Start slipping at ∆y

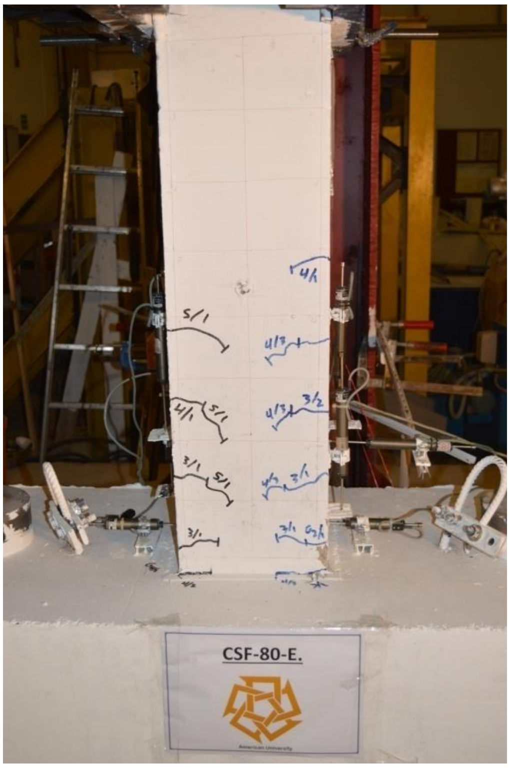

Figure 5.220: CSF-80-E Perpendicular side after tension loading of 1.69 ∆y

Figure 5.221: CSF-80-E Crushing concrete cover mid cycle of (1.69 ∆y)

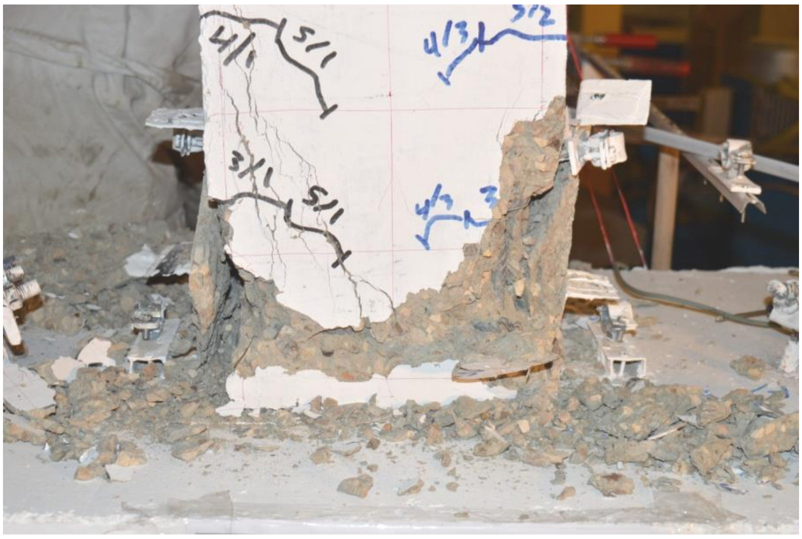

Figure 5.222: CSF-80-E Crushing concrete cover (2.85 ∆y)

Figure 5.223: End of the test

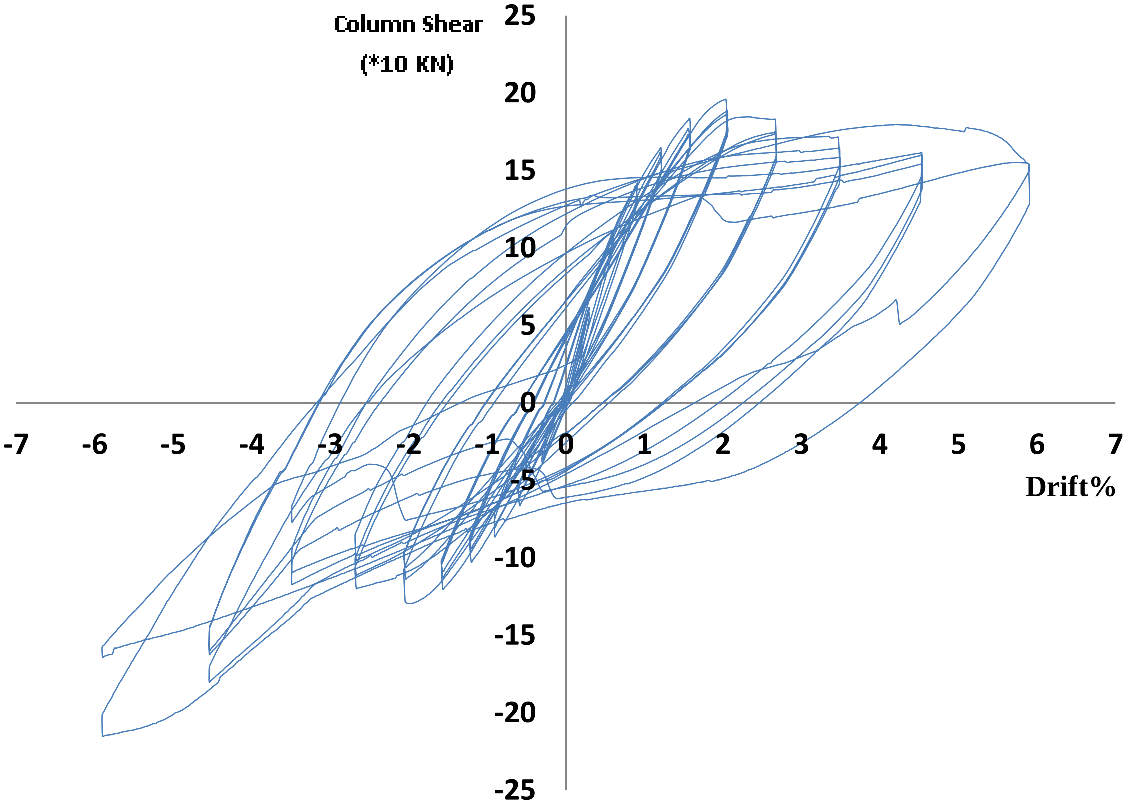

Figure 5.224: Shear force-drift hysteresis response of specimen CSF 80-E

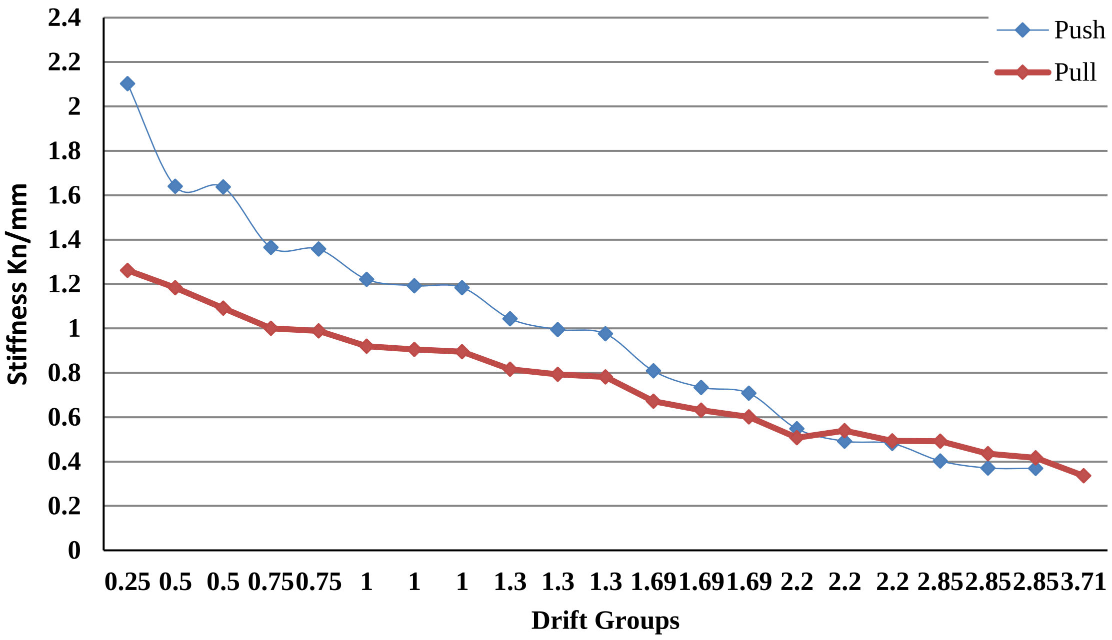

Figure 5.225: Peak to Peak stiffness of specimen CSF 80-E

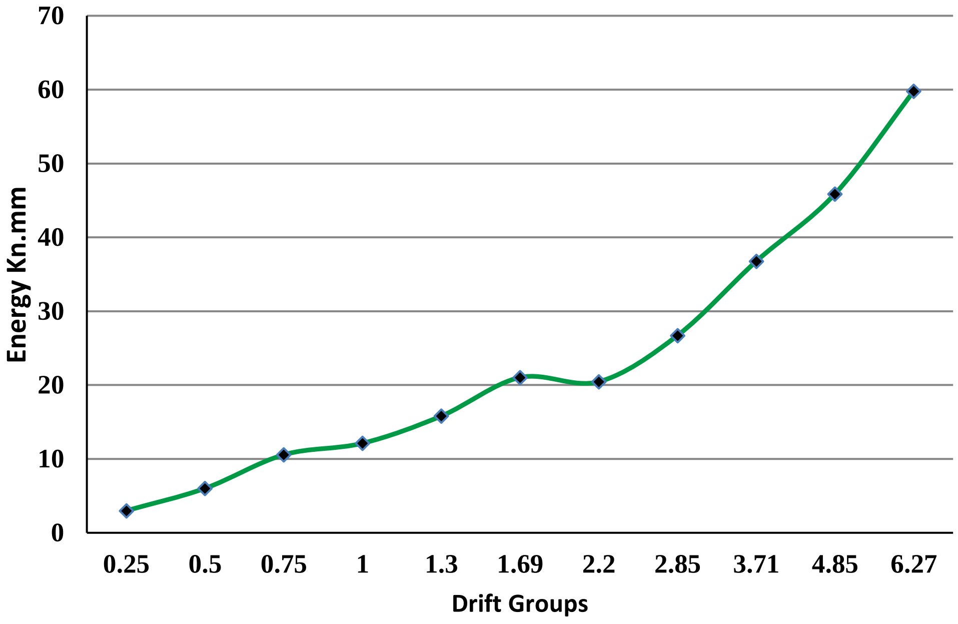

Figure 5.226: Peak to peak Energy of specimen CSF 80-E

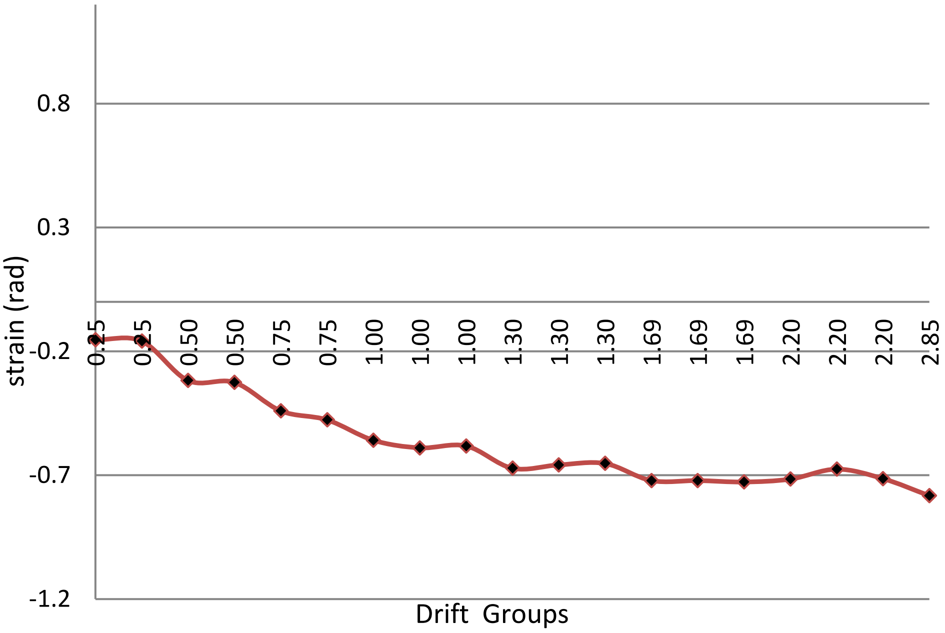

Figure 5.227: CSF-80-E Compression flange steel strain Vs Drift groups (300mm)

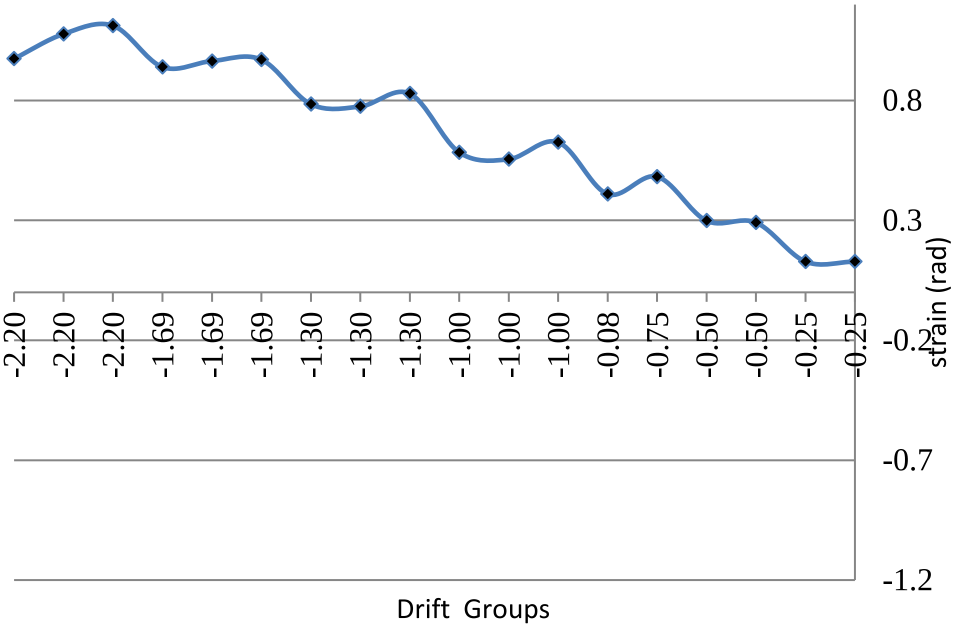

Figure 5.228: CSF-80-E Tension flange steel strain Vs Drift groups (300mm)

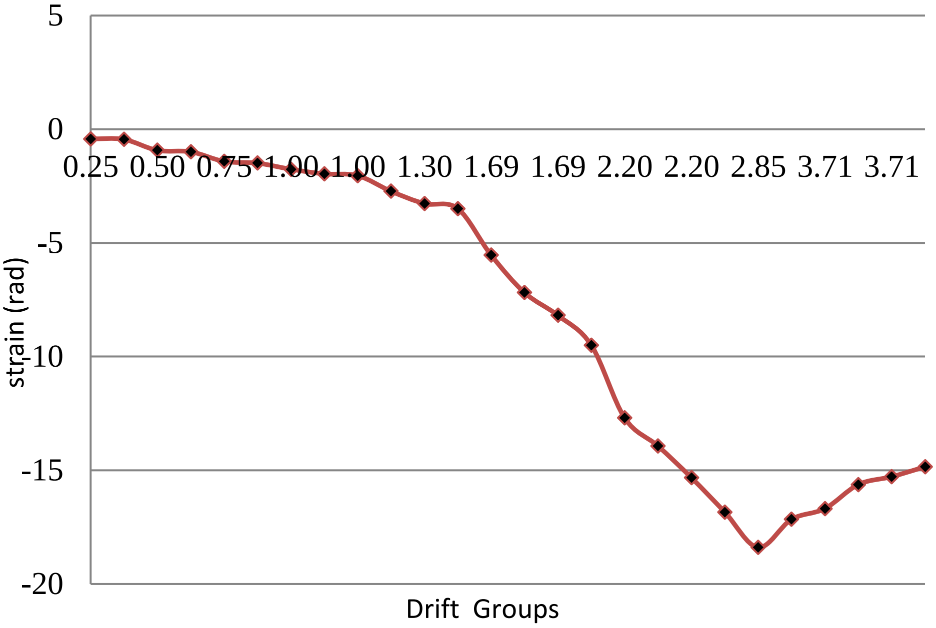

Figure 5.229: CSF-80-E Compression steel bar strain Vs Drift groups (50mm) (Compression side)

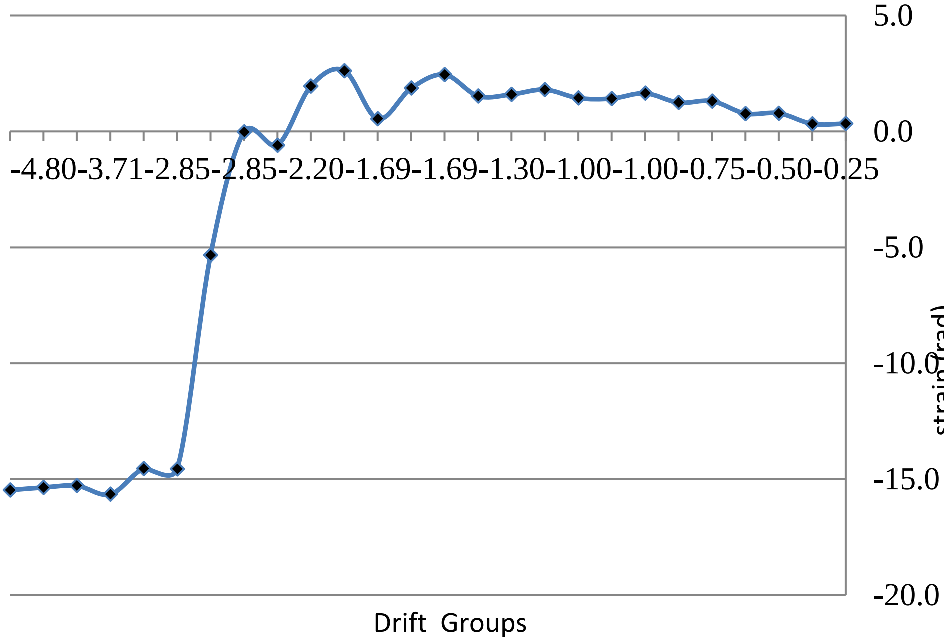

Figure 5.230: CSF-80-E Tension steel bar strain Vs Drift groups (50mm) (Compression side)

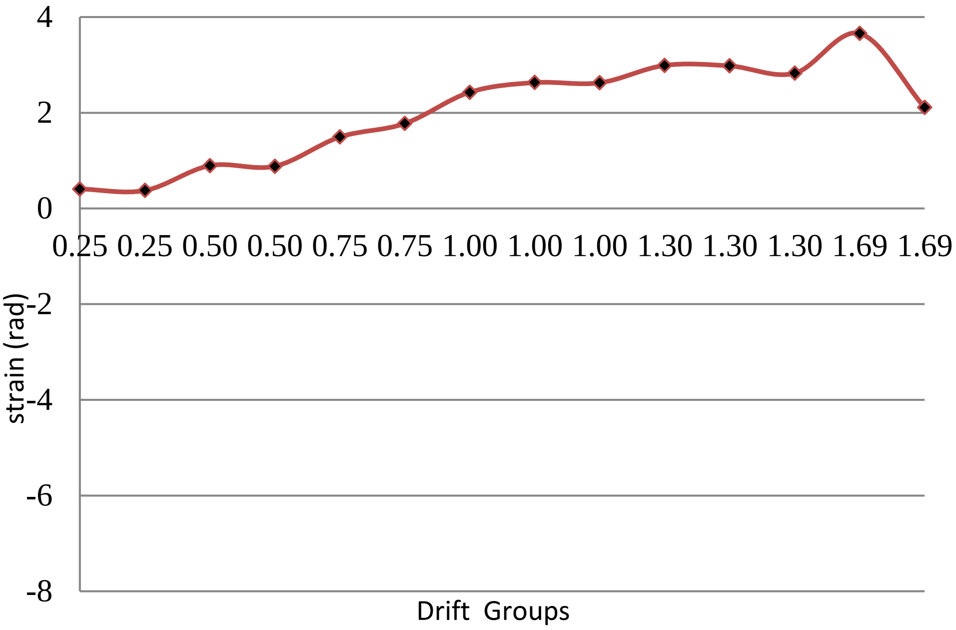

Figure 5.231: CSF-80-E Compression steel bar strain Vs Drift groups (50mm)(Compression side)

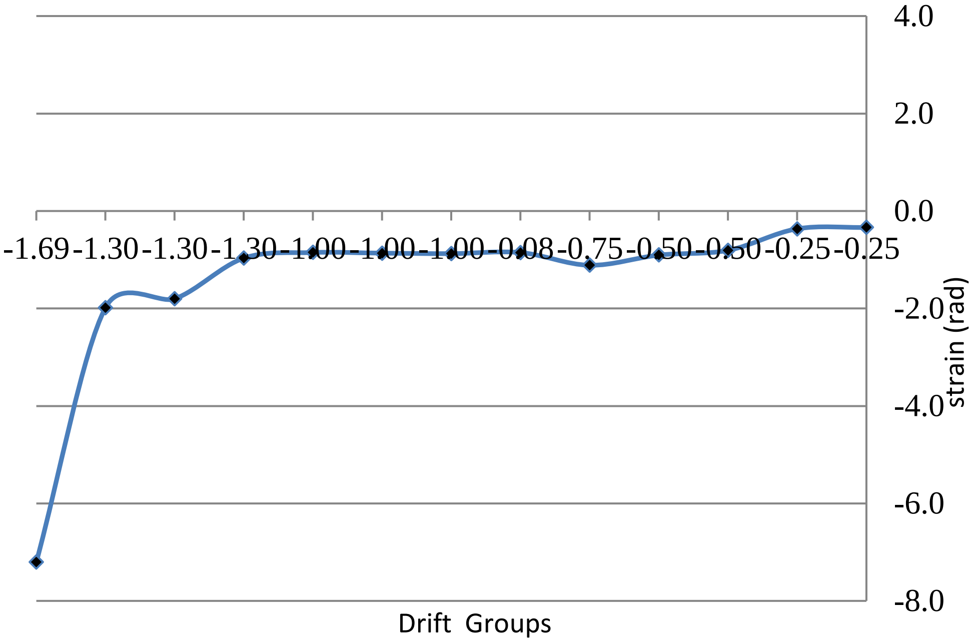

Figure 5.232: CSF-80-E Tension steel bar strain Vs Drift groups (50mm) (Compression side)

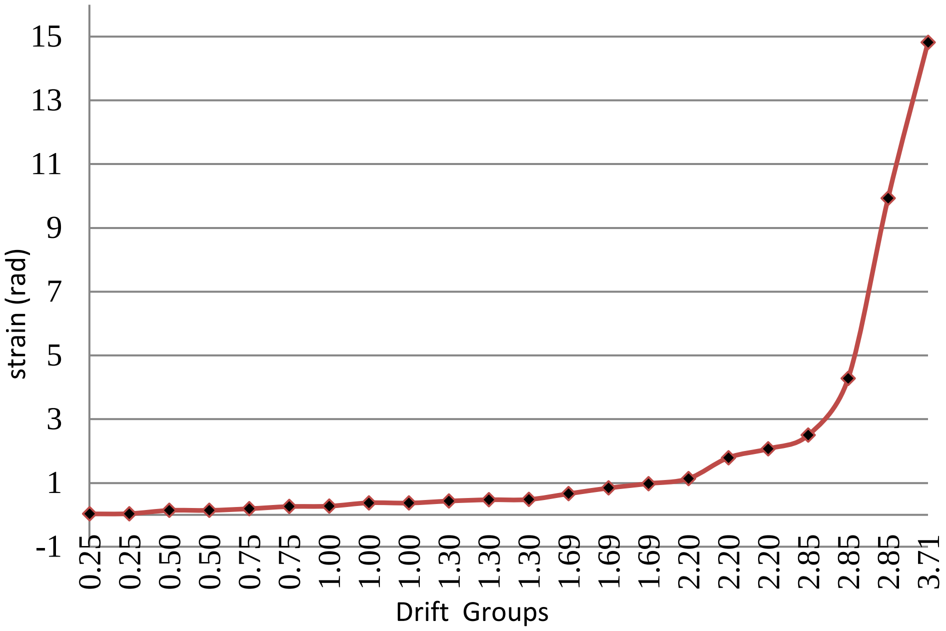

Figure 5.233: CSF-80-E Compression steel hoop strain Vs Drift groups (100mm)

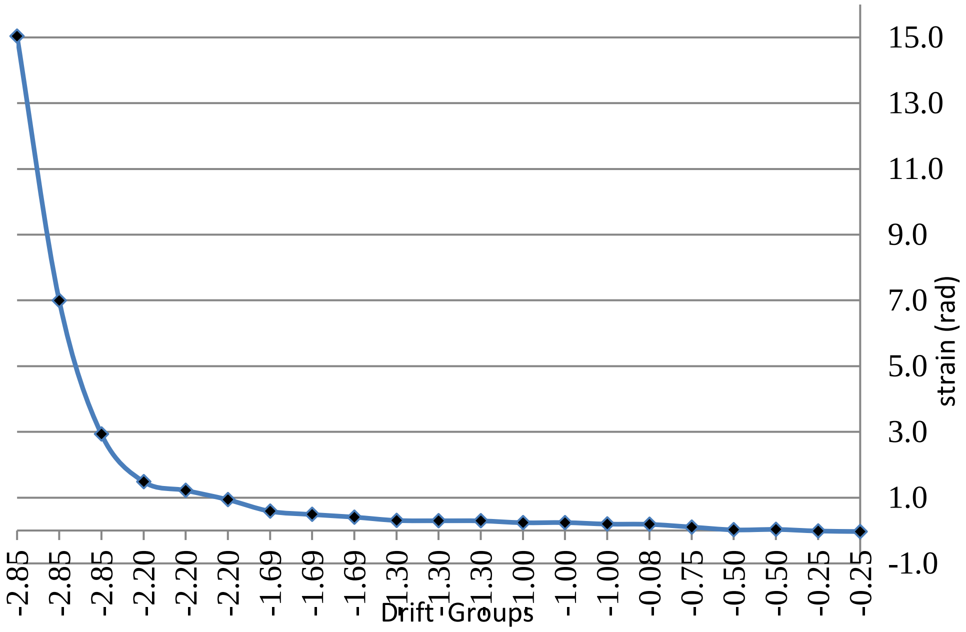

Figure 5.234: CSF-80-E Compression steel hoop strain Vs Drift groups (100mm)

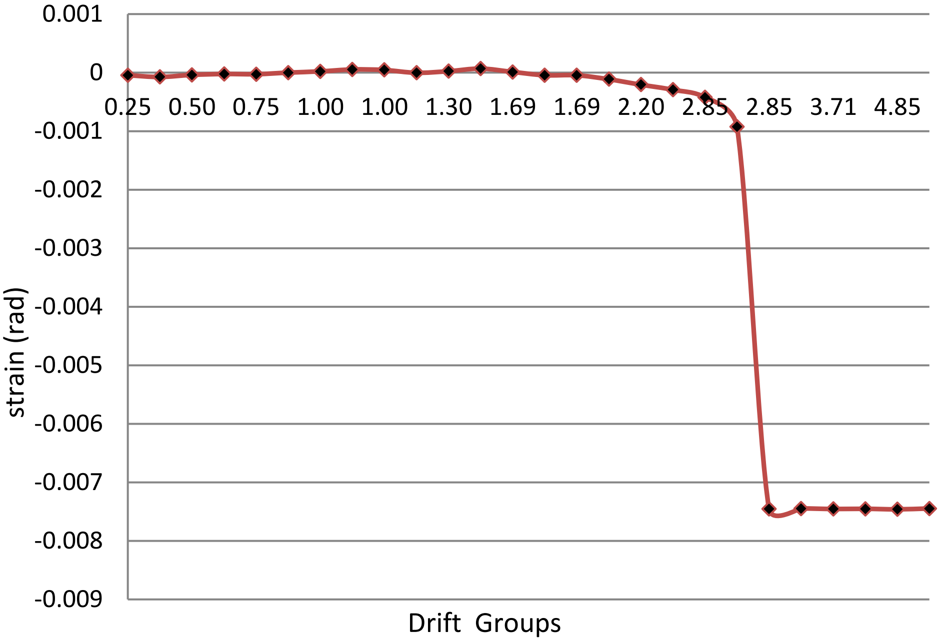

Figure 5.235: CSF-80-E Compression shear strain (rad) Vs Drift groups (vertical LVDTs 5-12) (Compression side)

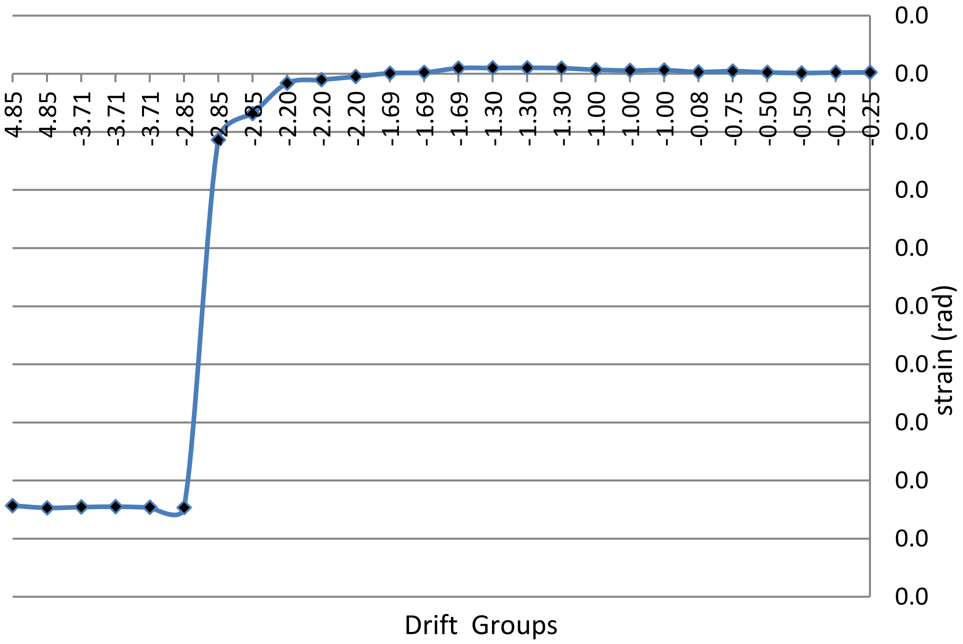

Figure 5.236: CSF-80-E Tension shear strain (rad) Vs Drift groups (vertical LVDTs 5-12) (compression side)

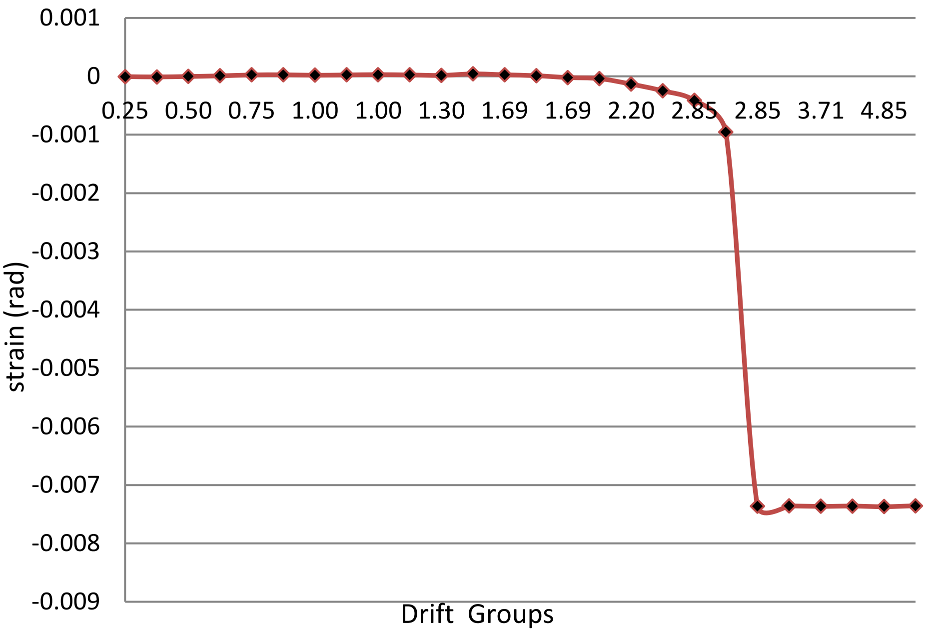

Figure 5.237: CSF-80-E Compression shear strain (rad) Vs Drift groups (Vertical LVDTs 5-12) (Tension side)

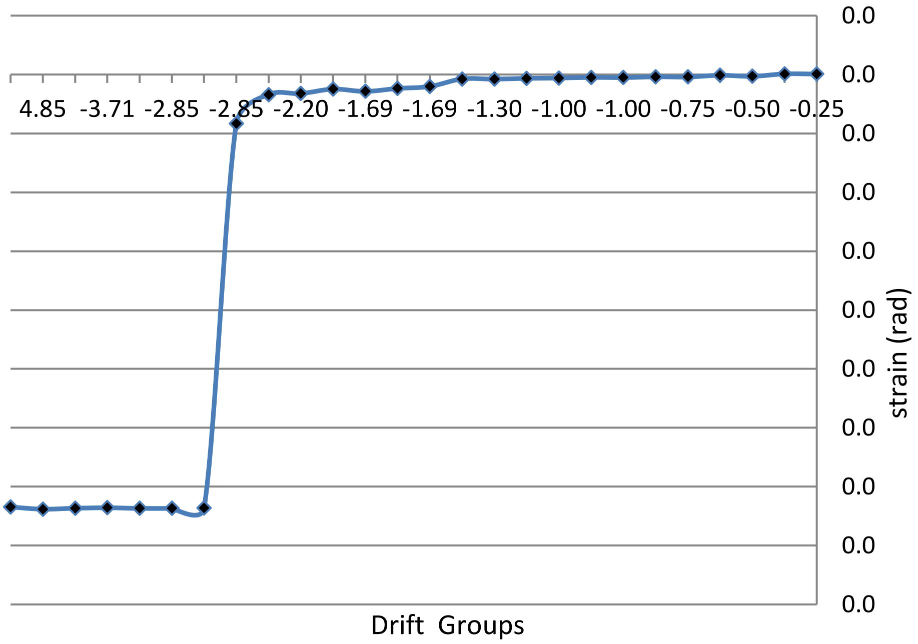

Figure 5.238: CSF-80-E Tension shear strain (rad) Vs Drift groups (vertical LVDTs 5-12) (tension side)

Table 5.5 shows the damage sequence for each specimen for each group cycles in displacement protocol. **Figures5.239. 5.240** and **5.241** show the backbone curve for shear force-drift hysteresis response for the both specimens to extract values from the curve. Table 5.6 shows the horizontal load and drift for both specimens for the yield, peak, and fracture which are extracted from previous curves. To show the damage deference between the two specimens **Figure 5.242:5.249**show the crack pattern for both in many levels of loading during the test.

Table 5.5: Qualitative damage description

Cycle	**Specimen 1 CSF 15-E**	**Specimen2 CSF 80-E**
0.25 Δy	No cracks	No cracks
0.5 Δy	Hairflexure cracking &Slipy	Haircracks
0.75 Δy	Cracking	Cracking
Δy	Yielding &cracking	Yielding &Cracking
1.3 Δy	Cracking & Start crushing concrete	Slipy& Stopping create new cracks
1.96 Δy	opening cracks & stopping create new cracks	opening cracks & Crushing concrete
2.2 Δy	Deeper cracking	Deeper cracking
2.85 Δy	Crushing concrete	Crushing concrete
3.72Δy	Two longitudinal bars was cut	Stirrups hoops opened & longitudinal bars and flanges buckled
4.87Δy	End of the test	End of the test

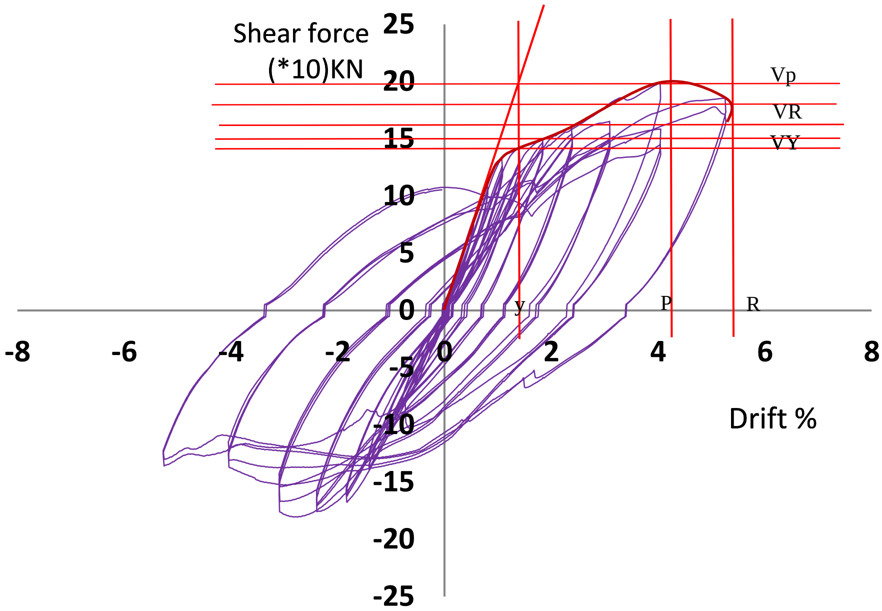

Figure 5.239: Specimen CSF 15 – E output curve data

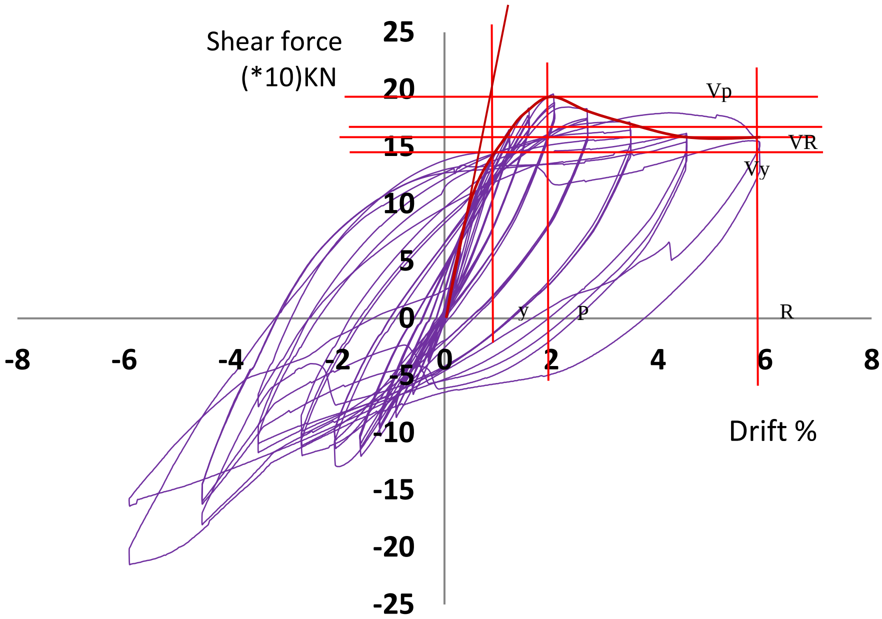

Figure 5.240: Specimen CSF 80-E output curve data

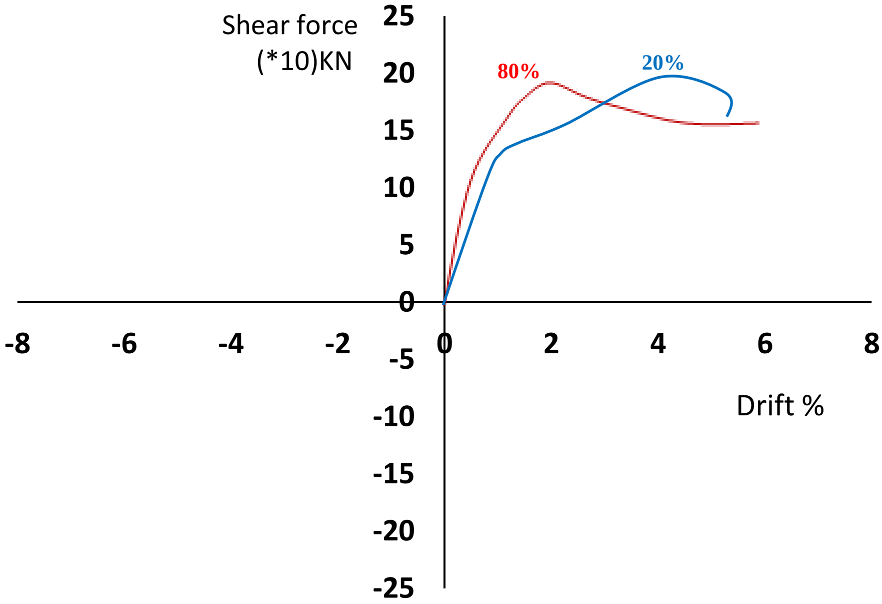

Figure 5.241: Envelope curves

Table 5.6: Comparison of flexure deficient specimens data curve outputs

#	Out put	CSF 15-E	CSF 80-E
1	**V peak Test**	150 KN	175 KN
2	**M peak Test**	225 KN M	262..5KN M
3	**Δ Vp%**	4.2%	2 %
4	**Vy Test**	120KN	140 KN
5	**Vy/Vpeak %**	80 %	80 %
6	**ΔVy%**	1.8 %	1.2 %
7	**V80%**	120 KN	140 KN
8	**ΔV80%**	4.6%	5.6 %
	VR	130 KN	95 KN
10	**VR/VP %**	86.67 %	54.28 %
11	**Δ VR**	6 %	6 %
12	**μΔ= ΔV80/ΔVy**	6.5 %	3.8 %
13	**μf= ΔVR/ΔVp**	1.43 %	3 %

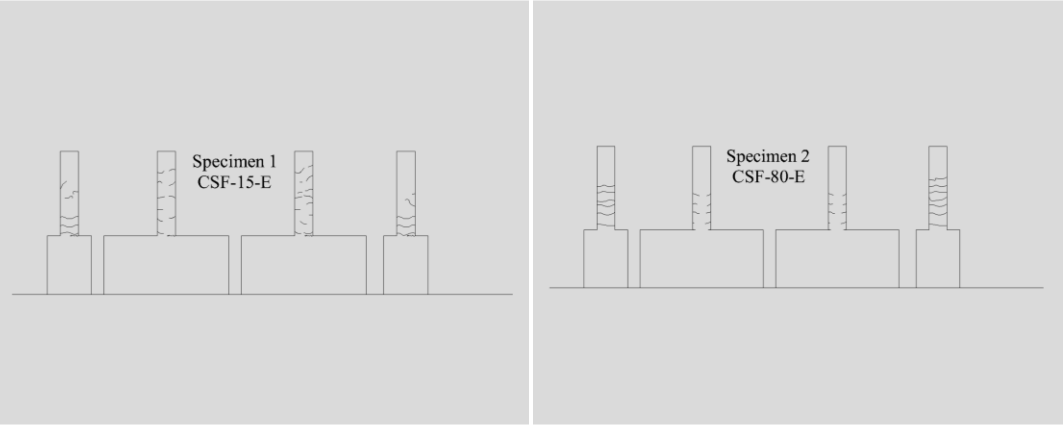

Figure 5.242: Crack pattern at (Δ y) lateral displacement

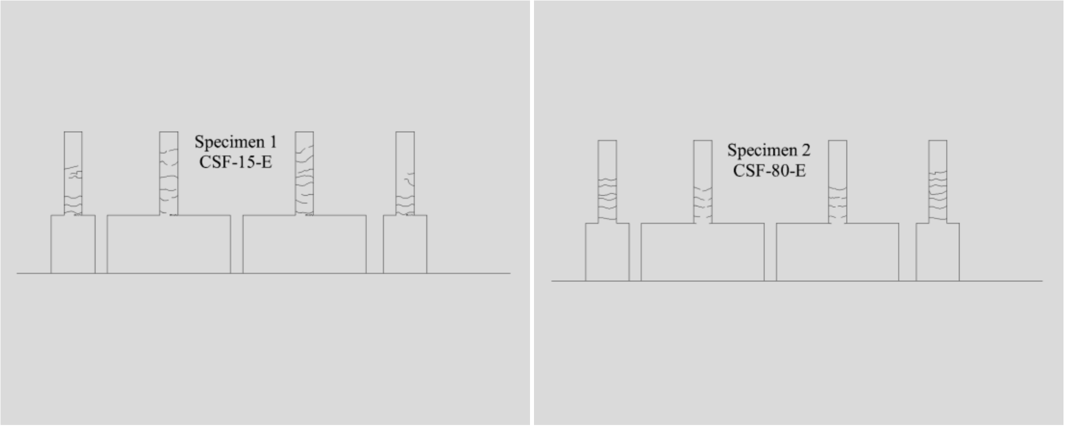

Figure 5.243: Crack pattern at (1.3 Δ y) lateral displacement

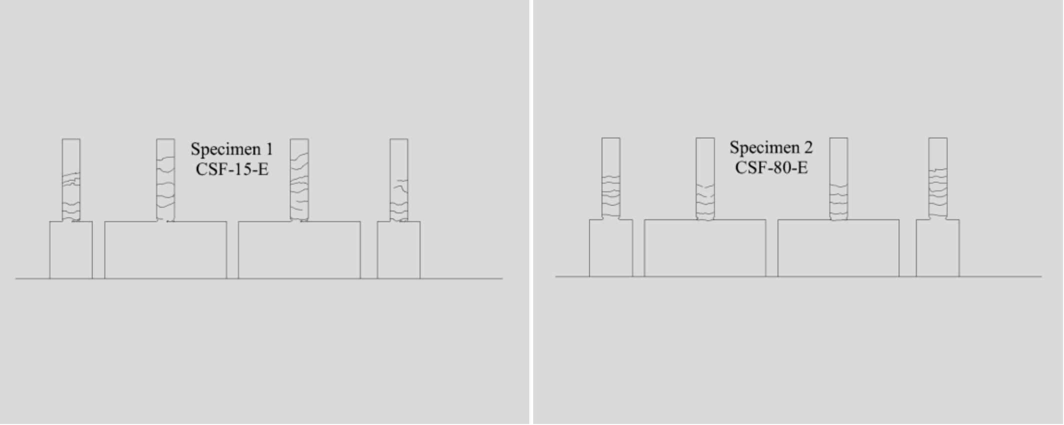

Figure 5.244: Crack pattern at (2.2 Δ y) lateral displacement

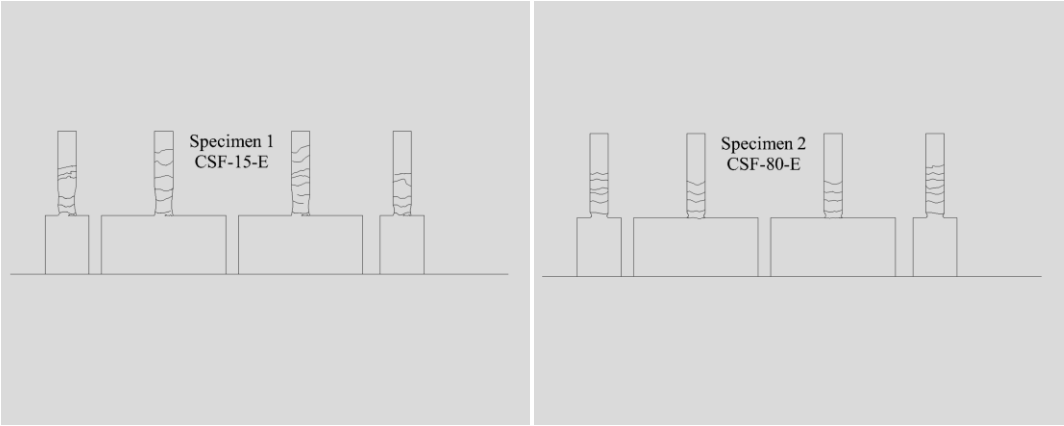

Figure 5.245: Crack pattern at (3.73 Δ y) lateral displacement

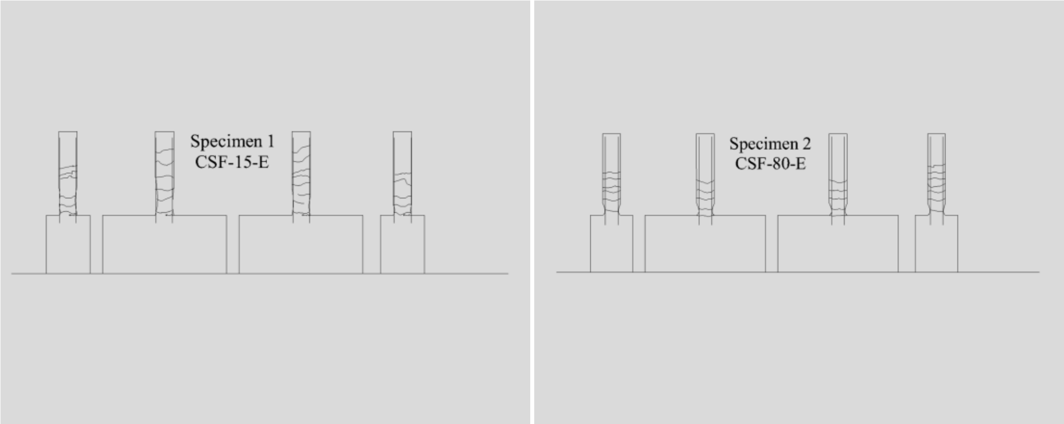

Figure 5.246: Crack pattern at (4.87 Δ y) lateral displacement

6. Chapter (6)

Discussion of Test Results

1. Modern building

1. Effect of axial load ratio

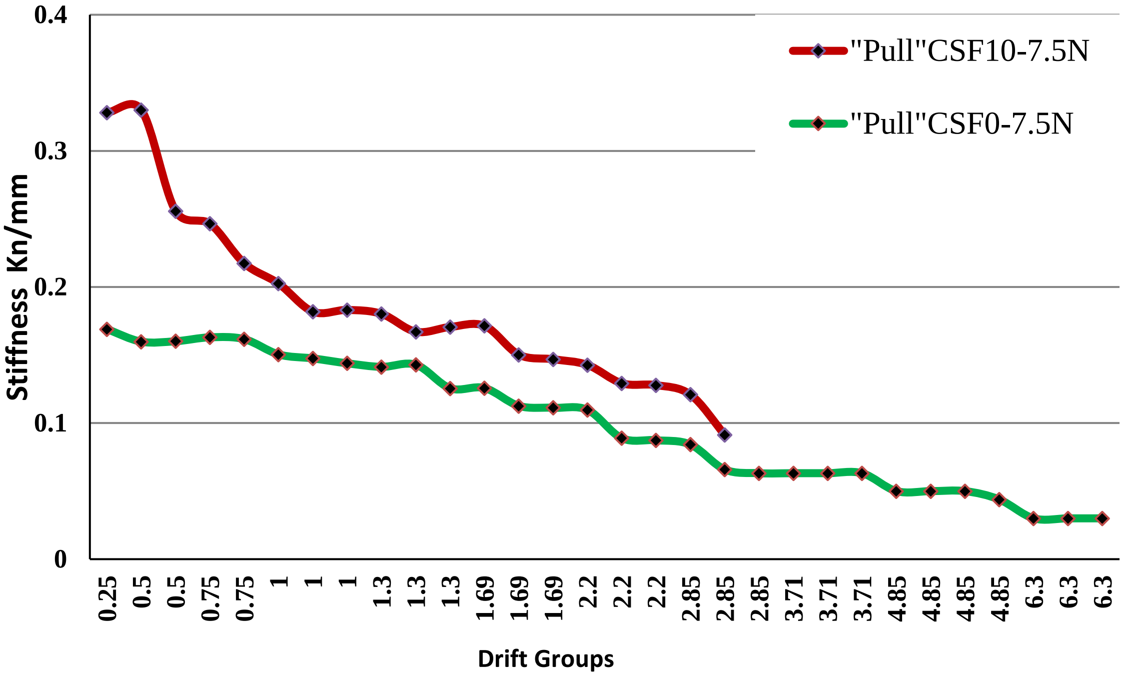

Figure 6.1: Peak to Peak stiffness of flexure modern building specimens (pull direction) (axial load effect)

- **Increasing axial load ratio from 0% to 10% increased the column stiffness peak about 200% in tension direction. Increasing loading, increase column resistance to horizontal loading**

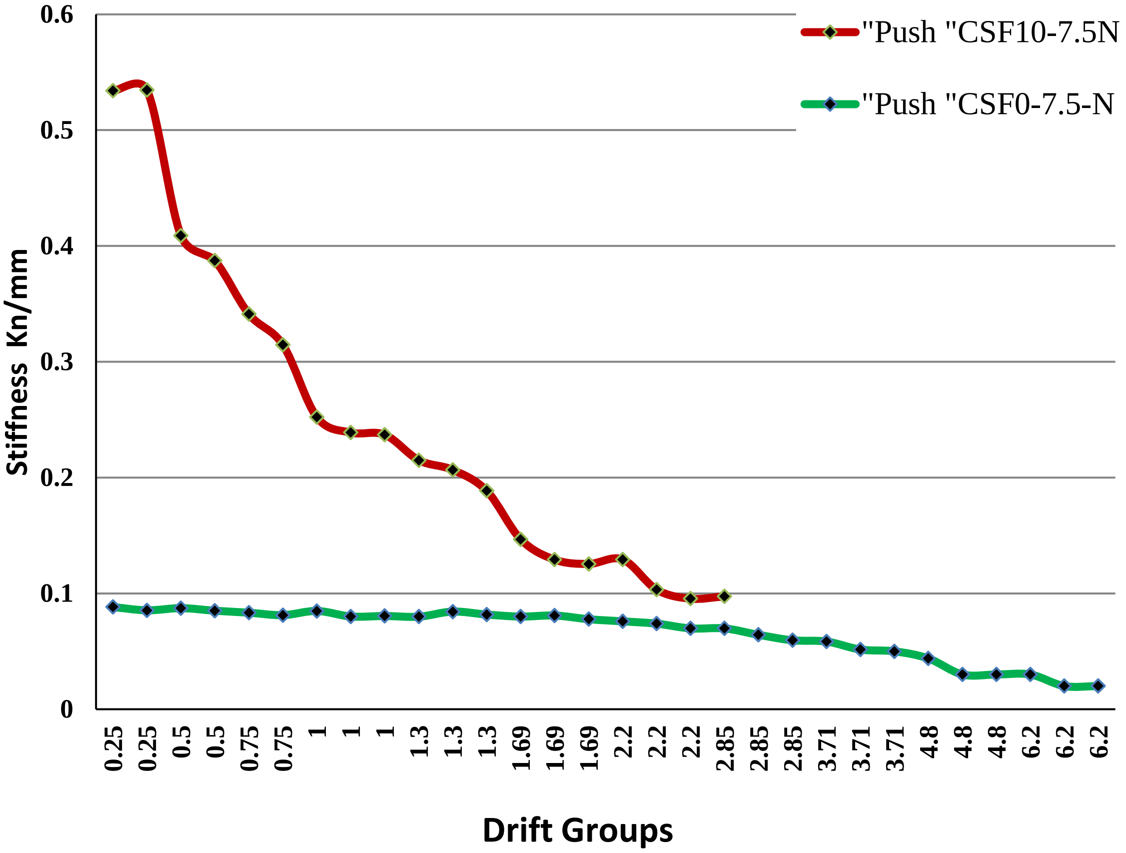

Figure 6.2: Peak to Peak stiffness of flexure modern building specimens (push direction) (axial load effect)

- **Increasing axial load ratio from 0% to 10% increased the column stiffness peak to about 500 % in compression direction.**

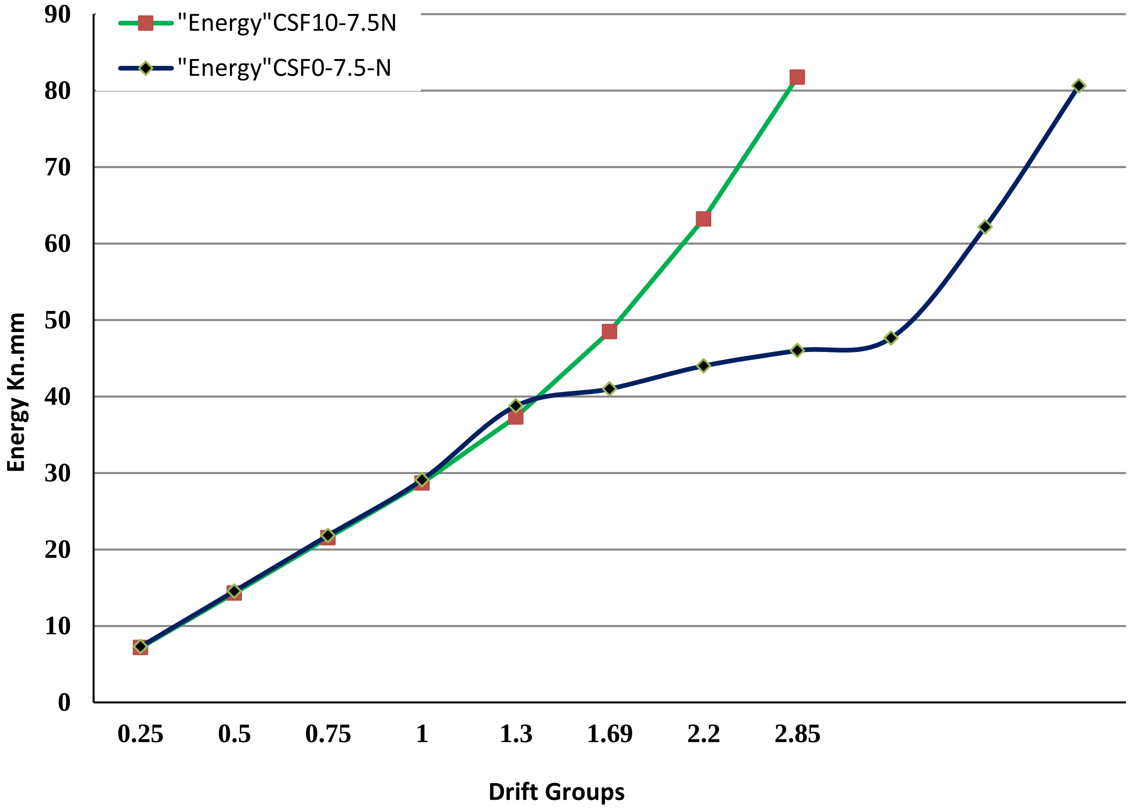

Figure 6.3: Peak to peak Energy of flexure modern building specimens (axial load effect)

- **Increasing axial load ratio from 0% to 10% decreased the column energy dissipation. As a predicted result the specimen of the higher axial load ratio, is less energetic than the low axial load specimen which has a higher drift capacity. Free specimen which only horizontally loaded without axial load can reach to higher drift values compared with the specimen that was axially loaded.**

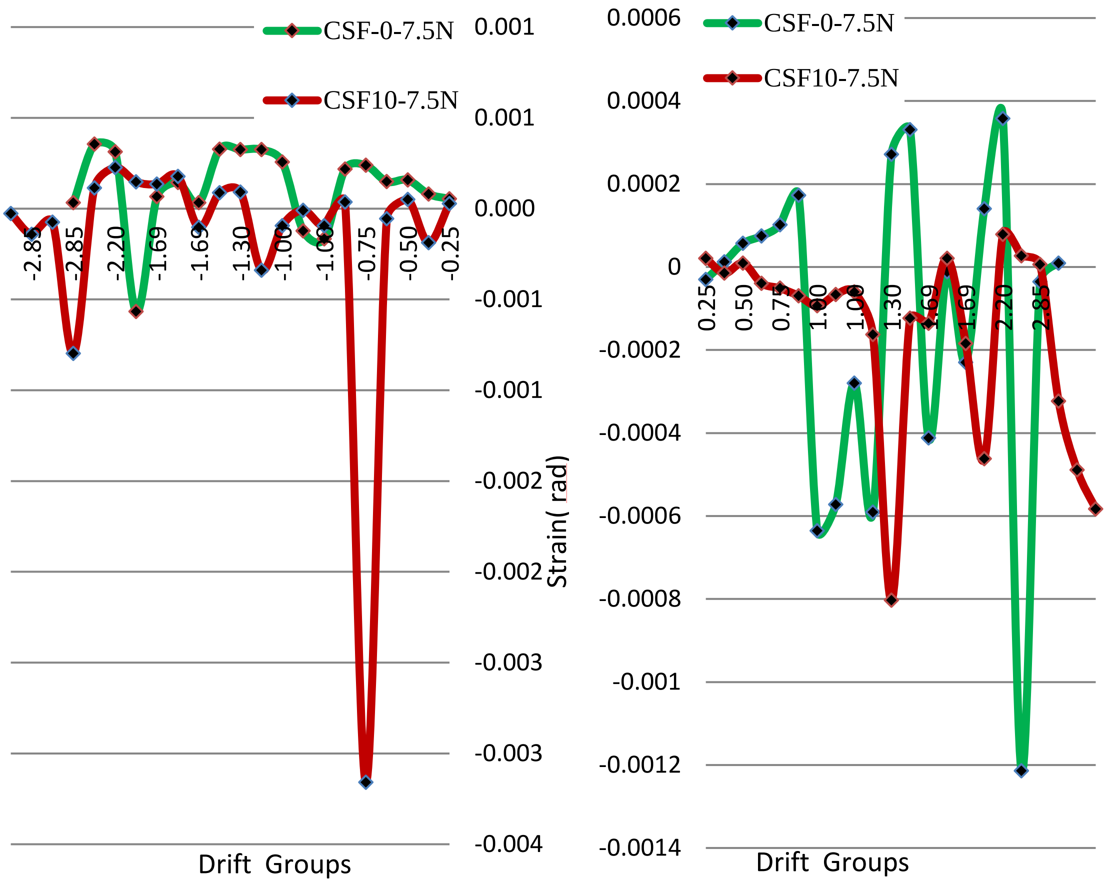

Figure 6.4: Compression and tension shear strain (rad) Vs Drift groups (Vertical LVDTs 5-12) (Tension side) (Axial load effect)

- **Increasing axial load ratio from 0% to 10% increase crack wide in CSF10-7.5N in compression loading direction than CSF-0-7.5N. Otherwise, CSF-0-7.5N had a wider crack in tension loading direction than CSF-10-7.5N.**

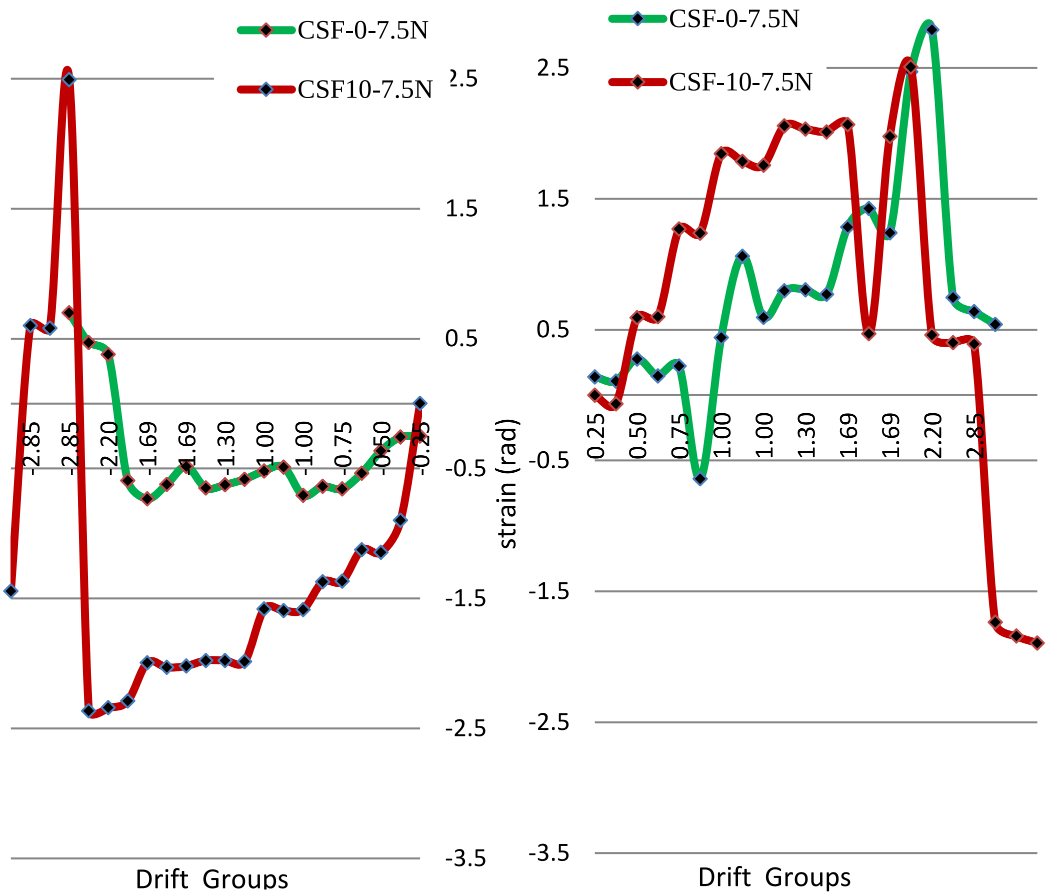

Figure 6.5: Compression and tension flange steel strain Vs Drift groups (125mm) (axial load effect)

- **Increasing axial load ratio from 0% to 10% appeared with more deformation of the steel section flange of CSF-10-75-N in both direction more than the deformation occurred in CSF-0-75-N**

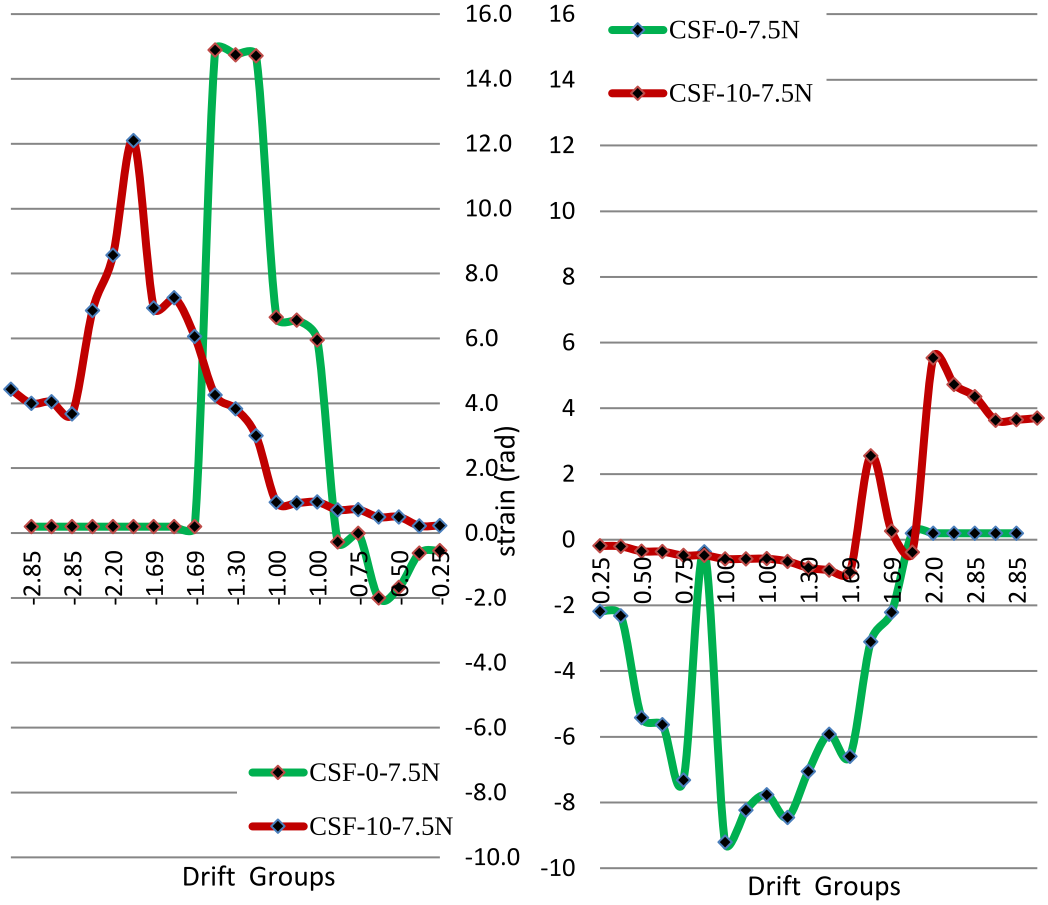

Figure 6.6: Compression and tension steel bar strain Vs Drift groups (125mm) (Compression side) (axial load effect)

- **Increasing axial load ratio from 0% to 10% affected on more tension force in steel bar in CSF-0-75-N axially loaded specimen was under a compression force that reduce tension force in longitudinal steel bars.**

2. Effect of confinement

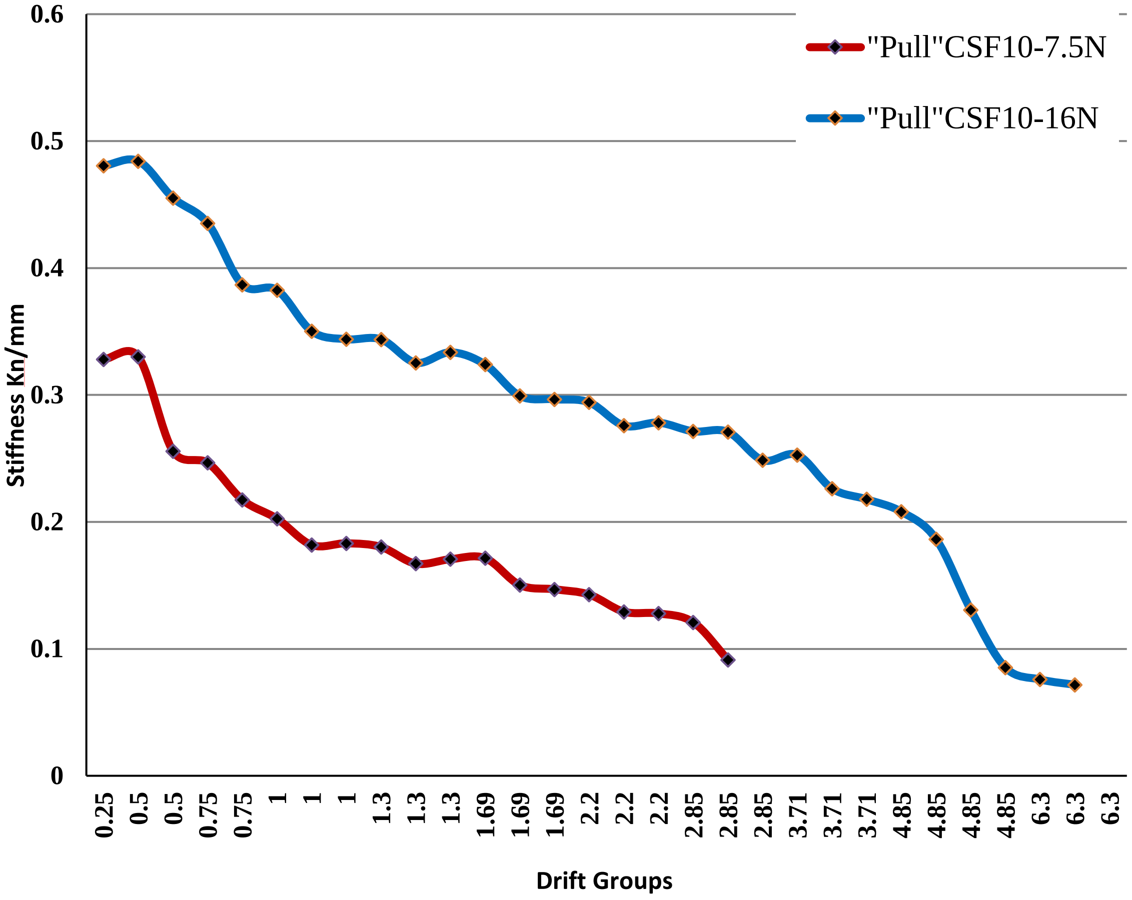

Figure 6.7: Peak to Peak stiffness of flexure modern building specimens (Pull direction) (confinement effect)

- **Increasing confinement by decreasing hoop spacing from 160 mm to 75 mm decreasing the stiffness peak from 0.48 to 0.33 in tension direction which was not predicted. Because of increasing confinement, increase the specimen load capacity which means stiffness increase.**

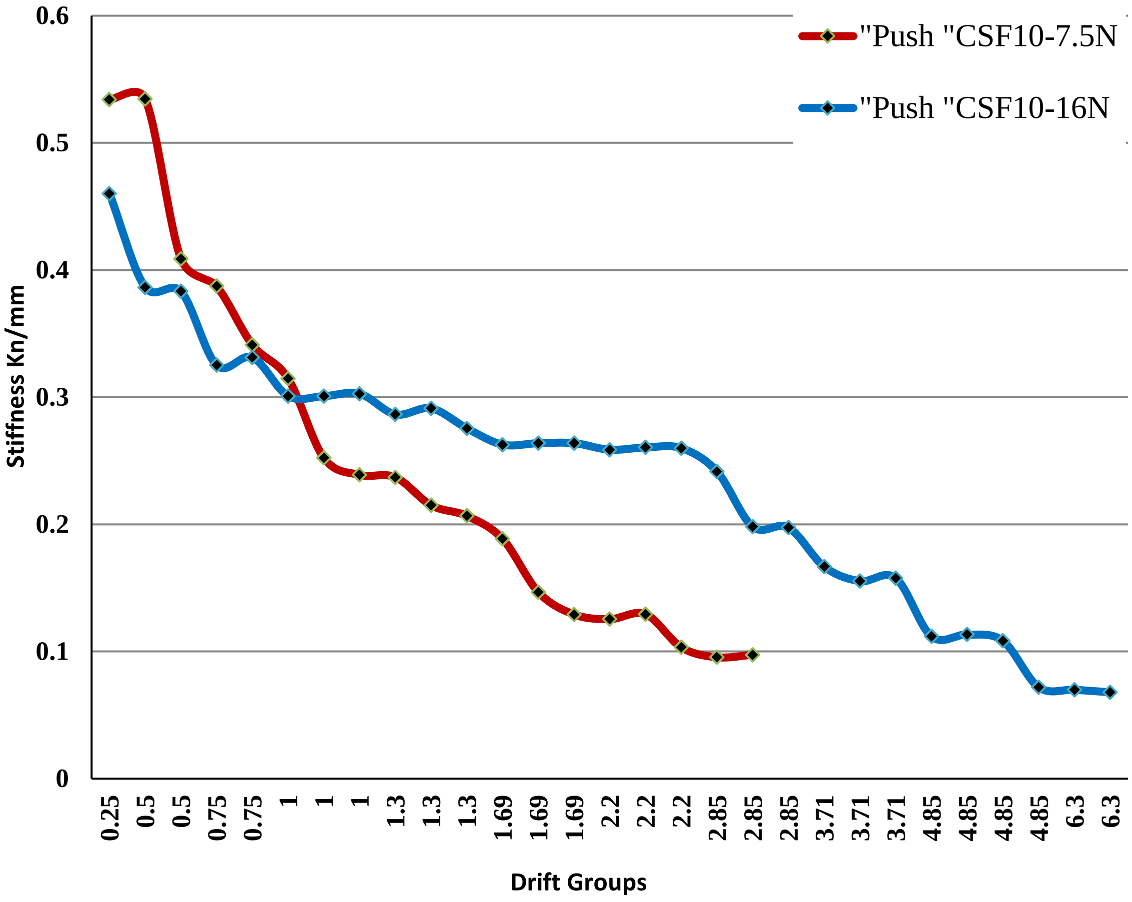

Figure 6.8: Peak to Peak stiffness of flexure modern building specimens (Push direction) (confinement effect)

- **Stiffness peak increased in compression with a few value less than 10% by increasing column confinement. Normally finding stiffness peak resulted from push direction higher than the stiffness value from pull direction. CSF-10-75N's stiffness value was higher but the slope curve was dramatically due the small spacing between stirrups increase the specimen brittleness. CSF-10-16N's stiffness value was lower but the blue curve show that increasing stirrups spacing lead to more ductility.**

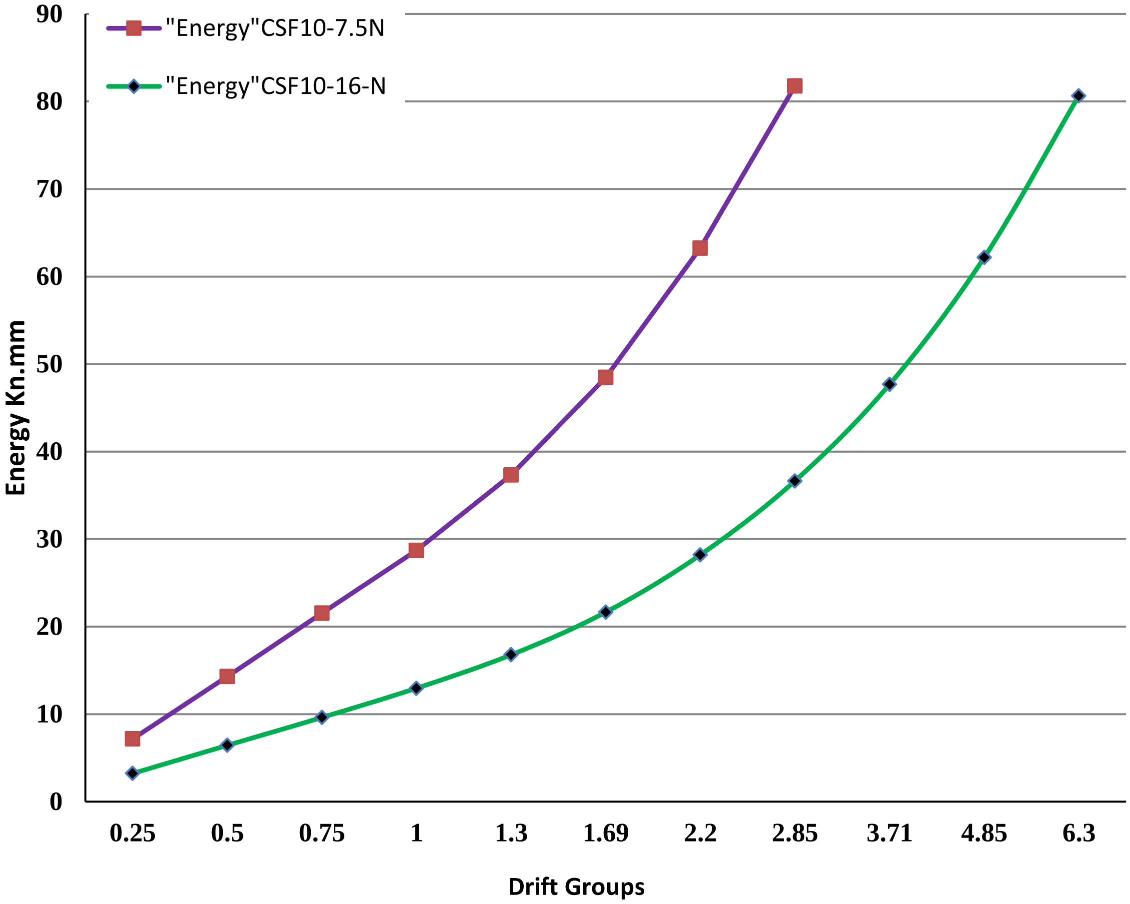

Figure 6.9: Peak to peak Energy of flexure modern building specimens (confinement effect)

- **More confinement, less energy specimen. Specimen with larger hoop spacing is higher drift capacity than the well confined specimen**

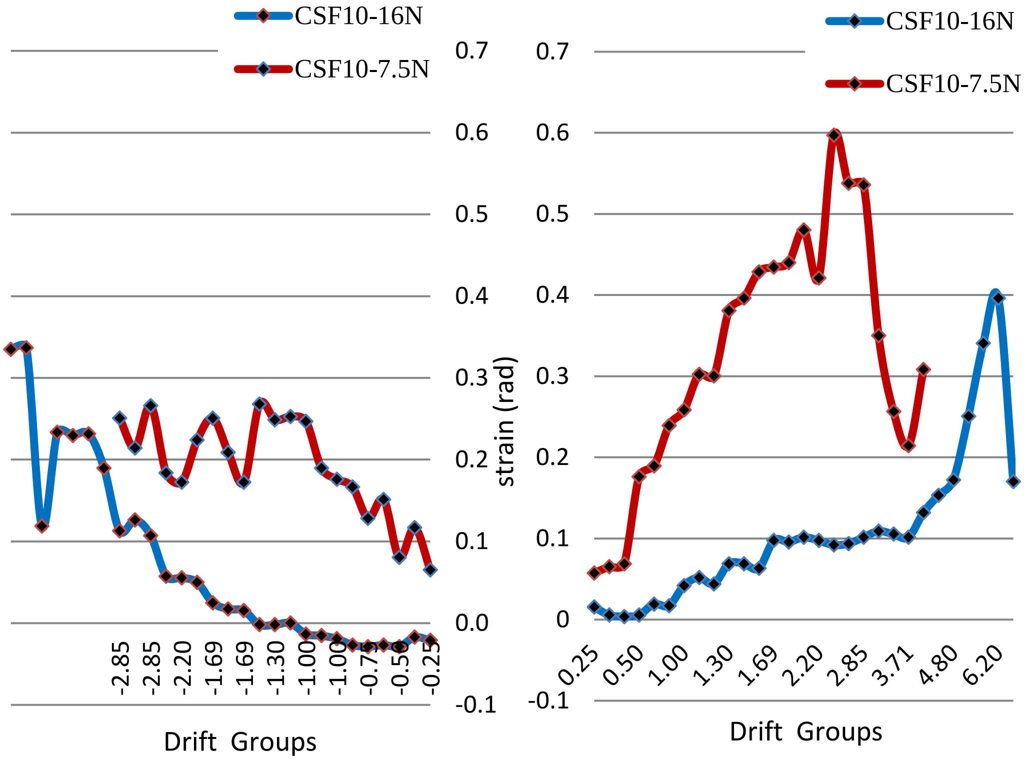

Figure 6.10: Compression and tension shear strain (rad) Vs Drift groups (Vertical LVDTs 5-12) (Tension side) (Confinement effect)

- **Concrete and steel web carry some of hoop strain in less confinement column.**

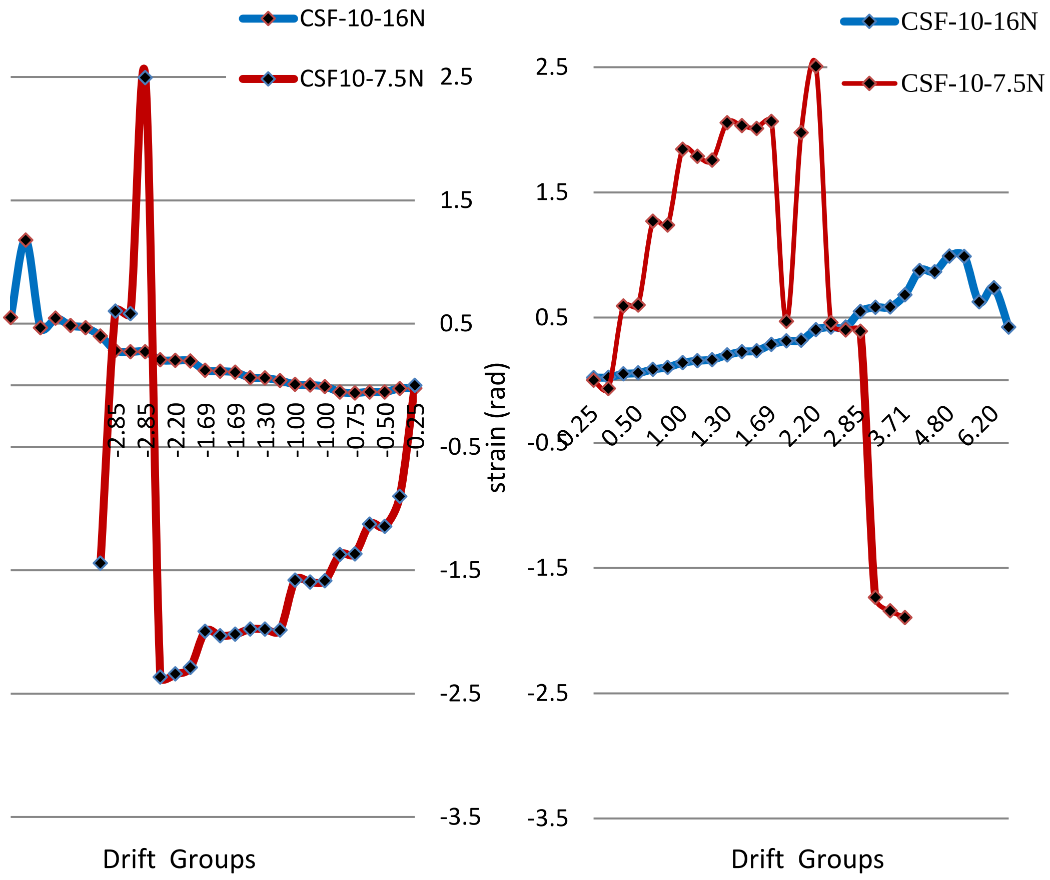

Figure 6.11: Compression and tension flange steel strain Vs Drift groups (125mm) (Confinement effect)

- **Steel section flanges reached to higher deformation in the more confinement column rather than the other one. Low stirrups space decreases the concrete ductility, so steel flanges resist the flexure deformation.**

2. Existing building

1. Effect of axial load ratio

1.1. Shear controlled specimens

S80. The peak shear strength reached was 220 KN which is significantly higher than the 158 KN theoretically predicted shear strength of AISC 341. On the contrary, the increase in the axial load ratio from 15% in specimen S15 to 80% in specimen S80 did not result in an increase in peak shear strength. However, the loading stiffness of specimen S80 is obviously higher than that of specimen S40 as can be clearly observed, which shows the backbone curves of all specimens in the positive (initial) loading direction. Higher axial load ratio resulted in increasing axial stiffness. The peak shear strength was reached at 2% drift ratio, which is about 32.2% less than that of specimen S15, 52.3% less than that of specimen S20, 52.3% less than that of specimen S40, emphasizing the effect of higher axial load in limiting the deformability and energy dissipation of the test specimen. This can be also observed by comparing the fatness of the hysteresis loops in specimen S15, S20 and S40 compared to those in specimen S80. Moreover, the axial failure drift capacity of specimen S80 was 3.9% which is about 32.7% less than the 5.8% drift capacity of specimen S15, 33.33% less than the 5.85% drift capacity of specimen S20, and 29% less than the 5.5% drift capacity of specimen S40. This further indicates the limited seismic deformation capacity imposed by the higher axial load in specimen S80. The post peak shear strength degradation in specimen S80 is better than that of specimen S15, S20, and S40 confirming the same observation. The axial failure corresponded to a 47.83 % drop in the lateral load capacity in specimen S15, 21.54 % drop in the lateral load capacity in specimen S20, and 15.4% drop in the lateral load capacity in specimen S40, while it corresponded to 12.44% drop in lateral load capacity in specimen S80. The drift ratio corresponding to reaching 20% shear strength degradation in specimen S80 was 3.5%, which is 23% less than its counterpart in specimen S40. This 3.5% reduced drift capacity is deemed relatively high compared to its counterpart in existing reinforced concrete buildings undergoing strong shaking and experiencing column shear failure; however, it is considered insufficient if compared to the modern building seismic drift capacity requirements under collapse prevention limit state as recommended by Tall Building Initiative (2011). Thus, retrofitting such shear deficient columns experiencing moderate to strong ground shaking under high axial loads seems inevitable.

As it mentioned before that specimen 1 (CSS-15-E) was loaded with axial load 15% of the concrete section strength with 255 KN, the specimen (CSS-20-E) was loaded with axial load 20% of the concrete section strength with 465 KN, the specimen (CSS-40-E) was loaded with axial load 40% of the concrete section strength with 670 KN, the specimen (CSS-60-E) was loaded with axial load 60% of the concrete section strength with 1400 KN, and the specimen (CSS-80-E) was loaded with axial load 80% of the concrete section strength with 1300 KN. The comparison between specimens show there are some effects of the axial load variables ratios of the column behavior under the seismic loading for the existing building.

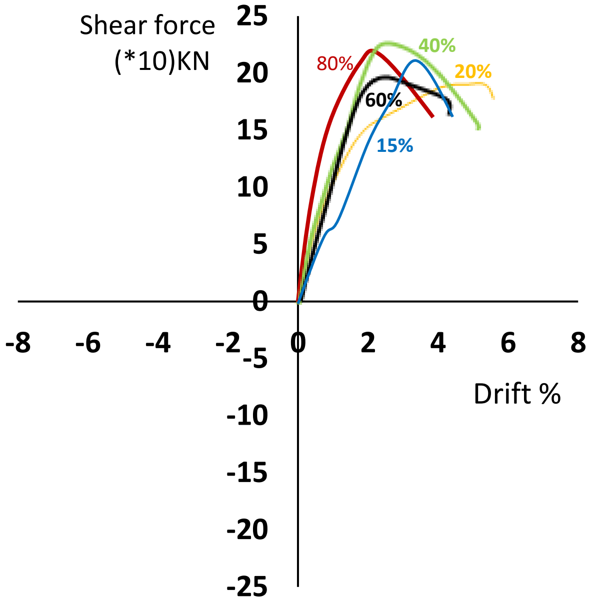

Figure 6.12: Shear deficient old building specimens Backbone curves

- **Increasing axial load ratio from 15% to 80% Decreased the drift Capacity gradually from Specimen CSS-15-E to CSS-80-E**

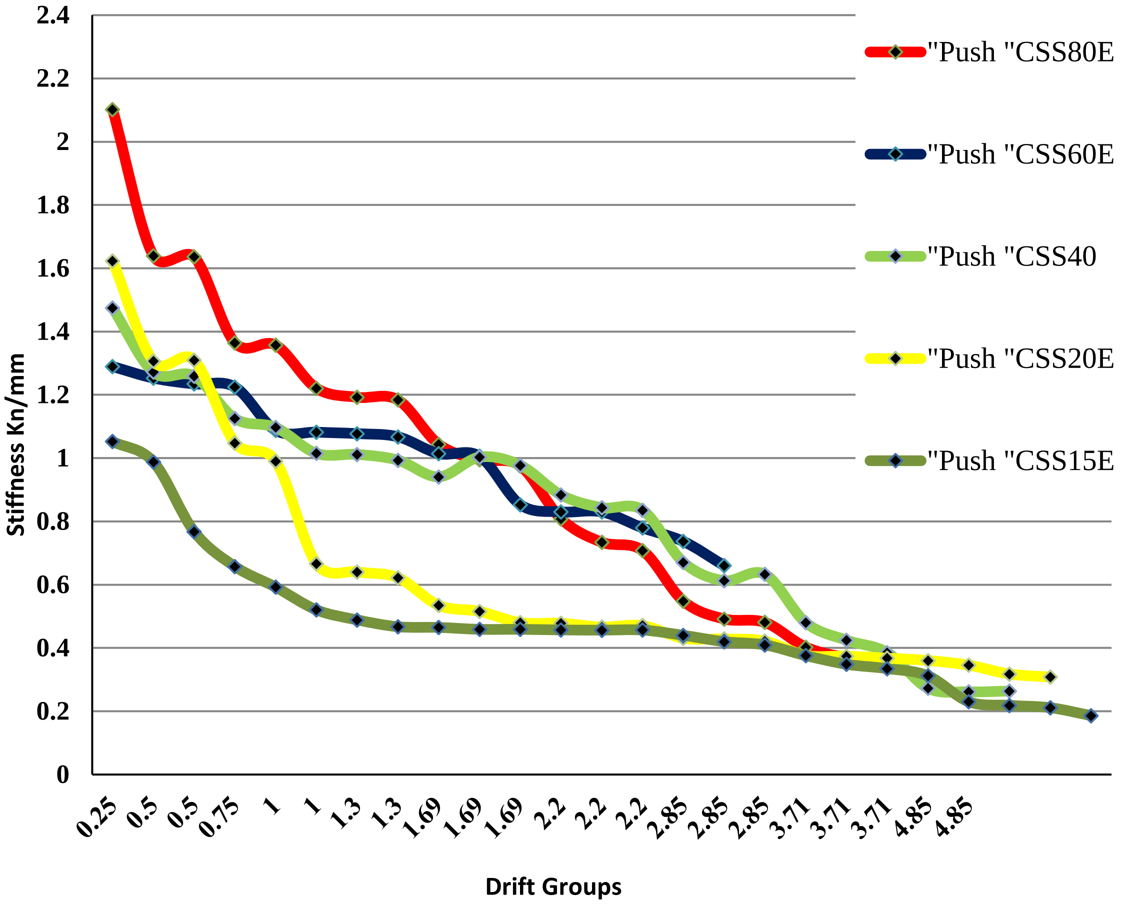

Figure 6.13: Peak to Peak stiffness of shear old building specimens (push direction)

- **Increasing axial load ratio from 15 % to 80% doubled the peak stiffness in compression direction. In CSS-15-E reach to about 1 Kn/ mm and with increasing load to 80% ratio CSS-80-E reach to 2.1 Kn/mm stiffness.**

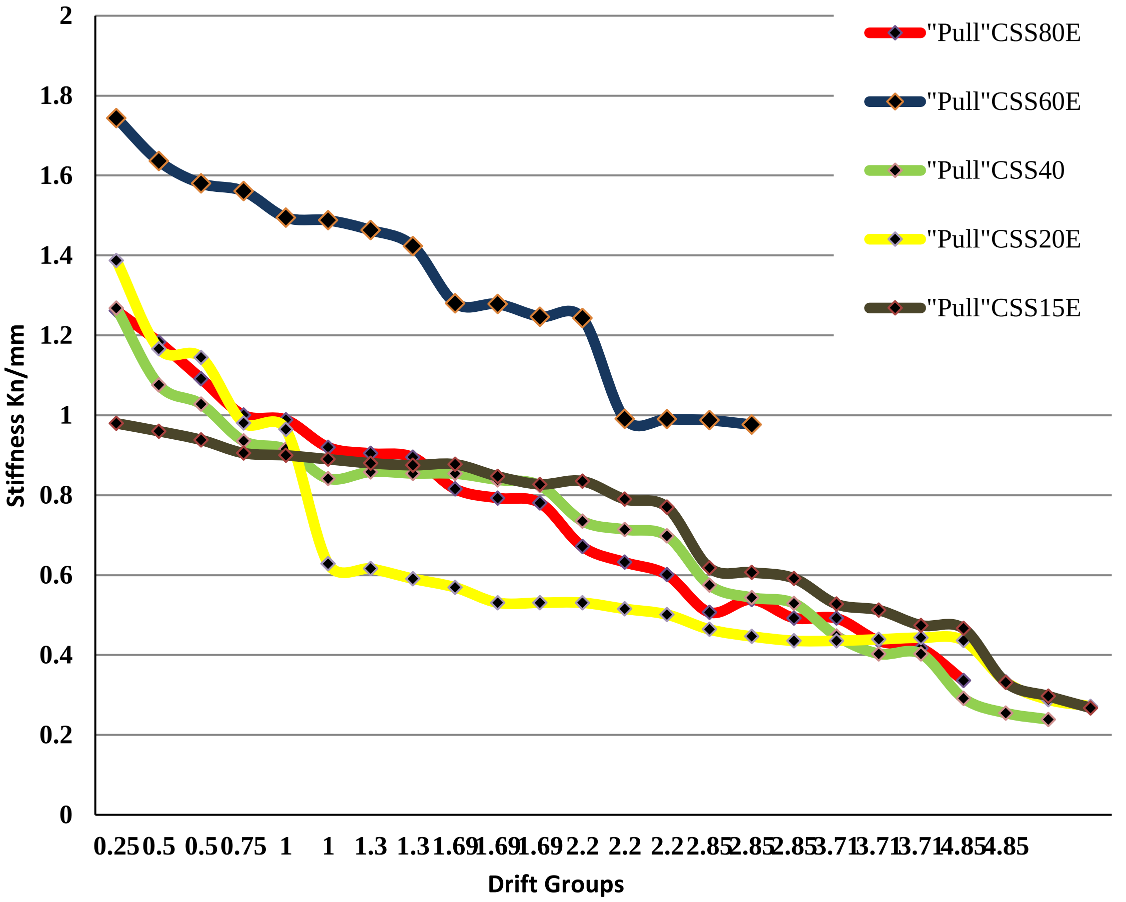

Figure 6.14: Peak to Peak stiffness of shear old building specimens (pull direction)

- **Increasing axial load ratio from 15 % to 80% has not a big effect on stiffness peak in tension direction. This result came from that concrete in tension direction already started cracking during loading compression direction to make a decreasing of tension direction stiffness.**

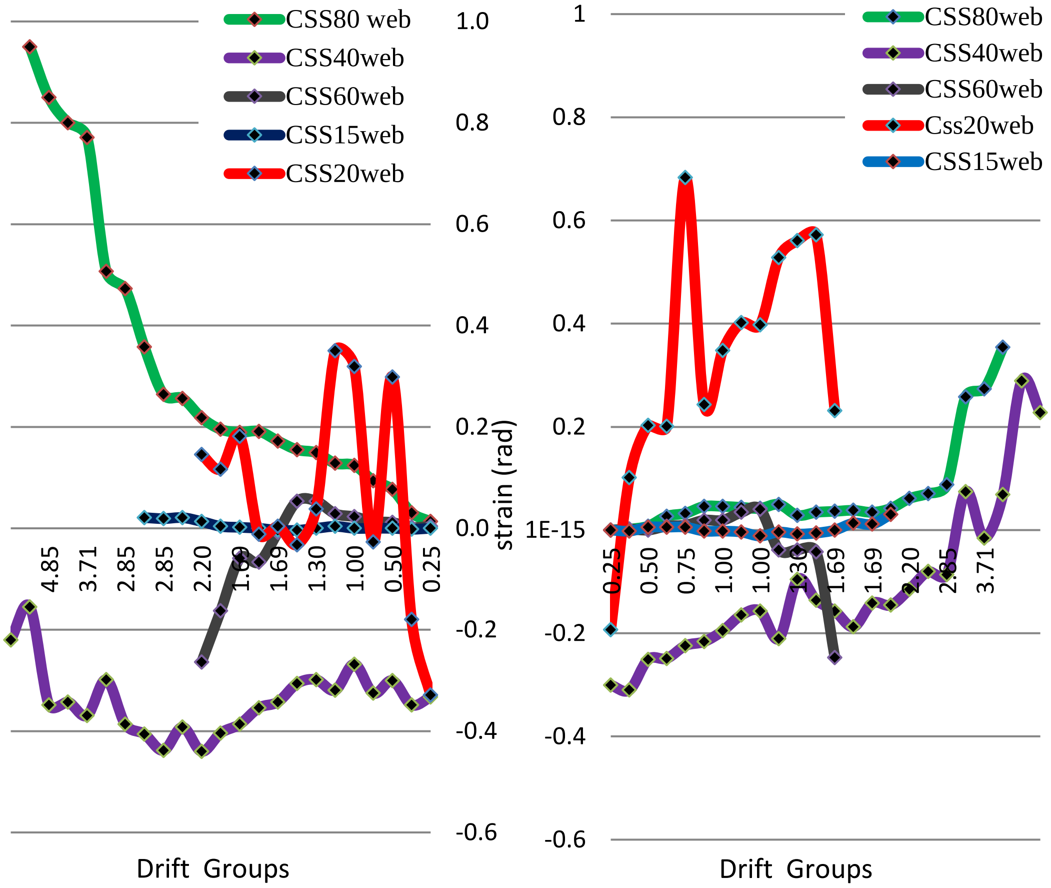

Figure 6.15: Compression and tension Web steel strain Vs Drift groups (320mm)

- **As predicted according to increasing axial load ratio from 15% to 80%, increased the deformation of steel web due to resisting more shear force.**

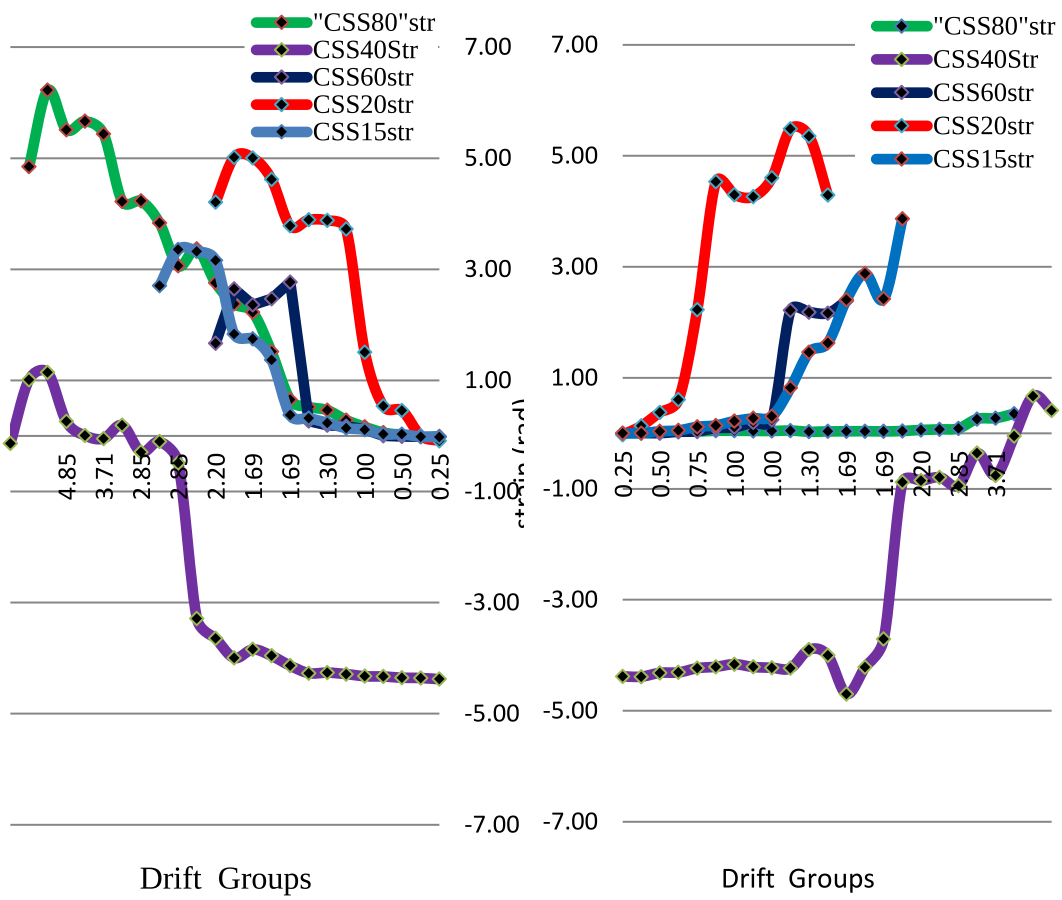

Figure 6.16: Compression and tension steel hoop strain Vs Drift groups (325 mm)

- **CSS-80-E's tension curve show a larger deformation in stirrup in level 325mm from bas surface. Under higher axial load ratio lower concrete area failed under compression which affected on stirrups in this part.**

2.2. Flexure controlled specimen

F80. The peak strength reached was 175 kN which is higher than the 128 kN theoretically predicted strength using XTRACT. The loading stiffness of specimen F80 is obviously higher than that of specimen F15 as can be clearly observed from, which shows the backbone curves of the two specimens in the positive (initial) loading direction. This is attributed to the higher axial load ratio effect in increasing axial stiffness. The peak strength was reached at 2% drift ratio, which is about 52.4% less than that of specimen F15, emphasizing the effect of higher axial load in limiting the deformability and energy dissipation of the test specimen. This can be also observed by comparing the characteristic fatness of the pre-peak hysteresis loops in specimen F15 indicating flexural tension yielding compared to the narrow ones in specimen F80 suggested more axially driven behavior. Moreover, the axial failure drift capacity of specimen F80 was 95KN at the same drift of F15 6% which is about 27% less than the 130 KN axial failure capacity of specimen F15. This further indicates the limited seismic deformation capacity imposed by the higher axial load in F80 specimen. The post-peak strength degradation in specimen F80 is much more pronounced than that of specimen F15 confirming the same observation. The highly flattened hysteretic loops in specimen F80 following the axial failure characterize that the specimen response is driven by the steel section residual capacity following out-of-plane deformations. Comparing the drift ratio at the onset of lateral strength loss (2%) to the MCE acceptance criteria of TBI 2011 (3% for the mean of a ground motion suite) indicates the limited deformability and the proneness to collapse of SRC columns in existing buildings with a strong seismic event. This suggests the need to retrofit existing SRC columns with high axial ratios. The unsymmetrical hysteresis loops following loss of lateral strength is resulted from the unsymmetrical loss of concrete compression zone and the out-of-plane buckling deformation of the steel section which is inherently unsymmetrical.

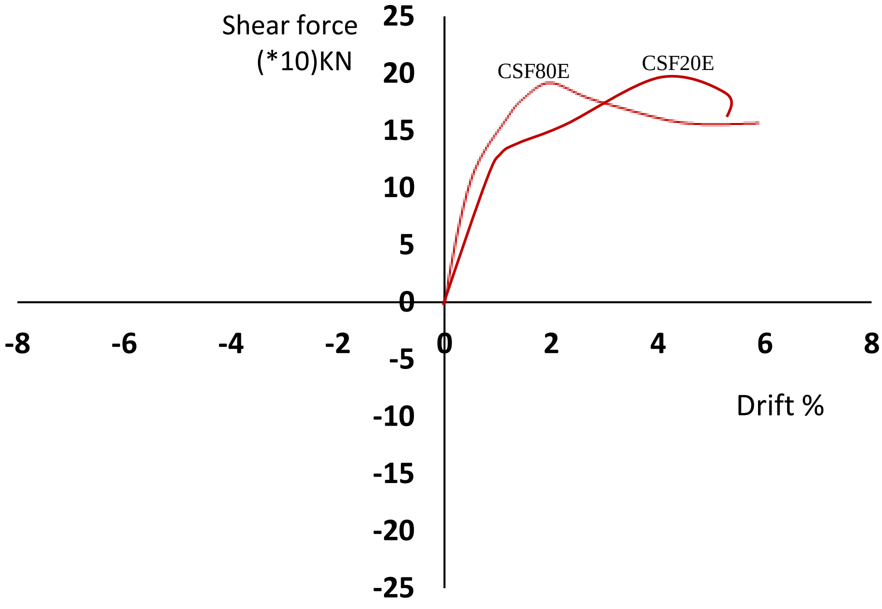

Figure 6.17: Shear deficient old building specimens Backbone curves

- **Increasing axial load ratio from 15 % in CSF-15-E to 80% in specimen CSF-80-E lead to 57% peak strength drift capacity reduction, 26% axial failure drift capacity reduction, higher loading stiffness, and accelerated post-peak stiffness & strength degradation.**

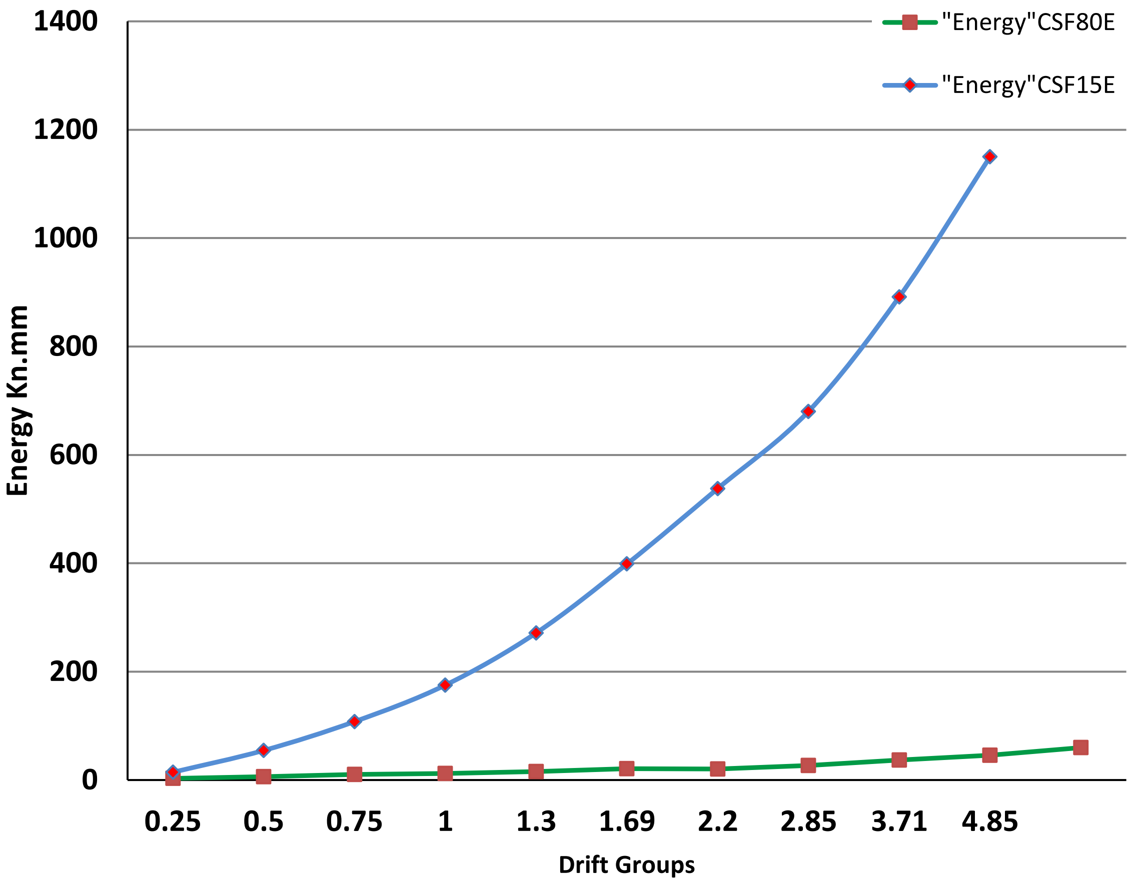

Figure 6.18: Peak to peak Energy of flexure old building specimens

- **The tension flexure failure specimen was more energetic than the flexure compression failure specimen due to the ductility of steel bars**

.

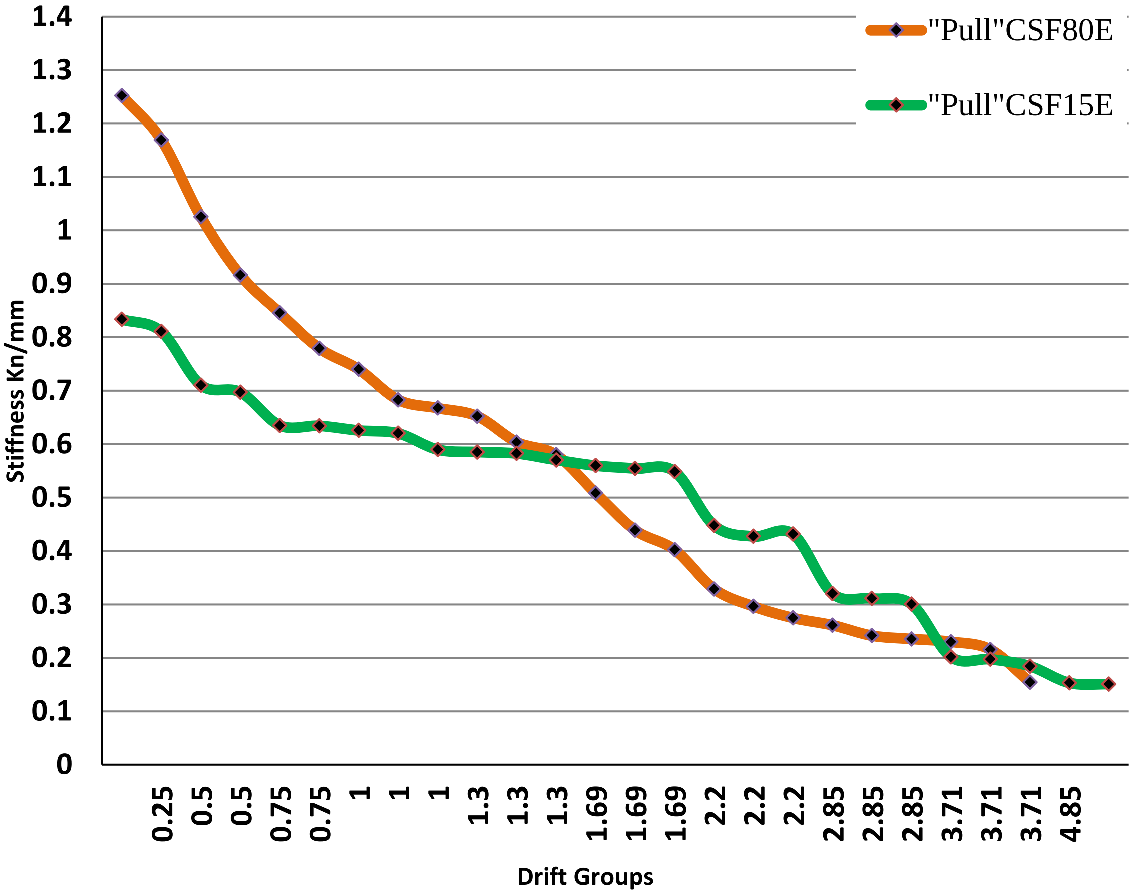

Figure 6.19: Peak to Peak stiffness of flexure old building specimens (pull direction)

- **Increasing axial load ratio from 15 % to 80% increased peak stiffness with 150% in tension direction**

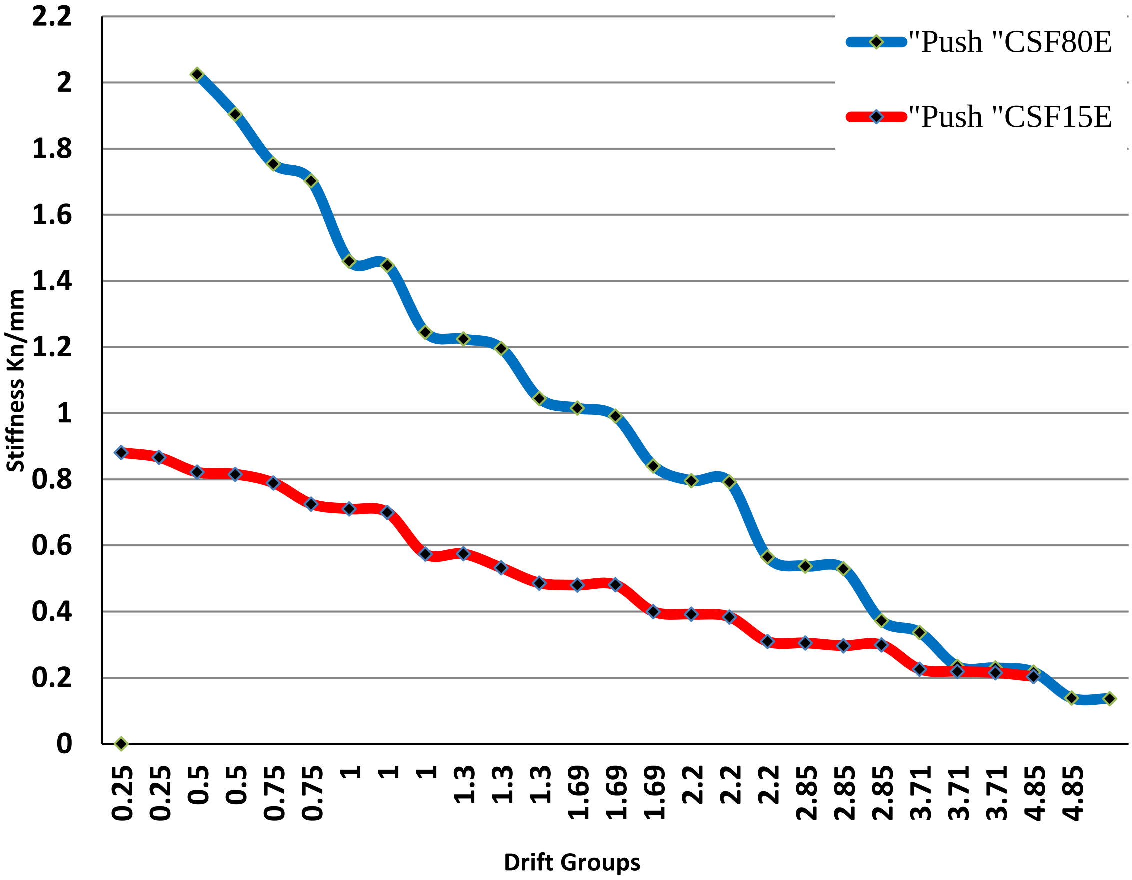

Figure 6.20: Peak to Peak stiffness of flexure old building specimens (push direction)

- **Increasing axial load ratio from 15 % to 80% increased peak stiffness with more than double in compression direction.**

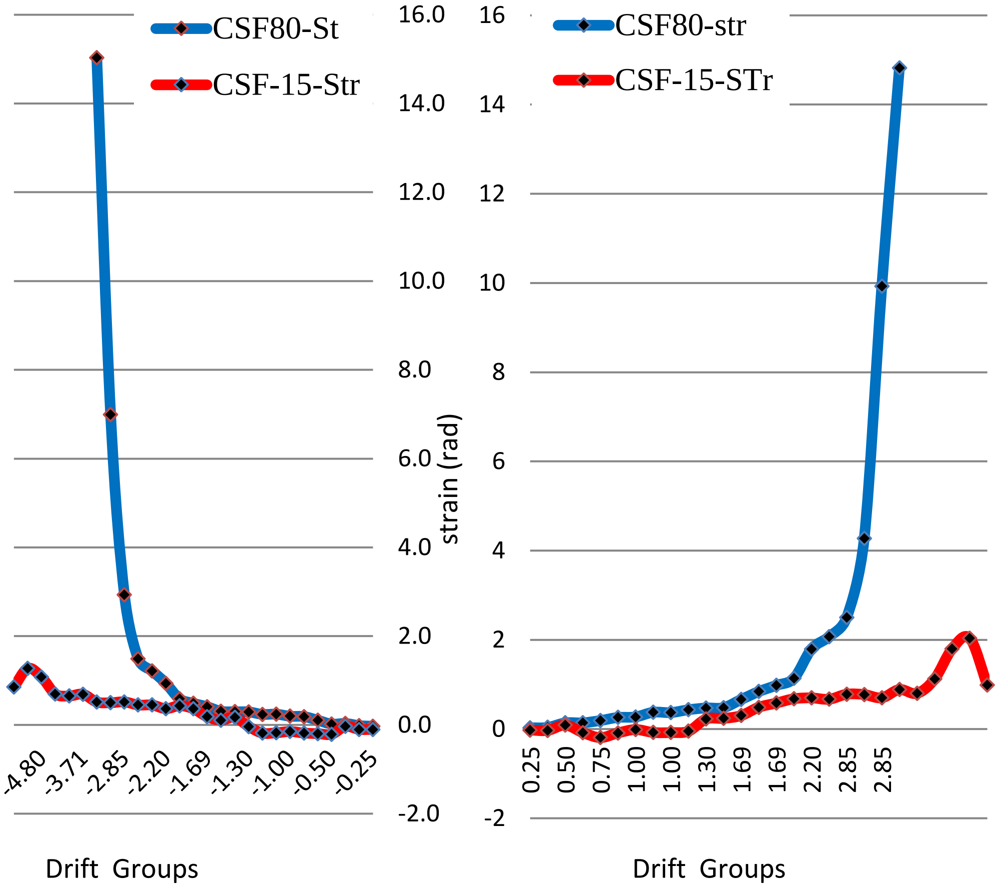

- **Blue line curve show a dramatic deformation for the higher axial loaded specimen CSF-80-E compared with CSF-15-E. The test show that stirrups opened under the high axial load and failed under compression flexure failure mood.**

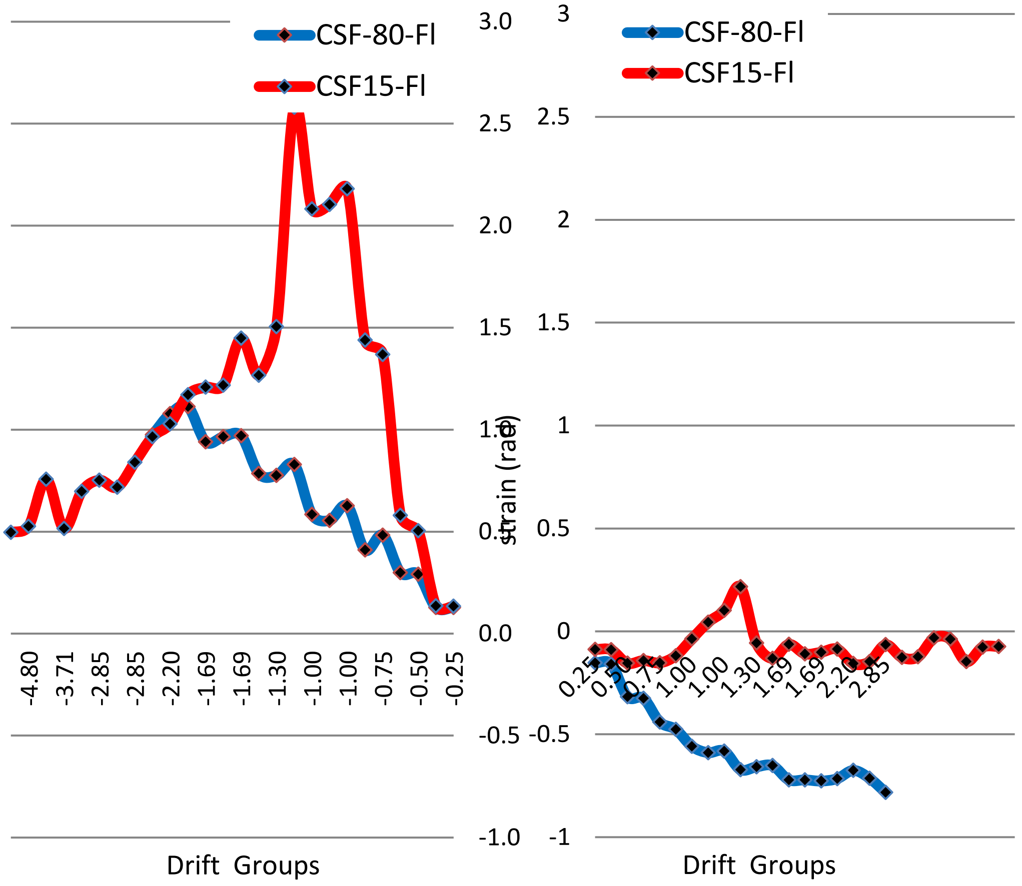

Figure 6.21: Compression and tension flange steel strain Vs Drift groups (300mm)

- **Under 80% axial load ratio the steel flange deformed higher comparing with 15% loading on specimen CSF-15-E**

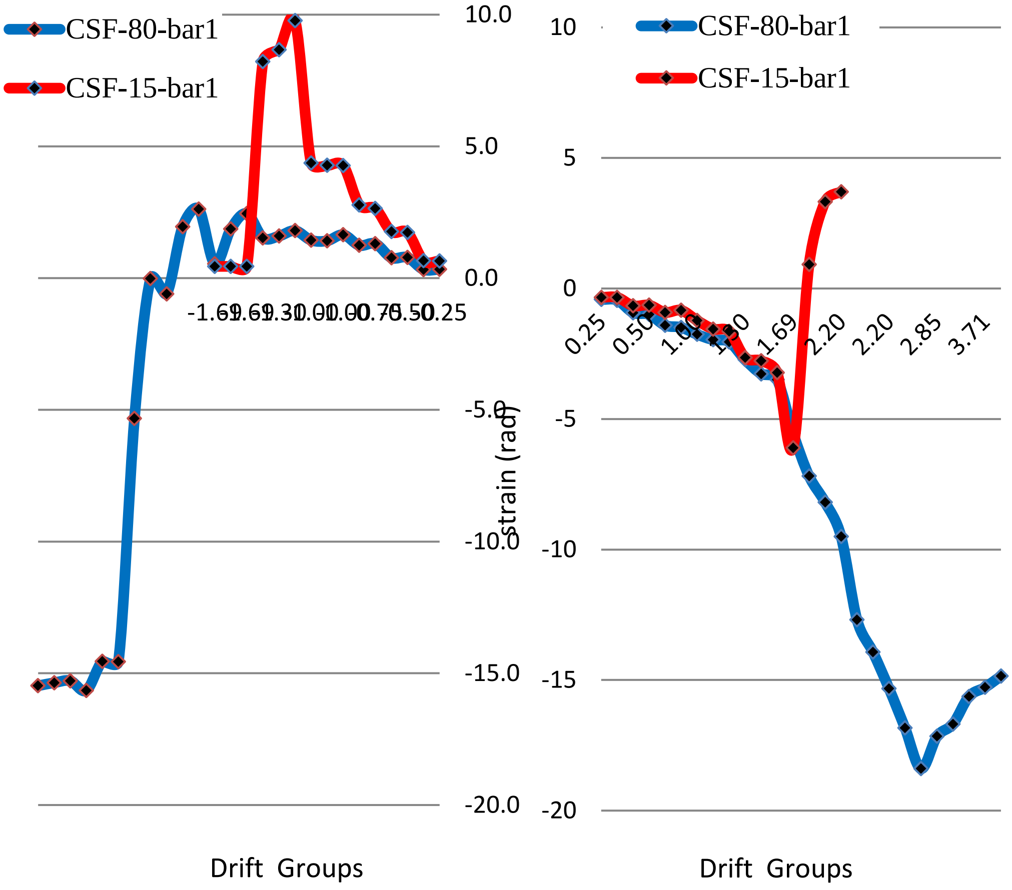

Figure 6.22: Compression and tension steel bar strain Vs Drift groups (50mm) (Compression side)

- **According to test figures and figure 6.22 last curve, steel bar buckled with big deformation larger than steel bar in CSF-15-E.**

7. Chapter (7)
Conclusion and recommendations

Based on the observation of failure modes and test results this chapter concludes all results from testing specimens for each group and how they fit with code’s recommendations. And also, there are some recommendations based on conclusions for each group.

7.1. Modern buildings

1.1. Conclusion

- Specimens show very satisfactory flexural performance without significant strength degradation until large drift ratio of 5.35 % which exceeds any practical drift ratio for collapse prevention.
- The steel section web and shear studs work to over-strength the column in shear. Thus, the shear failure of columns designed according to ACI 318-14 and AISC 341-2008 is not likely
- Modern building SRC column under flexural controlled in tension failure low axial load ratio with the maximum allowed hoop spacing showed slightly higher capacity in resisting lateral load with larger drift than column with smaller hoop spacing. That is not likely recommended by the code as it is counter-intuitive and could be attributed to test conditions. Thus, it could be concluded that since no apparent degradation of the more confined column was noticed until very large drift, using the maximum allowed hoop spacing recommended by ACI 318-14 seems suitable for good confinement with little strength loss at high drift.

1.2. Recommendations

- It is sufficient to use the maximum allowed ACI 318-14 hoop spacing in low axial load SRC column<15% experiencing flexural tension failure.
- More research needed to find the optimum hoop spacing which maximizes lateral and drift capacity for columns.
- More research needed with higher axial load ratio to further test the feasibility of code recommendation of hoop spacing

2. Existing buildings:

2.1. Conclusion:

2.1.1. Shear deficient

- The shear deficient SRC columns experienced early shear failure under cyclic load reversals and high axial load ratios.
- The tested specimens exhibited early shear failure at relatively low drift ratios of 2.28%-2.88%, which implies that SRC existing buildings are not fully conformant with modern building collapse prevention drift requirements under strong shaking. This could present losses of stability during strong seismic excitations. Thus, retrofitting such columns is needed.
- Increasing the axial load ratio from 15% to 80% has negatively affected deformation capacity of test specimens. It reduced peak shear drift by 32.2% and resulted in faster post peak shear strength degradation.

2.1.2. Flexure deficient

- The flexural compression controlled existing SRC columns with high axial load ratios (80%) are drift-critical since they can lose their lateral strength dramatically as early as 2% drift ratio and can reach axial failure at 6% drift ratio. Accordingly, these columns are considered seismically deficient if compared to the modern buildings deformation requirements.
- Increasing the axial load ratio from 15% to 80% shows a significantly different failure mode as the high axial load ratio led to the compression zone failure, buckling of longitudinal bars and steel section flanges, and opening the transverse hoops.
- Increasing the axial load ratio from 15% to 80% was detrimental to deformation capacity of test specimens. It reduced peak shear drift by 52.3%, axial failure load by 27% and resulted in faster post peak strength degradation.
- According to shear force hysteresis, after failure of concrete section, and losing a significant portion of lateral load capacity at relatively large drift, the steel section started increasing column energy and increased again the horizontal load capacity; however, this was at an unpractical large drift.

2.2. Recommendations

2.2.1. Shear and Flexure deficient

- Retrofitting shear deficient SRC columns under high axial loads (>40%) and flexure deficient columns under high axial loads (higher than the balanced load, i.e. compression controlled failure) experiencing moderate to strong ground shaking seems inevitable.

References

ACI 318-63. Building Code Requirements for Structural Concrete, American Concrete Institute, MI, USA.

ACI 318-14. Building Code Requirements for Structural Concrete, American Concrete Institute, MI, USA.

AISC 341-08.Specification for Seismic Design of Structural Steel, American Institute for Steel Construction, USA.

ASCE/SEI 41-13. Seismic Evaluation and Retrofit of Existing Buildings, American Society of Civil Engineers, USA.

AIJ (1987). “AIJ Standards for Calculation of Steel Reinforced Concrete Structures,” Architectural Institute of Japan, Tokyo (original in Japanese, English translation available from AIJ).

Chen, C., Wang, C., and Sun, H. 2014. Experimental Study on Seismic Behavior of Full Encased Steel-Concrete Composite Columns, ASCE Journal of Structural Engineering, Col.140, No.6.

Farag, M., and Hassan, W. 2015. Seismic Performance of Steel Reinforced Concrete Composite Columns, 10th Pacific Conference on Earthquake Engineering, Nov. 6-8, Sydney, Australia.

Farag, M. and Hassan, W., 2017. Seismic Performance of Flexural Controlled SRC Composite Columns in Existing Buildings, 16th World Conference on Earthquake Engineering, Jan 9-13, Santiago, Chile

Hassan, W., and Farag, M. 2017. Seismic Performance of Shear Controlled SRC Columns, 16th World Conference on Earthquake Engineering, Jan 9-13, Santiago,Chile.

Hassan W., and Farag, M. 2016. Cyclic Performance Assessment of Seismically Deficient SRC Composite Columns, 16th International Conference on Structural Faults and Repair, May 17-19, Edinburgh, Scotland, UK.

Hassan, W., Hodhod, O., Hilal, M.S., and Bahnasawy, H. 2017.Behavior of Eccentrically Loaded High Strength Concrete Columns Jacketed with FRP Laminates. Construction and Building Materials,138, pp. 508-527.

Hassan, W. M. 2011. Analytical and Experimental Assessment of Seismic Vulnerability of Beam-Column Joints without Transverse Reinforcement in Concrete Buildings.PhD Dissertation, University of California, Berkeley.

Ricle, J., and Paboojian, S. 1992. Experimental Study of Composite Columns Subjected to Seismic Loading Conditions, 10th World Conference on Earthquake Engineering, Balkema, Rotterdam.

Sezen, H. 2000. Seismic Behavior and Modeling of Reinforced Concrete Building Columns, PEER Report 2000/09, Pacific Earthquake Engineering Research Center, Berkeley, CA, USA.

Sarkisian, M. Long, E.D., and Hassan, W. M., 2013.Performance-Based Engineering of Core Wall Tall Buildings, Proceedings, ASCE Structures Congress, Pittsburg, PA, USA.

Tall Building Initiative.2011. Pacific Earthquake Engineering Research Center, University of California, Berkeley, CA, USA